2024

Environmental Controls On Carbon And Nitrogen Cycling In Alaskan Arctic Coastal Lagoons

Brian Seung Taek Kim
College of William and Mary - Virginia Institute of Marine Science, brian.st.kim@gmail.com

Environmental controls on carbon and nitrogen cycling in Alaskan Arctic coastal lagoons

---

A Dissertation

Presented to

The Faculty of the School of Marine Science

The College of William and Mary in Virginia

In Partial Fulfillment

of the Requirements for the Degree of

Doctor of Philosophy

By

Brian Seung Taek (승택) Kim

August 2024

APPROVAL PAGE

This dissertation is submitted in partial fulfillment of

the requirements for the degree of

Doctor of Philosophy

_____

Brian Seung Taek Kim

Approved by the Committee, July 2024

_____

Amber K. Hardison, Ph.D.
Advisor

_____

Bongkeun Song, Ph.D.

_____

Mark J. Brush, Ph.D.

_____

Chris J. Hein, Ph.D.

_____

Jim W. McClelland, Ph.D.
Marine Biological Laboratory
Woods Hole, MA, USA

This dissertation is dedicated to my family.

Thank you, mom and dad, for the sacrifices you made and the struggles you endured so that I could have a chance to pursue my passion.

To my sisters Eileen, Karen, and Jinna. Thank you for being role models and a source of inspiration in times of adversity and hardship.

To our collective future, health, and success.

Table of Contents

ACKNOWLEDGEMENTS

I would like to thank my advisor Dr. Amber K. Hardison for being my mentor throughout my graduate career. From persisting through post-Hurricane Harvey, moving from UTMSI to VIMS, and enduring COVID, thank you for supporting me during these past uncertain and tumultuous years. I would like to thank my committee members Drs. BK Song, Chris Hein, Jim McClelland, and Mark Brush for their help and support throughout my time at VIMS. I would like to give a special thank you to my committee member Dr. Iris C. Anderson who was a pillar of the biogeochemistry community and a constant source of radiant energy and curiosity.

During my time at VIMS, I have had the pleasure of working with many incredible members of the faculty, staff, administration, and student body. I would like to acknowledge the extensive support provided by Quinn Roberts and Hunter Walker who helped process thousands of my samples as well as provide sage life advice. I especially would like to thank my fellow Hardison lab mates, Ellie Gellerson, Novia Mann, Sarah Douglas, Xin Xu, Hengchen Wei and fellow VIMS graduate students Derek Detweiler, Stephanie Wilson, and Alyson Hall for years of support, advice, and friendship.

In the BLE-LTER, I would like to thank Drs. Andy Mahoney, Bailey McMeans, Byron Crump, Craig Tweedie, Emily Eidam, Jim McClelland, Katrin Iken, Ken Dunton, Mike Rawlings, Vanessa Lougheed, Vanessa von Biela, and Tim Whitaker for their academic and field support in the program. The unique experiences and opportunities have truly shaped who I am today as both a person and scientist. I would also like to give a special shoutout to Dr. Christina Bonsell, Dr. Nathan McTigue, and Kaylie Plumb who accomplish the impossible and make Arctic research feasible. As well as my fellow BLE-LTER graduate students, past and present, Kristina Baker, Tasha Griffin, Danny Fraser, Anne Krone, Sydney Wilkinson, Alina Spera, and Sasha Peterson for your unending support.

I would also like to thank the City of Utqiagvik and Kaktovik as well as the Ukpeagvik Inupiat Corporation (UIC) and Kaktovik Inupiat Corporation (KIC) for providing access to your native land. In particular, I would like to thank all of the people at the Barrow Arctic Research Center (BARC) who not only helped us with field logistics, but also welcomed us to engage in community events.

Finally, I would like to thank my friends and family for their endless support. Thank you for always listening and encouraging me to take the next step forward. I would truly not be here without you. Thank you to my family as well as my dear friends Alisha Lee, Jocelyn Ng, Josua Lutian, and Jackie Hang.

LIST OF TABLES

CHAPTER 2

Likewise, superscript letters (a,b,c) indicate significant internodal differences for a specific source within a given season based on ANOVA and post-hoc Tukey tests (a = 0.05).

Table 2.7. Net nutrient production and consumption (ΔN) according to deviations from the conservative mixing line of ammonium (NH_4^+; µmol N L^{-1}), nitrate (NO_3^-; µmol N L^{-1}), phosphate (PO_4^{3-}; µmol P L^{-1}), and dissolved silica (DSi; µmol SiO_2 L^{-1}) separated by season (Ice Cover, Break Up, Open Water), and node (BRW, SCC, BTI). NA: Fluxes of NH_4^+ and NO_3^- were not calculated due to lack of river nutrient data in BTI. Average ± standard error (n = sample number). For each nutrient, superscript letters (a,b,c) for the All Nodes Averages indicate statistically significant difference between seasons based on ANOVA and post-hoc Tukey tests (a = 0.05).

Table 2.8. Comparison of hypothetical nutrient concentrations from the conservative mixing line ($N_{conserved}$), observed nutrient concentrations, and deviation (ΔN) likely due to biotic processes during Ice Cover. Average ± standard error (n =sample number). To quantify the magnitude of biotic production ($\%_{biotic}$), ΔN was calculated as a percentage of ambient nutrient concentrations during Ice Cover.

APPENDIX A

Supplementary Table 2.1. Summary of nutrient analysis specification for ammonium (NH_4^+), orthophosphate (PO_4^{3-}), nitrate (NO_3^-) and nitrite (NO_2^-), and dissolved silica (DSi) for the Lachat autoanalyzer and FIAlyzer-1000.

Supplementary Table 2.2. Two-way ANOVA results on the effect of season and node on inorganic nutrient concentrations (NH_4^+, NO_3^-, PO_4^{3-}, DSi).

Supplementary Table 2.3. Multiple linear regression analysis results for environmental parameters (water column temperature, salinity, dissolved oxygen (DO), H_2O-$\delta^{18}O$) that may influence water column inorganic nutrient concentrations. For each parameter we calculated 1) slope: the estimated regression coefficient of the linear regression, 2) p-value: the statistical significance of the regression coefficient, 3) lmg: the relative importance of each parameter in explaining data variability, and 4) variance inflation factor (VIF): a measure of collinearity among independent variables, where values between 1 and 4 were considered an acceptable level of correlation between independent variables.

Supplementary Table 2.4. A two-way ANOVA was performed to analyze the effect of node and season on lagoon and river H_2O-$\delta^{18}O$ values.

Supplementary Table 2.5. A two-way ANOVA was performed to analyze the effect of node and season on the contribution of sea ice melt (SIM), meteoric water (MW), and the polar mixed layer (PML) to the lagoon.

Supplementary Table 2.6. A two-way ANOVA was performed to analyze the effect of node and season on the flux (ΔN deviation between $N_{Conserved}$ and $N_{observed}$) of inorganic nutrients (NH_4^+, NO_3^-, PO_4^{3-}, DSi).

CHAPTER 3

Table 3.1. Lagoon geomorphology (length (km), average depth (m), area (km^2), volume (km^3), annual river discharge (km^3), and ocean connectivity at Elson Lagoon (EWL, EEL), Simpson Lagoon (SIL), Stefansson Sound (SSL), Kaktovik Lagoon (KAL), and Jago Lagoon (JAL). Freshwater sources sampled by the BLE-LTER program are grouped by lagoon. Lagoon geomorphology was measured using the base World Imagery map on ArcGIS. (---) represents rivers with no published annual discharge rates. NA applies to lagoons with primarily diffusive inputs that cannot be or are difficult to quantify.

Table 3.2. Sediment organic carbon (SOC, %) and nitrogen (SON, %) content, C:N ratio, and carbon ($\delta^{13}C$) and nitrogen ($\delta^{15}N$) stable isotope composition (‰) in Shallow and Deep stations, or averaged across Shallow and Deep stations (All), at each node (BRW, SCC, BTI) or averaged across nodes (All) across all three seasons (Ice Cover, Break Up and Open Water) or averaged across Seasons (All). Values are average ± standard error (n = number of samples).

Table 3.3. Grain size average contribution (%) from sand (62.5 µm - 2000 µm), silt (4 µm - 62.5 µm), and clay (<4 µm) fractions (Wentworth, 1922) and median grain size values (µm) of BLE-LTER core program sediment samples (0-10 cm) grouped by water depth (Shallow, Deep), and node (BRW, SCC, BTI). Values are average ± standard error (n = number of samples).

Table 3.4. Elson Lagoon Focused Study: Sediment grain size, porosity (%), organic carbon (SOC, %) organic nitrogen (SON, %), C:N ratio, bottom water temperature (°C), and DOU rate (mmol O_2 m^{-2} d^{-1}) from Elson Lagoon surface sediments (0-2 cm) at Shallow and Deep stations during Ice Cover and Open Water seasons. Values are average ± standard error (n = number of samples). Shallow stations were not sampled during Ice Cover due to landfast ice. * indicates $p < 0.10$ from t-tests comparing Water Depth (Shallow vs. Deep) during Open Water; # indicates $p < 0.10$ from t-tests comparing deep stations across Season (Ice Cover vs. Open Water).

Table 3.5. Multiple linear regression analysis results for select characteristics (bottom water temperature, SOC content (%), C:N ratio, porosity (%), median grain size (µm)) that may influence benthic diffusive oxygen uptake (DOU, mmol O_2 m^{-2} d^{-1}). For each parameter we calculated 1) slope: the estimated regression coefficient of the linear regression, 2) p-value: the statistical significance of the regression coefficient, 3) lmg: the relative importance of each parameter in explaining data variability, and 4) variance inflation factor (VIF): a measure of collinearity among independent variables, where values between 1 and 4 were considered an acceptable level of correlation between independent variables.

Table 3.6. Benthic DOU was scaled up to the area of Elson Lagoon (207 km^2) over all three seasons (Ice Cover, Break Up, Open Water) between shallow and deep stations to calculate an annual sediment microbial respiration rate.

Appendix B

Supplementary Table 3.1. List of historical (1945-53) smooth sheets created from National Ocean Service (NOS) hydrographic surveys. Soundings were collected by

fathometers, and navigation was conducted by hydrographic sextant (visual triangulation) or Shoran (radio).

Supplementary Table 3.2. PERMANOVA results on the effect of node, season, and water depth on sediment organic carbon (SOC, %), organic nitrogen (SON, %), and C:N ratio. When significant, post-hoc pairwise comparisons were performed on independent and interaction factors.

Supplementary Table 3.3. PERMANOVA results on the effect of node, season, and water depth on sediment organic carbon and nitrogen stable isotopes ($\delta^{13}C$ and $\delta^{15}N$, ‰). When significant, post-hoc pairwise comparisons were performed on independent and interaction factors.

Supplementary Table 3.4. PERMANOVA results on the effect of node, season, and water depth on sediment grain size distribution (Sand %, Silt %, Clay %) for BLE-LTER core program sediment samples. When significant, post-hoc pairwise comparisons were performed on independent and interaction factors.

Supplementary Table 3.5. T-test comparing sediment characteristics (Sand %, Silt %, Clay %, median grain, porosity %) and organic matter content (SOC %, SON %, C:N ratio) between deep stations across Seasons (Ice Cover vs. Open Water) and Water Depth (Shallow vs. Deep) during the Open Water period.

Supplementary Table 3.6. The stepwise selection regression model output displays the model with the lowest prediction error using a defined number of parameters (1-4). For each model, we calculated RMSE and MAE, which measure the prediction error of each model, with lower values indicating a better model. Adjusted R^2 values represent the correlation between values observed and predicted by the model, with higher values indicating a better model.

CHAPTER 4

Table 4.1. Average hourly sediment fluxes of O_2 (mmol O_2 m^{-2} h^{-1}) and DIC (mmol C m^{-2} h^{-1}) across seasons (Ice Cover, Break Up, Open Water, Annual) and water depth (Deep, Shallow, Combined). n = sample size. Superscript letters denote significant differences between seasons. Asterisks (*) denote values which were set to 0 due to the lack of light incubations during Ice Cover. (---) represents samples not collected due to the presence of landfast ice.

Table 4.2. Average benthic respiration (BR; mmol C m^{-2} d^{-1}), gross benthic production (GBP; mmol C m^{-2} d^{-1}), and net benthic metabolism (NBM; mmol C m^{-2} d^{-1}) across seasons (Ice Cover, Break Up, Open Water) and water depth (Deep, Shallow, Combined). n = sample size. Superscript letters denote significant differences between seasons. (---) represents samples not collected due to the presence of landfast ice.

Table 4.3. Average net benthic N_2 fluxes (µmol N m^{-2} d^{-1}) and DIN fluxes (µmol N m^{-2} d^{-1}) across seasons (Ice Cover, Break Up, Open Water) and water depth (Deep, Shallow, Combined). n = sample size. Superscript letters denote significant differences between seasons. (---) represents samples not collected due to the presence of landfast ice.

Table 4.4. Average net benthic fluxes of NH_4^+ (µmol N m^{-2} d^{-1}), NO_3^- (µmol N m^{-2} d^{-1}), PO_4^{3-} (µmol P m^{-2} d^{-1}) and DSi (µmol SiO_2 m^{-2} d^{-1}) across seasons (Ice Cover, Break Up, Open Water, Annual) and water depth (Deep, Shallow, Combined). n = sample size. Superscript letters denote significant differences between seasons. (---) represents samples not collected due to the presence of landfast ice.

Table 4.5. Seasonal average ± standard error (n = sample number) of environmental parameters that were selected as input variables for the stepwise multiple linear regression model.

Table 4.6. The stepwise selection regression model output for Benthic Respiration (BR) displays the model with the lowest prediction error with two parameters (temperature, SOC; Model 2). For each model, we calculated RMSE and MAE, which measure the prediction error of each model, with lower values indicating a better model. Adjusted R^2 values represent the correlation between values observed and predicted by the model, with higher values indicating a better model. Once selected, the final model was assessed for 1) slope: the estimated regression coefficient of the linear regression, 2) p-value: the statistical significance of the regression coefficient, 3) lmg: the relative importance of each parameter in explaining data variability, and 4) variance inflation factor (VIF): a measure of collinearity among independent variables, where values between 1 and 4 were considered an acceptable level of correlation between independent variables.

Table 4.7. Seasonal rates of benthic metabolism (BR, GBP, NBM) and net nitrogen fluxes (N_2, DIN) were scaled up to annual rates based on the duration of each season (Ice Cover, Break Up, and Open Water).

APPENDIX C

Supplementary Table 4.1. Average hourly sediment fluxes of DIC (mmol C m^{-2} h^{-1}) across seasons (Ice Cover, Break Up, Open Water, Annual) and water depth (Deep, Shallow, Combined). n = sample size. Superscript letters denote significant differences between seasons. Asterisks (*) denote values which were set to 0 due to the lack of light incubations during Ice Cover. (---) represents samples not collected due to the presence of landfast ice.

Supplementary Table 4.2. Two-way ANOVA results on the effect of season (Ice Cover, Break Up, Open Water) and water depth (Shallow, Deep) on sediment fluxes of O_2 and DIC in dark and light incubations.

Supplementary Table 4.3. Two-way ANOVA results on the effect of season (Ice Cover, Break Up, Open Water) and water depth (Shallow, Deep) on benthic respiration (BR), gross benthic production (GBP) and net benthic metabolism (NBM).

Supplementary Table 4.4. Two-way ANOVA results on the effect of season (Ice Cover, Break Up, Open Water) and water depth (Shallow, Deep) on net benthic N_2 and DIN fluxes.

Supplementary Table 4.5. Two-way ANOVA results on the effect of season (Ice Cover, Break Up, Open Water) and water depth (Shallow, Deep) on net benthic inorganic nutrient fluxes (NH_4^+, NO_3^-, PO_4^{3-}, DSi).

Supplementary Table 4.6. Matrix of p-values from Pearson's correlation of all environmental parameters. Colors denote level of significant (yellow <0.1, green <0.05, red <0.01).

Supplementary Table 4.7. The stepwise selection regression model output for gross benthic production (GBP) displaying the model with the lowest prediction error with two parameters (Model 2; PAR, sediment chlorophyll-a).

Supplementary Table 4.8. The stepwise selection regression model output for net benthic metabolism (NBM) displaying the model with the lowest prediction error with one parameter (Model 1; salinity).

Supplementary Table 4.9. The stepwise selection regression model output for net sediment N_2 flux displaying the model with the lowest prediction error with one parameter (Model 1; water column DIN concentration).

Supplementary Table 4.10. The stepwise selection regression model output for net sediment NH_4^+ flux displaying the model with the lowest prediction error with one parameter (Model 1; temperature).

Supplementary Table 4.11. The stepwise selection regression model output for net sediment NO_3^- flux displaying the model with the lowest prediction error with three parameters (temperature, salinity, and δ^{13}C-SOC). The parameters of the final model were not significant.

Supplementary Table 4.12. The stepwise selection regression model output for net sediment PO_4^{3-} flux displaying the model with the lowest prediction error with one parameter (sediment chlorophyll-a). The final model was not significant.

Supplementary Table 4.13. The stepwise selection regression model output for net sediment DSi flux displaying the model with the lowest prediction error with one parameter (temperature).

Supplemental Table 4.14. Respiratory quotient (RQ, C:O_2) and photosynthetic quotient (PQ, O_2:C) calculated from linear regressions (R^2) of DO and DIC fluxes during dark and light incubations, respectively. Asterisks denote the levels of significance of the linear regression (p-value: ~<0.10, *<0.05, **<0.01, ***<0.001, ****<0.0001). RQ and PQ values were calculated for each season and annually. Due to the lack of significance of dark RQ values, RQ values were also calculated using both dark and light incubations.

LIST OF FIGURES

CHAPTER 2

CHAPTER 3

Figure 3.1. Location of the study sites at the Beaufort Lagoon Ecosystems Long-Term Ecological Research (BLE-LTER) program. a) Map of Alaska with Beaufort Sea Alaskan coast in box. b) Beaufort Sea Coast with BLE-LTER research nodes in boxes. c) The westernmost node (BRW) is based out of Utqiaġvik where Elson Lagoon is located. The central node (SCC) contains d) Simpson Lagoon and e) Stefansson Sound. The eastern node (BTI) is based out of Kaktovik and contains f) Kaktovik Lagoon and Jago Lagoon. Each sampled lagoon has two shallow (squares) and two deep (circles) stations.

Figure 3.2. BLE-LTER Core Program dataset (2019-2021) for a) sediment organic carbon (SOC, %), b) sediment organic nitrogen (SON, %), and c) C:N ratio across nodes (BRW, SCC, BTI), separated by water depth (Shallow, Deep) and colored by season: Ice Cover (blue), Break Up (green), and Open Water (yellow). The lower and upper extent of the boxplot represent the 25^{th} (Q1) and 75^{th} (Q3) percentiles, while the lower and upper extent of the whiskers represent 1.5 times the interquartile range (Q3-Q1) below Q1 and above Q3. The solid black line within each box represents the median value and the dashed black line and parentheses at the top of each panel denotes the average value across all nodes at each depth. The solid red line in c) represents the Redfield ratio of 106C:16N.

Figure 3.3. a) $\delta^{13}C$ and b) $\delta^{15}N$ values (‰) of lagoon sediments (circles) across nodes (BRW, SCC, BTI), separated by water depth (Shallow, Deep) and colored by season: Ice Cover (blue), Break Up (green), and Open Water (yellow). The lower and upper extent of the boxplot represent the 25^{th} (Q1) and 75^{th} (Q3) percentiles, while the lower and upper extent of the whiskers represent 1.5 times the interquartile range (Q3-Q1) below Q1 and above Q3. The average value across all nodes at each depth is denoted by the dashed black line and also written in parentheses at the top of the panel.

Figure 3.4. Ternary plot of grain size distribution showing % Sand (62.5 µm - 2000 µm), % Silt (4 µm - 62.5 µm), and % Clay (<4 µm) at Shallow (empty circle) and Deep stations (filled circle) for a) BLE-LTER and c) Elson Lagoon case study sediments. The same grain size data is visually represented as stacked barplots grouped by season (Ice Cover, Break Up, Open Water) and water depth (Deep, Shallow) for b) BLE-LTER and d) Elson Lagoon case study sediment samples. Shallow stations were not sampled during Ice Cover and Break Up was not sampled in the Elson Lagoon case study.

Figure 3.5. Surface sediment (0-2 cm depth) characteristics of a) SOC (%), b) SON (%), c) C:N ratio, d) porosity (%), and e) median grain size (µm) in Elson Lagoon separated by water depth (Deep, Shallow) and colored by season (blue=Ice Cover, yellow=Open Water). The lower and upper extent of the boxplot represent the 25^{th} (Q1) and 75^{th} (Q3) percentiles, while the lower and upper extent of the whiskers represent 1.5 times the interquartile range (Q3-Q1) below Q1 and above Q3. The solid black line within each box represents the median value. In the Elson Lagoon focused study, samples were not collected during Break Up or at shallow stations during Ice Cover.

Figure 3.6. a) Diffusive oxygen uptake (DOU, mmol O_2 m^{-2} d^{-1}) for Elson Lagoon focused study (2022) grouped by season (Ice Cover, Open Water) and water depth (Deep, Shallow). b) Regression of sediment organic carbon (SOC) content (%) and DOU (mmol O_2 m^{-2} d^{-1}) grouped by season (blue=Ice Cover, yellow=Open Water) and water depth

(filled=Shallow, hollow=Deep). DOU was not measured during the Break Up season. The average DOU rate for each season and depth is denoted in parentheses at the top of the panel.

Appendix B

Supplemental Figure 3.1. Bathymetry of study sites derived from inverse distance weighted (IDW) interpolation of point depth soundings from National Ocean Services surveys from 1945 to 1953 for a) Elson Lagoon, b) Simpson Lagoon, c) Stefansson Sound, Kaktovik Lagoon (d, left) and Jago Lagoon (d, right). Lagoon depth is colored in 0.5 m increments with white denoting a depth of 0 and black representing a depth > 5.0 m.

Supplemental Figure 3.2. Example sediment O_2 microprofiles from Unisense oxygen sensor. Two profiles during Open Water are shown to highlight the differences between Deep (EEL D1, filled circles) and Shallow (EWL S1, empty circles) stations.

CHAPTER 4

Figure 4.1. Location of the study sites at the Beaufort Lagoon Ecosystems Long-Term Ecological Research (BLE-LTER) program. a) Map of Alaska with Beaufort Sea Alaskan coast in box. b) Beaufort Sea Coast with BLE-LTER research nodes in boxes. c) The westernmost node (BRW) is based out of Utqiaġvik where Elson Lagoon is located. The central node (SCC) contains d) Simpson Lagoon and e) Stefansson Sound. The eastern node (BTI) is based out of Kaktovik and contains f) Kaktovik Lagoon and Jago Lagoon. Each sampled lagoon has two shallow (squares) and two deep (circles) stations.

Figure 4.2. Conceptual diagram based on Mahoney et al. (2007) showing annual cycles of landfast sea ice (background color, freeze-up = dark blue, Ice Cover = light blue, Break Up = turquoise, Open Water = grey) and river discharge (solid blue line) along the Alaskan Beaufort Sea coast (Mahoney et al. 2007). Diagram has been modified to denote periods with 24 hours of light (“midnight sun”) and 24 hours of darkness (“polar night”).

Figure 4.3. Boxplots of a) hourly sediment O_2 flux (mmol O_2 m^{-2} h^{-1}) and b) hourly sediment DIC flux (mmol C m^{-2} h^{-1}) from dark (grey bars) and light (white bars) incubations across seasons (Ice Cover, Break Up, Open Water) and water depth (Deep = filled circles, Shallow = empty circles). The lower and upper extent of the boxplot represent the 25^{th} (Q1) and 75^{th} (Q3) percentiles while the lower and upper extent of the whiskers represent 1.5 times the interquartile range (Q3-Q1) below Q1 and above Q3. The solid black line within each box represents the median rate. Brackets represent significant seasonal differences (p-value: ~<0.10, *<0.05, **<0.01, ***<0.001, ****<0.0001). c) Scatterplot of sediment O_2 flux and DIC flux during light (open circles) and dark (filled circles) incubations across Ice Cover (blue), Break Up (green), and Open Water (yellow). The dashed red line through the scatterplot represents a 1:1, C:O_2 ratio (i.e., respiratory quotient, RQ), while the solid black line represents the linear regression between O_2 and DIC fluxes averaged across the entire year for this study (Annual RQ: 0.71). Season-

specific linear regression lines are also shown for Ice Cover (blue), Break Up (green), and Open Water (yellow), with accompanying slopes, R^2, and p values.

Figure 4.4. Boxplot of daily rates of a) benthic respiration (BR, mmol C m^{-2} d^{-1}), b) gross benthic production (GBP, mmol C m^{-2} d^{-1}), and c) net benthic metabolism (NBM; mmol C m^{-2} d^{-1}) across seasons (Ice Cover [blue], Break Up [green], Open Water [yellow]) and water depth (Deep = filled circles, Shallow = empty circles). The lower and upper extent of the boxplot represent the 25th (Q1) and 75th (Q3) percentiles while the lower and upper extent of the whiskers represent 1.5 times the interquartile range (Q3-Q1) below Q1 and above Q3. The solid black line within each box represents the median rate. Brackets represent significant seasonal differences (p-value: ~<0.10, *<0.05, **<0.01, ***<0.001, ****<0.0001). Average rates of BR, GBP, and NBM (mmol C m^{-2} d^{-1}) by season are denoted in parentheses along the x-axis.

Figure 4.5. Boxplot of daily net benthic a) N_2 flux (µmol N m^{-2} d^{-1}) and b) DIN flux (µmol N m^{-2} d^{-1}) across seasons (Ice Cover [blue], Break Up [green], Open Water [yellow]) and water depth (Deep = filled circles, Shallow = empty circles). The lower and upper extent of the boxplot represent the 25th (Q1) and 75th (Q3) percentiles while the lower and upper extent of the whiskers represent 1.5 times the interquartile range (Q3-Q1) below Q1 and above Q3. The solid black line within each box represents the median rate. Brackets represent significant seasonal differences (p-value: ~<0.10, *<0.05, **<0.01, ***<0.001, ****<0.0001). Average rates of sediment N_2 and DIN flux by season are denoted in parentheses along the x-axis. Note the difference in scale for y-axis in panels a and b.

Figure 4.6. Boxplots of daily benthic fluxes of a) NH_4^+ (µmol N m^{-2} d^{-1}), b) NO_3^- (µmol N m^{-2} d^{-1}), c) PO_4^{3-} (µmol P m^{-2} d^{-1}), and d) DSi (µmol SiO_2 m^{-2} d^{-1}) across seasons (Ice Cover [blue], Break Up [green], Open Water [yellow]) and water depth (Deep = filled circles, Shallow = empty circles). The lower and upper extent of the boxplot represent the 25th (Q1) and 75th (Q3) percentiles while the lower and upper extent of the whiskers represent 1.5 times the interquartile range (Q3-Q1) below Q1 and above Q3. The solid black line within each box represents the median rate. Brackets represent significant seasonal differences (p-value: ~<0.10, *<0.05, **<0.01, ***<0.001, ****<0.0001). Average rates of sediment nutrient flux by season are denoted in parentheses along the x-axis.

Appendix C

Supplementary Figure 4.1. Hourly net benthic a) N_2 flux (µmol N m^{-2} h^{-1}) and b) DIN flux (µmol N m^{-2} h^{-1}) across seasons. Fluxes are separated between dark (gray boxplot) and light (white boxplot) incubations with water depth denoted by filled circles (Deep) or empty circles (Shallow). The lower and upper extent of the boxplot represent the 25th (Q1) and 75th (Q3) percentiles while the lower and upper extent of the whiskers represent 1.5 times the interquartile range (Q3-Q1) below Q1 and above Q3. The solid black line within each box represents the median rate. Note the difference in scale for y-axis in panels a and b.

Abstract

At the intersection of land, sea, and atmosphere, coastal lagoons act as bioreactors, processing both terrestrial and autochthonous organic matter production before export to the coastal ocean. Approximately half of the Beaufort Sea coast is outlined by barrier island chains that enclose shallow lagoons and sounds. These lagoons are subject to extreme seasonal variations in ice cover, temperature, and salinity, yet are home to a diverse and productive food web. Bound between the arctic tundra and Beaufort Sea, these shallow systems receive and process resources from both sea and particularly land in the form of coastal erosion and riverine export. While we know these terrestrial inputs are driving increasing rates of primary production in the Arctic Ocean, the role of nearshore coastal retention and processing of this material before export remains underexplored. To that end, the overarching goal of this dissertation was to assess seasonal and spatial dynamics of carbon and nutrient cycling in coastal Arctic lagoons as part of the Beaufort Lagoon Ecosystems Long-Term Ecological Research (BLE-LTER) program from 2018-2022. Water column and sediment samples were collected at five lagoons (Elson Lagoon, Simpson Lagoon, Stefansson Sound, Kaktovik Lagoon, Jago Lagoon) during Ice Cover (April), Break Up (June), and Open Water (August) in alignment with the major hydrological phases. In *Chapter 2, Abiotic and biotic controls on nutrient cycling in coastal Arctic lagoons,* I present seasonally collected water column nutrient data and estimated physical vs. biological controls on their concentrations. During Ice Cover, inorganic nutrient concentrations likely increased in response to brine exclusion and biotic remineralization. In contrast nutrient concentrations rapidly decreased during Break Up and Open Water through freshwater input dilution and autotrophic uptake during Break Up. In *Chapter 3, Physical drivers of sediment distribution and organic matter oxidation in coastal Arctic lagoons,* I focused on sediment characteristics and the physical conditions that drive organic matter distribution and microbial aerobic oxidation. Sediment grain size, organic matter content, and isotopic composition consistently differed between lagoons and water depths, reflecting the variability in sediment organic matter retention, source, and processing. In *Chapter 4, Seasonal cycles of benthic productivity and N cycling in Beaufort Sea lagoons* I present results from seasonal batch sediment incubations to quantify benthic metabolism and nitrogen cycling. In general, lagoon sediments shifted from net heterotrophy in Ice Cover, exhibiting net inorganic nutrient production and net denitrification before transitioning into net autotrophy during Break Up and Open Water with increased sediment nutrient consumption and nitrogen fixation. As the coastal Arctic undergoes rapid changes in temperature, duration of sea ice, river discharge, and coastal erosion, our understanding of seasonal nearshore coastal metabolism will help to better constrain future projections of coastal Arctic ecosystem productivity.

Environmental controls on carbon and nitrogen cycling in Alaskan Arctic coastal lagoons

Chapter 1: Introduction

1.1 Coastal lagoon ecosystems

Coastal marine zones receive, retain, and process significant amounts of terrestrial organic matter, making them among the most biologically active areas of the biosphere (Bianchi et al., 2018; Canuel & Hardison, 2016; Duarte, 2017). Coastal lagoons are shallow water bodies that are separated from the ocean by natural barriers, intermittently connected to the ocean, and characterized by their unique ecological features (Kjerfve, 1994; Kjerfve & Magill, 1989). Lagoons are effective sediment traps, with sediments originating from the shoreline, barrier island overwash during storms, tidal inlet processes (e.g., flood-tidal delta and recurved spit accretion), atmospheric deposition, and river discharge (Kjerfve & Magill, 1989; Snedden et al., 2023). Their shallow depths seldom exceed a few meters, making them distinct from other similar but deeper habitats such as estuaries and bays (Hardison et al., 2011; Kjerfve & Magill, 1989; Pérez-Ruzafa et al., 2011). Because lagoons are such effective sediment traps, the depth of most modern lagoons is controlled by their width along the coastline and primary wind direction, which determines fetch and therefore effective wave influence (Kjerfve & Magill, 1989; Snedden et al., 2023).

These estuarine coastal bodies exist as a continuum between terrestrial and marine ecosystems, encompassing several environmental gradients that host a wide variety of organisms including primary producers (Canuel & Hardison, 2016; Pérez-Ruzafa et al., 2011, 2020). Characterized by high resource availability, long retention times, and diverse primary producers, coastal lagoons support a highly productive

ecosystem (Kjerfve, 1994; Kjerfve & Magill, 1989; Pérez-Ruzafa et al., 2011; Snedden et al., 2023). Since these ecosystems are so shallow, benthic microbial loops also play an especially vital role in decomposing organic matter, recycling nutrients, and enhancing both benthic-pelagic cycling and primary productivity (Damashek & Francis, 2018; Liefer et al., 2014; Manini et al., 2003; Renaud et al., 2008). In turn, they provide essential sources of food and habitats that host numerous resident and migrant fish species, supporting local communities and overall ecological richness (Dunton et al., 2012; Fraley et al., 2021). However, due to climate change, coastal lagoons are subject to new environmental pressures such as sea-level rise, increasing temperatures and storm activity, and human pollution (Canuel et al., 2012; Carrasco et al., 2016; Ligorini et al., 2023; Pusceddu et al., 2005).

Favorable conditions including a shallow depth, high light availability, and benthic nutrient cycling, enhance primary production in coastal lagoon ecosystems (Manini et al., 2003; Pérez-Ruzafa et al., 2011, 2020). The mixing of fresh and marine waters enhances nutrient availability, promoting the growth of diverse vegetation and algae contributing to the status of coastal lagoons as being one of the most productive marine ecosystems globally (Duarte, 2017; Martins et al., 2022; Pérez-Ruzafa et al., 2011). Vegetated coastal habitats (i.e., mangroves, salt marshes, seagrass meadows) play a vital role in the ocean carbon budget by generating a substantial portion of global marine net primary production (Duarte, 2017; Duarte et al., 2005). Macroalgae can also be significant contributors to coastal primary production, even in polar regions, where annual primary production may be low (Gattuso et al., 2006).

The importance of coastal primary production also extends to their role in carbon sequestration, with these ecosystems exhibiting a disproportionate role in global carbon storage (Brevik & Homburg, 2004; Chen, 2020; Martins et al., 2022). Although coastal vegetated habitats, represent < 0.2% of the area of the ocean, they account for at least 50% of the total marine carbon sequestration (Duarte, 2017; Duarte et al., 2005). In fact, McLeod et al. (2011) found carbon storage rates in coastal vegetated areas could be up to 40 times higher than tropical rainforests per unit area. These habitats generate a surplus of organic carbon, which is often buried in sediments due to low carbon loss rates (Brevik & Homburg, 2004; Chen, 2020; Martins et al., 2022).

The morphological features of coastal lagoons, including the network of barrier islands, channels, and tidal flats, all influence water flow and therefore the burial of organic carbon in sediments (Bianchi et al., 2018; Petti et al., 2018), with higher residence times associated with higher rates of sediment trapping and burial (Hanna et al., 2018; Nichols, 1989). The accumulation of organic carbon in lagoon sediments is also influenced by sediment characteristics like grain size and organic carbon content, constraining redox conditions that dictate respiration and burial efficiency of carbon in these environments (Ahmerkamp et al., 2020; Van De Velde et al., 2023; Wilson et al., 2008). In addition, wind-driven sediment suspension and siltation processes also play a role in the burial of organic carbon within lagoon sediments (S. Lawson et al., 2012; S. E. Lawson et al., 2007; Petti et al., 2018).

As the boundary between several ecospheres, coastal lagoons can receive nutrients from various sources including groundwater, terrestrial runoff, atmospheric deposition, nitrogen fixation, and exchange with the ocean (Cervantes-Duarte et al., 2013;

Fertig et al., 2013; Leote et al., 2008; Rodellas et al., 2018). Coastal lagoons can act as both a source and sink of nutrients depending on local factors such as internal cycling, sediment interactions, and external inputs through groundwater and terrestrial discharge (Leote et al., 2008; Liefer et al., 2014; Rodellas et al., 2018). With long water residence times and restricted access to the sea, coastal lagoons can act as sites of organic matter accumulation, leading to nutrient retention within the lagoon ecosystem (Malta et al., 2017; Manini et al., 2003; Middelburg et al., 2004; Vybernaite-Lubiene et al., 2017). However, sediments can also act as a source of nutrients via remineralization and release to the overlying waters, fueling more primary production (McGlathery et al., 2007; Nowicki & Nixon, 1985; Webster et al., 2002). In some cases, coastal lagoons can behave as sources of dissolved inorganic nutrients due to high exchange rates with groundwater (Rodellas et al., 2018; Wang & Du, 2016). This retention and production highlights lagoons as bioreactors capable of fueling production, retaining nutrients, and exporting both new and regenerated organic and inorganic nutrients. This variability shows that coastal lagoons have the potential to act as both nutrient sinks and sources, depending on the specific hydrological conditions and biological processes occurring within the ecosystem.

In coastal lagoon ecosystems, seasonal and spatial variability in environmental conditions and resource availability facilitate an abundance of nitrogen (N) cycling pathways. The dominant N cycling pathway in sediments determines whether sediments act as a net source or sink for bioavailable N to the overlying water. Within anoxic sediments, N may be removed via denitrification or anaerobic ammonium oxidation (anammox) and released as dinitrogen gas (N_2). Denitrification is the stepwise reduction

of nitrate (NO_3^-) to N_2 gas by denitrifying, heterotrophic microbes. Nitrate fueling denitrification can come either from the overlying water column (direct denitrification) or from ammonium oxidation in the sediment porewater (coupled nitrification-denitrification; Devol, 2015). Denitrification rates are controlled by various environmental factors including overlying NO_3^- concentrations and redox conditions associated with organic matter content (Cornwell et al., 2014; Devol, 2015). Anammox is the anaerobic oxidation of ammonium (NH_4^+) coupled to the reduction of nitrite (NO_2^-) to produce N_2 gas. In contrast to denitrification, anammox is performed by autotrophic bacteria and may be more favorable in low organic matter conditions (Thamdrup & Dalsgaard, 2002). Dissimilatory nitrate reduction to ammonium (DNRA) is the reduction of NO_3^- to NH_4^+ performed by heterotrophic bacteria in anoxic settings (Giblin et al., 2013). DNRA is not considered a N removal pathway because it transforms NO_3^- into another bioavailable form, NH_4^+, thereby retaining the N in the system (Giblin et al., 2013). DNRA tends to dominate over denitrification in sulfide- and organic-rich sediments, and high organic matter loading can be seen as a prerequisite (Giblin et al., 2013; Hardison et al., 2015).

1.2 Beaufort Sea lagoons

As ubiquitous features, coastal lagoons are also found all around the Arctic Ocean. In fact, nearly half of the Beaufort Sea coast, located along the northernmost coast of Alaska, is bordered by an irregular and discontinuous chain of barrier islands that enclose numerous shallow (<7 m) lagoons and sounds (Dunton et al., 2006; Wiseman et al. 1973). Variations in barrier island morphology play a crucial role in shaping the hydrological balance between fresh and marine waters in the Arctic, creating a wide range of salinities,

circulation patterns, and flushing times that impact their hydrodynamics and overall ecological function (Snedden et al., 2023; Weingartner et al., 2017).

Seasonal shifts in temperature, sea ice dynamics, and freshwater inputs create large annual fluctuations in ecosystem conditions. Annually, water column temperatures range from -2 to 14 ^{o}C, and salinities vary drastically, from fresh (0) to hypersaline (45) (Harris et al., 2017; Miller et al., 2021; Connolly et al., 2021). The magnitude of seasonal temperature fluctuations in Arctic lagoons is notably larger compared to much of the rest of the Arctic Ocean (Carvalho & Wang, 2020). As early as October, seasonal sea ice begins to form and extends for eight months of the year, with shallow areas of the lagoons developing bottom fast ice (Mahoney et al., 2014). During sea ice formation, brine is ejected into the underlying water resulting in hypersaline conditions in shallow areas (<3 m) (Yamamoto-Kawai et al., 2005; McCart, 1977). In Spring, the freshet occurs as snow and sea ice melt, resulting in over half of the annual freshwater river discharge within a two-week period (McClelland et al., 2012; Stierle & Eicken, 2002). While freshwater inflow facilitates ice breakup, the lagoons remain largely ice-covered until late June. This lag between the freshet in May and ice break up in June promotes the retention and biological processing of river derived inputs, including vast quantities of dissolved organic matter (DOM), particulate organic matter (POM), and dissolved inorganic nutrients (McClelland et al., 2012). Once all the sea ice melts and the shoreline is exposed, wind and wave activity rapidly erode the coast (Barnhart et al., 2014b; Overeem et al., 2011). Located at roughly 70^{o}N , daylength varies from periods of no light (“polar night,” ~60 days) to periods of constant light (“midnight sun,” ~81 days) during winter and summer, respectively (www.timeanddate.com). Although surface sunlight exists for nine months of the year

(March – December), underwater light availability is further constrained to the late spring and summer months due to the presence of sea ice (Bonsell & Dunton, 2018).

Although the Arctic Ocean accounts for ~ 1% of total ocean volume, it receives >10% of global river discharge, resulting in a disproportionate impact of river inputs on the biogeochemistry of Arctic coastal waters (Dittmar & Kattner, 2003; McClelland et al., 2012). During a short period from May to July, Arctic rivers discharge >90% of their annual nutrient and organic matter export and most of their water inputs (Dittmar & Kattner, 2003; Holmes et al., 2012; McClelland et al., 2014). Relative to lower latitudes, Arctic rivers have some of the highest concentrations of organic matter, with annual exports on par with the Amazon River, while inorganic nutrients in the Arctic are among the lowest worldwide (Dittmar & Kattner, 2003). This pattern of high organic matter and low inorganic nutrient inputs is due to the Arctic watershed, which is primarily composed of permafrost that readily leaches high concentrations of dissolved organic carbon (DOC) (Bristol et al., 2021; Johnston et al., 2019; Connolly et al., 2020).

As the summer progresses and the lagoons become completely ice free, they receive additional terrestrial inputs in the form of permafrost through coastal erosion. Coastal erosion in the Beaufort Sea region is limited to the short ice-free season, lasting three to four months (Overduin et al., 2014). During this period, wind and wave activity along the coastline promotes mechanical permafrost degradation (Barnhart et al., 2014b; Overeem et al., 2011). Average rates of coastal erosion for the Arctic (0.5 m $year^{-1}$) are among the highest in the world, due in part to the ice-bonded nature of the coastal sediments (Jones et al., 2009; Lantuit et al., 2011). The Beaufort Sea coastline is characterized by the strongest retreat, with coastal erosion rates exceeding 1.1 m $year^{-1}$

on average (Lantuit et al., 2011). Rates have been observed to be even higher in regions of the Beaufort Sea coast exposed to northwestern winds and associated waves, leading to severe coastal changes (Barnhart et al., 2014a).

The coastal Arctic Ocean accounts for 80% of the total primary productivity in the Arctic Ocean (Hill and Cota, 2005). As with lower latitudes, seagrasses, macroalgae, and benthic microalgae (BMA) are present, and these benthic primary producers can be dominant in coastal Arctic systems. BMA contribute approximately 40% of total Arctic benthic primary production, despite only being found in 10-14% of the Arctic Ocean (Glud et al., 2009; Karsten et al., 2012). In shallow water systems, such as coastal lagoons, benthic diatoms typically contribute 1.5x more to overall primary production (1.6×10^{7} Gt C yr^{-1}) than pelagic communities (Glud et al., 2002). This may be due to their access to nutrients within sediment porewater, with concentrations typically 5-10x higher than in the adjacent water column (Glud et al., 2009; Woelfel et al., 2010). In addition to autotrophic production, the diversity of microbial communities and heterotrophic production in coastal Arctic ecosystems significantly contributes to lagoon food web productivity (Galand, et al., 2008; Kellogg et al., 2019). Studies have shown that external organic carbon from terrestrial runoff supports and integrates into lagoon food webs in the Arctic (Kellogg et al., 2019; Thibodeau et al., 2017).

In fact, around one third of current Arctic Ocean primary production could be sustained by rivers and coastal erosion, with terrestrial nitrogen inputs playing a crucial role in supporting Arctic Ocean production (Terhaar et al., 2021). Although the coastal Arctic appears to remain productive despite these drastic seasonal changes in

environmental conditions, this ecosystem is now subject to new and accelerating changes in environmental forces due to climate change.

1.3 Climate change in the Arctic

The Arctic climate system is in a transitional state, marked by declining summer sea ice extent, altered ecosystem dynamics, shifts in circulation patterns, and potential tipping points. Arctic amplification, characterized by enhanced warming in the Arctic compared to the global average, is a phenomenon largely attributed to the loss of sea ice cover (Previdi et al., 2021; Serreze & Barry, 2011). However, other local feedback loops such as the release of greenhouse gases stored in permafrost (Schuur et al., 2022), atmosphere-ocean heat transport (Boeke et al., 2020), and increased poleward heat transport (Screen & Simmonds, 2013) have all contributed to recent patterns of warming.

This warming in turn is increasing river discharge from major Arctic rivers with noticeable “freshening” of the coastal Arctic (Fichot et al., 2013). Discharge from the four largest Arctic-draining rivers along the Eurasian coast has increased 7% from 1936-1999 (Peterson et al., 2002), and approximately 14% from 1980-2009 (Ahmed et al., 2020). This phenomenon is also occurring along the Beaufort Sea coast which has experienced a 40% increase in liquid freshwater content from the 1970’s to 2018 (Proshutinsky et al., 2015). In addition to increased discharge, permafrost thawing and thermokarst formation are leading to increased surface water-groundwater interactions on land and increased groundwater discharge (Walvoord & Striegl, 2007; Connolly et al. 2020).

In addition to increasing freshwater inputs, warming atmospheric and water temperatures are expanding the open water period of the coastal Arctic by approximately 1-2 days per year (Markus et al., 2009; Stroeve et al., 2014). However, regional dynamics

can drastically amplify this effect with the open water period increasing by 1.2 days per year from 1979-2012 to 12.8 days per year from 2000 to 2012 along the Beaufort Sea coast (Frey et al., 2015). Several studies have documented a doubling (7 to 13.5 m^{-1} y^{-1}, Jones et al., 2009) or even tripling (6.8 to 19 m^{-1} y^{-}1, Barnhart et al., 2014) of rates of coastal erosion in response to the increasing open water period (Barnhart et al., 2014b; Günther et al., 2013; Overeem et al., 2011). With increased thaw of permafrost and more physical degradation through winds, waves, and storms, the coastal Arctic is releasing large amounts of previously frozen organic carbon, as well as greenhouse gases (Knoblauch et al., 2018; Voigt et al., 2017). In response to the thinning and diminishing ice cover and increasing light, pelagic and sea ice algal production rates are increasing (Lannuzel et al., 2020). In fact, Arctic Ocean primary production has increased ~30% over the past several decades (Arrigo et al., 2008; Arrigo & Van Dijken, 2015).

1.4 Beaufort Lagoon Ecosystems Long-Term Ecological Research program

To address both spatial and seasonal dynamics of coastal Arctic ecosystem metabolism, the research herein was conducted as part of the Beaufort Lagoon Ecosystems Long-Term Ecological Research (BLE-LTER) program. The National Science Foundation (NSF)-funded LTER program was first established in 1980 to address ecological questions that cannot be resolved with short-term observations or experiments. Today, there are 28 LTER sites that represent a wide spectrum of ecosystems including, but not limited to, temperate forests, coral reefs, deserts, and salt marshes. Although diverse in ecosystem type, LTER programs are centered around five consistent themes: 1) primary production, 2) population studies, 3) organic matter cycling, 4) inorganic nutrient cycling, and 5) environmental disturbance.

The BLE-LTER (ble.lternet.edu) was funded by NSF in 2017 and renewed again in 2023. The BLE-LTER operates out of three villages or “nodes,” Utqiaġvik (BRW), Prudhoe Bay (SCC), and Barter Island (BTI), representing spatial variability along the western, central, and eastern Beaufort Sea coast, respectively. Each region differs in the relative contribution it receives from terrestrial inputs, circulation, oceanic exchange, and sea ice dynamics. In the western node, the BLE-LTER samples Elson Lagoon, which divides into Elson Lagoon West and Elson Lagoon East for sampling purposes. The central node includes Simpson Lagoon and Stefansson Sound, and the eastern node includes Kaktovik Lagoon and Jago Lagoon. To study temporal and seasonal dynamics, samples were collected three times during each year (2018-2022) to capture key phases of the hydrological cycle: Ice Cover (April), Break Up (June), and Open Water (August).

1.5 Inupiat communities and subsistence hunting

Coastal lagoons play a significant role in supporting the Iñupiat community in Arctic Alaska, particularly in subsistence hunting practices. These ecosystems are crucial habitats for various fish species, including whitefishes, cods, and flounders, which are essential for subsistence harvesting (Dunton et al., 2012; Fraley et al., 2021). Subsistence hunting practices among the Iñupiat are not solely driven by economic considerations but are deeply rooted in a profound respect for the environment and a sustainable approach to resource utilization (Anthony, 2013). Traditional knowledge holders, such as hunters from Alaska Native communities, have observed and documented the impacts of climate change while hunting, particularly of marine mammals (Anthony, 2013; Huntington et al., 2020). Despite external pressures and challenges, subsistence hunting remains a vital aspect of Iñupiat life, serving not only as a means of acquiring food but also as a central

component of cultural identity reflected in the traditions of hunting, communal distribution of meat, and performance of cultural ceremonies (Sakakibara, 2017). This holistic perspective on subsistence hunting reflects a deep understanding of the interconnectedness of ecosystems and the need for responsible stewardship of natural resources to maintain ecological balance and biodiversity.

1.6 Dissertation objectives

Although foundational knowledge of coastal Arctic systems has been gradually learned over the past few decades, process studies that quantify nutrient transformations, ecosystem metabolism, and exchanges across the sediment-water interface in the shallow coastal nearshore are sorely needed to develop a complete understanding of complex biogeochemical cycling within the Arctic coast. Understanding seasonal patterns and biological mechanisms of coastal Arctic ecosystem metabolism and nutrient cycling is urgently needed to form a baseline for predictions about the changing Arctic system.

To that end, in this dissertation, I assessed carbon and nitrogen cycling in coastal Arctic lagoons as part of the BLE-LTER program. In *Chapter 2, Abiotic and biotic controls on nutrient cycling in coastal Arctic lagoons,* I present water column nutrient data collected seasonally from several Beaufort Sea lagoons and estimate physical vs. biological controls on their concentrations. In *Chapter 3, Physical drivers of sediment distribution and organic matter oxidation in coastal Arctic lagoons,* I focused on sediment characteristics and the physical conditions that drive organic matter distribution and aerobic oxidation. In *Chapter 4, Seasonal cycles of benthic productivity and N cycling in Beaufort Sea lagoons,* I present results from seasonal batch sediment incubations to quantify benthic metabolism and nutrient cycling. processes.

1.7 References

Ahmed, R., Prowse, T., Dibike, Y., Bonsal, B., & O'Neil, H. (2020). Recent Trends in Freshwater Influx to the Arctic Ocean from Four Major Arctic-Draining Rivers. Water, 12(4), 1189. https://doi.org/10.3390/w12041189

Ahmerkamp, S., Marchant, H. K., Peng, C., Probandt, D., Littmann, S., Kuypers, M. M. M., & Holtappels, M. (2020). The effect of sediment grain properties and porewater flow on microbial abundance and respiration in permeable sediments. Scientific Reports, 10(1), 3573. https://doi.org/10.1038/s41598-020-60557-7

Anthony, R. (2013). Animistic pragmatism and native ways of knowing: Adaptive strategies for overcoming the struggle for food in the sub-Arctic. International Journal of Circumpolar Health, 72(1), 21224. https://doi.org/10.3402/ijch.v72i0.21224

Arrigo, K. R., & Van Dijken, G. L. (2015). Continued increases in Arctic Ocean primary production. Progress in Oceanography, 136, 60–70. https://doi.org/10.1016/j.pocean.2015.05.002

Arrigo, K. R., Van Dijken, G., & Pabi, S. (2008). Impact of a shrinking Arctic ice cover on marine primary production. Geophysical Research Letters, 35(19), 2008GL035028. https://doi.org/10.1029/2008GL035028

Barnhart, K. R., Overeem, I., & Anderson, R. S. (2014a). Modeling erosion of ice-rich permafrost bluffs along the Alaskan Beaufort Sea coast. The Cryosphere, 8, 1777–1799. https://doi.org/10.5194/tc-8-1777-2014

Barnhart, K. R., Overeem, I., & Anderson, R. S. (2014b). The effect of changing sea ice on the physical vulnerability of Arctic coasts. The Cryosphere, 8(5), 1777–1799. https://doi.org/10.5194/tc-8-1777-2014

Bianchi, T. S., Cui, X., Blair, N. E., Burdige, D. J., Eglinton, T. I., & Galy, V. (2018). Centers of organic carbon burial and oxidation at the land-ocean interface. Organic Geochemistry, 115, 138–155. https://doi.org/10.1016/j.orggeochem.2017.09.008

Boeke, R., Taylor, P., & Sejas, S. (2020). On the Nature of the Arctic's Positive Lapse-Rate Feedback. Geophysical Research Letters. https://doi.org/10.1029/2020GL091109

Bonsell, C., & Dunton, K. H. (2018). Long-term patterns of benthic irradiance and kelp production in the central Beaufort sea reveal implications of warming for Arctic inner shelves. Progress in Oceanography, 162, 160–170. https://doi.org/10.1016/j.pocean.2018.02.016

Brevik, E. C., & Homburg, J. A. (2004). A 5000 year record of carbon sequestration from a coastal lagoon and wetland complex, Southern California, USA. CATENA, 57(3), 221–232. https://doi.org/10.1016/j.catena.2003.12.001

Bristol, E. M., Connolly, C. T., Lorenson, T. D., Richmond, B. M., Ilgen, A. G., Choens, R. C., Bull, D. L., Kanevskiy, M., Iwahana, G., Jones, B. M., & McClelland, J. W. (2021). Geochemistry of Coastal Permafrost and Erosion-Driven Organic Matter Fluxes to the Beaufort Sea Near Drew Point, Alaska. Frontiers in Earth Science, 8, 598933. https://doi.org/10.3389/feart.2020.598933

Canuel, E. A., Cammer, S. S., McIntosh, H. A., & Pondell, C. R. (2012). Climate Change Impacts on the Organic Carbon Cycle at the Land-Ocean Interface. Annual

Review of Earth and Planetary Sciences, 40(1), 685–711. https://doi.org/10.1146/annurev-earth-042711-105511
Canuel, E. A., & Hardison, A. K. (2016). Sources, Ages, and Alteration of Organic Matter in Estuaries. Annual Review of Marine Science, 8(1), 409–434. https://doi.org/10.1146/annurev-marine-122414-034058
Carrasco, A. R., Ferreira, Ó., & Roelvink, D. (2016). Coastal lagoons and rising sea level: A review. Earth-Science Reviews, 154, 356–368. https://doi.org/10.1016/j.earscirev.2015.11.007
Carvalho, K. S., & Wang, S. (2020). Sea surface temperature variability in the Arctic Ocean and its marginal seas in a changing climate: Patterns and mechanisms. Global and Planetary Change, 193, 103265. https://doi.org/10.1016/j.gloplacha.2020.103265
Cervantes-Duarte, R., Prego, R., López-López, S., Aguirre-Bahena, F., & Ospina-Alvarez, N. (2013). Annual patterns of nutrients and chlorophyll in a subtropical coastal lagoon under the upwelling influence (SW of Baja-California Peninsula). Estuarine, Coastal and Shelf Science, 120, 54–63. https://doi.org/10.1016/j.ecss.2013.01.020
Chen, A. (2020). The 400-year natural history of a tropical coastal mangrove-fringed lagoon: What can we learn? Global Change Biology, 26, 3185–3187.
Cornwell, J. C., Glibert, P. M., & Owens, M. S. (2014). Nutrient Fluxes from Sediments in the San Francisco Bay Delta. Estuaries and Coasts, 37(5), 1120–1133. https://doi.org/10.1007/s12237-013-9755-4
Damashek, J., & Francis, C. A. (2018). Microbial Nitrogen Cycling in Estuaries: From Genes to Ecosystem Processes. Estuaries and Coasts, 41(3), 626–660. https://doi.org/10.1007/s12237-017-0306-2
Devol, A. H. (2015). Denitrification, Anammox, and N2 Production in Marine Sediments. Annual Review of Marine Science, 7(1), 403–423. https://doi.org/10.1146/annurev-marine-010213-135040
Dittmar, T., & Kattner, G. (2003). The biogeochemistry of the river and shelf ecosystem of the Arctic Ocean: A review. Marine Chemistry, 83(3–4), 103–120. https://doi.org/10.1016/S0304-4203(03)00105-1
Duarte, C. M. (2017). Reviews and syntheses: Hidden forests, the role of vegetated coastal habitats in the ocean carbon budget. Biogeosciences, 14(2), 301–310. https://doi.org/10.5194/bg-14-301-2017
Duarte, C. M., Middelburg, J. J., & Caraco, N. (2005). Major role of marine vegetation on the oceanic carbon cycle.
Dunton, K. H., Schonberg, S. V., & Cooper, L. W. (2012). Food Web Structure of the Alaskan Nearshore Shelf and Estuarine Lagoons of the Beaufort Sea. Estuaries and Coasts, 35(2), 416–435. https://doi.org/10.1007/s12237-012-9475-1
Dunton, K. H., Weingartner, T., & Carmack, E. C. (2006). The nearshore western Beaufort Sea ecosystem: Circulation and importance of terrestrial carbon in arctic coastal food webs. Progress in Oceanography, 71(2–4), 362–378. https://doi.org/10.1016/j.pocean.2006.09.011
Fertig, B., O'Neil, J. M., Beckert, K. A., Cain, C. J., Needham, D. M., Carruthers, T. J. B., & Dennison, W. C. (2013). Elucidating terrestrial nutrient sources to a coastal

lagoon, Chincoteague Bay, Maryland, USA. Estuarine, Coastal and Shelf Science, 116, 1–10. https://doi.org/10.1016/j.ecss.2012.08.013
Fichot, C. G., Kaiser, K., Hooker, S. B., Amon, R. M. W., Babin, M., Bélanger, S., Walker, S. A., & Benner, R. (2013). Pan-Arctic distributions of continental runoff in the Arctic Ocean. Scientific Reports, 3(1), 1053. https://doi.org/10.1038/srep01053
Fraley, K. M., Robards, M. D., Rogers, M. C., Vollenweider, J., Smith, B., Whiting, A., & Jones, T. (2021). Freshwater input and ocean connectivity affect habitats and trophic ecology of fishes in Arctic coastal lagoons. Polar Biology, 44(7), 1401–1414. https://doi.org/10.1007/s00300-021-02895-4
Frey, K. E., Moore, G. W. K., Cooper, L. W., & Grebmeier, J. M. (2015). Divergent patterns of recent sea ice cover across the Bering, Chukchi, and Beaufort seas of the Pacific Arctic Region. Progress in Oceanography, 136, 32–49. https://doi.org/10.1016/j.pocean.2015.05.009
Galand, P. E., Lovejoy, C., Pouliot, Jé., Garneau, M.-ève, & Vincent, W. F. (2008). Microbial community diversity and heterotrophic production in a coastal Arctic ecosystem: A stamukhi lake and its source waters. Limnology and Oceanography, 53(2), 813–823. https://doi.org/10.4319/lo.2008.53.2.0813
Gattuso, J.-P., Gentili, B., Duarte, C. M., Kleypas, J. A., Middelburg, J. J., & Antoine, D. (2006). Light availability in the coastal ocean: Impact on the distribution of benthic photosynthetic organisms and their contribution to primary production. Biogeosciences, 3(4), 489–513. https://doi.org/10.5194/bg-3-489-2006
Giblin, A., Tobias, C., Song, B., Weston, N., Banta, G., & Rivera-Monroy, V. (2013). The Importance of Dissimilatory Nitrate Reduction to Ammonium (DNRA) in the Nitrogen Cycle of Coastal Ecosystems. Oceanography, 26(3), 124–131. https://doi.org/10.5670/oceanog.2013.54
Glud, R. N., Woelfel, J., Karsten, U., Kühl, M., & Rysgaard, S. (2009). Benthic microalgal production in the Arctic: Applied methods and status of the current database. Botm, 52(6), 559–571. https://doi.org/10.1515/BOT.2009.074
Günther, F., Overduin, P. P., Baranskaya, A., Opel, T., & Grigoriev, M. N. (2013). Observing Muostakh Island disappear: Erosion of a ground-ice-rich coast in response to summer warming and sea ice reduction on the East Siberian shelf. https://doi.org/10.5194/tcd-7-4101-2013
Hanna, A. J., Shanahan, T. M., Allison, M. A., Bianchi, T. S., & Schreiner, K. M. (2018). A multi-proxy investigation of late-Holocene temperature change and climate-driven fluctuations in sediment sourcing: Simpson Lagoon, Alaska. The Holocene, 28(6), 984–997. https://doi.org/10.1177/0959683617752845
Hardison, A. K., Algar, C. K., Giblin, A. E., & Rich, J. J. (2015). Influence of organic carbon and nitrate loading on partitioning between dissimilatory nitrate reduction to ammonium (DNRA) and N2 production. Geochimica et Cosmochimica Acta, 164, 146–160. https://doi.org/10.1016/j.gca.2015.04.049
Hardison, A. K., Anderson, I. C., Canuel, E. A., Tobias, C. R., & Veuger, B. (2011). Carbon and nitrogen dynamics in shallow photic systems: Interactions between macroalgae, microalgae, and bacteria. Limnology and Oceanography, 56(4), 1489–1503. https://doi.org/10.4319/lo.2011.56.4.1489

Harris, C. M., McClelland, J. W., Connelly, T. L., Crump, B. C., & Dunton, K. H. (2017). Salinity and Temperature Regimes in Eastern Alaskan Beaufort Sea Lagoons in Relation to Source Water Contributions. Estuaries and Coasts, 40(1), 50–62. https://doi.org/10.1007/s12237-016-0123-z

Holmes, R. M., McClelland, J. W., Peterson, B. J., Tank, S. E., Bulygina, E., Eglinton, T. I., Gordeev, V. V., Gurtovaya, T. Y., Raymond, P. A., Repeta, D. J., Staples, R., Striegl, R. G., Zhulidov, A. V., & Zimov, S. A. (2012). Seasonal and Annual Fluxes of Nutrients and Organic Matter from Large Rivers to the Arctic Ocean and Surrounding Seas. Estuaries and Coasts, 35(2), 369–382. https://doi.org/10.1007/s12237-011-9386-6

Huntington, H. P., Danielson, S. L., Wiese, F. K., Baker, M., Boveng, P., Citta, J. J., De Robertis, A., Dickson, D. M. S., Farley, E., George, J. C., Iken, K., Kimmel, D. G., Kuletz, K., Ladd, C., Levine, R., Quakenbush, L., Stabeno, P., Stafford, K. M., Stockwell, D., & Wilson, C. (2020). Evidence suggests potential transformation of the Pacific Arctic ecosystem is underway. Nature Climate Change, 10(4), 342–348. https://doi.org/10.1038/s41558-020-0695-2

Johnston, S. E., Carey, J. C., Kellerman, A., Podgorski, D., Jonathan, G., & Robert, S. (2019). Controls on Riverine Dissolved Organic Matter Composition Across an Arctic-Boreal Latitudinal Gradient. Geophysical Research Letters, 47. https://doi.org/10.1029/2019GL085897

Jones, B. M., Arp, C. D., Jorgenson, M. T., Hinkel, K. M., Schmutz, J. A., & Flint, P. L. (2009). Increase in the rate and uniformity of coastline erosion in Arctic Alaska. Geophysical Research Letters, 36(3), 2008GL036205. https://doi.org/10.1029/2008GL036205

Karsten, U., Schlie, C., Woelfel, J., & Becker, B. (2012). Benthic Diatoms in Arctic Seas – Ecological Functions and Adaptations. Polarforschung, 81(2), 77–84.

Kellogg, C. T. E., McClelland, J. W., Dunton, K. H., & Crump, B. C. (2019). Strong Seasonality in Arctic Estuarine Microbial Food Webs. Frontiers in Microbiology, 10, 2628. https://doi.org/10.3389/fmicb.2019.02628

Kjerfve, B. (1994). Chapter 1 Coastal Lagoons. In Elsevier Oceanography Series (Vol. 60, pp. 1–8). Elsevier. https://doi.org/10.1016/S0422-9894(08)70006-0

Kjerfve, B., & Magill, K. E. (1989). Geographic and hydrodynamic characteristics of shallow coastal lagoons. Marine Geology, 88(3–4), 187–199. https://doi.org/10.1016/0025-3227(89)90097-2

Knoblauch, C., Beer, C., Liebner, S., Grigoriev, M. N., & Pfeiffer, E.-M. (2018). Methane production as key to the greenhouse gas budget of thawing permafrost. Nature Climate Change, 8(4), 309–312. https://doi.org/10.1038/s41558-018-0095-z

Lannuzel, D., Tedesco, L., Van Leeuwe, M., Campbell, K., Flores, H., Delille, B., Miller, L., Stefels, J., Assmy, P., Bowman, J., Brown, K., Castellani, G., Chierici, M., Crabeck, O., Damm, E., Else, B., Fransson, A., Fripiat, F., Geilfus, N.-X., … Wongpan, P. (2020). The future of Arctic sea-ice biogeochemistry and ice-associated ecosystems. Nature Climate Change, 10(11), 983–992. https://doi.org/10.1038/s41558-020-00940-4

Lantuit, H., Atkinson, D., Paul Overduin, P., Grigoriev, M., Rachold, V., Grosse, G., & Hubberten, H.-W. (2011). Coastal erosion dynamics on the permafrost-dominated

Bykovsky Peninsula, north Siberia, 1951–2006. Polar Research, 30(1), 7341. https://doi.org/10.3402/polar.v30i0.7341
Lawson, S. E., Wiberg, P. L., McGlathery, K. J., & Fugate, D. C. (2007). Wind-driven sediment suspension controls light availability in a shallow coastal lagoon. Estuaries and Coasts, 30(1), 102–112. https://doi.org/10.1007/BF02782971
Lawson, S., McGlathery, K., & Wiberg, P. (2012). Enhancement of sediment suspension and nutrient flux by benthic macrophytes at low biomass. Marine Ecology Progress Series, 448, 259–270. https://doi.org/10.3354/meps09579
Leote, C., Ibánhez, J. S., & Rocha, C. (2008). Submarine Groundwater Discharge as a nitrogen source to the Ria Formosa studied with seepage meters. Biogeochemistry, 88(2), 185–194. https://doi.org/10.1007/s10533-008-9204-9
Liefer, J. D., MacIntyre, H. L., Su, N., & Burnett, W. C. (2014). Seasonal Alternation Between Groundwater Discharge and Benthic Coupling as Nutrient Sources in a Shallow Coastal Lagoon. Estuaries and Coasts, 37(4), 925–940. https://doi.org/10.1007/s12237-013-9739-4
Ligorini, V., Crayol, E., Huneau, F., Garel, E., Malet, N., Garrido, M., Simon, L., Cecchi, P., & Pasqualini, V. (2023). Small Mediterranean coastal Lagoons Under Threat: Hydro-ecological Disturbances and Local Anthropogenic Pressures (Size Matters). Estuaries and Coasts, 46(8), 2220–2243. https://doi.org/10.1007/s12237-023-01182-1
Mahoney, A. R., Eicken, H., Gaylord, A. G., & Gens, R. (2014). Landfast sea ice extent in the Chukchi and Beaufort Seas: The annual cycle and decadal variability. Cold Regions Science and Technology, 103, 41–56. https://doi.org/10.1016/j.coldregions.2014.03.003
Malta, E.-J., Stigter, T. Y., Pacheco, A., Dill, A. C., Tavares, D., & Santos, R. (2017). Effects of External Nutrient Sources and Extreme Weather Events on the Nutrient Budget of a Southern European Coastal Lagoon. Estuaries and Coasts, 40(2), 419–436. https://doi.org/10.1007/s12237-016-0150-9
Manini, E., Fiordelmondo, C., Gambi, C., Pusceddu, A., & Danovaro, R. (2003). Benthic microbial loop functioning in coastal lagoons: A comparative approach. Oceanologica Acta, 26(1), 27–38. https://doi.org/10.1016/S0399-1784(02)01227-6
Markus, T., Stroeve, J. C., & Miller, J. (2009). Recent changes in Arctic sea ice melt onset, freezeup, and melt season length. Journal of Geophysical Research: Oceans, 114(C12), 2009JC005436. https://doi.org/10.1029/2009JC005436
Martins, M., De Los Santos, C. B., Masqué, P., Carrasco, A. R., Veiga-Pires, C., & Santos, R. (2022). Carbon and Nitrogen Stocks and Burial Rates in Intertidal Vegetated Habitats of a Mesotidal Coastal Lagoon. Ecosystems, 25(2), 372–386. https://doi.org/10.1007/s10021-021-00660-6
McClelland, J. W., Holmes, R. M., Dunton, K. H., & Macdonald, R. W. (2012). The Arctic Ocean Estuary. Estuaries and Coasts, 35(2), 353–368. https://doi.org/10.1007/s12237-010-9357-3
McClelland, J. W., Townsend-Small, A., Holmes, R. M., Pan, F., Stieglitz, M., Khosh, M., & Peterson, B. J. (2014). River export of nutrients and organic matter from the North Slope of Alaska to the Beaufort Sea. Water Resources Research, 50(2), 1823–1839. https://doi.org/10.1002/2013WR014722

McGlathery, K., Sundbäck, K., & Anderson, I. (2007). Eutrophication in shallow coastal bays and lagoons: The role of plants in the coastal filter. Marine Ecology Progress Series, 348, 1–18. https://doi.org/10.3354/meps07132

Mcleod, E., Chmura, G. L., Bouillon, S., Salm, R., Björk, M., Duarte, C. M., Lovelock, C. E., Schlesinger, W. H., & Silliman, B. R. (2011). A blueprint for blue carbon: Toward an improved understanding of the role of vegetated coastal habitats in sequestering CO 2. Frontiers in Ecology and the Environment, 9(10), 552–560. https://doi.org/10.1890/110004

Middelburg, J. J., Soetaert, K., Boschker, H. T. S., & Heip, C. H. R. (2004). Burial of nutrient in coastal sediments: the role of primary producers. Estuarine Nutrient Cycling: The Influence of Primary Producers. Aquatic Ecology Book Series, vol 2. Springer, Dordrecht.

Miller, C. A., Bonsell, C., McTigue, N. D., & Kelley, A. L. (2021). The seasonal phases of an Arctic lagoon reveal the discontinuities of pH variability and CO_2 flux at the air–sea interface. Biogeosciences, 18(3), 1203–1221. https://doi.org/10.5194/bg-18-1203-2021

Nichols, M. M. (1989). Sediment accumulation rates and relative sea-level rise in lagoons. Marine Geology, 88(3–4), 201–219. https://doi.org/10.1016/0025-3227(89)90098-4

Nowicki, B. L., & Nixon, S. W. (1985). Benthic Nutrient Remineralization in a Coastal Lagoon Ecosystem. Estuaries, 8(2), 182. https://doi.org/10.2307/1352199

Overduin, P. P., Strzelecki, M. C., Grigoriev, M. N., Couture, N., Lantuit, H., St-Hilaire-Gravel, D., Günther, F., & Wetterich, S. (2014). Coastal changes in the Arctic. Geological Society, London, Special Publications, 388(1), 103–129. https://doi.org/10.1144/SP388.13

Overeem, I., Anderson, R. S., Wobus, C. W., Clow, G. D., Urban, F. E., & Matell, N. (2011). Sea ice loss enhances wave action at the Arctic coast. Geophysical Research Letters, 38(17) https://doi.org/10.1029/2011GL048681

Pérez-Ruzafa, A., Marcos, C., Pérez-Ruzafa, I. M., & Pérez-Marcos, M. (2011). Coastal lagoons: “Transitional ecosystems” between transitional and coastal waters. Journal of Coastal Conservation, 15(3), 369–392. https://doi.org/10.1007/s11852-010-0095-2

Pérez-Ruzafa, A., Morkune, R., Marcos, C., Pérez-Ruzafa, I. M., & Razinkovas-Baziukas, A. (2020). Can an oligotrophic coastal lagoon support high biological productivity? Sources and pathways of primary production. Marine Environmental Research, 153, 104824. https://doi.org/10.1016/j.marenvres.2019.104824

Peterson, B. J., Holmes, R. M., McClelland, J. W., Vörösmarty, C. J., Lammers, R. B., Shiklomanov, A. I., Shiklomanov, I. A., & Rahmstorf, S. (2002). Increasing River Discharge to the Arctic Ocean. Science, New Series, 298(5601), 2171–2173.

Petti, M., Bosa, S., & Pascolo, S. (2018). Lagoon Sediment Dynamics: A Coupled Model to Study a Medium-Term Silting of Tidal Channels. Water, 10(5), 569. https://doi.org/10.3390/w10050569

Previdi, M., Smith, K. L., & Polvani, L. M. (2021). Arctic amplification of climate change: A review of underlying mechanisms. Environmental Research Letters, 16(9), 093003. https://doi.org/10.1088/1748-9326/ac1c29

Proshutinsky, A., Dukhovskoy, D., Timmermans, M.-L., Krishfield, R., & Bamber, J. L. (2015). Arctic circulation regimes. Philosophical Transactions of the Royal Society A: Mathematical, Physical and Engineering Sciences, 373(2052), 20140160. https://doi.org/10.1098/rsta.2014.0160

Pusceddu, A., Grémare, A., Escoubeyrou, K., Amouroux, J. M., Fiordelmondo, C., & Danovaro, R. (2005). Impact of natural (storm) and anthropogenic (trawling) sediment resuspension on particulate organic matter in coastal environments. Continental Shelf Research, 25(19–20), 2506–2520. https://doi.org/10.1016/j.csr.2005.08.012

Renaud, P. E., Morata, N., Carroll, M. L., Denisenko, S. G., & Reigstad, M. (2008). Pelagic–benthic coupling in the western Barents Sea: Processes and time scales. Deep Sea Research Part II: Topical Studies in Oceanography, 55(20–21), 2372–2380. https://doi.org/10.1016/j.dsr2.2008.05.017

Rodellas, V., Stieglitz, T. C., Andrisoa, A., Cook, P. G., Raimbault, P., Tamborski, J. J., Van Beek, P., & Radakovitch, O. (2018). Groundwater-driven nutrient inputs to coastal lagoons: The relevance of lagoon water recirculation as a conveyor of dissolved nutrients. Science of The Total Environment, 642, 764–780. https://doi.org/10.1016/j.scitotenv.2018.06.095

Sakakibara, C. (2017). People of the Whales: Climate Change and Cultural Resilience Among Iñupiat of Arctic Alaska. Geographical Review, 107(1), 159–184. https://doi.org/10.1111/j.1931-0846.2016.12219.x

Schuur, E. A. G., Abbott, B. W., Commane, R., Ernakovich, J., Euskirchen, E., Hugelius, G., Grosse, G., Jones, M., Koven, C., Leshyk, V., Lawrence, D., Loranty, M. M., Mauritz, M., Olefeldt, D., Natali, S., Rodenhizer, H., Salmon, V., Schädel, C., Strauss, J., … Turetsky, M. (2022). Permafrost and Climate Change: Carbon Cycle Feedbacks From the Warming Arctic. Annual Review of Environment and Resources, 47(1), 343–371. https://doi.org/10.1146/annurev-environ-012220-011847

Screen, J., & Simmonds, I. (2013). Exploring links between Arctic amplification and mid-latitude weather. Geophysical Research Letters, 40, 959–964. https://doi.org/10.1002/GRL.50174, 2013

Serreze, M. C., & Barry, R. G. (2011). Processes and impacts of Arctic amplification: A research synthesis. Global and Planetary Change, 77(1–2), 85–96. https://doi.org/10.1016/j.gloplacha.2011.03.004

Snedden, G., Cable, J., & Kjerfve, B. (2023). Estuarine Geomorphology, Circulation, and Mixing. In Wiley (Ed) *Estuarine Ecology* (3rd edition, pp 16-35). Wiley. https://pubs.usgs.gov/publiucation/70238656.

Stierle, A. P., & Eicken, H. (2002). Sediment Inclusions in Alaskan Coastal Sea Ice: Spatial Distribution, Interannual Variability, and Entrainment Requirements. Arctic, Antarctic, and Alpine Research, 34(4), 465–476. https://doi.org/10.1080/15230430.2002.12003518

Stroeve, J. C., Markus, T., Boisvert, L., Miller, J., & Barrett, A. (2014). Changes in Arctic melt season and implications for sea ice loss. Geophysical Research Letters, 41(4), 1216–1225. https://doi.org/10.1002/2013GL058951

Terhaar, J., Lauerwald, R., Regnier, P., Gruber, N., & Bopp, L. (2021). Around one third of current Arctic Ocean primary production sustained by rivers and coastal

erosion. Nature Communications, 12(1), 169. https://doi.org/10.1038/s41467-020-20470-z

Thamdrup, B., & Dalsgaard, T. (2002). Production of N2 through Anaerobic Ammonium Oxidation Coupled to Nitrate Reduction in Marine Sediments. Applied and Environmental Microbiology, 68(3), 1312–1318. https://doi.org/10.1128/AEM.68.3.1312-1318.2002

Thibodeau, B., Bauch, D., & Voss, M. (2017). Nitrogen dynamic in Eurasian coastal Arctic ecosystem: Insight from nitrogen isotope. Global Biogeochemical Cycles, 31(5), 836–849. https://doi.org/10.1002/2016GB005593

Van De Velde, S. J., Hylén, A., Eriksson, M., James, R. K., Kononets, M. Y., Robertson, E. K., & Hall, P. O. J. (2023). Exceptionally high respiration rates in the reactive surface layer of sediments underlying oxygen-deficient bottom waters. Proceedings of the Royal Society A: Mathematical, Physical and Engineering Sciences, 479(2275), 20230189. https://doi.org/10.1098/rspa.2023.0189

Voigt, C., Marushchak, M. E., Lamprecht, R. E., Jackowicz-Korczyński, M., Lindgren, A., Mastepanov, M., Granlund, L., Christensen, T. R., Tahvanainen, T., Martikainen, P. J., & Biasi, C. (2017). Increased nitrous oxide emissions from Arctic peatlands after permafrost thaw. Proceedings of the National Academy of Sciences, 114(24), 6238–6243. https://doi.org/10.1073/pnas.1702902114

Vybernaite-Lubiene, I., Zilius, M., Giordani, G., Petkuviene, J., Vaiciute, D., Bukaveckas, P. A., & Bartoli, M. (2017). Effect of algal blooms on retention of N, Si and P in Europe's largest coastal lagoon. Estuarine, Coastal and Shelf Science, 194, 217–228. https://doi.org/10.1016/j.ecss.2017.06.020

Walvoord, M. A., & Striegl, R. G. (2007). Increased groundwater to stream discharge from permafrost thawing in the Yukon River basin: Potential impacts on lateral export of carbon and nitrogen. Geophysical Research Letters, 34(12), 2007GL030216. https://doi.org/10.1029/2007GL030216

Wang, X., & Du, J. (2016). Submarine groundwater discharge into typical tropical lagoons: A case study in eastern Hainan Island, China. Geochemistry, Geophysics, Geosystems, 17(11), 4366–4382. https://doi.org/10.1002/2016GC006502

Webster, I. T., Ford, P. W., & Hodgson, B. (2002). Microphytobenthos contribution to nutrient-phytoplankton dynamics in a shallow coastal lagoon. Estuaries, 25(4), 540–551. https://doi.org/10.1007/BF02804889

Weingartner, T. J., Danielson, S. L., Potter, R. A., Trefry, J. H., Mahoney, A., Savoie, M., Irvine, C., & Sousa, L. (2017). Circulation and water properties in the landfast ice zone of the Alaskan Beaufort Sea. Continental Shelf Research, 148, 185–198. https://doi.org/10.1016/j.csr.2017.09.001

Wilson, A. M., Huettel, M., & Klein, S. (2008). Grain size and depositional environment as predictors of permeability in coastal marine sands. Estuarine, Coastal and Shelf Science, 80(1), 193–199. https://doi.org/10.1016/j.ecss.2008.06.011

Woelfel, J., Schumann, R., Peine, F., Flohr, A., Kruss, A., Tegowski, J., Blondel, P., Wiencke, C., & Karsten, U. (2010). Microphytobenthos of Arctic Kongsfjorden (Svalbard, Norway): Biomass and potential primary production along the shore line. Polar Biology, 33(9), 1239–1253. https://doi.org/10.1007/s00300-010-0813-0

Yamamoto-Kawai, M., Tanaka, N., & Pivovarov, S. (2005). Freshwater and brine behaviors in the Arctic Ocean deduced from historical data of $\delta^{18}O$ and alkalinity (1929–2002 A.D.). Journal of Geophysical Research, 110. https://doi.org/doi:10.1029/2004JC002793

Chapter 2: Abiotic and biotic controls on nutrient cycling in coastal Arctic lagoons

2.1 Abstract

Approximately half of the Alaska Beaufort Sea coast is outlined by barrier island chains that enclose shallow lagoons. These lagoons are subject to extreme seasonal variations in ice cover, temperature, and salinity, yet are home to a diverse and productive food web. Situated at the interface between the Arctic tundra and Beaufort Sea, these systems receive and process resources from both land and sea as well as internal loading from the sediments. Due to extreme seasonal variations in environmental conditions, the input, transformation, and fate of these nutrients are likely dynamic, but not well studied. To quantify the impacts of these seasonal forces on lagoon nutrients, we measured biogeochemical and physical parameters (temperature, salinity, pH, dissolved oxygen, inorganic nutrients, H_2O-$\delta^{18}O$) of six lagoons along the Beaufort Sea coast. Samples were collected seasonally, during “Ice Cover” (April), “Break Up” (June), and “Open Water” (August) periods from 2018-2022. Using a three-end-member mixing model and conservative mixing line, we quantified the abiotic and biotic effects associated with seasonal changes in inorganic nutrients and, by proxy, net ecosystem productivity. We observed seasonal changes in nutrient concentrations likely driven by abiotic processes like brine exclusion during Ice Cover and freshwater dilution during Break Up. We also observed net accumulation of nutrients during Ice Cover likely due to biotic remineralization and uptake during Break Up and Open Water by microalgae. As the Open Water period lengthens, along with rapidly increasing Arctic temperatures, there will

likely be cascading impacts on winter nutrient accumulation, spring primary productivity, and summer organic matter cycling.

2.2 Introduction

Arctic-wide average surface air temperatures have increased at nearly four times the rate of global mean temperatures since 1979 (Rantanen et al., 2022) — a phenomenon known as Arctic amplification (Serreze & Barry, 2011). Records of atmospheric temperature in the Alaskan Arctic indicate warming by 3.1 ^{o}C during the cold season and 1.8 ^{o}C during the warm season since the 1970s (Box et al., 2019). Mechanisms for Arctic amplification include reduced summer albedo due to sea-ice and snow-cover loss, decreased cloud cover in summer and increased cloud cover in winter, and marine heat maintained later into the fall (Pithan & Mauritsen, 2014). In 2011–2020, annual average Arctic sea ice area reached its lowest level since 1850, and late summer Arctic sea ice area was smaller than at any time in at least the past 1000 years (IPCC 2021). In addition to decreasing sea ice area, ice formation in the Beaufort Sea, a marginal sea of the Arctic Ocean, is occurring progressively later. For example, in 2012, sea ice formed five weeks later compared to the 1981-2010 average (Bonsell & Dunton, 2018).

Arctic coastal environments are recognized as one of the most vulnerable ecosystems on Earth in response to global warming (Lantuit et al., 2011), and represent an interface between marine, cryospheric, and terrestrial systems. In many areas, sustained warming is changing coastal ice conditions (Mahoney et al., 2014) and increasing coastal erosion (Jones et al., 2009). Several studies have highlighted how changes in sea ice extent can impact barrier island geomorphology and terrestrial processes (Bhatt et al., 2014; Tweedie et al., 2016). For example, permafrost thaw controls coastal erosion and, therefore, watershed export to the coastal ocean (Mahoney

et al., 2014; Aguirre eta al, 2011). Due to these significant changes in freshwater inflow, coastal erosion, ice cover, and exchange with the ocean, Alaska's northern Arctic coastal ecosystem has been primed to undergo dramatic changes in ecosystem function.

Nearly half of the Alaskan Beaufort Sea coast is bordered by an irregular and discontinuous chain of barrier islands that enclose numerous shallow (<7 m) lagoons and sounds (Fig. 2.1.). Situated north of the Arctic Circle, the lagoons are subject to extreme seasonal variations in physical conditions (i.e., hydrology, temperature). Beginning in October, seasonal ice cover extends for eight months of the year, with shallow areas of the lagoons developing ice down to the sediment surface (Mahoney et al., 2014). Annually, water column temperatures range from -2 to 14 ^{o}C, and salinities vary drastically, from fresh (0) to hypersaline (45) (Harris et al., 2017; Miller et al., 2021). This large salinity range is a result of both the spring freshet introducing large volumes of freshwater into the lagoons during the "Break Up" period, and the hypersaline conditions under ice due to salt extrusion during sea ice formation (McCart, 1977). The spring freshet, driven by snowmelt, delivers over half of the annual freshwater river discharge from Alaska's North Slope during a two-week period from late May to mid-June (McClelland et al., 2014). While freshwater inflow facilitates ice break up, the lagoons remain largely ice-covered until late June. This lag between the spring freshet and ice break up promotes retention and biological processing of river derived inputs, including vast quantities of DOM, POM, and dissolved inorganic nutrients (McClelland et al., 2012). During the Open Water period (August through September), the absence of sea ice exposes the lagoons to wind energy, which promotes wind-driven sediment resuspension and coastal erosion (Stierle and Eicken, 2002; Zimmerman et al. 2022).

The Arctic coast is characterized by extreme seasonal variability of terrestrial discharge, particularly with peak inflows during the freshet. Seasonal changes in water discharge alone can account for much of the variation in nutrient and organic matter inputs from rivers to the coastal ocean (Holmes et al., 2012). During the freshet, Arctic rivers discharge >90% of their annual nutrient and organic matter export and most of their water inputs (Dittmar & Kattner, 2003; Holmes et al., 2012; McClelland et al., 2014). In fact, although the Arctic Ocean accounts for ~1% of the total ocean volume, it receives >10% of global river discharge, resulting in a disproportionate impact of river inputs on the biogeochemistry of Arctic coastal waters (Dittmar & Kattner, 2003; McClelland et al., 2012). Compared globally, Arctic rivers have some of the highest concentrations of organic matter, with annual exports on par with the Amazon River. In contrast, inorganic nutrients in the Arctic are among the lowest worldwide, except for silicate in some rivers (Dittmar & Kattner, 2003).

In addition to large seasonal differences in river discharge, the presence of the Brooks Range mountains in eastern Alaska establishes a gradient in watershed slope, with primarily flat coastal plains in the west and steeper terrain toward the east. This elevation gradient impacts the stable oxygen isotope value of water (H_2O-$\delta^{18}O$) in precipitation. As clouds approach the mountains, they are forced up and, in this process, cool and precipitate out heavier $\delta^{18}O$ isotopes. As these clouds continue to rise and repeat this process, isotopically depleted atmospheric moisture is eventually forced to precipitate at higher elevations resulting in snow with very depleted H_2O-$\delta^{18}O$ values (Retamal et al., 2008). In this way, the hydrology of these lagoons can vary significantly both spatially and temporally.

Coastal arctic lagoons are subject to extreme seasonal changes in environmental forces including large fluctuations in temperature, hydrology, nutrient supply, and light availability on an annual scale. Regardless, at the boundary between the land and sea, these lagoons play a vital role in coastal carbon (C) and nitrogen (N) cycling within the coastal Arctic Ocean accounting for 80% of the total primary productivity in the Arctic Ocean (Retamal et al. 2007). Furthermore, a recent study in these coastal Arctic systems found that microbial communities mediate terrestrial inputs to the Arctic Ocean, determining the form and quantity of resources that sustain over one-third of Arctic Ocean production (Terhaar et al., 2021). Increasing rates of primary production in the Arctic Ocean are projected due to increasing terrestrial nutrient inputs alongside sea ice retreat (Arrigo & Van Dijken, 2015; Lewis et al., 2020); however, the nearshore ecosystem processes controlling these inputs are systematically understudied (Fritz et al., 2017), particularly outside the open water period. To quantify the potential impacts of these environmental forces on net ecosystem productivity, we measured chemical (i.e., inorganic nutrients, H_2O-$\delta^{18}O$) and physical (i.e., salinity, temperature) parameters of water column samples across five lagoons during three seasons. Using a three end-member mixing model and conservative mixing line, we quantified spatial and temporal patterns of water source contribution and deviations from the mixing line to determine potential abiotic and biotic processes that drive seasonal changes in inorganic nutrients and by proxy ecosystem productivity.

2.3 Methods

2.3.1 Study area

The study area is composed of several lagoons and sounds along the Alaskan coast of the Beaufort Sea in alignment with the Beaufort Lagoon Ecosystems Long-Term Ecological Research (BLE-LTER) program (ble.lternet.edu). The BLE-LTER program operates out of three nodes, spanning ~100 km of the Alaskan coastline: Utqiaġvik (formerly Barrow; BRW), Prudhoe Bay (SCC), and Barter Island (BTI) to represent the western, central, and eastern Beaufort Sea coast, respectively (Fig. 2.1). Each region differs in the relative contribution it receives from terrestrial inputs, oceanic exchange, and sea ice dynamics. Each node has two lagoons. In the western node, the BLE-LTER samples Elson Lagoon, which divides into Elson Lagoon West and Elson Lagoon East for sampling purposes. The central node includes Simpson Lagoon and Stefansson Sound, and the eastern node includes Kaktovik Lagoon and Jago Lagoon.

The western node is located near the village of Utqiaġvik. Elson Lagoon is the largest lagoon among the BLE-LTER lagoons (Fig. 2.1, Table 2.1). It is delineated by a 25 km chain of barrier islands and receives freshwater inputs from several streams (Lewellen, 1972). Exchange between Elson Lagoon and the Beaufort Sea occurs through several and sometimes intermittent channels within the barrier island chain (Okkonen, 2008). The central node is in the oil field region of Prudhoe Bay and contains Simpson Lagoon and Stefansson Sound. In Simpson Lagoon, the Kuparuk River discharges directly into Gwyder Bay at the eastern end while the largest river on the North Slope of Alaska, the Colville River, discharges at the western end (Craig et al., 1984). Stefansson Sound which is located roughly 50 km east of Simpson Lagoon primarily receives inputs

from the Sagavanirktok River and has the smallest barrier islands and is the least enclosed coastal system among the BLE-LTER lagoons. The eastern node is located near the village of Kaktovik. Kaktovik Lagoon receives freshwater input from streams, runoff, and groundwater seepage and is only connected to the Beaufort Sea by two shallow narrow entrances. In contrast, Jago Lagoon is fed by the Jago River and has broader deeper channels connected toward the Beaufort Sea (Alkire & Trefry, 2006).

2.3.2 Sampling scheme

Samples were collected as part of the BLE-LTER core sampling program. To examine seasonal variations, water samples were collected three times during each year to capture key phases of the hydrological cycle: Ice Cover, Break Up, and Open Water. To determine spatial variation, samples were collected at the six BLE-LTER lagoons, with each lagoon containing one shallow (<1 m water depth) and one deep (3-5 m water depth) station, with the latter having surface (10-30 cm below surface) and bottom (10-30 cm above sediment) water column sampling depths (Fig. 2.1). During Ice Cover, samples were not collected at shallow stations due to the presence of landfast ice but were sampled at the deep stations, where surface measurements were made 10-30 cm below the bottom of the sea ice. Although sampling efforts are ongoing, this study presents data from 2018 to 2022 across all lagoons with some exceptions due to the COVID-19 pandemic. During 2020, all field excursions were canceled and resumed in April 2021 for BRW and SCC and in August 2021 for BTI. In addition to the lagoon water, surrounding water bodies such as the Beaufort Sea and major rivers were sampled during Break Up and Open Water to characterize terrestrial and marine end-members (Table 2.1).

2.3.3 Water column collection

Water column samples were collected with a peristaltic pump equipped with Masterflex C-flex tubing at the surface (10-30 cm below surface) and at depth (10-30 cm above sediment). Water samples were collected in 1 L sample-rinsed high-density polyethylene (HDPE) bottles in the field and kept at near-ambient temperatures in a cooler during transport to the field lab. In the lab, samples for dissolved inorganic nutrient analysis (n=1) were passed through a 0.45 µm high-capacity polyethersulfone (PES) capsule filter and frozen in either 2 oz Whirl-Pak bags or sample-rinsed 60 mL HDPE bottles at -20 ^{o}C until analysis. Unfiltered water (30 mL) for H_2O-$\delta^{18}O$ (n=1) measurement was transferred to a sample-rinsed HDPE bottle without headspace, sealed with electrical tape, and stored at room temperature until analysis.

2.3.4 Inorganic nutrient (NH_4^+, NO_3^-, PO_4^{3-}, DSi) analysis

Water column dissolved inorganic nutrients analyzed included ammonium (NH_4^+), nitrate + nitrite (NO_3^-), orthophosphate (PO_4^{3-}), and dissolved silica (DSi; Beaufort Lagoon Ecosystems LTER, Core Program, 2023). Nitrate and nitrite concentrations were measured separately during 2018 and 2019, however nitrite values were consistently below the detection limit (< 0.05 µmol N L^{-1}), so hereafter NO_3^- will refer to combined nitrate and nitrite. Nutrients were measured at the Core Facilities Laboratory at the University of Texas Marine Science Institute (UTMSI) on a continuous flow-analyzer Lachat Quick Chem 8500 (2018-2020) and in the Hardison Lab at the Virginia Institute of Marine Science (VIMS) on a multi-channel FIAlyzer-1000 from Fluidic Intelligently Automated (FIA, 2021-2022). Duplicates were analyzed on both instruments to test precision and continuity during the transition from UTMSI to VIMS. The technical

specifications and sample precision for each instrument and parameter are listed in Supplemental Table 2.1.

2.3.4 Oxygen isotope composition of water (H_2O-$\delta^{18}O$) analysis

Oxygen stable isotope composition of water samples was measured at the Core Facilities Laboratory at UTMSI (Beaufort Lagoon Ecosystems LTER, Core Program, 2023). In the lab, 200 µL of sample was placed into a 13 mL glass vial (Exetainer) and capped with a rubber septum. The vials were then equilibrated with a mixed helium and carbon dioxide (0.3% CO_2) gas for 5 days at room temperature. After equilibration, the headspace CO_2 was analyzed for oxygen-isotope composition ($\delta^{18}O$, mass 46/44) using a GasBench II device (Thermo Fisher Scientific) coupled to a Thermo Fisher Scientific Delta V stable isotope ratio mass spectrometer (IRMS). All δ values were reported relative to VSMOW (Coplen, 1996) using a two-point calibration standard (VSMOW2: 0 ‰, SLAP2: -55.50 ‰) from the International Atomic Energy Agency.

2.3.5 Averaging and statistical analyses

All statistical analyses were run in R (version 4.3.0). Average concentrations of nutrients across season and node were calculated including both surface and bottom water samples with each discrete sample treated as an independent data point . The effects of season and spatial gradients on biogeochemical parameters (NH_4^+, NO_3^-, PO_4^{3-}, DSi, H_2O-$\delta^{18}O$) were assessed with a two-way analysis of variance (ANOVA). Prior to analysis, the dataset was tested for normal distribution using a Shapiro Wilk test, and any necessary transformations were applied. The ANOVA included fixed effects of seasons (Ice Cover, Break Up, Open Water) and geographic node (BRW, SCC, BTI). When the

ANOVA indicated a significant effect (a = 0.05), a post-hoc Tukey multiple comparisons of means was used, with 95% confidence intervals.

To identify environmental drivers of measured parameters, multivariate regression models were used to find relationships between observed concentrations and environmental parameters. *A priori*, we selected several environmental parameters that are known factors to influence or reflect ambient nutrient concentrations. Nutrient concentrations were treated as dependent variables while water temperature, salinity, DO and H_2O-$\delta^{18}O$ were treated as independent variables. Four metrics were used to determine the influence of each independent variable on explaining data variability: 1) slope: the estimated regression coefficient of the linear regression, 2) p-value: the statistical significance of the regression coefficient, 3) lmg: the relative importance of each parameter in explaining data variability (R package: relaimpo; Groemping, 2006), and 4) variance inflation factor (VIF): a measure of collinearity among independent variables (R package: car; Fox & Weisberg, 2019), where values between 1 and 4 were considered an acceptable level of correlation between independent variables.

2.3.6 Mixing model calculations

To quantify the proportion of lagoon water that originated from sea ice melt (SIM), runoff/riverine inputs (i.e., meteoric water; MW), and ocean water (i.e., polar mixed layer; PML), a three-end-member mixing model was applied using salinity and H_2O-$\delta^{18}O$ as conservative tracers. For freshwater end-member H_2O-$\delta^{18}O$ and inorganic nutrient values, we used BLE-LTER samples collected from lagoon freshwater sources (Table 2.2): BRW (Avak Creek, Mayoeak River, No Name River), SCC (Kuparuk River, Putuligayuk River, Sagavanirktok River) and BTI (Jago River), averaged across seasons from 2018 to 2022

(Table 2.2). However, the BLE-LTER lacks representative samples of sea ice melt and Arctic Ocean water end-members, so literature values from the Beaufort Sea coast were applied. SIM and PML salinity and H_2O-$\delta^{18}O$ were sourced from Alkire and Trefry (2006), where seawater and ice cores were collected along a transect from the shore to the Beaufort Sea in late May in Stefansson Sound, our central node. PML values represented shelf waters off the Beaufort coast as defined by MacDonald et al. (1987). Sea ice nutrient concentrations from Utqiagvik (Manes & Gradinger, 2009) were used for SIM, and samples collected in the Beaufort Sea (0.4 km outside of Gwyder Bay) by the BLE-LTER (July 2019) were used to represent PML nutrients (Table 2.2).

To calculate the fractional contribution (f) of each water source (SIM, MW, PML), Equations 2.1 through 2.3 were solved simultaneously, following Harris et al. (2017). Values for end-member parameters (salinity, H_2O-$\delta^{18}O$, inorganic nutrients) are listed in Table 2.2.

Equation 2.1. $f_{SIM} + f_{MW} + f_{PML} = 1.$

The observed salinity ($S_{observed}$) was equal to the sum of the salinity of each end-member (Table 2.2) multiplied by its fractional contribution, (Equation 2.2):

Equation 2.2. $(S_{SIM} \times f_{SIM}) + (S_{MW} \times f_{MW}) + (S_{PML} \times f_{PML}) = S_{observed}$.

The observed $\delta^{18}O$ ($\delta^{18}O_{observed}$) of the water sample was equal to the sum of the measured $\delta^{18}O$ of each end-member (Table 2.2) multiplied by its fractional contribution (Equation 2.3):

Equation 2.3. $(\delta^{18}O_{SIM} \times f_{SIM}) + (\delta^{18}O_{MW} \times f_{MW}) + (\delta^{18}O_{PML} \times f_{PML}) = \delta^{18}O_{observed}$.

Fractional contributions of end-members (from Equation 2.1) were multiplied by end-member nutrient concentrations (Table 2.2) to calculate a conservative mixing line that represents the potential nutrient concentrations resulting from only the physical mixing of the three water sources, following Equation 2.4:

Equation 2.4. $(N_{SIM} \times f_{SIM}) + (N_{MW} \times f_{MW}) + (N_{PML} \times f_{PML}) = N_{Conserved}$.

The term $N_{Conserved}$ quantifies the hypothetical nutrient concentration due to abiotic physical mixing without the influence of biotic activity. The disparity ("ΔN") between the $N_{Conserved}$ and the observed values ($N_{observed}$) from the lagoons represents either net production or net consumption of the nutrient through biological processes (Equation 2.5):

Equation 2.5. $N_{Observed} - N_{Conserved}$ = *"ΔN" = Net nutrient production or Net nutrient consumption*.

A positive ΔN indicates net nutrient production, while a negative ΔN indicates net nutrient consumption. These calculations were performed for NH_4^+, PO_4^{3-}, NO_3^- , and DSi. These estimates rely on salinity and H_2O-$\delta^{18}O$ as conservative elements in the lagoons and assume homogenous mixing of the water sources.

2.4 Results

2.4.1 Environmental Parameters

Lagoon water temperatures were coldest during Ice Cover (-1.9 ± 0.1 °C) and increased gradually during Break Up (2.9 ± 0.6 °C) and Open Water (7.3 ± 0.3 °C; Table 2.3; Fig. 2.2). Salinities were lowest during Break Up (6.6 ± 1.5) and increased substantially during Open Water (24.4 ± 0.6) before becoming hypersaline during Ice

Cover (36.2 ± 0.8; Table 2.3; Fig. 2.2). Salinity reached levels as high as 56 during Ice Cover and as low as 0.2 during Break Up (Fig. 2.2). Temperature and salinity were most variable during Break Up, with the largest coefficient of variation (CV, temperature: 19.5%, salinity: 22.9%) compared to Ice Cover (temperature: 4.4%, salinity: 2.2%) and Open Water (temperature: 3.5%, salinity: 2.4%). DO concentrations were lowest during Ice Cover (10.5 ± 0.4 mg L^{-1}), peaked during Break Up (12.8 ± 0.2 mg L^{-1}) and returned closer to Ice Cover levels during the Open Water period (10.9 ± 0.2 mg L^{-1}; Table 2.3). The lowest average pH (7.6 ± 0.1) corresponded with the lowest average DO during Ice Cover before increasing slightly during Break Up (7.9 ± 0.2) and staying constant through the Open Water period (7.9 ± 0.02; Table 2.3).

2.4.2 Water Column Nutrients and H_2O-$\delta^{18}O$

All inorganic nutrients changed significantly across seasons, with the highest concentrations during Ice Cover and the lowest during Open Water (Table 2.4, Fig. 2.3). Averaged across all nodes, NH_4^+ levels were highest during Ice Cover (2.1 ± 0.5 µmol N L^{-1}), decreased by half during break-up (1.0 ± 0.4 µmol N L^{-1}), and decreased again by half during Open Water (0.5 ± 0.1 µmol N L^{-1}; Fig. 2.3a, Table 2.4). Averaged across all nodes, NO_3^- levels were also highest during Ice Cover (5.2 ± 0.4 µmol N L^{-1}), decreased by ~70% during break-up (1.5 ± 0.3 µmol N L^{-1}), then decreased another ~70% by Open Water (0.5 ± 0.1 µmol N L^{-1}; Fig. 2.3b, Table 2.4). During Ice Cover, average NO_3^- levels were more than twice as high as NH_4^+ levels, while values were comparable during the Break Up and Open Water periods. Averaged across all nodes, PO_4^{3-} levels were high during Ice Cover (2.2 ± 0.3 µmol P L^{-1}), then decreased ~60% during Break Up (0.9 ± 0.3

μmol P L^{-1}) and remained low for Open Water (0.6 ± 0.1 μmol P L^{-1}; Fig. 2.3c, Table 2.4). Like PO_4^{3-}, averaged across all nodes, DSi levels were high during Ice Cover (18.8 ± 1.1 μmol SiO_2 L^{-1}), then decreased substantially during Break Up (7.2 ± 1.0 μmol SiO_2 L^{-1}) and remained low for Open Water (6.6 ± 0.7 μmol SiO_2 L^{-1}; Fig. 2.3d, Table 2.4). Relative to the lowest concentrations observed during Open Water, all nutrients were significantly higher (3-10x) during the Ice Cover period, with maximum values of NH_4^+: 20.2 μmol N L^{-1}, NO_3^-: 12.8 μmol N L^{-1}, PO_4^{3-}: 6.4 μmol P L^{-1}, and DSi: 60.3 μmol SiO_2 L^{-1} (Fig. 2.3).

Nutrient concentration variations between nodes were less consistent than between seasons, with a few notable Season-by-Node interactions (Supplementary Table 2.2, Fig. 2.3). NH_4^+ exhibited no significant spatial variability between nodes during any season (Fig. 2.3a, Supplementary Table 2.2,). In contrast, NO_3^- significantly varied across nodes during Ice Cover, with higher concentrations in BRW (5.9 ± 0.5 μmol N L^{-1}) and SCC (5.6 ± 0.6 μmol N L^{-1}) than BTI (3.0 ± 0.4 μmol N L^{-1}) (Table 2.4, Supplementary Table 2.2, Fig. 2.3b). Likewise, PO_4^{3-} varied between nodes, with lower concentrations at SCC (0.5 ± 0.3 μmol P L^{-1}) compared to BTI (2.0 ± 0.9 μmol P L^{-1}) during Break Up (Fig. 2.3c, Table 2.2). DSi concentrations varied between nodes during Break Up and Open Water periods, with generally higher concentrations in SCC (Fig. 2.3d, Table 2.4, Supplementary Table 2.2,).

Seasonal patterns in water column H_2O-$\delta^{18}O$ values were consistent across all nodes, where mean values were most enriched during Ice Cover (-3.5 ± 0.1 ‰) and most depleted during Break Up (-11.6 ± 0.9 ‰; Fig. 2.4a, Table 2.5). Lagoon H_2O-$\delta^{18}O$ also displayed notable Season-by-Node interactions, with SCC having more depleted values compared to BRW and BTI during Break Up (-15.1 ± 1.3 ‰) and Open Water (-8.0 ± 0.8

‰), but there were no node differences during Ice Cover (Table 2.5). Samples collected during Break Up and Open Water from riverine end-member inputs exhibited a longitudinal gradient across the nodes, with the most enriched riverine H_2O-$\delta^{18}O$ values at the westernmost node, BRW (-11.5 ± 0.4 ‰), intermediate levels at the central node, SCC (-18.8 ± 0.5 ‰), and the most depleted values at the easternmost node, BTI (-21.4 ‰; Fig. 2.4b, Table 2.5).

2.4.3 Multiple Linear Regression

Multiple linear regression analysis demonstrated that water temperature was the most consistently highly correlated environmental parameter to the concentrations of all four inorganic nutrients (Supplementary Table 2.3). DO displayed the strongest correlation with NH_4^+ concentration with DO (46%) and temperature (45%) together explaining over 90% of the variance. For NO_3^-, temperature explained the majority (70%) of variance, while salinity (17%) and H_2O-$\delta^{18}O$ (8%) were smaller, but still significant factors. For PO_4^{3-}, temperature (56%) and H_2O-$\delta^{18}O$ (26%) explained 82% of the total variance, while DSi was most correlated with temperature (42%), then H_2O-$\delta^{18}O$ (31%), and salinity (21%).

2.4.4 Water Source Contribution and Conservative Mixing Line

The three-end-member mixing model displayed consistent seasonal trends in the contribution of sea ice melt (SIM), meteoric waters (MW), and polar mixed layer (PML) waters (Fig. 2.5, Table 2.6, Supplementary Table 2.5). During Ice Cover, SIM contributions averaged across nodes were negative (-16 ± 3%; Fig. 2.5a). Average MW contribution

was negligible (1 ± 3%), and the contribution of PML waters exceeded 100% (115 ± 4 %; Fig. 2.5a, Table 2.6). During Break Up, MW contributions increased dramatically (64 ± 5%), with the SIM and PML representing the next major contributors (19 ± 6% and 17 ± 5%; Fig. 2.5b), respectively. During the Open Water period, PML waters were the dominant source (76 ± 2%), with secondary inputs from MW (19 ± 2 %) and some remnants of SIM (5 ± 1%; Fig. 2.5c). In addition to the seasonal trends, the ANOVA and post-hoc Tukey tests revealed some spatial variability for the source water contributions during Break Up, with higher MW inputs into SCC (76 ± 8 %) compared to BTI (35 ± 12%; Table 2.6, Supplementary Table 2.5).

All inorganic nutrients exhibited seasonal deviations from the conservative mixing line, indicating net nutrient production and consumption across seasons (Table 2.7; Fig. 2.6, Supplementary Table 2.7). Averaged across all nodes, NH_4^+ exhibited net production (i.e., a positive value) during Ice Cover (1.2 ± 0.4 μmol N L^{-1}) and net consumption (i.e., a negative value) during Open Water (-0.4 ± 0.09 μmol N L^{-1}; Fig. 2.6a, Table 2.7). NO_3^- was also produced during Ice Cover (5.6 ± 0.4 μmol N L^{-1}) before shifting to net consumption during both Break Up (-0.7 ± 0.4 μmol N L^{-1}) and Open Water (-0.2 ± 0.1 μmol N L^{-1}, Fig. 2.6b). PO_4^{3-} was produced during all seasons but decreased in magnitude over time from Ice Cover (2.1 ± 0.3 μmol P L^{-1}) to Open Water (0.3 ± 0.1 μmol P L^{-1}, Fig. 2.6c). Like NO_3^-, DSi was produced during Ice Cover (13.4 ± 1.2 μmol SiO_2 L^{-1}) before shifting to consumption during both Break Up (-6.6 ± 1.0 μmol SiO_2 L^{-1}) and Open Water (-0.9 ± 0.3 μmol SiO_2 L^{-1}, Fig. 2.6d). Significant variability between nodes was not found for any of the nutrients; however, DSi exhibited some minor differences during Break Up,

with SCC (-11.2 ± 1.3 μmol SiO_2 L^{-1}) having higher net consumption compared to BRW (-3.1 ± 0.3 μmol SiO_2 L^{-1}; Table 2.7, Supplementary Table 2.6).

2.5 Discussion

2.5.1 Seasonal and spatial variability in environmental parameters

Environmental conditions fluctuated dramatically between seasons. As anticipated, lagoon water temperatures were coldest during Ice Cover (-1.9 ± 0.1 °C), which corresponded with hypersaline waters (36.2 ± 0.8), reaching as high as 56. Hypersaline waters under sea ice are a known phenomenon related to brine exclusion during the formation of sea ice during winter. This brine is a source of salts to underlying waters, resulting in hypersaline conditions in shallow areas (<3 m) including lagoons (Yamamoto-Kawai et al., 2005). As daylight duration increased and atmospheric temperatures warmed in late spring during Break Up (May - June), snowmelt fueled numerous streams and rivers that drained into the Beaufort Sea (Rawlins et al., 2019), providing a flush of freshwater that lowered lagoon salinities (6.6 ± 1.5). During Open Water (July - September), storms and wind-driven upwelling are thought to enhance water exchange, causing more saline water from the Beaufort Sea to intrude into the lagoons (Schell et al., 1984; McCart, 1977). Open Water lagoon temperatures were highest (7.3 ± 0.3 °C), and salinities were more reflective of a typical estuarine system (24.4 ± 0.6). This dramatic seasonal pattern has been previously demonstrated in Arctic lagoons along the Beaufort Sea coast (e.g., Connolly et al., 2021; Craig et al., 1984; Harris et al., 2017; McClelland et al., 2012) and pan-Arctic lagoon habitats more broadly (Dugan & Lamoureux, 2011; Gattuso et al., 2023; Herzog et al., 2019).

This seasonal pattern was also reflected in the lagoon water column H_2O-$\delta^{18}O$ content. High freshwater inputs during Break Up coincided with the most depleted H_2O-$\delta^{18}O$ levels in the lagoons (-11.6 ± 0.9 ‰). The river H_2O-$\delta^{18}O$ values were significantly depleted (-15.4 ± 0.8 ‰) relative to the PML end-member (-3.5 ‰). Most Arctic rivers tend to be depleted in H_2O-$\delta^{18}O$ because the snow stored over the winter months, which then melts, is also characterized by very depleted H_2O-$\delta^{18}O$ values (Harris et al., 2017). Polar precipitation can be particularly depleted relative to marine waters due to Rayleigh distillation where, as water vapor moves poleward, isotopically heavier rain is dropped, resulting in lighter source water vapor at higher latitudes (Lachniet et al., 2016).

In addition to the poleward gradient, our rivers exhibited a longitudinal gradient across the nodes. The westernmost node (BRW) was most enriched (-11.5 ± 0.4 ‰), followed by the central node (SCC; -18.8 ± 0.5 ‰), with the easternmost node (BTI) being the most depleted (-21.4 ‰). This longitudinal gradient may be explained by the topography of the North Slope, which drains into the Beaufort Sea. The watershed in BRW is primarily lowland flat, Arctic coastal plains, while the watersheds at SCC and BTI also include the Arctic foothills and the Brooks Range mountains (Lachniet et al., 2016; Rawlins et al., 2019). With increasing elevation, the H_2O-$\delta^{18}O$ of precipitation decreases due to the altitude effect, where isotopically depleted atmospheric moisture is forced to rain out at higher elevations (Lachniet et al., 2016). Thus, precipitation in the node with the highest average watershed elevation (BTI) is more depleted in H_2O-$\delta^{18}O$ relative to the node with the lowest watershed elevation (BRW; Lachniet et al., 2016).

Transitioning to the Open Water period, the lagoon water column was ~5 ‰ more enriched in H_2O-$\delta^{18}O$ than during Break Up, likely driven by increased inputs and

exchange with the Beaufort Sea (Alkire & Trefry, 2006). This was anticipated, as marine waters from the Beaufort Sea shelf entering the lagoons are more enriched (-3.5 ‰), reflected in the PML end-member value (Alkire & Trefry, 2006).

We observed a seasonal enrichment of H_2O-$\delta^{18}O$ from Open Water (-6.1 ± 0.4 ‰) to Ice Cover (-3.5 ± 0.1 ‰). If the lagoon water during the Open Water period was used during sea ice formation in October, equilibrium isotope fractionation would dictate that the ice would be enriched in $\delta^{18}O$ while the remaining underlying water would be diluted by brine with depleted H_2O-$\delta^{18}O$ values. Since this is the opposite of what we observed, it is likely that water column H_2O-$\delta^{18}O$ values at the time of freeze up (October) were more enriched than what we measured in Open Water (August), suggesting that the lagoons became more marine by October (Johnson & Eicken, 2016; Mahoney et al., 2014).

DO and pH levels showed some seasonality but at a smaller magnitude compared with temperature, salinity, and H_2O-$\delta^{18}O$. DO concentrations were highest during Break Up, and pH was lowest during Ice Cover. These seasonal high and low periods in DO and pH respectively, could be explained by photosynthesis, which would produce DO, consume CO_2, and increase pH, and respiration, which would consume DO, produce CO_2, and decrease pH. This is in line with other ice covered systems that exhibit a wide range of pH annually (Miller et al., 2021; Muth et al., 2022), with decreases in pH due to respiration (Matson et al., 2014) and ice formation (DeGrandpre et al., 2019) during winter and increases with atmospheric exchange during the Open Water period (Sievers et al., 2015).

The environmental parameters measured in this study may be categorized into two groups: those with primarily abiotic, hydrologic control (i.e., temperature, salinity, H_2O-$\delta^{18}O$) and those also influenced by biotic factors (i.e., DO, pH). The multivariate regression model demonstrated that, of the parameters considered, temperature was the dominant driver of most inorganic nutrients (NO_3^-, PO_4^{3-}, DSi). Temperature is a well-known factor influencing metabolic activities such as photosynthesis and respiration (Barton et al., 2020), thus temperature is likely to influence nutrient concentrations (Marañón et al., 2018). However, in Arctic lagoons, temperature is also tightly linked to the large pulse of freshwater during the freshet. Thus, it is difficult to attribute changes in nutrient concentrations to either abiotic or biotic forces alone.

In addition to temperature, other environmental parameters had significant influences on nutrient concentrations and may provide insight into abiotic vs. biotic controls on each nutrient. For example, variability in NH_4^+ concentrations was best explained by DO levels, potentially reflecting the link between NH_4^+ production during respiration, and uptake during photosynthesis. For NO_3^- and DSi, salinity and H_2O-$\delta^{18}O$ explained a significant amount of the variability, which may indicate a stronger riverine influence for those nutrients compared to NH_4^+. Lastly, temperature and H_2O-$\delta^{18}O$ explained 82% of the total variance in PO_4^{3-} concentrations, suggesting primarily riverine influence as well. Although temperature largely drove seasonal variability of inorganic nutrients, hydrologic influence was also evident. To further tease apart the role of abiotic and biotic factors on nutrient variability, we present the results of the water source contribution and conservative mixing line below.

2.5.2 Ice Cover period

One of the strongest trends observed in the dataset was consistently high water column nutrient concentrations during Ice Cover. Elevated dissolved inorganic nutrients and dissolved organic carbon (DOC) concentrations have been observed previously in coastal Arctic under-ice waters during the winter (Connolly et al., 2021; Macdonald & Yu, 2006). Brine excluded during sea ice formation contains concentrated solute levels and can accumulate in surface waters, most noticeably for parameters with existing high ambient concentrations (Macdonald & Yu, 2006; Yamamoto-Kawai et al., 2005).

Our water source contribution model indicated negative inputs of SIM (-16 ± 3 %), negligible inputs of MW (1 ± 3 %), and dominance by PML contributions (115 ± 4 %) during Ice Cover. A negligible contribution from MW was expected during the winter, with temperatures well below 0 ^{o}C, when freshwater reservoirs on land and sea are frozen in place and provide no inputs into the lagoons. The negative SIM values potentially represent sea ice formation in the lagoons, where freshwater was removed from and brine accumulated in the lagoon water (Yamamoto-Kawai et al., 2005). Similarly, the “oversaturation” of PML waters possibly reflects dissolved nutrients and solutes condensed in the lagoon during sea ice formation due to freshwater removal and brine inputs.

High nutrient concentrations during Ice Cover can be partially attributed to physical controls on solutes such as brine exclusion (Fang et al., 2016; Giannelli et al., 2001; Vancoppenolle et al., 2013); however, high ΔN values for all inorganic nutrients (Fig 2.6) during Ice Cover also suggest significant biotic controls. Biotic net nutrient production (i.e., positive ΔN) was greatest during Ice Cover compared to the warmer seasons. In coastal

systems, inorganic nutrient fluxes from benthic remineralization have been shown to be a significant source of nutrients to the overlying water (Nixon, 1981). During the Ice Cover period, with little to no light under the ice, remineralization likely dominates, resulting in the accumulation of inorganic nutrients. Indeed, these lagoons have been observed with lower DO concentrations and microbially-derived OM during Ice Cover, reflecting a net heterotrophic environment during winter (Connelly et al., 2015). Benthic flux, while an important component of Arctic shelf ecosystems (Hardison et al. 2017), with high rates of benthic remineralization potentially contributing nutrients to pelagic primary production (Albert et al., 2021; Bourgeois et al., 2017; Sun et al., 2021).

By comparing ambient nutrient concentrations and the assumed biotic flux (ΔN) values, we identified the proportion of ambient Ice Cover nutrient concentrations represented by biotic processes. During the winter ~60% of ambient NH_4^+ was from biotic production, leaving ~40% resulting from abiotic processes (Table 2.8). In contrast, biotic production was the source of all (108%) ambient NO_3^-. This offset between NH_4^+ and NO_3^- production via biological activities was likely driven by the activity of ammonium-oxidizing archaea (AOA) during the Ice Cover period. AOA are chemoautotrophs that play an important role in nitrogen and carbon cycling of polar ecosystems (Tolar et al., 2016), including Beaufort Sea lagoon water, particularly during the winter (Baker et al., 2021). As light-independent, aerobic autotrophs that thrive in high NH_4^+ concentrations and low light conditions, these archaea use the oxidation of NH_4^+ into NO_3^- as a source of energy to fix inorganic carbon (Shiozaki et al., 2019). Through this microbially mediated transformation, we observed a greater accumulation of NO_3^- compared to NH_4^+ during Ice Cover, suggesting active nitrification.

Despite the significant biotic production of dissolved inorganic nitrogen (DIN = NH_4^+ + NO_3^-), the DIN:DIP ratio of nutrients produced during Ice Cover was ~3:1, which is significantly lower than Redfield (16:1; Redfield et al. 1963). One potential explanation for this deficit in DIN during Ice Cover is the removal of DIN from the lagoons via denitrification. Denitrification is a respiratory process where heterotrophic microbes use the stepwise reduction of NO_3^- to N_2 gas as the terminal electron receptor (Damashek & Francis, 2018). Denitrification occurs in suboxic and anoxic sediment and can be fueled by NO_3^- from the overlying water column (termed direct denitrification) or in conjunction with nitrification (coupled nitrification-denitrification; Anderson et al. 2013). In fact, several studies in the coastal Arctic have observed significant rates of denitrification (Canion et al., 2014; Chang & Devol, 2009; Rysgaard et al., 2004), with some showing rates exceeding sediment NH_4^+ flux resulting in net inorganic nitrogen removal by the sediment (Hardison et al., 2017; McTigue et al., 2016). When comparing DIN and DSi, we observed a similar deficit in the N:Si ratio (7.7:15) relative to expected Redfield ratio (16:15), further indicating DIN removal during Ice Cover.

2.5.3 Break Up period

Nutrient concentrations decreased notably transitioning from the Ice Cover period to the Break Up period. NH_4^+ levels decreased by 50%, NO_3^- levels decreased by ~70%, and PO_4^{3-} and DSi levels decreased ~60% compared to Ice Cover. This dramatic change in lagoon water nutrients has been previously observed in Arctic coastal systems and attributed to both dilution and biological uptake (Carey et al., 2020; Holmes et al., 2012; McClelland et al., 2012). With such significant volumes of freshwater draining into the

coast during Break Up, the majority of under ice lagoon waters are flushed out into the coastal sea and replaced with MW and SIM inputs (Harris et al., 2017; Kellogg et al., 2019).

In this study, lagoon waters during Break Up were primarily composed of MW (64 ± 5 %) and secondarily of SIM (19 ± 6 %), together exemplifying the dominant freshwater influence during this season. There were spatial differences in the balance between freshwater and marine influence during Break Up, with the greatest MW inputs in SCC compared to BRW and BTI. SCC is the node with the most MW influence, with several major rivers (Kuparuk, Colville, Sagavanirktok, and Atigun) draining into SIL and SSL. The Sagavanirktok, Kuparuk, and Colville rivers are the three largest rivers draining the North Slope of Alaska, with a combined export of ~23 km^3 annually (McClelland et al., 2014). As the dominant environmental influence during this period, MW inputs determine the delivery and ambient concentrations of organic matter and nutrients in these lagoons (McClelland et al., 2014).

Compared to systems globally, river waters entering the Arctic Ocean are rich in organic matter and depleted in inorganic nutrients (McClelland et al., 2012). Nitrate concentrations in Arctic rivers fall toward the lower end of global values (McClelland et al., 2014). In most Arctic rivers, including in this study (Table 2.2), NO_3^- strongly dominates the DIN pool (Carey et al., 2020; Holmes et al., 2012; McClelland et al., 2014). However, previous studies suggest that riverine dissolved organic nitrogen (DON) inputs may play a significantly larger role than DIN inputs in supplying coastal N demand (Connolly et al., 2020; Holmes et al., 2012; Tank et al., 2012). Phosphate concentrations in our rivers were low (Table 2.2) and typical of rivers in the region (Carey et al., 2020; Holmes et al., 2012).

In Arctic rivers DIN:DIP ratios are generally greater than Redfield, suggesting relative scarcity and lack of DIP in waters delivered to the coast (Carey et al., 2020; Holmes et al., 2012). This was exemplified in our lagoons, where DIN:DIP ratios increased from 8.7 ± 1.3 during Ice Cover to 89.5 ± 0.3 during Break Up, shifting from moderate nitrogen limitation to extreme phosphorus limitation. In contrast, riverine discharge is a well-known control on silica export globally (Carey et al., 2020). Arctic rivers supply ample DSi to support primary production, particularly by diatoms, which are a major constituent of Arctic Ocean phytoplankton (Holmes et al., 2012). In our lagoons, DIN and DSi concentrations were higher in the MW than the PML end-member, and PO_4^{3-} concentrations were lower in the MW relative to the PML. Thus, relative to inputs from the Beaufort Sea, our rivers acted to enrich the lagoons in DIN and DSi and dilute the lagoons with respect to PO_4^{3-}.

During Break Up, the replacement of hypersaline, nutrient-rich under ice waters by MW and SIM inputs resulted in a significant dilution of inorganic nutrients. However, in addition to dilution, net biotic nutrient consumption was observed for NO_3^- and DSi, further depleting ambient nutrient concentrations. With longer and more intense light availability and increased temperatures, NO_3^- and DSi uptake suggests diatom production and a shift toward net ecosystem autotrophy. In much of the Arctic Ocean, diatoms are the most abundant primary producers and account for >80% of high-latitude marine primary productivity (Carey et al., 2020). In addition to marine diatoms (*Chaetoceros* and *Thalassiosira*) found in the Beaufort and Chukchi Seas, diatoms typically associated with freshwater and sea-ice environments (e.g., *Melosira*, *Navicula*, *Carteria*, *Chlamydomonas*) were also found during Break Up in Arctic coastal lagoons (Kellogg et al., 2019).

Despite expectations for PO_4^{3-} consumption due to biotic uptake for photosynthesis as for NO_3^- and DSi, we observed net biotic PO_4^{3-} production during Break Up. This may be explained by the release of sorbed PO_4^{3-} from terrestrial organic matter entering the lagoons. As river-borne terrestrial organic matter flows into the coast and mixes with marine waters, the presence of sulfide may enhance the dissolution of Fe-P and form Fe-sulfide precipitates, resulting in the release of PO_4^{3-} (Jordan et al., 2008; Zhang & Huang, 2011). These lagoons receive large pulses of iron during the spring snow melt (Rember & Trefry, 2004). As ion exchange frees the bound PO_4^{3-}, sorbed P is thus transported from the watershed to coastal waters. This PO_4^{3-} release may contribute to the general shift from P limitation to N limitation along the fresh to marine continuum. In contrast to the other three nutrients, NH_4^+ exhibited neither net biotic production nor net biotic consumption. One possible explanation is rapid turnover rates for NH_4^+, where high rates of biotic NH_4^+ consumption by phytoplankton may be offset by similarly high rates of NH_4^+ released during remineralization (Baer et al., 2017; Bruesewitz et al., 2013, 2015; Fulweiler et al., 2010).

2.5.4 Open Water period

During the relatively warm Open Water period, nutrients reached their lowest values. Lagoon waters were primarily composed of the PML (76 ± 2 %) with secondary inputs from MW (19 ± 2 %). Without the physical barrier of sea ice during Open Water, marine exchange increases, and waters from the adjacent Beaufort Sea intrude into the lagoons (Harris et al., 2017; Hale, 1990). In addition to the PML and MW, we observed minor but significant remnants of SIM (5 ± 1 %) within the lagoons. However, because

SIM also exists in the coastal Beaufort Sea, it is difficult to isolate its origin as retained lagoon SIM or Beaufort Sea SIM advected into the lagoons with marine water intrusion (Harris et al., 2017).

In our conservative mixing model, the PML water end-member had lower NO_3^- and DSi concentrations but higher PO_4^{3-} concentration relative to the measured BLE riverine (MW) end-member. Previous work has shown that Arctic waters are generally N-limited during the summer (Ko et al., 2020; Krisch et al., 2020; Lewis et al., 2020), further supported by the DIN:DIP ratios observed in our lagoons during Open Water, 7.3 ± 3.2 which indicated a strong N deficit relative to Redfield (16:1). The lagoons exhibited no significant positive or negative Δ values for all nutrients during Open Water, suggesting a balance between remineralization and photosynthesis. However, external nutrients (DON) and sources (i.e., groundwater) not accounted for in the conservative mixing model may limit what we can infer about lagoon productivity, particularly during the Open Water period.

Phytoplankton in temperate systems have been observed comprising up to 10% of their N uptake in the form of DON (Mulholland et al., 1998), and uptake of urea has been shown to supply as much as 80% of N demand in coastal systems (Bronk et al., 2007). In the Laptev Sea near Siberia, ~70% of the DON was taken up and removed within shelf water (Letscher et al., 2013; Thibodeau et al., 2017). Similarly, primary production was heavily dependent on NH_4^+ and remineralization of organic substrates in Elson Lagoon (Baer et al., 2017). This pattern has also been supported by microbial data, which showed a shift from large diatoms during Break Up to a diverse array of small-celled microbes such as dinoflagellates and heterotrophic bacteria during Open Water

(Kellogg et al., 2019; Millette et al., 2024). This aligns with our results from Open Water which exhibited low ambient DIN concentrations and little to no deviation from the conservative mixing line, likely driven by simultaneous remineralization and uptake.

During the summer, surface waters can flow through deeper seasonally thawed active soil layers with leachable organic matter as supra-permafrost ground water (SPGW; Connolly et al., 2020). While small by volume compared to river discharge (1-5%), the high DOM concentrations result in 15-70% of total terrestrial DOC and DON export annually (Connolly et al., 2020). Unfortunately, the salinity and H_2O-$\delta^{18}O$ water source contribution model does not isolate the inputs of SPGW nor factor in the role of organic nutrient supply. However, the source of salinity and H_2O-$\delta^{18}O$ signals between terrestrial MW and SPGW are both local precipitation and therefore likely to be captured in the water source contribution model as just MW.

2.6 Conclusion

Arctic coastal environments are highly dynamic ecosystems at the intersection of cryospheric, terrestrial, and marine systems. Although covered in sea ice for most of the year, these coastal lagoons experience extreme seasonality, receiving significant terrestrial inputs during Break Up and becoming ice free during the summer. In response to these seasonal environmental forces, we observed seasonal changes in nutrient concentrations likely attributed to abiotic processes like brine exclusion during Ice Cover and freshwater flushing during Break Up. We also observed net biotic nutrient production during Ice Cover, likely due to remineralization, as well as net biotic nutrient uptake during Break Up, likely by diatoms. During the Open Water period, nutrient concentrations were

the lowest potentially reflecting a microbial shift from autotrophs during Break Up to mixo- and heterotrophs in response to limited inorganic nutrients and high dissolved organic nutrient availability.

As the Arctic rapidly warms, these coastal lagoons will experience significant ecosystem state changes in the coming decades from both the land and sea. Warming is decreasing sea ice extent during the summer across the Arctic, expanding the duration of the Open Water period (Bonsell & Dunton, 2018). Changes in the timing and the magnitude of freshwater and marine inputs are likely to impact both hydrologic and biological processes in these lagoons. Studies across the Arctic have observed increases in nutrient delivery (Le Fouest et al., 2013; Terhaar et al., 2021), temperature, and dissolved inorganic carbon (Ardyna & Arrigo, 2020), all linked to enhanced phytoplankton production. Specifically on the North coast of Alaska, studies indicate increasing inputs from land are providing more resources to support lagoon food webs and coastal primary productivity (Connolly et al., 2020; Harris et al., 2017; McClelland et al., 2014).

Based on the current expansion rates of the Open Water period in the Beaufort Sea (Frey et al., 2015; Markus et al., 2009; Stroeve et al., 2014), in 20 years we can expect the Open Water period to increase by approximately three weeks. This will result in a corresponding contraction of the Ice Cover period with no significant changes to the duration of Break Up (Bonsell & Dunton, 2021). Decreasing Ice Cover duration will likely diminish the amount of inorganic nutrient accumulation in the water column during the winter. In turn, it is possible that limited accumulation of nutrients will result in less supply for primary producers initially during Break Up. Furthermore, although net nutrient uptake was highest during Break Up potentially indicating net autotrophy, because the duration

of Break Up is likely to remain constant, future changes may not facilitate a longer net nutrient uptake or net autotrophic season. In contrast, the Open Water period displays a net balance between biotic consumption and production possibly reflecting a microbial shift from diatoms to mixotrophs and heterotrophs. As this summer period of intense organic matter cycling continues to lengthen, it is likely to impact the quantity and quality of organic matter within these lagoons. As these lagoons are subject to drastic environmental fluctuations and ongoing climate change, it is critical to understand the biogeochemical processes and linkages among these distinct, sequential, seasonal periods.

2.7 References

Albert, S., Bonaglia, S., Stjärnkvist, N., Winder, M., Thamdrup, B., & Nascimento, F. J. A. (2021). Influence of settling organic matter quantity and quality on benthic nitrogen cycling. Limnology and Oceanography, 66(5), 1882–1895. https://doi.org/10.1002/lno.11730

Alkire, M. B., & Trefry, J. H. (2006). Transport of spring floodwater from rivers under ice to the Alaskan Beaufort Sea. Journal of Geophysical Research, 111(C12), C12008. https://doi.org/10.1029/2005JC003446

Ardyna, M., & Arrigo, K. R. (2020). Phytoplankton dynamics in a changing Arctic Ocean. Nature Climate Change, 10(10), 892–903. https://doi.org/10.1038/s41558-020-0905-y

Arrigo, K. R., & Van Dijken, G. L. (2015). Continued increases in Arctic Ocean primary production. Progress in Oceanography, 136, 60–70. https://doi.org/10.1016/j.pocean.2015.05.002

Baer, S. E., Sipler, R. E., Roberts, Q. N., Yager, P. L., Frischer, M. E., & Bronk, D. A. (2017). Seasonal nitrogen uptake and regeneration in the western coastal Arctic. Limnology and Oceanography, 62(6), 2463–2479. https://doi.org/10.1002/lno.10580

Baker, K. D., Kellogg, C. T. E., McClelland, J. W., Dunton, K. H., & Crump, B. C. (2021). The Genomic Capabilities of Microbial Communities Track Seasonal Variation in Environmental Conditions of Arctic Lagoons. Frontiers in Microbiology, 12, 601901. https://doi.org/10.3389/fmicb.2021.601901

Barton, S., Jenkins, J., Buckling, A., Schaum, C.-E., Smirnoff, N., Raven, J. A., & Yvon-Durocher, G. (2020). Evolutionary temperature compensation of carbon fixation in marine phytoplankton. Ecology Letters, 23(4), 722–733. https://doi.org/10.1111/ele.13469

Beaufort Lagoon Ecosystems LTER, Core Program. (2023a). Stable oxygen isotope ratios of water (H2O-d18O) from river, lagoon, and open ocean sites along the Alaska Beaufort Sea coast, 2019-ongoing (Version 5) [dataset]. Environmental Data Initiative. https://doi.org/10.6073/pasta/e22a2f3ed737fb437a46a58c5afe5b60

Beaufort Lagoon Ecosystems LTER, Core Program. (2023b). Water column and sediment porewater nutrient concentrations from lagoon, river, and ocean sites along the Alaska Beaufort Sea coast, 2018-ongoing (Version 6) [dataset]. Environmental Data Initiative. https://doi.org/10.6073/pasta/91eec1c3e67f7cdbacc4629523984b99

Bhatt, U. S., Walker, D. A., Walsh, J. E., Carmack, E. C., Frey, K. E., Meier, W. N., Moore, S. E., Parmentier, F.-J. W., Post, E., Romanovsky, V. E., & Simpson, W. R. (2014). Implications of Arctic Sea Ice Decline for the Earth System. Annual Review of Environment and Resources, 39(1), 57–89. https://doi.org/10.1146/annurev-environ-122012-094357

Bonsell, C., & Dunton, K. H. (2018). Long-term patterns of benthic irradiance and kelp production in the central Beaufort sea reveal implications of warming for Arctic inner shelves. Progress in Oceanography, 162, 160–170. https://doi.org/10.1016/j.pocean.2018.02.016

Bonsell, C., & Dunton, K. H. (2021). Slow Community Development Enhances Abiotic Limitation of Benthic Community Structure in a High Arctic Kelp Bed. Frontiers in Marine Science, 8, 592295. https://doi.org/10.3389/fmars.2021.592295

Bourgeois, S., Archambault, P., & Witte, U. (2017). Organic matter remineralization in marine sediments: A Pan-Arctic synthesis. Global Biogeochemical Cycles, 31, 190–213. https://doi.org/10.1002/2016GB005378

Box, J. E., Colgan, W. T., Christensen, T. R., Schmidt, N. M., Lund, M., Parmentier, F.-J. W., Brown, R., Bhatt, U. S., Euskirchen, E. S., Romanovsky, V. E., Walsh, J. E., Overland, J. E., Wang, M., Corell, R. W., Meier, W. N., Wouters, B., Mernild, S., Mård, J., Pawlak, J., & Olsen, M. S. (2019). Key indicators of Arctic climate change: 1971–2017. Environmental Research Letters, 14(4), 045010. https://doi.org/10.1088/1748-9326/aafc1b

Bronk, D. A., See, J. H., Bradley, P., & Killberg, L. (2007). DON as a source of bioavailable nitrogen for phytoplankton. Biogeosciences, 4, 283-296, https://doi.org/10.5194/bg-4-283-2007.

Bruesewitz, D. A., Gardner, W. S., Mooney, R. F., & Buskey, E. J. (2015). Seasonal Water Column NH_4^+ Cycling Along a Semi-arid Sub-tropical River–Estuary Continuum: Responses to Episodic Events and Drought Conditions. Ecosystems, 18(5), 792–812. https://doi.org/10.1007/s10021-015-9863-z

Bruesewitz, D. A., Gardner, W. S., Mooney, R. F., Pollard, L., & Buskey, E. J. (2013). Estuarine ecosystem function response to flood and drought in a shallow, semiarid estuary: Nitrogen cycling and ecosystem metabolism. Limnology and Oceanography, 58(6), 2293–2309. https://doi.org/10.4319/lo.2013.58.6.2293

Canion, A., Overholt, W. A., Kostka, J. E., Huettel, M., Lavik, G., & Kuypers, M. M. M. (2014). Temperature response of denitrification and anaerobic ammonium oxidation rates and microbial community structure in Arctic fjord sediments. Environmental Microbiology, 16(10), 3331–3344. https://doi.org/10.1111/1462-2920.12593

Carey, J. C., Gewirtzman, J., Johnston, S. E., Kurtz, A., Tang, J., Vieillard, A. M., & Spencer, R. G. M. (2020). Arctic River Dissolved and Biogenic Silicon Exports—Current Conditions and Future Changes With Warming. Global Biogeochemical Cycles, 34(3). https://doi.org/10.1029/2019GB006308

Chang, B. X., & Devol, A. H. (2009). Seasonal and spatial patterns of sedimentary denitrification rates in the Chukchi sea. Deep Sea Research Part II: Topical Studies in Oceanography, 56(17), 1339–1350. https://doi.org/10.1016/j.dsr2.2008.10.024

Connelly, T., McClelland, J., Crump, B., Kellogg, C., & Dunton, K. (2015). Seasonal changes in quantity and composition of suspended particulate organic matter in lagoons of the Alaskan Beaufort Sea. Marine Ecology Progress Series, 527, 31–45. https://doi.org/10.3354/meps11207

Connolly, C. T., Cardenas, M. B., Burkart, G. A., Spencer, R. G. M., & McClelland, J. W. (2020). Groundwater as a major source of dissolved organic matter to Arctic coastal waters. Nature Communications, 11(1), 1479. https://doi.org/10.1038/s41467-020-15250-8

Connolly, C. T., Crump, B. C., Dunton, K. H., & McClelland, J. W. (2021). Seasonality of dissolved organic matter in lagoon ecosystems along the Alaska Beaufort Sea

coast. Limnology and Oceanography, 66(12), 4299–4313. https://doi.org/10.1002/lno.11962
Craig, P. C., Griffiths, W. B., Johnson, S. R., & Schell, D. M. (1984). TROPHIC DYNAMICS IN AN ARCTIC LAGOON. In The Alaskan Beaufort Sea (pp. 347–380). Elsevier. https://doi.org/10.1016/B978-0-12-079030-2.50023-X
Damashek, J., & Francis, C. A. (2018). Microbial Nitrogen Cycling in Estuaries: From Genes to Ecosystem Processes. Estuaries and Coasts, 41(3), 626–660. https://doi.org/10.1007/s12237-017-0306-2
DeGrandpre, M. D., Lai, C., Timmermans, M., Krishfield, R. A., Proshutinsky, A., & Torres, D. (2019). Inorganic Carbon and pCO2 Variability During Ice Formation in the Beaufort Gyre of the Canada Basin. Journal of Geophysical Research: Oceans, 124(6), 4017–4028. https://doi.org/10.1029/2019JC015109
Dittmar, T., & Kattner, G. (2003). The biogeochemistry of the river and shelf ecosystem of the Arctic Ocean: A review. Marine Chemistry, 83(3–4), 103–120. https://doi.org/10.1016/S0304-4203(03)00105-1
Dugan, H. A., & Lamoureux, S. F. (2011). The chemical development of a hypersaline coastal basin in the High Arctic. Limnology and Oceanography, 56(2), 495–507. https://doi.org/10.4319/lo.2011.56.2.0495
Fang, Y., Changyou, L., Leppäranta, M., Xiaonghong, S., Shengnan, Z., & Chengfu, Z. (2016). Notable increases in nutrient concentrations in a shallow lake during seasonal ice growth. Water Science and Technology, 74(12), 2773–2783. https://doi.org/10.2166/wst.2016.433
Fox, J., & Weisberg, S. (2019). An R Companion to Applied Regression. Sage. Thousand Oaks CA.
Frey, K. E., Moore, G. W. K., Cooper, L. W., & Grebmeier, J. M. (2015). Divergent patterns of recent sea ice cover across the Bering, Chukchi, and Beaufort seas of the Pacific Arctic Region. Progress in Oceanography, 136, 32–49. https://doi.org/10.1016/j.pocean.2015.05.009
Fritz, M., Vonk, J. E., & Lantuit, H. (2017). Collapsing Arctic coastlines. Nature Climate Change, 7(1), 6–7. https://doi.org/10.1038/nclimate3188
Fulweiler, R. W., Nixon, S. W., & Buckley, B. A. (2010). Spatial and Temporal Variability of Benthic Oxygen Demand and Nutrient Regeneration in an Anthropogenically Impacted New England Estuary. Estuaries and Coasts, 33(6), 1377–1390. https://doi.org/10.1007/s12237-009-9260-y
Gattuso, J.-P., Alliouane, S., & Fischer, P. (2023). High-frequency, year-round time series of the carbonate chemistry in a high-Arctic fjord (Svalbard). Earth System Science Data, 15(7), 2809–2825. https://doi.org/10.5194/essd-15-2809-2023
Giannelli, V., Thomas, D. N., Haas, C., Kattner, G., Kennedy, H., & Dieckmann, G. S. (2001). Behaviour of dissolved organic matter and inorganic nutrients during experimental sea-ice formation. Annals of Glaciology, 33, 317–321. https://doi.org/10.3189/172756401781818572
Groemping, U. (2006). Relative Importance for Linear Regression in R: The Package relaimpo. Journal of Statistical Software, 17(1), 1–27.
Hardison, A. K., McTigue, N. D., Gardner, W. S., & Dunton, K. H. (2017). Arctic shelves as platforms for biogeochemical activity: Nitrogen and carbon transformations in

the Chukchi Sea, Alaska. Deep Sea Research Part II: Topical Studies in Oceanography, 144, 78–91. https://doi.org/10.1016/j.dsr2.2017.08.004
Harris, C. M., McClelland, J. W., Connelly, T. L., Crump, B. C., & Dunton, K. H. (2017). Salinity and Temperature Regimes in Eastern Alaskan Beaufort Sea Lagoons in Relation to Source Water Contributions. Estuaries and Coasts, 40(1), 50–62. https://doi.org/10.1007/s12237-016-0123-z
Herzog, S. D., Conrad, S., Ingri, J., Persson, P., & Kritzberg, E. S. (2019). Spring flood induced shifts in Fe speciation and fate at increased salinity. Applied Geochemistry, 109, 104385. https://doi.org/10.1016/j.apgeochem.2019.104385
Holmes, R. M., McClelland, J. W., Peterson, B. J., Tank, S. E., Bulygina, E., Eglinton, T. I., Gordeev, V. V., Gurtovaya, T. Y., Raymond, P. A., Repeta, D. J., Staples, R., Striegl, R. G., Zhulidov, A. V., & Zimov, S. A. (2012). Seasonal and Annual Fluxes of Nutrients and Organic Matter from Large Rivers to the Arctic Ocean and Surrounding Seas. Estuaries and Coasts, 35(2), 369–382. https://doi.org/10.1007/s12237-011-9386-6
Johnson, M., & Eicken, H. (2016). Estimating Arctic sea-ice freeze-up and break-up from the satellite record: A comparison of different approaches in the Chukchi and Beaufort Seas. Elementa: Science of the Anthropocene, 4, 000124. https://doi.org/10.12952/journal.elementa.000124
Jones, B. M., Arp, C. D., Jorgenson, M. T., Hinkel, K. M., Schmutz, J. A., & Flint, P. L. (2009). Increase in the rate and uniformity of coastline erosion in Arctic Alaska. Geophysical Research Letters, 36(3), 2008GL036205. https://doi.org/10.1029/2008GL036205
Jordan, T. E., Cornwell, J. C., Boynton, W. R., & Anderson, J. T. (2008). Changes in phosphorus biogeochemistry along an estuarine salinity gradient: The iron conveyer belt. Limnology and Oceanography, 53(1), 172–184. https://doi.org/10.4319/lo.2008.53.1.0172
Kellogg, C. T. E., McClelland, J. W., Dunton, K. H., & Crump, B. C. (2019). Strong Seasonality in Arctic Estuarine Microbial Food Webs. Frontiers in Microbiology, 10, 2628. https://doi.org/10.3389/fmicb.2019.02628
Kim, S.-H., Choi, A., Jin Yang, E., Lee, S., & Hyun, J.-H. (2016). Low benthic respiration and nutrient flux at the highly productive Amundsen Sea Polynya, Antarctica. Deep Sea Research Part II: Topical Studies in Oceanography, 123, 92–101. https://doi.org/10.1016/j.dsr2.2015.10.004
Ko, E., Gorbunov, M. Y., Jung, J., Joo, H. M., Lee, Y., Cho, K., Yang, E. J., Kang, S., & Park, J. (2020). Effects of Nitrogen Limitation on Phytoplankton Physiology in the Western Arctic Ocean in Summer. Journal of Geophysical Research: Oceans, 125(11), e2020JC016501. https://doi.org/10.1029/2020JC016501
Krisch, S., Browning, T. J., Graeve, M., Ludwichowski, K.-U., Lodeiro, P., Hopwood, M. J., Roig, S., Yong, J.-C., Kanzow, T., & Achterberg, E. P. (2020). The influence of Arctic Fe and Atlantic fixed N on summertime primary production in Fram Strait, North Greenland Sea. Scientific Reports, 10(1), 15230. https://doi.org/10.1038/s41598-020-72100-9
Lachniet, M. S., Lawson, D. E., Stephen, H., Sloat, A. R., & Patterson, W. P. (2016). Isoscapes of δ18O and δ2H reveal climatic forcings on Alaska and Yukon

precipitation: Alaska isoscape. Water Resources Research, 52(8), 6575–6586. https://doi.org/10.1002/2016WR019436
Lantuit, H., Atkinson, D., Paul Overduin, P., Grigoriev, M., Rachold, V., Grosse, G., & Hubberten, H.-W. (2011). Coastal erosion dynamics on the permafrost-dominated Bykovsky Peninsula, north Siberia, 1951–2006. Polar Research, 30(1), 7341. https://doi.org/10.3402/polar.v30i0.7341
Le Fouest, V., Babin, M., & Tremblay, J.-É. (2013). The fate of riverine nutrients on Arctic shelves. Biogeosciences, 10(6), 3661–3677. https://doi.org/10.5194/bg-10-3661-2013
Letscher, R. T., Hansell, D. A., Kadko, D., & Bates, N. R. (2013). Dissolved organic nitrogen dynamics in the Arctic Ocean. Marine Chemistry, 148, 1–9. https://doi.org/10.1016/j.marchem.2012.10.002
Lewis, K. M., Van Dijken, G. L., & Arrigo, K. R. (2020). Changes in phytoplankton concentration now drive increased Arctic Ocean primary production. Science, 369(6500), 198–202. https://doi.org/10.1126/science.aay8380
Link, H., Chaillou, G., Forest, A., Piepenburg, D., & Archambault, P. (2013). Multivariate benthic ecosystem functioning in the Arctic – benthic fluxes explained by environmental parameters in the southeastern Beaufort Sea. Biogeosciences, 10(9), 5911–5929. https://doi.org/10.5194/bg-10-5911-2013
Macdonald, R. W., & Yu, Y. (2006). The Mackenzie Estuary of the Arctic Ocean. In P. J. Wangersky (Ed.), Estuaries (Vol. 5H, pp. 91–120). Springer-Verlag. https://doi.org/10.1007/698_5_027
Mahoney, A. R., Eicken, H., Gaylord, A. G., & Gens, R. (2014). Landfast sea ice extent in the Chukchi and Beaufort Seas: The annual cycle and decadal variability. Cold Regions Science and Technology, 103, 41–56. https://doi.org/10.1016/j.coldregions.2014.03.003
Manes, S. S., & Gradinger, R. (2009). Small scale vertical gradients of Arctic ice algal photophysiological properties. Photosynthesis Research, 102(1), 53–66. https://doi.org/10.1007/s11120-009-9489-0
Marañón, E., Lorenzo, M. P., Cermeño, P., & Mouriño-Carballido, B. (2018). Nutrient limitation suppresses the temperature dependence of phytoplankton metabolic rates. The ISME Journal, 12(7), 1836–1845. https://doi.org/10.1038/s41396-018-0105-1
Markus, T., Stroeve, J. C., & Miller, J. (2009). Recent changes in Arctic sea ice melt onset, freezeup, and melt season length. Journal of Geophysical Research: Oceans, 114(C12), 2009JC005436. https://doi.org/10.1029/2009JC005436
Matson, P. G., Washburn, L., Martz, T. R., & Hofmann, G. E. (2014). Abiotic versus Biotic Drivers of Ocean pH Variation under Fast Sea Ice in McMurdo Sound, Antarctica. PLoS ONE, 9(9), e107239. https://doi.org/10.1371/journal.pone.0107239
McClelland, J. W., Holmes, R. M., Dunton, K. H., & Macdonald, R. W. (2012). The Arctic Ocean Estuary. Estuaries and Coasts, 35(2), 353–368. https://doi.org/10.1007/s12237-010-9357-3
McClelland, J. W., Townsend-Small, A., Holmes, R. M., Pan, F., Stieglitz, M., Khosh, M., & Peterson, B. J. (2014). River export of nutrients and organic matter from the

North Slope of Alaska to the Beaufort Sea. Water Resources Research, 50(2), 1823–1839. https://doi.org/10.1002/2013WR014722
McTigue, N. D., Gardner, W. S., Dunton, K. H., & Hardison, A. K. (2016). Biotic and abiotic controls on co-occurring nitrogen cycling processes in shallow Arctic shelf sediments. Nature Communications, 7(1), 13145. https://doi.org/10.1038/ncomms13145
Miller, C. A., Bonsell, C., McTigue, N. D., & Kelley, A. L. (2021). The seasonal phases of an Arctic lagoon reveal the discontinuities of pH variability and CO_2 flux at the air–sea interface. Biogeosciences, 18(3), 1203–1221. https://doi.org/10.5194/bg-18-1203-2021
Millette, N. C., Leles, S. G., Johnson, M. D., Maloney, A. E., Brownlee, E. F., Cohen, N. R., Duhamel, S., Poulton, N. J., Princiotta, S. D., Stamieszkin, K., Wilken, S., & Moeller, H. V. (2024). Recommendations for advancing mixoplankton research through empirical-model integration. Frontiers in Marine Science, 11, 1392673. https://doi.org/10.3389/fmars.2024.1392673
Mulholland, M., Glibert, P., Berg, G., Van Heukelem, L., Pantoja, S., & Lee, C. (1998). Extracellular amino acid oxidation by microplankton: A cross-ecosystem comparison. Aquatic Microbial Ecology, 15, 141–152. https://doi.org/10.3354/ame015141
Muth, A. F., Kelley, A. L., & Dunton, K. H. (2022). HIGH-FREQUENCY PH TIME SERIES reveals pronounced seasonality in Arctic coastal waters. Limnology and Oceanography, 67(7), 1429–1442. https://doi.org/10.1002/lno.12080
Okkonen, S. (2008). Exchange Between Elson Lagoon and the Nearshore Beaufort Sea and Its Role in the Aggregation of Zooplankton.
Pithan, F., & Mauritsen, T. (2014). Arctic amplification dominated by temperature feedbacks in contemporary climate models. Nature Geoscience, 7(3), 181–184. https://doi.org/10.1038/ngeo2071
Rantanen, M., Karpechko, A. Yu., Lipponen, A., Nordling, K., Hyvärinen, O., Ruosteenoja, K., Vihma, T., & Laaksonen, A. (2022). The Arctic has warmed nearly four times faster than the globe since 1979. Communications Earth & Environment, 3(1), 168. https://doi.org/10.1038/s43247-022-00498-3
Rawlins, M. A., Cai, L., Stuefer, S. L., & Nicolsky, D. (2019). Changing characteristics of runoff and freshwater export from watersheds draining northern Alaska. The Cryosphere, 13(12), 3337–3352. https://doi.org/10.5194/tc-13-3337-2019
Rember, R. D., & Trefry, J. H. (2004). Increased concentrations of dissolved trace metals and organic carbon during snowmelt in rivers of the alaskan arctic. Geochimica et Cosmochimica Acta, 68(3), 477–489. https://doi.org/10.1016/S0016-7037(03)00458-7
Retamal, L., Bonilla, S., & Vincent, W. F. (2008). Optical gradients and phytoplankton production in the Mackenzie River and the coastal Beaufort Sea. Polar Biology, 31(3), 363–379. https://doi.org/10.1007/s00300-007-0365-0
Rysgaard, S., Glud, R. N., Risgaard-Petersen, N., & Dalsgaard, T. (2004). Denitrification and anammox activity in Arctic marine sediments. Limnology and Oceanography, 49(5), 1493–1502. https://doi.org/10.4319/lo.2004.49.5.1493
Schell, D. M., Parrish, D. M., & Ziemann, P. J. (1984). Primary Production, Nutrient Dynamics, and Trophic Energetic. 369–432.

Serreze, M. C., & Barry, R. G. (2011). Processes and impacts of Arctic amplification: A research synthesis. Global and Planetary Change, 77(1–2), 85–96. https://doi.org/10.1016/j.gloplacha.2011.03.004

Shiozaki, T., Ijichi, M., Fujiwara, A., Makabe, A., Nishino, S., Yoshikawa, C., & Harada, N. (2019). Factors Regulating Nitrification in the Arctic Ocean: Potential Impact of Sea Ice Reduction and Ocean Acidification. Global Biogeochemical Cycles, 33(8), 1085–1099. https://doi.org/10.1029/2018GB006068

Sievers, J., Sørensen, L. L., Papakyriakou, T., Else, B., Sejr, M. K., Haubjerg Søgaard, D., Barber, D., & Rysgaard, S. (2015). Winter observations of CO_2 exchange between sea ice and the atmosphere in a coastal fjord environment. The Cryosphere, 9(4), 1701–1713. https://doi.org/10.5194/tc-9-1701-2015

Stroeve, J. C., Markus, T., Boisvert, L., Miller, J., & Barrett, A. (2014). Changes in Arctic melt season and implications for sea ice loss. Geophysical Research Letters, 41(4), 1216–1225. https://doi.org/10.1002/2013GL058951

Sun, X., Humborg, C., Mörth, C., & Brüchert, V. (2021). The Importance of Benthic Nutrient Fluxes in Supporting Primary Production in the Laptev and East Siberian Shelf Seas. Global Biogeochemical Cycles, 35(7), e2020GB006849. https://doi.org/10.1029/2020GB006849

Tank, S. E., Manizza, M., Holmes, R. M., McClelland, J. W., & Peterson, B. J. (2012). The Processing and Impact of Dissolved Riverine Nitrogen in the Arctic Ocean. Estuaries and Coasts, 35(2), 401–415. https://doi.org/10.1007/s12237-011-9417-3

Terhaar, J., Lauerwald, R., Regnier, P., Gruber, N., & Bopp, L. (2021). Around one third of current Arctic Ocean primary production sustained by rivers and coastal erosion. Nature Communications, 12(1), 169. https://doi.org/10.1038/s41467-020-20470-z

Thibodeau, B., Bauch, D., & Voss, M. (2017). Nitrogen dynamic in Eurasian coastal Arctic ecosystem: Insight from nitrogen isotope. Global Biogeochemical Cycles, 31(5), 836–849. https://doi.org/10.1002/2016GB005593

Tolar, B. B., Ross, M. J., Wallsgrove, N. J., Liu, Q., Aluwihare, L. I., Popp, B. N., & Hollibaugh, J. T. (2016). Contribution of ammonia oxidation to chemoautotrophy in Antarctic coastal waters. The ISME Journal, 10(11), 2605–2619. https://doi.org/10.1038/ismej.2016.61

Vancoppenolle, M., Meiners, K. M., Michel, C., Bopp, L., Brabant, F., Carnat, G., Delille, B., Lannuzel, D., Madec, G., Moreau, S., Tison, J.-L., & Van Der Merwe, P. (2013). Role of sea ice in global biogeochemical cycles: Emerging views and challenges. Quaternary Science Reviews, 79, 207–230. https://doi.org/10.1016/j.quascirev.2013.04.011

Yamamoto-Kawai, M., Tanaka, N., & Pivovarov, S. (2005). Freshwater and brine behaviors in the Arctic Ocean deduced from historical data of D18O and alkalinity (1929–2002 A.D.). Journal of Geophysical Research, 110. https://doi.org/doi:10.1029/2004JC002793

Zhang, J.-Z., & Huang, X.-L. (2011). Effect of Temperature and Salinity on Phosphate Sorption on Marine Sediments. Environmental Science & Technology, 45(16), 6831–6837. https://doi.org/10.1021/es200867p

2.8 Tables

Table 2.1. Lagoon geomorphology (depth (m), length (km), annual river discharge (km^3), ocean connectivity) at Elson Lagoon, Simpson Lagoon, Stefansson Sound, Kaktovik Lagoon, and Jago Lagoon. Freshwater sources sampled by the BLE-LTER program are grouped by lagoon. Lagoon length was measured using the base World Imagery map on ArcGIS, and depths were derived from Kim et al. (unpublished). (---) represents rivers with no published annual discharge rates. *McClelland et al. 2014 **Stuefer et al. 2017. NA applies to lagoons with primarily diffusive inputs that cannot be or are difficult to quantify.

Lagoon	Average depth (m)	Length (km)	Freshwater sources sampled	Annual river discharge (km^3)	Ocean connectivity
Elson Lagoon West (EWL) and Elson Lagoon East (EEL)	2.4	25	Avak Creek No Name River Mayoeak River	--- --- ---	Several intermittent channels
Simpson Lagoon (SIL)	1.8	25	Kuparak River Colville River	1.3* 19.7*	Several intermittent channels
Stefansson Sound (SSL)	4.3	35	Sagavanirktok River Putuligauyuk River Atigun River	1.6* 0.05** ---	Semi-enclosed
Kaktovik Lagoon (KAL)	2.8	7	Streams, runoff	NA	1 channel to JAL
Jago Lagoon (JAL)	2.6	7	Jago River	---	1 channel to Beaufort Sea

Table 2.2. End-member (sea ice melt (SIM), meteoric water (MW), and polar mixed layer (PML)) values for salinity, H_2O-$\delta^{18}O$, and inorganic nutrients used in the water source contribution and conservative mixing model. MW inputs were node-specific due to spatial heterogeneity in end-member values. All MW salinity, $\delta^{18}O$-H_2O, and nutrients were collected by the BLE-LTER from 2018-2022. *SIM and PML salinity and $\delta^{18}O$-H_2O were from Alkire and Trefry, 2006. **SIM nutrients were from Manes and Gradinger, 2009. Beaufort Sea surface nutrients collected by the BLE-LTER was used for PML nutrients.

Water Source		Salinity	$\delta^{18}O$ (‰)	NH_4^+ (µmol N L^{-1})	PO_4^{3-} (µmol P L^{-1})	NO_3^- (µmol N L^{-1})	DSi (µmol SiO_2 L^{-1})
SIM		5.0*	-2.4*	1.3**	1.2**	0.14**	2.7**
MW	BRW	0.1	-11.5	1.5	0.4	2.0	7.7
	SCC	0.1	-18.8	0.4	0.0	3.6	28.8
	BTI	0.1	-21.4	NA	0.1	NA	9.2
PML		31.6*	-3.5*	0.9	0.4	0.0	4.9

Table 2.3. Water column temperature (°C), salinity, dissolved oxygen (DO, mg L^{-1}), and pH during Ice Cover, Break Up, and Open Water seasons, averaged across nodes. Average ± standard error (n = sample number). Superscript letters (a,b,c) for each parameter indicate statistically significant difference between seasons based on ANOVA and post-hoc Tukey tests (a = 0.05).

Parameter	Mean ± standard error (n)		
	Ice Cover	Break Up	Open Water
Temperature (°C)	-1.9 ± 0.1 (n=39)[a]	2.9 ± 0.6 (n=40)[b]	7.3 ± 0.3 (n=84)[c]
Salinity	36.2 ± 0.8 (n=39)[a]	6.6 ± 1.5 (n=40)[b]	24.4 ± 0.6 (n=83)[c]
DO (mg L^{-1})	10.5 ± 0.4 (n=39)[b]	12.8 ± 0.2 (n=40)[a]	10.9 ± 0.2 (n=84)[b]
pH	7.6 ± 0.1 (n=39)[a]	7.9 ± 0.1 (n=40)[b]	7.9 ± 0.02 (n=84)[b]

Table 2.4. Water column concentrations of ammonium (NH_4^+; µmol N L^{-1}), nitrate (NO_3^-; µmol N L^{-1}), phosphate (PO_4^{3-}; µmol P L^{-1}), molar N:P ratio, and dissolved silica (DSi; µmol SiO_2 L^{-1}) across season (Ice Cover, Break Up, Open Water) and node (BRW, SCC, BTI). Average ± standard error (n = sample number). For each nutrient, superscript letters (a,b,c) for the All Node averages indicate statistically significant difference between seasons based on ANOVA and post-hoc Tukey tests (a = 0.05). Likewise, for each nutrient, superscript letters (a,b,c) indicate significant internodal differences within a given season based on ANOVA and post-hoc Tukey tests (a = 0.05).

	Ice Cover					Break Up					Open Water				
Node	NH_4^+ µmol N L^{-1}	NO_3^- µmol N L^{-1}	PO_4^{3-} µmol P L^{-1}	NP Ratio	DSi µmol SiO_2 L^{-1}	NH_4^+ µmol N L^{-1}	NO_3^- µmol N L^{-1}	PO_4^{3-} µmol P L^{-1}	NP Ratio	DSi µmol SiO_2 L^{-1}	NH_4^+ µmol N L^{-1}	NO_3^- µmol N L^{-1}	PO_4^{3-} µmol P L^{-1}	NP Ratio	DSi µmol SiO_2 L^{-1}
BRW	1.9 ± 0.2 (n=18)	5.9 ± 0.5 (n=18)^{b}	2.0 ± 0.5 (n=18)	13.4 ± 2.9 (n=18)	20.8 ± 0.9 (n=18)	1.4 ± 1.0 (n=14)	0.7 ± 0.3 (n=16)	1.0 ± 0.4 (n=17)	48.5 ± 36.7 (n=13)	2.7 ± 0.4 (n=17)^{a}	0.6 ± 0.2 (n=35)	0.4 ± 0.1 (n=33)	0.8 ± 0.2 (n=35)	1.1 ± 0.2 (n=33)	3.7 ± 0.3 (n=35)^{b}
SCC	1.5 ± 0.6 (n=20)	5.6 ± 0.6 (n=22)^{b}	2.0 ± 0.4 (n=21)	6.8 ± 1.1 (n=19)	19.1 ± 2.3 (n=22)	0.7 ± 0.1 (n=17)	2.2 ± 0.5 (n=19)	0.5 ± 0.3 (n=19)	128.5 ± 34.4 (n=16)	11.8 ± 1.5 (n=19)^{b}	0.4 ± 0.1 (n=31)	0.7 ± 0.2 (n=28)	0.4 ± 0.1 (n=32)	17.1 ± 8.3 (n=28)	10.7 ± 1.6 (n=32)^{a}
BTI	3.7 ± 1.9 (n=10)	3.0 ± 0.4 (n=10)^{a}	3.0 ± 0.7 (n=10)	3.9 ± 1.1 (n=10)	14.4 ± 1.3 (n=10)	0.6 ± 0.3 (n=4)	0.7 ± 0.7 (n=2)	2.0 ± 0.9 (n=6)	0.3 (n=1)	5.1 ± 1.8 (n=6)^{b}	0.8 ± 0.1 (n=16)	0.3 ± 0.2 (n=14)	0.7 ± 0.2 (n=16)	2.3 ± 0.6 (n=14)	4.7 ± 0.7 (n=16)^{b}
All Nodes	2.1 ± 0.5 (n=48)^{a}	5.2 ± 0.4 (n=50)^{a}	2.2 ± 0.3 (n=49)^{a}	8.7 ± 1.3 (n=47)	18.8 ± 1.1 (n=50)^{a}	1.0 ± 0.4 (n=35)^{b}	1.5 ± 0.3 (n=37)^{b}	0.9 ± 0.3 (n=42)^{b}	89.5 ± 25.1 (n=30)	7.2 ± 1.0 (n=42)^{b}	0.5 ± 0.1 (n=82)^{b}	0.5 ± 0.1 (n=75)^{c}	0.6 ± 0.1 (n=83)^{b}	7.3 ± 3.2 (n=75)	6.6 ± 0.7 (n=83)^{b}

Table 2.5. Average lagoon and river H_2O-$\delta^{18}O$ values (‰) separated by node (BRW, SCC, and BTI). Lagoon water column H_2O-$\delta^{18}O$ values are further separated by season (Ice Cover, Break Up, Open Water). Average ± standard error (n = sample number). Superscript letters (a,b,c) for the All Nodes Averages indicate statistically significant difference between seasons based on ANOVA and post-hoc Tukey tests (a = 0.05). Likewise, superscript letters (a,b,c) indicate significant internodal differences within a given season (for lagoons) or for the rivers based on ANOVA and post-hoc Tukey tests (a = 0.05).

	H_2O-$\delta^{18}O$ (‰, mean ± standard error)			
	Lagoon			River
	Ice Cover	Break Up	Open Water	
BRW	-3.3 ± 0.2 (n=14)	-7.9 ± 0.6 (n=14)^{b}	-4.7 ± 0.3 (n=33)^{a}	-11.5 ± 0.4 (n=15)^{a}
SCC	-4.6 ± 0.8 (n=22)	-15.1 ± 1.3 (n=18)^{a}	-8.0 ± 0.8 (n=29)^{b}	-18.8 ± 0.5 (n=15)^{b}
BTI	-3.5 ± 0.3 (n=10)	-9.6 ± 2.0 (n=6)^{b}	-5.5 ± 0.4 (n=15)^{a,b}	-21.4 (n=1)^{b}
All Nodes	-3.5 ± 0.1 (n=46)^{a}	-11.6 ± 0.9 (n=38)^{b}	-6.1 ± 0.4 (n=77)^{c}	-15.4 ± 0.8 (n=31)

Table 2.6. Contributions (%) of sea ice melt (SIM), meteoric water (MW), and polar mixed layer (PML) waters in the lagoons based on outputs of the salinity and H_2O-$\delta^{18}O$ water source mixing model separated by season (Ice Cover, Break Up, Open Water) and node (BRW, SCC, BTI). Average ± standard error (n = sample number). For each source, superscript letters (a,b,c) for the All Nodes averages indicate statistically significant difference between seasons based on ANOVA and post-hoc Tukey tests (a = 0.05). Likewise, superscript letters (a,b,c) indicate significant internodal differences for a specific source within a given season based on ANOVA and post-hoc Tukey tests (a = 0.05).

Node	Water Source Contribution (%)								
	Ice Cover			Break Up			Open Water		
	SIM	MW	PML	SIM	MW	PML	SIM	MW	PML
BRW	-11 ± 4 (n=14)	-4 ± 2 (n=14)	116 ± 2 (n=14)	31 ± 8 (n=14)	60 ± 6^{a,b} (n=14)	9 ± 3 (n=14)	8 ± 3 (n=33)	16 ± 3 (n=33)	76 ± 2 (n=33)
SCC	-16 ± 7 (n=15)	-8 ± 8 (n=15)	108 ± 10 (n=15)	10 ± 10 (n=18)	76 ± 8^{b} (n=18)	14 ± 8 (n=18)	0 ± 2 (n=28)	27 ± 5 (n=28)	74 ± 4 (n=28)
BTI	-22 ± 4 (n=10)	-1 ± 1 (n=10)	123 ± 3 (n=10)	18 ± 12 (n=6)	35 ± 12^{a} (n=6)	46 ± 23 (n=6)	6 ± 3 (n=15)	12 ± 2 (n=15)	83 ± 3 (n=15)
All Nodes	-16 ± 3 (n=39)^{a}	1 ± 3 (n=39)^{a}	115 ± 4 (n=39)^{a}	19 ± 6 (n=38)^{b}	64 ± 5 (n=38)^{b}	17 ± 5 (n=38)^{b}	5 ± 1 (n=76)^{c}	19 ± 2 (n=76)^{c}	76 ± 2 (n=76)^{c}

Table 2.7. Net nutrient production and consumption (ΔN) according to deviations from the conservative mixing line of ammonium (NH_4^+; µmol N L^{-1}), nitrate (NO_3^-; µmol N L^{-1}), phosphate (PO_4^{3-}; µmol P L^{-1}), and dissolved silica (DSi; µmol SiO_2 L^{-1}) separated by season (Ice Cover, Break Up, Open Water), and node (BRW, SCC, BTI). NA: Fluxes of NH_4^+ and NO_3^- were not calculated due to lack of river nutrient data in BTI. Average ± standard error (n = sample number). For each nutrient, superscript letters (a,b,c) for the All Nodes averages indicate statistically significant difference between seasons based on ANOVA and post-hoc Tukey tests (a = 0.05).

	Ice Cover				Break Up				Open Water			
Node	ΔNH_4^+ µmol N L^{-1}	ΔNO_3^- µmol N L^{-1}	ΔPO_4^{3-} µmol P L^{-1}	ΔDSi µmol SiO_2 L^{-1}	ΔNH_4^+ µmol N L^{-1}	ΔNO_3^- µmol N L^{-1}	ΔPO_4^{3-} µmol P L^{-1}	ΔDSi µmol SiO_2 L^{-1}	ΔNH_4^+ µmol N L^{-1}	ΔNO_3^- µmol N L^{-1}	ΔPO_4^{3-} µmol P L^{-1}	ΔDSi µmol SiO_2 L^{-1}
BRW	1.2 ± 0.3 (n=14)	5.9 ± 2.2 (n=14)	2.0 ± 0.7 (n=14)	15.9 ± 1.0 (n=14)	0.4 ± 1.3 (n=11)	-0.7 ± 0.3 (n=13)	0.9 ± 0.4 (n=14)	-3.1 ± 0.3 (n=14)	-0.4 ± 0.2 (n=32)	-0.0 ± 0.1 (n=30)	0.5 ± 0.2 (n=32)	-1.4 ± 0.4 (n=32)
SCC	1.2 ± 0.8 (n=13)	5.2 ± 2.6 (n=15)	2.0 ± 0.5 (n=15)	14.1 ± 3.2 (n=15)	0.2 ± 0.1 (n=16)	-0.7 ± 0.6 (n=18)	0.5 ± 0.3 (n=17)	-11.2 ± 1.3 (n=18)	-0.3 ± 0.1 (n=27)	-0.3 ± 0.2 (n=25)	0.1 ± 0.1 (n=28)	-0.4 ± 0.7 (n=28)
BTI	NA	NA	2.5 ± 0.7 (n=10)	9.0 ± 1.3 (n=10)	NA	NA	1.7 ± 0.8 (n=6)	-0.9 ± 1.9 (n=6)	NA	NA	0.4 ± 0.2 (n=15)	-1.1 ± 0.4 (n=15)
All Nodes	1.2 ± 0.4 (n=27)^{a}	5.6 ± 0.4 (n=29)^{a}	2.1 ± 0.3 (n=39)^{a}	13.4 ± 1.2 (n=39)^{a}	0.3 ± 0.5 (n=27)^{a,b}	-0.7 ± 0.4 (n=31)^{b}	0.8 ± 0.3 (n=37)^{b}	-6.6 ± 1.0 (n=38)^{a,b}	-0.4 ± 0.1 (n=59)^{b}	-0.2 ± 0.1 (n=55)^{b}	0.3 ± 0.1 (n=75)^{b}	-0.9 ± 0.3 (n=75)^{b}

Table 2.8. Comparison of hypothetical nutrient concentrations from the conservative mixing line ($N_{conserved}$), observed nutrient concentrations, and deviation (ΔN) likely due to biotic processes during Ice Cover. Average ± standard error (n =sample number). To quantify the magnitude of biotic production ($\%_{biotic}$), ΔN was calculated as a percentage of ambient nutrient concentrations during Ice Cover.

Nutrient	$N_{conserved}$	$N_{observed}$	ΔN	$\%_{biotic}$
NH_4^+	0.8 ± 0.0 (n=29)	2.1 ± 0.5 (n=48)	1.2 ± 0.4 (n=27)	57
NO_3^-	-0.2 ± 0.1 (n=29)	5.2 ± 0.4 (n=50)	5.6 ± 0.5 (n=29)	107
PO_4^{3-}	0.4 ± 0.0 (n=39)	2.2 ± 0.3 (n=49)	2.1 ± 0.4 (n=39)	97
DSi	5.2 ± 0.2 (n=39)	18.8 ± 1.1 (n=50)	13.4 ± 1.4 (n=39)	71

2.9 Figures

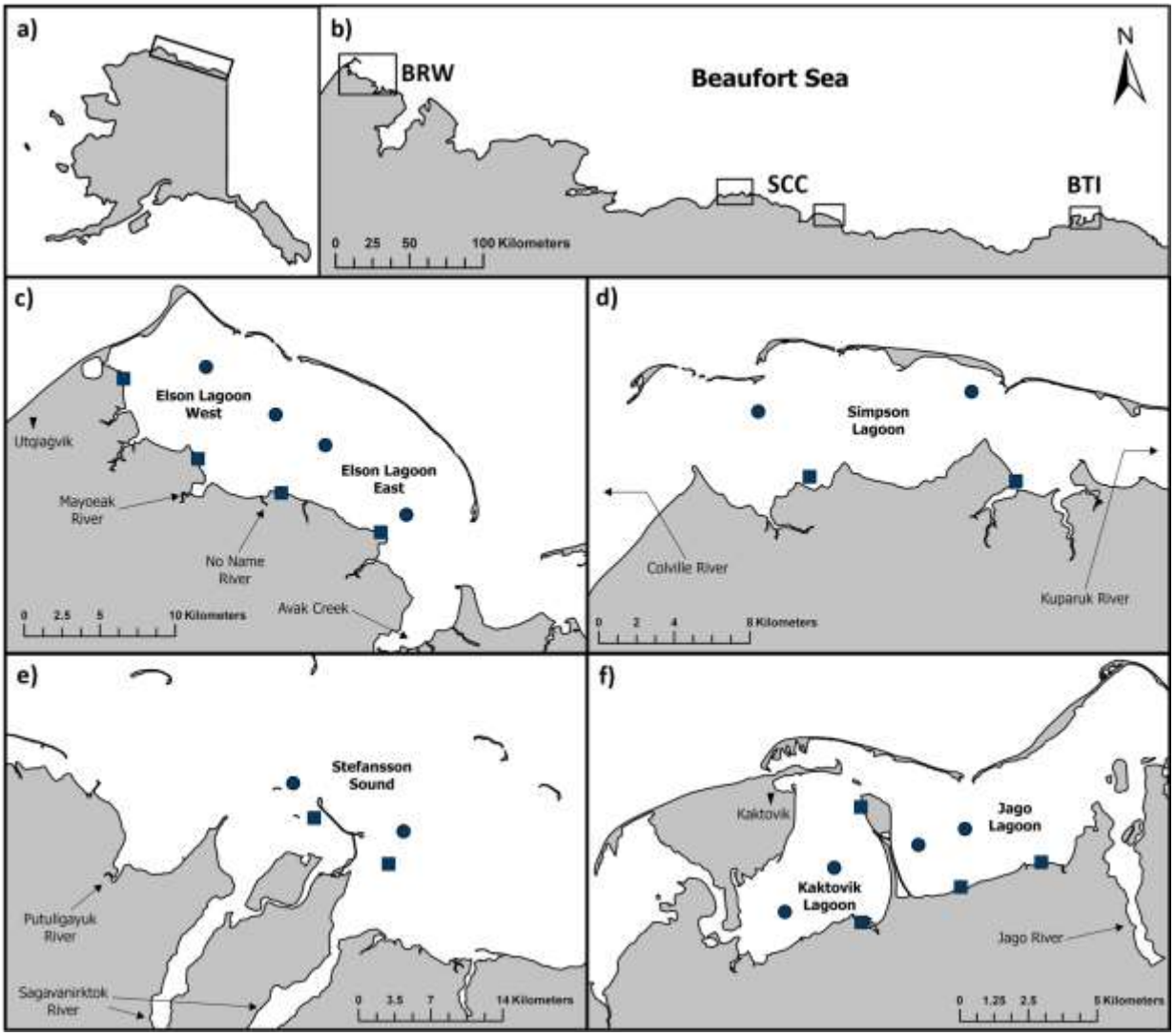

Figure 2.1 Location of the study sites at the Beaufort Lagoon Ecosystems Long-Term Ecological Research (BLE-LTER) program. a) Map of Alaska with Beaufort Sea Alaskan coast in box. b) Beaufort Sea Coast with BLE-LTER research nodes in boxes. c) The westernmost node (BRW) is based out of Utqiaġvik where Elson Lagoon is located. The central node (SCC) contains d) Simpson Lagoon and e) Stefansson Sound. The eastern node (BTI) is based out of Kaktovik and contains f) Kaktovik Lagoon and Jago Lagoon. Each sampled lagoon has two shallow (squares) and two deep (circles) stations.

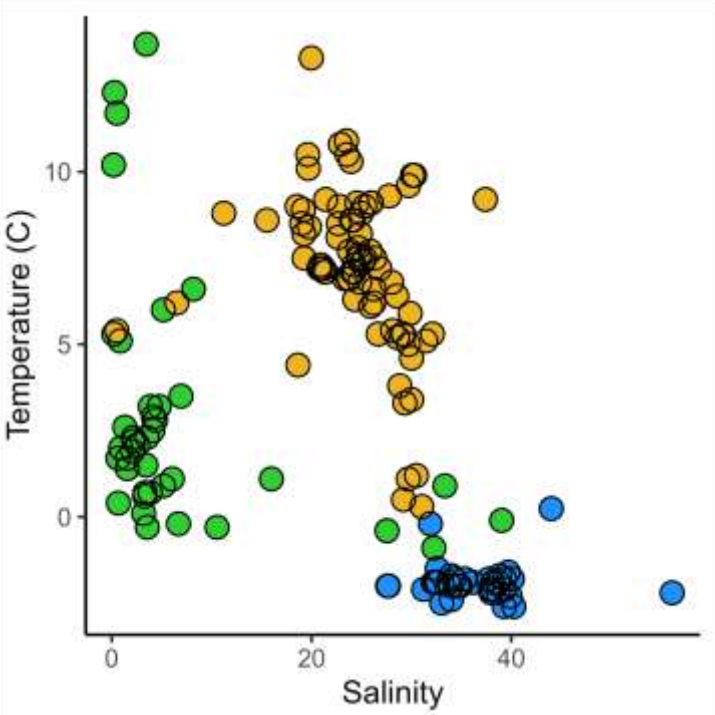

Figure 2.2. Water column temperature (°C) and salinity during Ice Cover (blue), Break Up (green), and Open Water (yellow) across all nodes from 2018 to 2021.

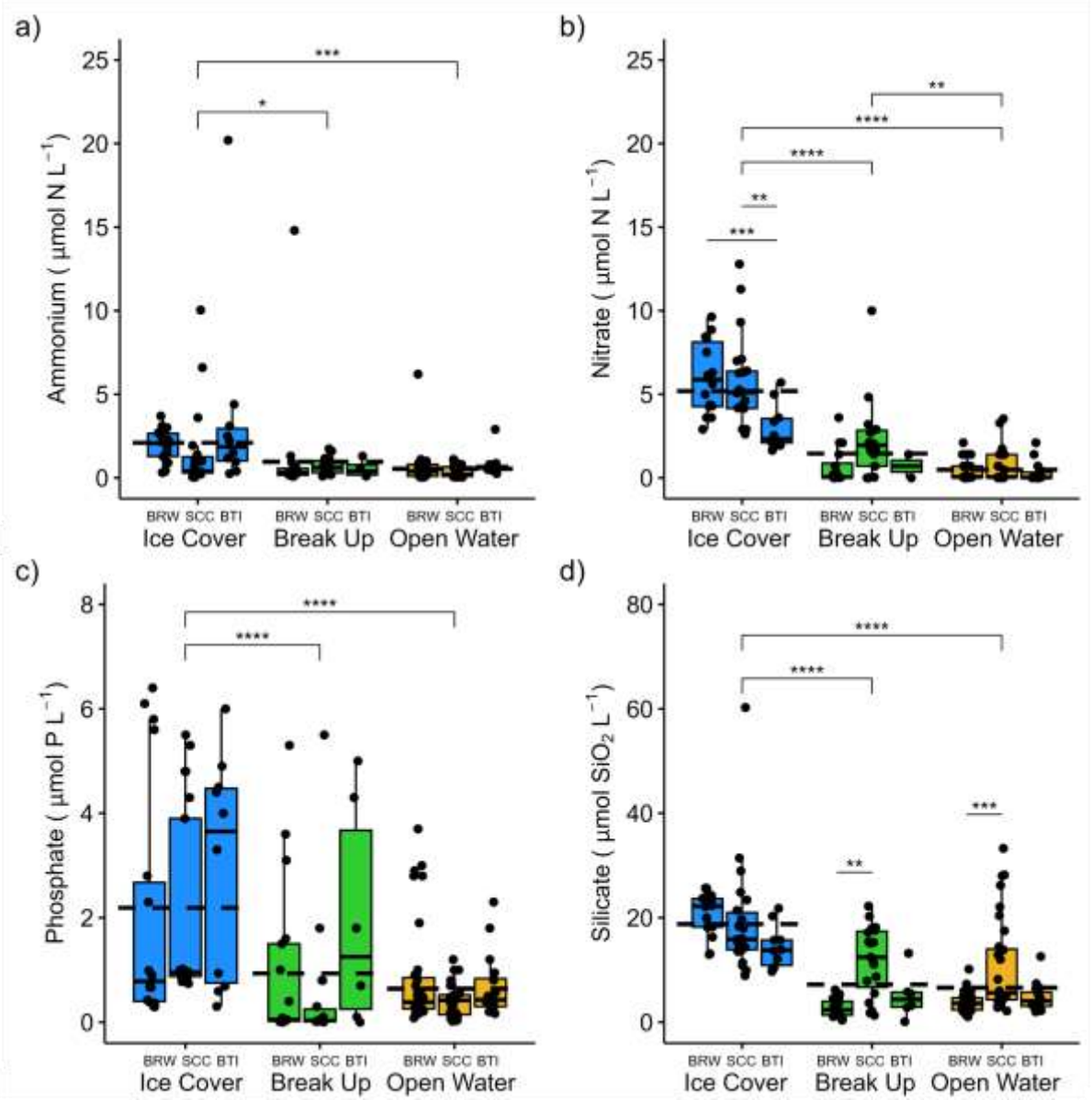

Figure 2.3. Water column concentrations of a) ammonium (NH_4^+; µmol N L^{-1}), b) nitrate (NO_3^-; µmol N L^{-1}), c) phosphate (PO_4^{3-}; µmol P L^{-1}), and d) dissolved silica (DSi; µmol SiO_2 L^{-1}) across seasons (Ice Cover [blue], Break Up [green], Open Water [yellow]) and nodes (BRW, SCC, BTI). The lower and upper extent of the boxplot represent the 25th (Q1) and 75th (Q3) percentiles while the lower and upper extent of the whiskers represent 1.5 times the interquartile range (Q3-Q1) below Q1 and above Q3. The solid black line within each box represents the median concentration, and the dashed black lines represent the average concentration across all nodes for that season. Brackets and horizontal lines represent significant seasonal and internodal differences, respectively. Asterisks represent level of significance (*<0.05, **<0.01, ***<0.001, ****<0.0001).

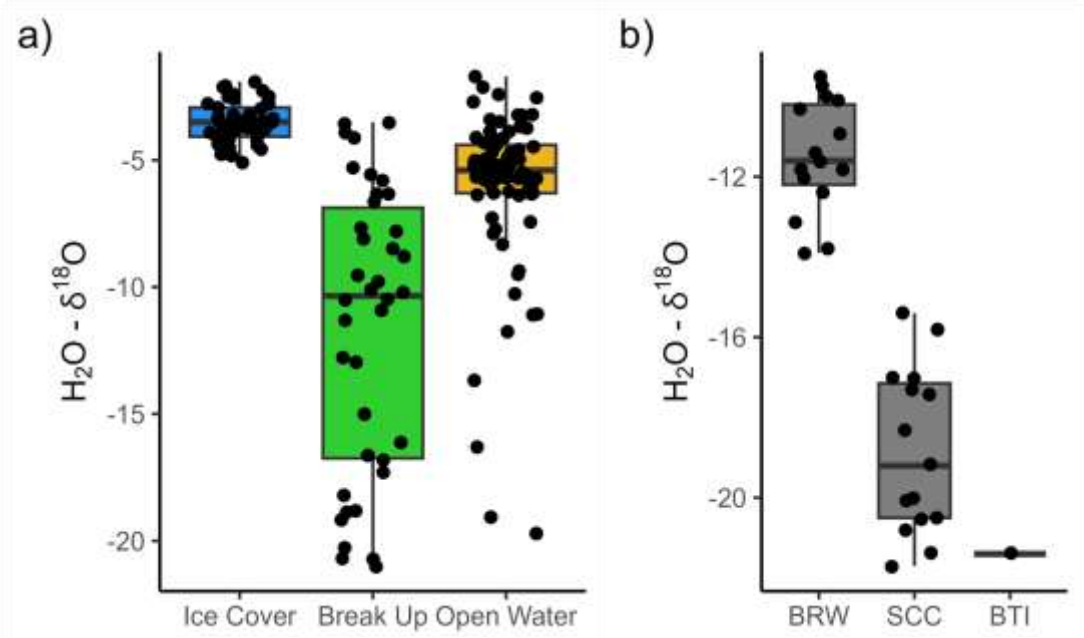

Figure 2.4. a) Lagoon water column H_2O-$\delta^{18}O$ (‰) values during Ice Cover (blue), Break Up (green), and Open Water (yellow). b) Meteoric water H_2O-$\delta^{18}O$ (‰) values from BLE-LTER river stations during Break Up and Open Water separated by node, moving from west to east (BRW, SCC, BTI).

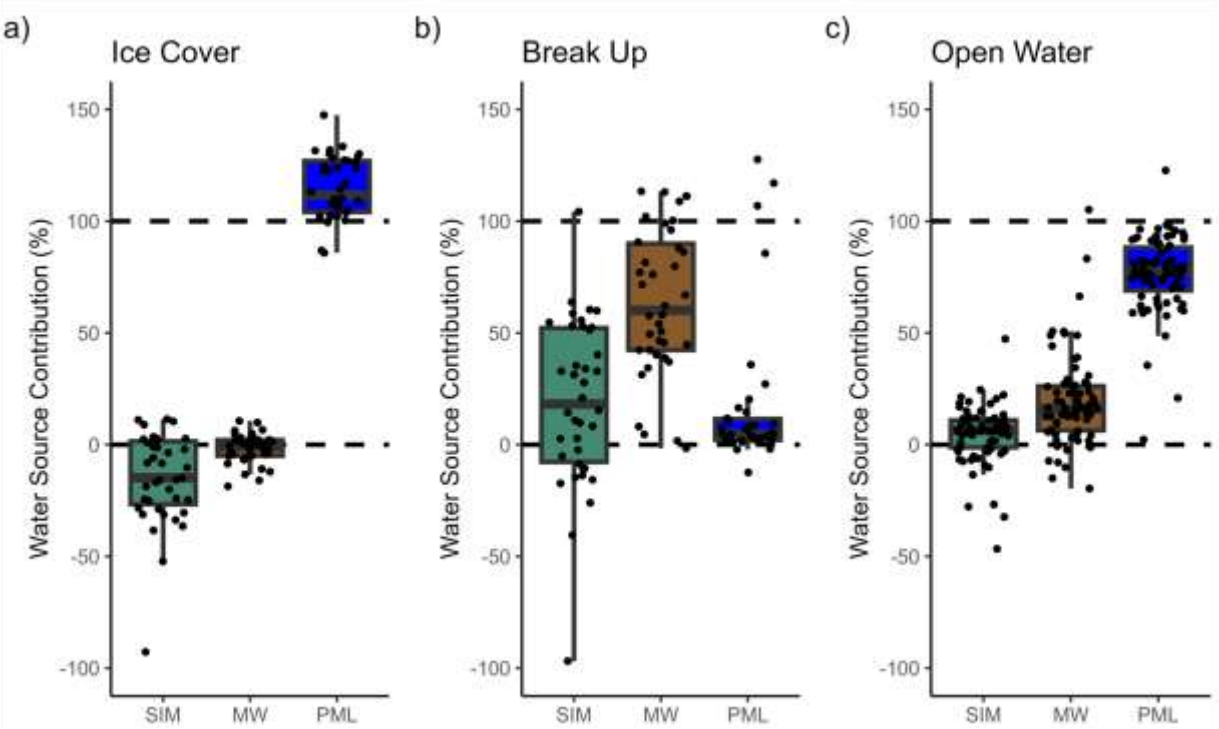

Figure 2.5. Water source contribution (%) from sea ice melt (SIM; green), riverine input (meteoric water, MW; brown), and polar mixed layer (PML; blue), according to salinity and H_2O-$\delta^{18}O$ mixing model output during a) Ice Cover, b) Break Up, and c) Open Water. Each panel shows contributions from each water source. Dashed lines represent 0% and 100% contribution from a water source.

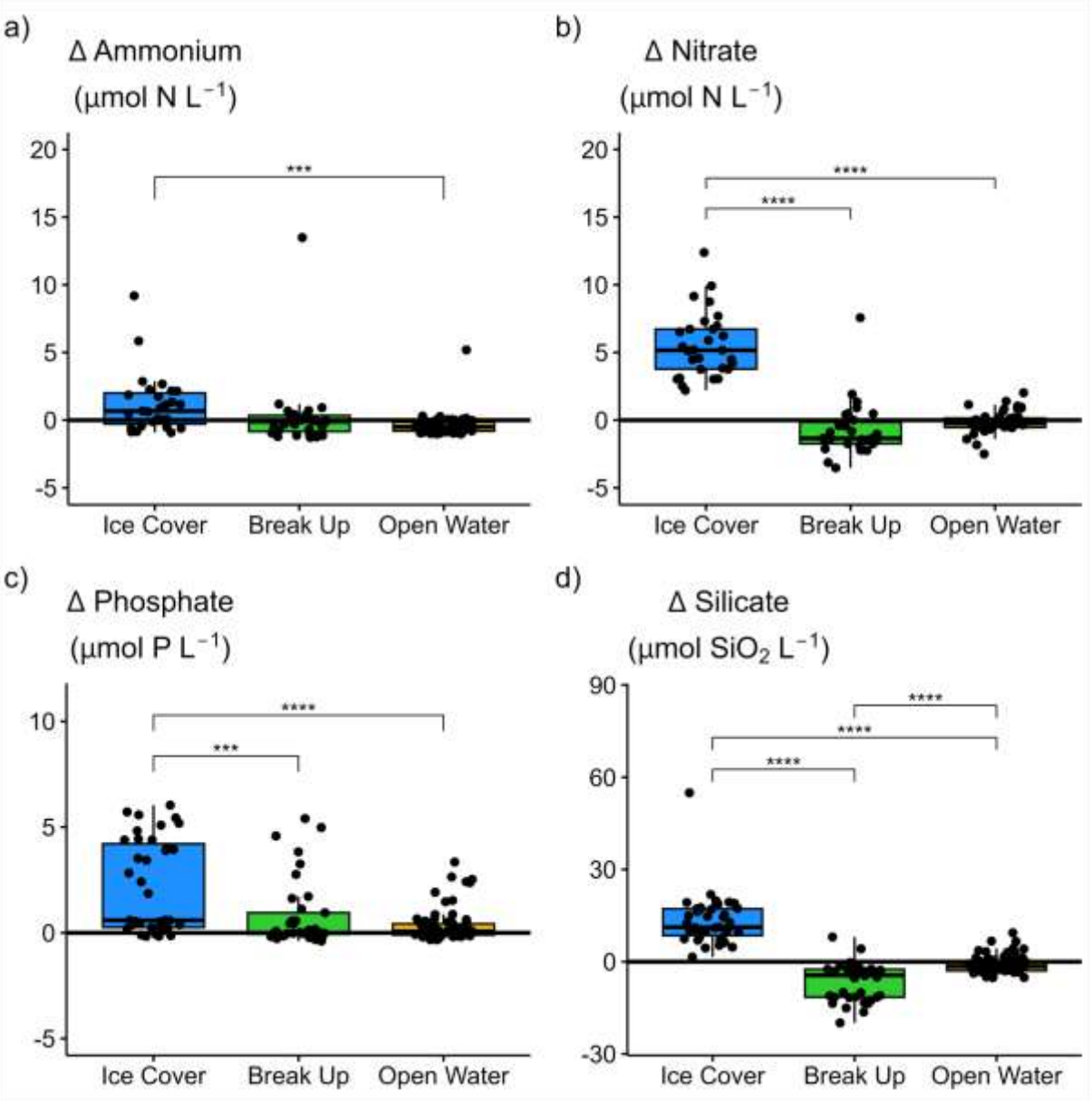

Figure 2.6. Net nutrient production and consumption (ΔN) according to deviations from the conservative mixing line of a) ammonium, b) nitrate, c) phosphate, and d) dissolved silica during Ice Cover (blue), Break Up (green), and Open Water (yellow). Positive ΔN values indicate net production, and negative ΔN values indicate net consumption. The solid black lines within each box represent the median ΔN concentration. Brackets represent significant seasonal differences with asterisks denoting level of significance (*<0.05, **<0.01, ***<0.001, ****<0.0001).

2.10 Appendix A

Supplemental Table 2.1. Summary of nutrient analysis specification for ammonium (NH_4^+), orthophosphate (PO_4^{3-}), nitrate (NO_3^-) and nitrite (NO_2^-), and dissolved silica (DSi) for the Lachat autoanalyzer and FIAlyzer-1000.

	Chemistry	Unit	Reaction	Wavelength (nm)	Detection limit	Applicable Range
Lachat	NH_4^+	ug N L^{-1}	Berthelot indophenol blue	540	0.7	5-600
	PO_4^{3-}	µg P L^{-1}	Phosphomolybdenum blue complex	880	1.0	4-400
	NO_2^- + NO_3^-	mg N L^{-1}	N-1-Napthylethelendiamine dihydrochloride (azo dye)	540	0.025	0.25-30
	SiO_2	mg SiO_2 L^{-1}	Molybdenum blue	820	0.2	1202-6009
FIA	NH_4^+	umol N L^{-1}	OPA fluorescence	NA	0.5	0.5-20
	PO_4^{3-}	µmol P L^{-1}	Phosphomolybdenum blue complex	880	0.05	0.25-10
	NO_2^- + NO_3^-	µmol N L^{-1}	N-1-Napthylethelendiamine dihydrochloride (azo dye)	540	0.05	0.5-50
	SiO_2	µmol SiO_2 L^{-1}	Molybdenum blue	820	0.10	1-100

Supplementary Table 2.2. Two-way ANOVA results on the effect of season and node on inorganic nutrient concentrations (NH_4^+, NO_3^-, PO_4^{3-}, DSi).

2-way ANOVA NH_4^+	Sum of Squares	Df	Mean Square	F	P
Season	74.2	2	37.11	8.223	0.000402
Node	18.3	2	9.17	2.032	0.134587
Season:node	21.5	4	5.37	1.190	0.317218
Tukey HSD Season	**p adj**				
break up - ice cover	0.0446868				
open water - ice cover	0.0002485				
open water - break up	0.5912008				
2-way ANOVA NO_3^- + NO_2^-	**Sum of Squares**	**Df**	**Mean Square**	**F**	**P**
Season	690.2	2	345.1	131.251	<2e-16
Node	37.2	2	18.6	7.074	0.00115
Season:node	47.0	4	11.7	4.468	0.00192
Tukey HSD Season	**p adj**				
break up - ice cover	0				
open water - ice cover	0				
open water - break up	0.0096162				
Tukey HSD Node	**p adj**	**P adj**			
		Under ice	**Break up**	**Open water**	
SCC - BRW	0.238904	-----	-----	-----	
BTI - BRW	0.0374547	0.000	1.000	1.000	
BTI - SCC	0.0008664	0.002	0.948	0.999	
2-way ANOVA PO_4^{3-}	**Sum of Squares**	**Df**	**Mean Square**	**F**	**P**
Season	77.1	2	38.53	19.155	3.31e-8
Node	12.2	2	6.12	3.045	0.0503
Season:node	8.4	4	2.10	1.044	0.3861
Tukey HSD Season	**P adj**				
break up - ice cover	0.0000883				
open water - ice cover	0				
open water - break up	0.5743207				
Tukey HSD Node	**P adj**				
SCC - BRW	0.3590742				
BTI - BRW	0.380478				
BTI - SCC	0.0437912				
2-way ANOVA DSi	**Sum of Squares**	**Df**	**Mean Square**	**F**	**P**
Season	5143	2	2571.4	65.76	2e-16
Node	1231	2	615.7	15.74	5.48e-7
Season:node	707	4	176.7	4.52	0.00172
Tukey HSD Season	**P adj**				
break up - ice cover	0				
open water - ice cover	0				
open water - break up	0.8772881				
Tukey HSD Node	**P adj**	**P adj**			
		Under ice	**Break up**	**Open water**	
SCC - BRW	0.0000069	0.995	0.001	0.000	
BTI - BRW	0.8533337	-----	-----	-----	
BTI - SCC	0.0000567	0.538	0.346	0.053	

Supplementary Table 2.3. Multiple linear regression analysis results for environmental parameters (water column temperature, salinity, dissolved oxygen (DO), H_2O-$\delta^{18}O$) that may influence water column inorganic nutrient concentrations. For each parameter we calculated 1) slope: the estimated regression coefficient of the linear regression, 2) p-value: the statistical significance of the regression coefficient, 3) lmg: the relative importance of each parameter in explaining data variability, and 4) variance inflation factor (VIF): a measure of collinearity among independent variables, where values between 1 and 4 were considered an acceptable level of correlation between independent variables.

Multiple Regression	slope	p value	lmg	VIF
Ammonium				
Intercept	6.89	0.0001	NA	NA
Temperature (°C)	-0.17	0.0001	0.45	1.17
Salinity	-0.02	0.50	0.06	2.74
DO (mg L^{-1})	-0.40	0.0001	0.46	1.24
$\delta^{18}O$ (‰)	0.02	0.77	0.02	2.22
Nitrate				
Intercept	1.84	0.21	NA	NA
Temperature (°C)	-0.31	3.13×10^{-14}	0.70	1.15
Salinity	0.07	0.0006	0.17	2.89
DO (mg L^{-1})	-0.16	0.078	0.05	1.34
$\delta^{18}O$ (‰)	-0.19	0.0001	0.08	2.28
Phosphate				
Intercept	3.19	0.006	NA	NA
Temperature (°C)	-0.13	7.66×10^{-6}	0.56	1.16
Salinity	-0.004	0.78	0.16	2.81
DO (mg L^{-1})	-0.06	0.36	0.02	1.29
$\delta^{18}O$ (‰)	0.09	0.017	0.26	2.27
Dissolved Silica				
Intercept	2.39	0.63	NA	NA
Temperature (°C)	-0.84	5.86×10^{-10}	0.42	1.16
Salinity	0.38	3.51×10^{-7}	0.21	2.81
DO (mg L^{-1})	-0.60	0.49	0.06	1.29
$\delta^{18}O$ (‰)	-1.29	2.36×10^{-12}	0.31	2.27

Supplementary Table 2.4. A two-way ANOVA was performed to analyze the effect of node and season on lagoon and river H_2O-$\delta^{18}O$ values.

Lagoon H_2O-$\delta^{18}O$	Sum of Squares	Df	Mean Square	F	P
Season	1399.4	2	699.7	74.201	2E-16
Node	396.2	2	198.1	21.010	8.79×10^{-9}
Season:node	203.7	4	50.9	5.401	0.000429
Tukey HSD Season	**p adj**				
break up - ice cover	0				
open water - ice cover	4.21×10^{-5}				
open water - break up	0				
Tukey HSD Node	**p adj**	**P adj**			
		Ice cover	**Break up**	**Open water**	
SCC - BRW	9.25×10^{-9}	0.9999767	0	0.00159	
BTI - BRW	0.3305284	-----	-----	-----	
BTI - SCC	0.0009905	1	0.0071498	0.2239404	
River H_2O-$\delta^{18}O$	**Sum of Squares**	**Df**	**Mean Square**	**F**	**P**
Season	5.5	1	5.48	1.647	0.211
Node	436.4	2	218.18	65.555	6.98×10^{-11}
Season:node	1.3	1	1.26	0.380	0.543
Residuals	86.5		3.33		
Tukey HSD Node	**p adj**				
SCC - BRW	9.497×10^{-11}				
BTI - BRW	0.0000988				
BTI - SCC	0.5067238				

Supplementary Table 2.5. A two-way ANOVA was performed to analyze the effect of node and season on the contribution of sea ice melt (SIM), meteoric water (MW), and the polar mixed layer (PML) to the lagoon.

2-way ANOVA SIM	Sum of Squares	Df	Mean Square	F	P
Season	2.263	2	1.1314	21.992	4.63E-9
Node	0.341	2	0.1706	3.317	0.0391
Season:node	0.203	4	0.0507	0.987	0.4172
Tukey HSD Season	**p adj**				
break up - ice cover	0				
open water - ice cover	0.0000634				
open water - break up	0.0047784				
Tukey HSD Node	**p adj**				
SCC - BRW	0.034055				
BTI - BRW	0.3015366				
BTI - SCC	0.8284208				
2-way ANOVA MW	**Sum of Squares**	**Df**	**Mean Square**	**F**	**P**
Season	8.782	2	4.391	101.947	2E-16
Node	0.669	2	0.334	7.762	0.000629
Season:node	0.401	4	0.1	2.33	0.058809
Residuals	6.202	144	0.043		
Tukey HSD Season	**p adj**				
break up - ice cover	0				
open water - ice cover	2.80E-06				
open water - break up	0				
Tukey HSD Node	**p adj**	**P adj**			
		Under ice	**Break up**	**Open water**	
SCC - BRW	0.014435	1.000	0.412	0.588	
BTI - BRW	0.3925019	-----	-----	-----	
BTI - SCC	0.0011145	1.000	0.002	0.370	
2-way ANOVA PML	**Sum of Squares**	**Df**	**Mean Square**	**F**	**P**
Season	19.398	2	9.699	201.991	2E-16
Node	0.459	2	0.229	4.778	0.00979
Season:node	0.305	4	0.076	1.589	0.18037
Residuals	304.42	143	2.13		
Tukey HSD Season	**P adj**				
break up - ice cover	0				
open water - ice cover	0				
open water - break up	0				
Tukey HSD Node	**P adj**				
SCC - BRW	0.9968333				
BTI - BRW	0.0170545				
BTI - SCC	0.0142865				

Supplementary Table 2.6. A two-way ANOVA was performed to analyze the effect of node and season on the flux (ΔN deviation between $N_{Conserved}$ and $N_{observed}$) of inorganic nutrients (NH_4^+, NO_3^-, PO_4^{3-}, DSi).

2-way ANOVA ΔNH_4^+	Sum of Squares	Df	Mean Square	F	P
Season	46.8	2	23.41	6.943	0.00146
Node	0	1	0.001	0	0.98574
Season:node	0.3	2	0.145	0.043	0.95804
Tukey HSD Season	**p adj**				
break up - ice cover	0.1509283				
open water - ice cover	0.0009632				
open water - break up	0.2893688				
2-way ANOVA $\Delta NO_3^- + NO_2^-$	**Sum of Squares**	**Df**	**Mean Square**	**F**	**P**
Season	768.1	2	384	136.306	2E-16
Node	2.8	1	2.8	0.983	0.324
Season:node	1.8	2	0.9	0.324	0.724
Tukey HSD Season	**p adj**				
break up - ice cover	0				
open water - ice cover	0				
open water - break up	0.2815169				
2-way ANOVA ΔPO_4^{3-}	**Sum of Squares**	**Df**	**Mean Square**	**F**	**P**
Season	82.84	2	41.42	19.456	3.36E-08
Node	6.62	2	3.31	1.555	0.215
Season:node	5	4	1.25	0.587	0.673
Tukey HSD Season	**P adj**				
break up - ice cover	0.000331				
open water - ice cover	0				
open water - break up	0.2416778				
2-way ANOVA ΔDSi	**Sum of Squares**	**Df**	**Mean Square**	**F**	**P**
Season	8486	2	4243	165.864	2E-16
Node	141	2	70	2.75	0.0673
Season:node	906	4	227	8.858	2.03E-06
Tukey HSD Season	**P adj**				
break up - ice cover	0				
open water - ice cover	0				
open water - break up	3.00E-07				
Tukey HSD Node	**P adj**	**P adj**			
		Under ice	**Break up**	**Open water**	
SCC - BRW	0.0598149	0.988	0.000	0.998	
BTI - BRW	0.3607088	-----	-----	-----	
BTI - SCC	0.8617228	-----	-----	-----	

Chapter 3: Physical drivers of sediment distribution and organic matter oxidation in coastal Arctic lagoons

3.1 Abstract

The Arctic is warming at a rate four times the global average. With this warming, Alaska's northern coastal ecosystem will continue to experience drastic increases in temperature, ice-free duration, coastal erosion, and river inputs. At the intersection of land, sea, and atmosphere, coastal lagoons act as bioreactors, processing both terrestrial and autochthonous organic matter before export to the coastal ocean. While terrestrial inputs are driving increasing rates of primary production in the Arctic Ocean, the role of nearshore coastal retention and processing of this material before export off the coast remains underexplored. In this study, we investigated the seasonal trends and spatial distribution of sediment characteristics (SOC, SON, C:N ratio, $\delta^{13}C$, $\delta^{15}N$, porosity, grain size) across five coastal Arctic lagoons along the Beaufort Sea coast and identified potential environmental drivers of benthic oxygen (O_2) consumption. Sediments were collected as part of the Beaufort Lagoon Ecosystems Long-Term Ecological Research (BLE-LTER) program from 2019 to 2022, and samples for diffusive O_2 uptake (DOU) were collected in Elson Lagoon in 2022. In alignment with the major hydrological phases, samples were collected during complete sea Ice Cover (April), Break Up (June), and the Open Water period (August). The results of this study demonstrate that surface sediment characteristics in coastal lagoons along the Alaskan Beaufort Sea coast are primarily influenced by physical differences in geomorphology and terrestrial inputs. Sediment grain size, organic matter content, and stable isotopic composition consistently differed between lagoons and water depths, reflecting variability in organic matter source, quantity,

and processing. DOU rates for Elson Lagoon ranged from 0.22 - 1.96 mmol O_2 m^2 d^{-1} and were primarily explained by SOC distribution, while also showing a seasonal component, with higher sediment respiration at Deep stations during the Open Water period with warmer waters. Here, we discuss the physical and spatial variations within and between BLE-LTER lagoon sites that influence the quantity, distribution, and composition of surface sediment organic matter and microbial SOC remineralization.

3.2 Introduction

Coastal marine zones receive, retain, and process significant amounts of terrestrial organic matter, making them among the most biologically active areas of the biosphere (Bianchi et al., 2018; Canuel & Hardison, 2016; Duarte, 2017). The coastal margin is a known hotspot of organic carbon burial in the ocean, with river deltas and non-deltaic shelf regions burying significantly more carbon (70+ Tg C y^{-1}) compared to the open ocean (6 Tg C y^{-1}; Bianchi et al., 2018; Burdige, 2005). These ecosystems function as hotspots of carbon burial due to high inputs of autochthonous and allochthonous production. Receiving resources from both land and sea, coastal zones support a diverse array of primary producers ranging from benthic microalgae to mangrove forests that outperform terrestrial counterparts per unit area (Mcleod et al., 2011). In fact, while coastal vegetated habitats represent < 0.2% of the area of the ocean, they account for at least 50% of the total marine carbon sequestration (Duarte, 2017; Duarte et al., 2005) and exhibit burial rates up to 40 times higher than tropical rainforests per unit area (Mcleod et al., 2011). In addition to autochthonous production, coastal zones receive significant inputs of terrestrial organic matter through river discharge and coastal erosion with approximately one third of the organic matter in marine sediments being of terrestrial origin (Burdige, 2005).

While it has been long established that continental shelves represent the largest sink of both terrestrial and marine carbon globally (Bianchi et al., 2018; Burdige, 2005; Muller-Karger et al., 2005), the coastal margin exhibits large spatial and temporal heterogeneity and will be subject to extreme environmental shifts in the coming decades due to climate change (Canuel et al., 2012). There is significant interest in the processing

and transformation of organic matter in the continental margin, ranging from identifying the source and fate of organic carbon released into the coast (Bianchi et al., 2016; Blair & Aller, 2012; Ward, 2017), to determining whether the coastal ocean is a net source or sink of CO_2 to the atmosphere (Cai, 2011; Miller et al., 2021).

One such system is coastal Arctic lagoons, which represent >50% of the Alaskan Arctic coastline (Wiseman et al. 1973). In Alaska, the Beaufort Sea coast contains numerous shallow estuarine lagoons enclosed by barrier islands with tributaries and rivers that primarily drain Arctic coastal plains in the west and the Brooks Range in the east (Dunton et al., 2006). Forming a physical boundary, barrier islands obstruct the free exchange of water between the lagoons and the Beaufort Sea, impacting their hydrography and creating shallow systems with a seasonally and spatially variable estuarine environment (Fraley et al., 2021; Miller et al., 2021). Variations in barrier island morphology play a crucial role in shaping the hydrological balance between fresh and marine waters, creating a wide range of salinities, circulation patterns, and flushing times that impact their hydrodynamics and overall ecological dynamics (Snedden et al., 2023; Weingartner et al., 2017). The morphological features of coastal lagoons, including the network of barrier islands, channels, and tidal flats, all influence residence time and therefore burial of organic carbon in sediments (Bianchi et al., 2018; Petti et al., 2018), with higher residence times associated with higher rates of sediment trapping, accumulation, and burial (Hanna et al., 2018; Nichols, 1989). Sediment accumulation rates in coastal lagoons vary globally, (0.09 - 0.70 cm y^{-1}, Cuellar-Martinez et al., 2017), but the few rates available in Arctic lagoons are within the global range (Simpson Lagoon:

0.02 - 0.46 cm y^{-1}, Hanna et al., 2018; Elson Lagoon: 0.23 - 0.27 cm y^{-1}, Naidu et al., 2003).

In the Arctic, the large seasonal pulse in the transport of terrestrial material through river discharge and permafrost erosion substantially contributes to carbon burial. The Arctic Ocean, which is almost land locked, receives the discharge of some of the world's largest rivers, representing 11% of global river discharge while accounting for only 1% of the global ocean volume (McClelland et al., 2012). The spring freshet, an annual discharge event in major Arctic rivers lasting approximately 2-4 weeks, contributes the vast majority of freshwater inflow to the coast and Arctic Ocean (Ahmed et al., 2020). With drainage basins consisting of primarily permafrost soils, Arctic rivers function as a major vector of ancient organic carbon export to the coastal environment (Benner et al., 2004; Connolly et al., 2020; McClelland et al., 2014). In fact, the carbon-rich soils at higher latitudes result in a disproportionate export of organic carbon via rivers to the Arctic Ocean as compared to other major basins (Dittmar & Kattner, 2003; McClelland et al., 2014). While freshwater inflow facilitates ice break up, the lagoons remain largely ice-covered until late June. This lag between the freshet in May and ice break up in June promotes retention and biological processing of river derived inputs (Weingartner et al., 2017), including vast quantities of dissolved organic matter (DOM), particulate organic matter (POM), and dissolved inorganic nutrients (McClelland et al., 2012, 2014, 2016).

Coastal erosion is also a significant source of sediment and carbon to the Arctic and may have doubled since 1955 (Rowland et al., 2010). Due to the uneven geomorphology along the Beaufort Sea coastline, erosion rates and quantities of sediment delivered to the nearshore zone exhibit wide variability (Lantuit et al., 2013).

Rates of coastal erosion in the Arctic (0.5 m $year^{-1}$) are known to be among the highest in the world, due in part to the ice-bonded nature of the coastal sediments (Jones et al., 2009; Lantuit et al., 2012). Although erosion rates vary along the Beaufort Sea coast, ranging from <1 m $year^{-1}$ in the Yukon and Kaktovik (Couture et al., 2018) to more than 8 m $year^{-1}$ at Drew Point (Barnhart et al., 2014), the Beaufort Sea coastline as a whole is characterized by the strongest retreat in the Arctic, with coastal erosion rates exceeding 1.1 m $year^{-1}$ on average (Lantuit et al., 2012). Additionally, erosion rates along the Arctic coast have been accelerating due to the increasing length of the ice-free period (Barnhart et al., 2014; Günther et al., 2013; Overeem et al., 2011). These terrestrial inputs are further confirmed by Arctic shelf sediment biomarker and stable carbon isotopes which indicate highly degraded materials derived from vascular plants (Goñi et al., 2000; Van Dongen et al., 2008), with the potential for preferential burial of permafrost-derived organic carbon in Arctic shelf waters (Jong et al., 2024).

Sediment distribution and preservation dynamics can be seasonally influenced by several physical factors including coastal geomorphology, grain size, and water depth. During the ice cover period, sea ice reaches the sediments (~November) within narrow straits and coastal areas, creating landfast ice (Mahoney et al., 2014; Trishchenko et al., 2022). On the Beaufort Sea coast, the sea ice is on average 1.7 meters thick, lasting for ~9 months (Harris et al., 2017; Pedrazas et al., 2020). As the sea ice grows down toward the benthos, it can trap sediments, incorporating them into the ice matrix. This process can then lead to the transport of sediments and associated organic matter within the ice during the spring melt and subsequent release back into the water column during the melting season (Eicken et al., 2005; Ito et al., 2019; Wegner et al., 2017). During the open

water period when the lagoons are free of sea ice cover, their shallow nature makes the sediments particularly susceptible to wave-induced sediment resuspension (Carr et al., 2010; Lawson et al., 2007; Macdonald et al., 2015). In particular, fine-grained sediments such as silt (<65 μm), which are commonly found in the Arctic, are subject to sediment resuspension (Macdonald et al., 2015; Radosavljevic et al., 2022) due to their low mobilization threshold (Eidam et al., 2024). Through this disturbance and re-working, sediments are exposed to oxygenated water, enhancing remineralization of organic matter, and decreasing burial efficiency (Burdige, 2005; Wainright & Hopkinson, 1997; Yahel et al., 2008).

Sediments and associated organic matter in the coastal Arctic are therefore influenced by a complex interaction of factors including sea ice cover, river export, coastal erosion, and microbial activity. With projected decreases in sea ice cover (Frey et al., 2015; Markus et al., 2009; Stroeve et al., 2014) and increases in coastal erosion (Jones et al., 2009; Barnhart et al., 2014b; Günther et al., 2013; Overeem et al., 2011) and river discharge (Ahmed et al., 2020; Proshutinsky et al. 2015), the Arctic is undergoing rapid changes, and the fate of the organic matter within these lagoons is not well defined. The processing of this organic matter as climate changes will have significant implications for carbon and nutrient cycling within the coastal Arctic environment. The overarching objectives of this study were therefore to 1) quantify and describe sediment grain size and organic matter distribution across several Beaufort Sea lagoons, 2) quantify dissolved O_2 uptake (DOU) rates for Elson Lagoon over time and space, and 3) identify potential environmental drivers of DOU rates in Elson Lagoon.

3.3 Methods

3.3.1 BLE-LTER Study Site Description

The study area is composed of several lagoons and sounds along the northern coast of Alaska bordering the Beaufort Sea. These lagoons and sounds are part of the Beaufort Lagoon Ecosystems Long-Term Ecological Research (BLE-LTER) program (ble.lternet.edu) which spans ~100 km of the Alaskan coastline and operates out of three nodes, Utqiaġvik (formerly Barrow; BRW), Prudhoe Bay (SCC), and Barter Island (BTI) (Fig. 3.1). These three nodes, which represent the western, central, and eastern portions of Alaska's Beaufort Sea coast, differ in their relative contribution from terrestrial inputs, circulation, ocean exchange, and sea ice dynamics (Table 3.1). Each node has two lagoons.

The BLE-LTER's westernmost node is based out of Utqiaġvik and contains Elson Lagoon (Fig. 3.1b,c; Table 3.1). Elson Lagoon sits at the intersection between the Chukchi Sea to the west and the Beaufort Sea to the north. Elson lagoon is ~25 km long, and 6 km wide and bound by well-defined barrier islands. In addition to the three intermittent tidal inlets, the eastern side of the lagoon contains the mouth of Avak Creek and a 3.7 km-wide passage to the Beaufort Sea. The average depth of Elson Lagoon is 2.4 m, with an area of 207 km^2 and volume of 0.50 km^3. Elson Lagoon has the second lowest mean depth of the BLE-LTER lagoons partially due to the larger percentage of lagoon area with shallow depths (Table 3.1, Supplementary Figure 3.1). Placed in the Arctic lowland and foothills, Elson Lagoon receives terrestrial runoff from several small tributaries, creeks, and rivers (Rawlins et al. 2021).

The BLE-LTER's central node is located in the middle of the Alaskan Beaufort Sea coastline and is based at the Prudhoe Bay oil field (Fig. 3.1b,d,e; Table 3.1). Simpson Lagoon is located to the west of Prudhoe Bay and Stefansson Sound to the east (Fig. 3.1b). Like Elson Lagoon, Simpson Lagoon is bound by well-defined barrier islands and is ~25 km long and 6 km wide (Fig. 3.1d). There are two tidal inlets along the western barrier islands and one to the east. To the west and east, Simpson Lagoon opens to the Beaufort Sea and the mouths of the Colville and Kuparuk rivers, respectively. In addition to the two major rivers at the far ends of Simpson Lagoon, there are also several tributaries that flow directly into the lagoon. Simpson Lagoon is the shallowest of the lagoons with an average depth of 1.8 m, an area of 173 km^2 and a volume of 0.30 km^3. Although similar in size, Simpson Lagoon and Elson Lagoon differ considerably in terms of riverine inputs and marine connectivity. Unlike Simpson Lagoon which receives high river inputs from the Colville and Kuparuk rivers, Elson Lagoon receives only minor riverine inputs from Avak Creek and some small tributaries and is only open to the Beaufort Sea on the eastern end with the western boundary enclosed by a continuous barrier island (Point Barrow; Fig. 3.1c). In contrast to the other lagoons, Stefansson Sound is the least enclosed study site of the BLE-LTER with four small (3-5 km wide) barrier islands located ~14 km off the coast (Fig. 3.1e). With wide openings rather than small tidal inlets, Stefansson Sound is exposed to much more marine influence. From land, the Sagavanirktok River empties directly into Stefansson Sound with two separate inflows. With an average depth of 4.3 m, area of 749 km^2, and a volume of 3.25 km^3, Stefansson Sound is the deepest and largest BLE-LTER coastal system by both area and volume (Table 3.1, Supplementary Figure 3.1).

The BLE-LTER's easternmost node is based out of the village of Kaktovik and contains Kaktovik and Jago Lagoons, the smallest of the BLE-LTER lagoons (Fig. 3.1b,f; Table 3.1). Both lagoons are ~7 km long and are enclosed by well-defined barrier islands. Kaktovik Lagoon connects to Arey Lagoon in the west through a series of winding channels and to Jago Lagoon in the east through a 1 km wide channel. With no direct tidal inlet or major river, Kaktovik Lagoon experiences the least marine exchange and freshwater through surface runoff. In contrast, Jago Lagoon receives inputs from the Jago River to the east as well as a narrow (0.5 km) tidal inlet to the Beaufort Sea. Both lagoons are also relatively shallow (Kaktovik: 2.8 m, Jago 2.6 m) and have the smallest area and volume (Table 3.1).

3.3.2 BLE-LTER Core Program sediment sampling

To investigate spatial variability of surface sediments along the coast and within each lagoon, samples were collected at the six BLE-LTER lagoons, with each lagoon containing two shallow (<1 m water depth) and two deep (3-5 m water depth) stations (Fig. 3.1). To examine potential seasonal dynamics, sediment samples were collected in alignment with the major hydrological phases of Ice Cover (April), Break Up (June), and Open Water (August). During the Ice Cover period, samples were collected at deep stations but not at shallow stations due to the presence of landfast ice. Sediment samples were collected annually from 2019 - 2021 across all six lagoons, with some exceptions in 2020 and 2021 due to the COVID-19 pandemic. In 2020 no sampling occurred; however, in 2021, sample collection resumed for BRW and SCC during Ice Cover and BTI during Open Water.

BLE-LTER Core Program sediment samples were collected using a 20.3 cm^2 sediment PONAR grab for sediment organic carbon and nitrogen, stable carbon and nitrogen isotopes ($\delta^{13}C$, $\delta^{15}N$), and benthic pigments. Organic carbon and nitrogen content and stable isotopes (n=1) were subsampled from the top 2 cm of the PONAR grab sample using a modified 20 mL syringe (I.D.: 1 cm, vol.: 5 mL). Wet sediment samples were transferred to a 7 mL snap cap vial, dried in the oven at 60^oC, and stored at room temperature until analysis at The University of Texas Marine Science Institute (UTMSI). Grain size samples (depth: 10 cm) were collected opportunistically from PONAR grabs in 2021 using a modified 60 mL syringe (I.D.: 2.5 cm, vol.: 60 mL) and frozen at -20^oC until analysis.

3.3.3 Elson Lagoon focused study sampling

In addition to the BLE-LTER Core Program sediment samples, we conducted a focused study in Elson Lagoon (BRW, the westernmost node) during Open Water 2022 and Ice Cover 2023. Alongside bulk organic matter content, we measured sediment porosity, grain size, and benthic diffusive oxygen uptake (DOU) rates to investigate the environmental drivers of benthic organic matter respiration. For this focused study, sediment samples were collected using a HYPOX sediment corer (Gardner et al., 2009) to better retain vertical sediment structure integrity and minimize potential disturbances at the sediment-water interface. Sediment cores (I.D.: 5 cm, height: 20 cm, sediment depth: 15 cm) were collected in triplicate at 2 deep stations during Ice Cover and 4 deep and 4 shallow stations during Open Water. One sediment core was used to measure DOU rates while the other two cores were used for sediment characterization. For the sediment characterization cores, we gently extruded and collected the top 2 cm, transferred to 18

oz Whirl-Pak bags, and froze the samples at -20°C until analysis for grain size, porosity, and bulk organic matter content.

3.3.4 Organic carbon and nitrogen content and stable isotopes

For the BLE-LTER dataset, sediment organic carbon (SOC, %) and sediment organic nitrogen (SON, %) content and stable isotopic composition ($\delta^{13}C$ and $\delta^{15}N$, ‰) were analyzed at the Core Facilities Laboratory at UTMSI. Prior to analysis, samples for carbon content and $\delta^{13}C$ were acidified with 10% HCl to remove any carbonates (Hedges & Stern, 1984). Acidification was carried out in silver capsules using 20-40 mg of dry sediment, which were then wrapped in tin capsules. Samples for nitrogen content and $\delta^{15}N$ were not acidified. Once wrapped, samples were analyzed using a Thermo Fisher EA-Isolink-CNSOH coupled to a Thermo Fisher Scientific Delta V continuous flow (He) stable isotope ratio mass spectrometer. Isotopic composition is presented using the conventional δ-notation (Equation 3.1):

Equation 3.1. $\delta^{13}C$ or $\delta^{15}N$ (‰) = $[(R_{sample}/R_{standard})-1]$,

where

R_{sample} and $R_{standard}$ = $^{13}C/^{12}C$ or $^{15}N/^{14}N$ of the sample and analytical standard, respectively. A two-point calibration of $\delta^{13}C$ or $\delta^{15}N$ to VPDB or AIR, respectively, was achieved using USGS-40 ($\delta^{13}C$ =−26.39 ‰, $\delta^{15}N$ =−4.5 ‰) and USGS-41a ($\delta^{13}C$ = +36.55 ‰, $\delta^{15}N$ = +47.55 ‰) standards. An internal standard (Casein protein; $\delta^{13}C$ = -26.98 ‰, $\delta^{15}N$ = +65.94 ‰) was used to confirm instrument accuracy and analytical precision (≤ ±0.2‰ standard deviation).

3.3.5 Sediment grain size

For both the BLE-LTER dataset and the Elson Lagoon focused study, sediment grain size was analyzed using a Beckman Coulter LS 13 320 Laser Diffraction Particle Size Analyzer (LDPSA) with an aqueous module in the Coastal Geology Lab at the Virginia Institute of Marine Science (VIMS). The LDPSA applies the theory of Fraunhofer diffraction where the size of a particle is proportional to the intensity and angle of light scattered (Loizeau et al., 1994). Prior to analysis, wet sediment samples (2-4 mL) were vortexed with 5 mL of a surfactant (Calgone) for particle separation and resuspension during analysis. When the sample is suspended in the aqueous module, it is pumped across the flow-cell, where sensors detect the diffraction of the laser beam and provide the grain size distribution. Based on the Udden-Wentworth size classification, we calculated the percent composition (%) of each sediment class: gravel (>2000 μm), sand (62.5 μm - 2000 μm), silt (4 μm - 62.5 μm), and clay (<4 μm; Wentworth, 1922).

3.3.6 Sediment porosity and bulk organic matter content

For the Elson Lagoon focused study, we measured porosity, bulk sediment organic matter (OM) content, and carbon and nitrogen content. Water content was used as a proxy for porosity, where sediment samples were weighed before and after drying at 60°C for seven days to observe changes in mass due to loss of water (Equation 3.2). Dry sediments were then combusted at 500°C for 5 hours to measure the mass loss on ignition (LOI) for bulk OM content (Equation 3.3),

Equation 3.2. Porosity (%) = $\left(\frac{\text{mass}_{wet} - \text{mass}_{dry}}{\text{mass}_{wet}}\right) * 100$

Equation 3.3. Organic matter content (LOI, %) $= \left(\frac{\text{mass}_{dry} - \text{mass}_{combusted}}{\text{mass}_{dry}}\right) * 100.$

In addition to bulk OM content, dried samples were run on a Thermo Scientific Flash Elemental Analyzer 1112 Series NC Soil Analyzer at VIMS for SOC (%) and SON (%) content (without stable isotopes) using the same sample preparation protocols as for the BLE-LTER samples described above, including acidification with 10% HCl.

3.3.7 Diffusive Oxygen Uptake (DOU)

Diffusive oxygen uptake (DOU) represents aerobic respiration by benthic microbes while excluding oxygen (O_2) uptake by benthic fauna and is widely used in coastal sediments (Arrigo and Dijken, 2011; Hardison et al. 2017; McTigue et al. 2016). DOU was modeled from O_2 profile measurements using a Unisense O_2 microelectrode (Supplemental Fig 3.2). Sensors were calibrated using a 2-point calibration: at 0% O_2 saturation, using a 1:1 mixture of 0.1 M sodium ascorbate and 0.1 M sodium hydroxide, and at 100% O_2 saturation, using fully aerated deionized (DI) water (Unisense, 2020). Oxygen microprofiles were conducted by measuring O_2 concentrations every 0.5 mm moving vertically from the water column, across the sediment-water interface, and into the sediments, until O_2 concentrations reached 0% (Xu et al., 2021; Hardison et al., 2017; Supplemental Fig 3.2). Diffusive O_2 flux (mmol O_2 m^{-2} d^{-1}) was calculated using a classic steady-state one-dimensional equation (Equation 3.4) because concentration and diffusion coefficients are independent of time (Boudreau, 1997):

Equation 3.4. $\varphi\left(\frac{DO_2}{\theta^2}\right)\left(\frac{d^2O_2}{dt^2}\right) = v_{max}\left(\frac{O_2}{O_2+k_{O2}}\right),$

where φ refers to sediment porosity of the core (0-2 cm), DO_2 is the diffusive coefficient for O_2, which is determined by temperature and salinity, θ^2 is tortuosity, which refers to porosity and can be calculated using Equation 3.5 (Boudreau, 1997):

Equation 3.5. $\theta^2 = 1 - ln(\varphi^2)$,

and v_{max} and k_{O2} are Monod-type kinetic parameters that describe O_2 consumption in sediment (Boudreau, 1997; Brin et al., 2014; Hardison et al., 2017; Xu et al., 2021). The model was performed in R (version 4.2.2) using the packages ReacTran (Soetaert and Meysman, 2009) and FME (Soetaert and Petzoldt, 2012).

3.3.8 BLE-LTER lagoon bathymetry

To assess internodal spatial variability in lagoon geomorphology as well as sediment distribution patterns, bathymetry maps were created for each lagoon to calculate water depth and depth distribution within the lagoons. Between 1945 and 1953, the NOAA National Ocean Service (NOS) created hydrographic smooth sheets using single beam soundings along the Beaufort Sea coast which are stored at the National Centers for Environmental Information (NCEI) database (https://www.ncei.noaa.gov/). Although there are more recent surveys with a higher resolution and updated values, the NOS survey provides one cohesive dataset that encompasses all the lagoons in this study (Supplemental Table 3.1). Descriptions from the surveys indicate some access limitations offshore due to sea ice and nearshore due to landfast ice and waters too shallow for safe navigation. To describe coastal geomorphology, we used ArcGIS (v.10.8.2, ESRI) to measure the width of the lagoons and channels on the World Imagery base map. To quantify the bathymetry and volume of each lagoon, we digitized the NOS single beam

sounding transects as described in Zimmermann et al. (2013). First, the scanned NOS maps were georectified using the latitude and longitude intersections as source control points. Due to significant rates of coastal erosion, barrier island migration, and changes in infrastructure, landmarks were not used as reference points. Next, each point depth measurement was manually digitized into a multi-point layer with attribute depth. Once completely digitized, an inverse distance weighted (IDW) interpolation was performed on the multi-point layer, bound by a perimeter polygon with depth 0 m, to create a raster bathymetry map across each lagoon.

3.3.9 Statistical analyses

Due to field logistics and COVID-19 limitations, the dataset was unbalanced. Consequently, we performed permutational multivariate ANOVA (PERMANOVA) for non-parametric data in R (version 4.3.0). PERMANOVA was used to investigate the effects of node (BRW, SCC, BTI), season (Ice Cover, Break Up, Open Water), and water depth (Shallow, Deep) on sediment parameters (SOC, SON, $\delta^{13}C$, $\delta^{15}N$, porosity, grain size). When the PERMANOVA indicated a significant effect at an alpha level of 0.05, a post-hoc pairwise comparison was performed (R package: vegan; Oksanen et al., 2024) to identify the significant independent or interaction effects.

To identify the environmental drivers of sediment DOU, a stepwise multivariate regression model was used to find relationships between observed DOU and environmental parameters. *A priori*, we selected several environmental parameters that are known factors to influence or reflect benthic respiration rates. Sediment DOU was treated as a dependent variable, while water temperature, SOC content, benthic

SOC:SON ratio, porosity, and median grain size were treated as independent variables. In a stepwise selection regression model, predictors are iteratively added and removed to find the subset of variables in the dataset resulting in the lowest prediction error (R package: leaps; Miller, 2020). With the addition and removal of each parameter, the significance of each regression term is tested. Parameter selection and elimination are repeated until the model cannot be significantly improved with new parameters. Three metrics were used to compare the accuracy of the models: root mean square error (RMSE) and mean absolute error (MAE) measure the prediction error of each model, with lower values indicating a better model; R^2 indicates the correlation between the predicted and observed values, with values closer to 1 indicating a better model.

3.4 Results

3.4.1 BLE-LTER sediment organic carbon and nitrogen content and stable isotopes

SOC content did not vary significantly by season but did exhibit spatial variability across nodes as well as water depth (i.e., Shallow and Deep stations; Table 3.2; Supplemental Table 3.2; Fig. 3.2a). Averaged across water depth and season, SOC was higher at BRW (2.0 ± 0.2 %) and BTI (1.5 ± 0.1) compared to SCC (1.0 ± 0.1 %) (Fig. 3.2a, Table 3.2, Supplemental Table 3.2). Averaged across node and season, SOC was significantly lower at Shallow stations (1.0 ± 0.2 %) compared to Deep stations (1.9 ± 0.1 %), with the greatest contrast between Shallow and Deep stations observed in BRW (Table 3.2; Fig. 3.2a). There was no significant difference in SOC between Shallow (1.2 ± 0.3 %) and Deep (0.9 ± 0.1 %) stations at SCC (Table 3.2; Supplemental Table 3.2; Fig. 3.2a).

SON also varied by node and water depth, but also by season. Like SOC, averaged across all depths and seasons, SON was higher at BRW (0.15 ± 0.02 %) and BTI (0.14 ± 0.01 %) compared to SCC (0.08 ± 0.01 %) (Table 3.2; Fig. 3.2b; Supplemental Table 3.2). Averaged across all nodes and seasons, SON was about twice as high at Deep stations (0.15 ± 0.01 %) compared to Shallow stations (0.08 ± 0.01 %) (Fig. 3.2b, Supplemental Table 3.2). And like SOC, there was no significant difference in SON between Shallow (0.09 ± 0.02 %) and Deep (0.08 ± 0.01 %) stations at SCC (Table 3.2; Supplemental Table 3.2; Fig. 3.2b).

Although SOC and SON appeared to change in parallel across nodes (Fig. 3.2a,b), the ratio of SOC:SON (i.e., C:N; Fig. 3.2c) varied significantly by node, decreasing moving from west to east (Supplemental Table 3.2). Averaged across water depth and season, the highest C:N ratios were observed in BRW: 15.3 ± 0.6, followed by SCC: 13.6 ± 0.4, then BTI: 12.2 ± 0.4 (Table 3.2).

SOC-$\delta^{13}C$ values varied across node, water depth, and season, listed in order of significance, although the overall variability was quite small (Table 3.2, Supplemental Table 3.3). Averaged across water depth and seasons, SOC-$\delta^{13}C$ values were significantly more depleted at SCC (-26.3 ± 0.1 ‰) compared to BRW (-25.7 ± 0.2 ‰) and BTI (-25.9 ± 0.1 ‰) (Table 3.2, Fig. 3.3a). Furthermore, interaction effects between node and season revealed that this pattern of SOC-$\delta^{13}C$ primarily occurred during Break Up. When averaged across season and node, SOC-$\delta^{13}C$ values differed significantly, with more enriched SOC-$\delta^{13}C$ at Shallow stations (-25.7 ± 0.2 ‰) compared to Deep stations (-26.2 ± 0.1 ‰). Seasonally, averaged across node and water depth, SOC-$\delta^{13}C$ values were most depleted during Ice Cover (-26.4 ± 0.1 ‰) and became slightly enriched during

Break Up (-25.8 ± 0.2 ‰) and Open Water (-25.9 ± 0.1 ‰; Table 3.2, Supplemental Table 3.3).

SON-$\delta^{15}N$ values did not vary by season or water depth but did vary by node, although like SOC-$\delta^{13}C$ over a narrow range. Averaged across water depth and season, SCC had a lower mean $\delta^{15}N$ values (2.7 ± 0.1 ‰) relative to BRW (3.3 ± 0.1 ‰) and BTI (3.2 ± 0.1 ‰) (Table 3.2, Fig. 3.3b, Supplemental Table 3.3). Significant interaction effects between node and water depth also revealed that the significant inter-nodal differences were primarily observed at Deep stations rather than Shallow stations.

3.4.2 BLE-LTER sediment grain size distribution

Grain size distribution for BLE-LTER sediments did not vary appreciably by season or node but did differ substantially based on water depth (Fig. 3.4a,b Table 3.3, Supplemental Table 3.4). Averaged across nodes, Shallow stations were primarily composed of sand (59 ± 10 %), followed by silt (30 ± 7 %), then clay (11 ± 4 %), with a median grain size of 105 ± 25 μm (Table 3.3). In contrast, Deep stations were dominated by silt (53 ± 3 %), followed by sand (27 ± 4 %), then clay (19 ± 2 %), with a smaller median grain size of 28 ± 5 μm (Table 3.3).

3.4.3 Elson Lagoon sediment characteristics

Sediment characteristics from the focused study of Elson Lagoon (2022) followed the overall trends of the BLE-LTER Core Program samples (2019-2021), with most of the variability explained by water depth and less explained by season (Table 3.4,

Supplemental Table 3.5). Since Shallow stations were not sampled during Ice Cover due to the presence of landfast ice, we performed the Shallow vs. Deep comparison only for Open Water samples (Supplemental Table 3.5). During Open Water, SOC content was higher at Deep stations (2.6 ± 0.1 %) than Shallow stations (0.5 ± 0.2 %) (Fig. 3.5a, Table 3.4). Similarly, SON content was higher at Deep stations (0.20 ± 0.01 %) compared to Shallow stations (0.05 ± 0.01 %). The C:N ratio did not vary over time or space, with an average across seasons and nodes of 15.2 ± 0.9 (Fig. 3.5c, Table 3.4).

Sediment grain size distribution in Elson Lagoon was also consistent with the overall trends of the BLE-LTER Core Program samples, with the variability explained by water depth and not by season (Table 3.4, Supplemental Table 3.5). During Open Water, Shallow stations were primarily composed of sand (70 ± 9 %), and Deep stations were primarily composed of silt (56 ± 2 %) (Fig. 3.4c,d, Table 3.4). Median grain size was considerably higher at Shallow stations (119 ± 28 μm) versus Deep stations (19 ± 5 μm) during Open Water. Grain size for the Deep stations during Ice Cover were similar to Deep stations during Open Water, with silt as the dominant fraction (57 ± 4 %), and a median grain size of 22 ± 7 μm (Table 3.4). During Open Water, sediment porosity in Deep stations (50 ± 3 %) was twice that of Shallow stations (23 ± 2 %; Table 3.4). Porosity for the Deep stations during Ice Cover (52 ± 4 %) was similar to that at Deep stations during Open Water. The porosity values reflect the unconsolidated, fine-grained nature of surface sediments observed at the Deep stations.

3.4.4 Elson Lagoon diffusive oxygen uptake

DOU rates for the Elson Lagoon focused study varied by season and water depth. As with the sediment characteristics for the Elson Lagoon focused study, Shallow stations were not sampled during Ice Cover due to the presence of landfast ice, so we performed the Shallow vs. Deep comparison only for Open Water samples. Similarly, the seasonal comparison was performed for Deep stations only in Ice Cover vs. Open Water (Table 3.4, Supplemental Table 3.5). Sediment DOU rates were lowest at Shallow stations during Open Water (0.48 ± 0.08 mmol O_2 m^{-2} d^{-1}), followed by Deep stations during Ice Cover (0.75 ± 0.07 mmol O_2 m^{-2} d^{-1}), and highest at Deep stations during Open Water (1.42 ± 0.27 mmol O_2 m^{-2} d^{-1}) (Table 3.4; Fig. 3.6a). Average DOU rates at Deep stations were nearly three times as high as Shallow rates during Open Water. DOU rates at Deep stations during Open Water were twice as high as Deep stations during Ice Cover (Fig. 3.6a, Table 3.4, Supplemental Table 3.5).

Previous studies demonstrate that sediment DOU rates can have numerous environmental controls including temperature, sediment organic matter content, water depth, organic carbon lability, porosity, and median grain size, encompassing all variables targeted in this study (Glud, 2008; Jorgensen et al., 2022; Ahmerkamp et al. 2020). To identify potential drivers of sediment DOU, we performed a stepwise selection multivariate regression model to find the subset out of the five variables (bottom water temperature, SOC content (%), C:N ratio, porosity (%), median grain size (μm)) in the data resulting in the lowest prediction error. The stepwise selection linear regression function provided four models with varying (1-4) numbers of parameters (Supplemental Table 3.6). Based on the RMSE, MAE, and adjusted R^2 values, which represent the accuracy of the models,

Model 2 with two parameters (bottom water temperature and SOC content) was selected as the best fitting model. Further analysis of the model demonstrated that SOC content (%) was the dominant explanatory variable for DOU rates in Elson Lagoon, accounting for 72% of the variance, with temperature accounting for the remaining 28% (Table 3.5, Supplemental Table 3.6, Fig. 3.6b).

3.5 Discussion

This study suggests that surface sediment characteristics in coastal lagoons along the Alaskan Beaufort Sea coast are likely linked to physical differences in geomorphology and terrestrial inputs. Sediment grain size, organic matter content, and isotopic composition consistently differed between nodes and water depths. DOU rates in Elson Lagoon also varied by water depth and were primarily explained by SOC distribution, while also exhibiting a seasonal trend. Here, we discuss the physical and spatial variability within and between BLE-LTER lagoon sites that influences the quantity, distribution, and composition of surface sediment organic matter and microbial SOC remineralization.

3.5.1 Sediment organic matter distribution

In this study of Beaufort Sea coastal lagoons, SOC content (average: 1.5 ± 0.1 %, range: 0.1 - 6.7 %) was consistent with previous values for the coasts of the Siberian Sea (0.36 - 1.96 %, Guo et al., 2004; Karlsson et al., 2016) and Chukchi Sea (0.66 - 1.99 %, Goñi et al., 2013; Schreiner et al., 2013). SOC levels in BLE-LTER lagoon sediments varied significantly across nodes and water depths. Between nodes, average SOC concentrations were highest at BRW (2.0 ± 0.2 %), then BTI (1.5 ± 0.1 %), and lowest at

SCC (1.0 ± 0.1 %;), and all fell within the range of 0.1 % to 6.7 %. Notably, deep stations at BTI and BRW had SOC values two to three times higher than SCC deep stations. The overall lower SOC levels at SCC may be attributed to the significantly higher discharge of two large rivers at SCC during the freshet coupled with wider inlets than the other nodes, likely enhancing marine exchange and export to the shelf, rather than entrainment of material within the lagoons.

BRW and SCC had the highest and lowest average SOC levels, respectively. In contrast to Simpson Lagoon and Stefansson Sound (SCC), Elson Lagoon (BRW) had lower river discharge, and smaller inlets, leading to less exchange with the adjacent Beaufort Sea. With less freshwater input and less marine connectivity, Elson Lagoon likely has a longer residence time than lagoons at SCC, allowing for more sediment retention and deposition. In comparison, Kaktovik and Jago Lagoons (BTI) are also more closed off than Simpson Lagoon and Stefansson Sound, and even Elson Lagoon, with only one direct channel reaching the Beaufort Sea. Overall, the two nodes with less marine exchange (BRW, BTI) tended to have higher SOC in Deep stations relative to Shallow stations.

Within each lagoon, the sites were categorized as Shallow or Deep based on water depth, with deep stations (>1.5 m) representing a majority of the lagoons by area (>70%, Table 3.1). The sediments at the Deep stations were mostly fine-grained unconsolidated silt with low settling velocities, suggesting a zone of deposition (Falco et al. 2004). In contrast, Shallow stations had a larger median grain size and were primarily composed of sand, which indicated persistent higher energy conditions and winnowing of low density and fine sediments (Radosavljevic et al., 2022). The separation in median grain size

between Shallow and Deep stations was reflected in SOC, with highest SOC in Deep stations for BRW and BTI and the lowest SOC at Shallow stations for BRW and BTI. This positive relationship between SOC and silt content has been consistently observed in silt and clay-rich sediments which provide a larger surface area and better binding sites for organic carbon (De Falco et al., 2004; Ramaswamy et al., 2008). Although the lagoon sediments are likely subject to frequent resuspension events and some export off the coast, based on the relatively high sediment organic matter content and fine sediment grain composition at deep sites, it appears that the deeper portion of the lagoons function as deposition zones with lower hydrodynamic energy.

3.5.2 Sediment organic matter source

In estuaries, sediment organic matter can be derived from a variety of sources including terrestrial material, tidally advected marine inputs, as well as autochthonous production by a wide variety of pelagic and benthic primary producers (Canuel & Hardison, 2016). Bulk proxies of organic matter source such as C:N ratio and $\delta^{13}C$ values can be used to determine organic matter sources in various sedimentary environments (Cloern et al., 2002). In general, C:N ratios are higher in terrestrial primary producers (>12) than in marine producers (3-10) due to the presence of carbon-rich structures (i.e., cellulose, lignin) in the former but not the latter. Similarly, the $\delta^{13}C$ values of primary producers are also distinct due to the source of their carbon and specific carbon fixation pathway, with terrestrial carbon fixation resulting in more depleted values compared to marine primary production (Cloern et al., 2002 and references therein). However, without distinct and

defined organic matter source end-members for a given system, interpretation of C:N ratios and $\delta^{13}C$ values may be qualitative and ambiguous.

Averaged across seasons, water depths, and nodes, the lagoons had a relatively high C:N ratio (13.9 ± 0.3) indicating substantial terrestrial contribution to the coastal sediment. These relatively high C:N values have also been observed in the Beaufort Sea shelf sediments (7.3 - 11.5, Morris et al., 2015; Simpson Lagoon: 13.2 - 18.4, Schreiner et al., 2013; Herschel Basin: 11.3 - 25.9, Couture et al., 2018). Notably, sediment C:N ratios exhibited a spatial gradient decreasing eastward along the coast, with the highest average values in BRW (15.3 ± 0.6), followed by SCC (13.6 ± 0.4), and lowest in BTI (12.2 ± 0.4). Consistent with patterns of SOC distribution, the dominant pattern of sediment organic matter stable isotopes and C:N ratio was inter-nodal. SOC- $\delta^{13}C$ and SON- $\delta^{15}N$ values were similar to previous values for Arctic sediments (Dunton et al., 2012; Goñi et al., 2013; Naidu et al., 2000), but varied by node, with more depleted values at SCC ($\delta^{13}C$: -26.3 ± 0.1 ‰, $\delta^{15}N$: 2.7 ± 0.1 ‰) compared to BRW ($\delta^{13}C$: -25.7 ± 0.2 ‰, $\delta^{15}N$: 3.3 ± 0.1 ‰) and BTI ($\delta^{13}C$: -25.9 ± 0.1 ‰, $\delta^{15}N$: 3.2 ± 0.1 ‰).

For the Arctic coast, riverine POM export and coastal erosion of permafrost bluffs are two important vectors of sediment and organic matter transport (Goñi et al., 2013; Macdonald et al., 2015; Whalen et al., 2022). For the Alaskan Beaufort Sea (Reimnitz et al., 1988) and the Laptev Sea (Rachold et al., 2000), sediments derived from coastal erosion can be greater than the riverine influx. Coastal erosion rates widely vary along the Beaufort Sea coast depending on local geomorphology, ranging from <1 m $year^{-1}$ in the Yukon and Kaktovik (Couture et al., 2018) to more than 8 m $year^{-1}$ at Drew Point (located ~midway between BRW and SCC; Jones et al., 2009). Typically, exposed bluffs

occur on the eastern and western ends of the Beaufort Sea coast (Jorgenson & Brown, 2005) and hold large stocks of organic-rich soils, particularly in the upper active layers (12 - 45% TOC), primed to enter the nearshore (Bristol et al., 2021). A study of permafrost along the Beaufort Sea, including the regions of this study, found an average C:N ratio of 26.3 with no significant longitudinal trend (Ping et al., 2011). Other studies along the Beaufort Sea coast also exhibit a high C:N ratio, although with more variability within a local region of coastline and between permafrost depth horizons (Bristol et al., 2021; Goñi et al., 2000; Tanski et al., 2017). Although the sediments in this study clearly reflect a terrestrial signal of permafrost inputs, the large gap in C:N ratio between the sediments (13.9, this study) and permafrost (26.3, Ping et al., 2011) suggests significant contributions of organic matter with a lower C:N ratio.

From land, Arctic rivers also export POC with C:N values slightly elevated above the Redfield ratio (C:N, 6.6) ranging from 9 to 13.2 (Bell et al., 2016; Connelly et al., 2015; Lobbes et al., 2000; McClelland et al., 2016). The C:N ratio of Arctic river POC export is relatively consistent across watersheds and more variable between seasons (McClelland et al., 2016), suggesting the eastward decrease in sediment C:N ratio is a result of differences in relative contributions from eroding coastlines (higher C:N ratio) and river-borne POM (lower C:N ratio) rather than C:N variability of the source organic matter along the coast.

The impacts of these relative contributions are reflected in sediment $\delta^{13}C$ values in Beaufort Sea sediments. Patterns and values of settling POC-$\delta^{13}C$ and surface sediments in the Beaufort Seas are consistent and similar highlighting the tight benthic-pelagic connections between riverine POC discharge and rapid deposition to the

sediments (Dunton et al., 2012; Naidu et al., 2000). For example, in the Beaufort Sea coast, water column POC exhibits depleting values with longitude (west to east along the coast) in response to increasing terrestrial loads from the Mackenzie River delta (-21 to -27 ‰; Dunton et al., 2012; Goñi et al., 2013; Naidu et al., 2000). However, while sediment patterns of $\delta^{13}C$ align with higher terrestrial inputs via river discharge at SCC, the lowest C:N ratios were not observed at SCC but rather BTI.

Interestingly, this decreasing eastward trend in C:N ratio was also observed for water column DOM along the Beaufort coast, explained by an eastward increase in landscape elevation and an associated decrease in terrestrial microbial degradation rather than organic matter composition (Connolly et al., 2021). This spatial pattern in microbial degradation created by elevation on land may parallel in lagoon sediments in the form of sediment resuspension. Sediment resuspension facilitates benthic gas exchange and the transport of organic matter into the water column, enhancing remineralization and nutrient cycling in coastal areas (Moriarty et al., 2021; Pusceddu et al., 2005; Wainright & Hopkinson, 1997). Indeed, Stahlberg et al. (2006) observed a five time increase in sediment respiration during controlled incubations with resuspension events. In shallow coastal systems such as lagoons, stronger interactions between the atmosphere, water, and sediments result in more continuous resuspension events, facilitating even more enhanced organic matter remineralization (Moriarty et al., 2018; Niemistö & Lund-Hansen, 2019). While organic matter degradation may not significantly impact $\delta^{13}C$ signals on shorter time scales (months), it may be reflected in C:N ratios with the preferential breakdown of labile N-containing fractions (Lehmann et al., 2002; McArthur et al., 1991). Spanning a relatively long length of coastline, allowing for a longer

fetch, and also representing the two shallowest lagoons, Elson Lagoon and SIL are likely to experience frequent resuspension events during the Open Water period. Although SSL is the deepest lagoon, large inputs from the Sagavanirktok River and open access to the Beaufort Sea are likely to facilitate sufficient water turbulence to initiate resuspension. In contrast, Jago and Kaktovik Lagoons represent the smallest lagoons with the most land protection resulting in minimal resuspension activity.

3.5.3 Sediment microbial respiration in Elson Lagoon

Given the large variability in SOC between BLE-LTER lagoons, we conducted a focused study in a single lagoon (Elson Lagoon) to more accurately assess controls on sediment microbial activities. Although the general patterns were consistent, the sampling techniques used between the BLE-LTER Core Program (0-10 cm) and Elson Lagoon 2022 (0-2 cm) differed slightly, with the latter providing a more precise and accurate representation of surface sediments. Notably, compared to the BLE Core Program samples, the samples from Elson Lagoon 2022 displayed a more prominent distinction between Shallow and Deep stations across almost all sediment characteristics.

The DOU rates in Elson Lagoon ranged from 0.22 – 1.96 mmol O_2 m^2 d^{-1}, displaying both seasonal and spatial variability. During Open Water, DOU rates were three times as high at Deep stations compared to Shallow stations, while Deep stations during Open Water were only twice as high as Deep stations during Ice Cover. The stepwise multiple linear regression of DOU rates indicated that 72% and 28% of the variance was explained by SOC and temperature, respectively. Thus, in this study, DOU rates were more strongly controlled by SOC than temperature, despite the large seasonal

temperature difference in bottom waters (min (Ice Cover): -2.1°C, max (Open Water): 8.6°C).

DOU rates in this study were on the lower end of the range when compared to global shelf (9 – 21 mmol O_2 m^2 d^{-1}; Jørgensen et al., 2022), pan-Arctic (10.5 mmol O_2 m^2 d^{-1}, Bourgeois et al., 2017) and coastal Arctic (2.8 – 13.4 mmol O_2 m^2 d^{-1}, Jorgenson & Brown, 2005; 4.5 – 9.1 mmol O_2 m^2 d^{-1}, Glud et al., 1998; 2.5 – 2.8 mmol O_2 m^2 d^{-1}, Attard et al., 2016; 2.8 – 6.8 mmol m^{-2} d^{-1}, Sørensen et al., 2015) sediments. However, DOU rates comparable to this study have been observed on the Barent Sea shelf (0.16 – 1.13 mmol O_2 m^2 d^{-1}; Kiesel et al., 2020) and in the Arctic Fram Strait (0.5 – 2.1 mmol O_2 m^2 d^{-1}, Hoffmann et al., 2018), suggesting spatial heterogeneity along the Beaufort Sea and Arctic coast.

Several studies have also observed that sediment respiration rates in the Arctic appear to be limited by the availability of organic matter more than temperature (Bourgeois et al., 2017; Glud et al., 1998; Kiesel et al., 2020; Renaud et al., 2008). SOC is often correlated with sediment O_2 demand due to tight benthic-pelagic connections supplying labile organic matter to the sediments (Link et al., 2011, 2013; Renaud et al., 2008). In addition to quantity, the composition and quality of POM reaching the benthos are particularly related to sediment O_2 use especially during the winter with low export to the benthos (Morata & Renaud, 2008).

Although temperate coastal environments are characterized by high rates of sediment O_2 uptake and remineralization during summer and low rates during winter, attributed to temperature controls on metabolic rates (Thamdrup et al., 1998), respiration rates in Arctic sediments do not appear to be limited by the predominantly low

temperatures (Glud et al., 1998; Thamdrup & Fleischer, 1998). Arctic benthic microbial communities are well-adapted to the cold with optimal growth yields at low in situ temperature maintaining relatively high activity (Arnosti & Jørgensen, 2006; Knoblauch et al., 1999; Rysgaard et al., 1998; Thamdrup & Fleischer, 1998) and O_2 consumption rates similar to those in temperate sediments (Glud et al., 1998).

To quantify the ecosystem scale impact of sediment DOU, annual benthic DOU rates were calculated by applying depth-specific SOC content, temperature, and lagoon area to the stepwise regression model (Table 3.6). The vast majority (95%) of sediment respiration occurred at Deep stations, which represented more than 70% of the lagoons by area and have higher SOC content. Surprisingly, even though daily rates of DOU were the lowest during Ice Cover, the long duration of the winter (~7.5 months) resulted in Ice Cover representing nearly half (~49%) of annual sediment respiration. In contrast, even though it was a shorter period of the year (~2.5 months), Open Water constituted 42% of annual DOU facilitated by higher daily respiration rates. Annually, Elson Lagoon benthic microbial respiration consumed ~138 Mmol O_2 y^{-1} or released approximately 1.65 Gg C y^{-1} assuming a 1:1: C:O_2 respiratory quotient (RQ).

For comparison, carbon inputs from coastal erosion and pelagic primary production were calculated for Elson Lagoon. Using the length of coastline (34 km, (Rawlins, 2021) and permafrost characteristics for Elson Lagoon described by Ping et al. (2011), who measured annual rates of coastal erosion (1.27 m y^{-1}), average bluff height (2.5 m) and permafrost carbon values (50 kg m^{-3}), annual erosional inputs into Elson Lagoon were estimated to be ~5.40 Gg C y^{-1}. Similarly, assuming consistent rates of pelagic primary production within Elson Lagoon and Beaufort Sea shelf waters (~24 g C

m^{-2} y^{-1}, Brugel et al., 2009; Lavoie et al., 2009), when scaled up to the area of Elson Lagoon (207 km^2), annual pelagic carbon fixation rates occurred at levels (4.97 Gg C y^{-1}) on par with carbon inputs from coastal erosion. Relative to these potential sources individually, sediment DOU in Elson Lagoon could be responsible for the remineralization of approximately ~16% of organic carbon inputs from coastal erosion and marine primary production with the remaining ~84% being buried or exported out of the lagoons.

3.6 Conclusion

Using grain size data and bulk geochemical indicators of SOC, we determined the patterns of SOC distribution in Arctic coastal lagoons along permafrost coasts of the Beaufort Sea. The association of SOC with fine grain size fractions indicated that geochemical parameters generally followed spatial trends in grain size. Although their shallow depths and silt dominant composition are conducive to sediment resuspension, the lagoons still function as deposition zones of organic matter due to the presence of the barrier islands which inhibit the offshore export of sediments. This was reflected in internodal variability, where SOC was higher at BRW and BTI with less connectivity to the Beaufort Sea. Lagoon sediments exhibited a relatively high C:N ratio, suggesting significant terrestrial inputs, but values fell between permafrost, riverine POM, and autochthonous marine production, suggesting considerable input from sources other than erosion of permafrost. Furthermore, sediment C:N ratios varied spatially, decreasing eastward between BLE nodes, suggesting higher permafrost organic carbon inputs relative to riverine and pelagic POM inputs. Alternatively, this pattern may be driven by higher rates of overall organic matter degradation in response to higher sediment

resuspension frequency. In the sediments, DOU rates were primarily driven by SOC but also increased seasonally in response to rising water temperatures. On an annual scale, Elson Lagoon sediments respired approximately 1.7 Gg C y^{-1}, representing ~16% of carbon inputs into the lagoon from coastal erosion and pelagic primary production .

3.7 References

Ahmed, R., Prowse, T., Dibike, Y., Bonsal, B., & O'Neil, H. (2020). Recent Trends in Freshwater Influx to the Arctic Ocean from Four Major Arctic-Draining Rivers. Water, 12(4), 1189. https://doi.org/10.3390/w12041189

Arnosti, C., & Jørgensen, B. B. (2006). Organic Carbon Degradation in Arctic Marine Sediments, Svalbard: A Comparison of Initial and Terminal Steps. Geomicrobiology Journal, 23(7), 551–563. https://doi.org/10.1080/01490450600897336

Attard, K., Hancke, K., Sejr, M., & Glud, R. (2016). Benthic primary production and mineralization in a High Arctic fjord: In situ assessments by aquatic eddy covariance. Marine Ecology Progress Series, 554, 35–50. https://doi.org/10.3354/meps11780

Barnhart, K. R., Overeem, I., & Anderson, R. S. (2014). The effect of changing sea ice on the physical vulnerability of Arctic coasts. The Cryosphere, 8(5), 1777–1799. https://doi.org/10.5194/tc-8-1777-2014

Bell, L., Bluhm, B., & Iken, K. (2016). Influence of terrestrial organic matter in marine food webs of the Beaufort Sea shelf and slope. Marine Ecology Progress Series, 550, 1–24. https://doi.org/10.3354/meps11725

Benner, R., Benitez-Nelson, B., Kaiser, K., & Amon, R. M. W. (2004). Export of young terrigenous dissolved organic carbon from rivers to the Arctic Ocean. Geophysical Research Letters, 31(5), 2003GL019251. https://doi.org/10.1029/2003GL019251

Bianchi, T. S., Cui, X., Blair, N. E., Burdige, D. J., Eglinton, T. I., & Galy, V. (2018). Centers of organic carbon burial and oxidation at the land-ocean interface. Organic Geochemistry, 115, 138–155. https://doi.org/10.1016/j.orggeochem.2017.09.008

Bianchi, T. S., Schreiner, K. M., Smith, R. W., Burdige, D. J., Woodard, S., & Conley, D. J. (2016). Redox Effects on Organic Matter Storage in Coastal Sediments During the Holocene: A Biomarker/Proxy Perspective. Annual Review of Earth and Planetary Sciences, 44(1), 295–319. https://doi.org/10.1146/annurev-earth-060614-105417

Blair, N. E., & Aller, R. C. (2012). The Fate of Terrestrial Organic Carbon in the Marine Environment. Annual Review of Marine Science, 4(1), 401–423. https://doi.org/10.1146/annurev-marine-120709-142717

Bourgeois, S., Archambault, P., & Witte, U. (2017). Organic matter remineralization in marine sediments: A Pan-Arctic synthesis. Global Biogeochemical Cycles, 31, 190–213. https://doi.org/10.1002/2016GB005378

Bristol, E. M., Connolly, C. T., Lorenson, T. D., Richmond, B. M., Ilgen, A. G., Choens, R. C., Bull, D. L., Kanevskiy, M., Iwahana, G., Jones, B. M., & McClelland, J. W. (2021). Geochemistry of Coastal Permafrost and Erosion-Driven Organic Matter Fluxes to the Beaufort Sea Near Drew Point, Alaska. Frontiers in Earth Science, 8, 598933. https://doi.org/10.3389/feart.2020.598933

Brugel, S., Nozais, C., Poulin, M., Tremblay, J., Miller, L., Simpson, K., Gratton, Y., & Demers, S. (2009). Phytoplankton biomass and production in the southeastern

Beaufort Sea in autumn 2002 and 2003. Marine Ecology Progress Series, 377, 63–77. https://doi.org/10.3354/meps07808
Burdige, David. (2005). Burial of terrestrial organic matter in marine sediments: A re-assessment David J. Burdige. Global Biogeochemical Cycles, 19. https://doi.org/doi:10.1029/2004GB002368
Cai, W.-J. (2011). Estuarine and Coastal Ocean Carbon Paradox: CO 2 Sinks or Sites of Terrestrial Carbon Incineration? Annual Review of Marine Science, 3(1), 123–145. https://doi.org/10.1146/annurev-marine-120709-142723
Canuel, E. A., Cammer, S. S., McIntosh, H. A., & Pondell, C. R. (2012). Climate Change Impacts on the Organic Carbon Cycle at the Land-Ocean Interface. Annual Review of Earth and Planetary Sciences, 40(1), 685–711. https://doi.org/10.1146/annurev-earth-042711-105511
Canuel, E. A., & Hardison, A. K. (2016). Sources, Ages, and Alteration of Organic Matter in Estuaries. Annual Review of Marine Science, 8(1), 409–434. https://doi.org/10.1146/annurev-marine-122414-034058
Carr, J., D'Odorico, P., McGlathery, K., & Wiberg, P. (2010). Stability and bistability of seagrass ecosystems in shallow coastal lagoons: Role of feedbacks with sediment resuspension and light attenuation. Journal of Geophysical Research: Biogeosciences, 115(G3), 2009JG001103. https://doi.org/10.1029/2009JG001103
Cloern, J. E., Canuel, E. A., & Harris, D. (2002). Stable carbon and nitrogen isotope composition of aquatic and terrestrial plants of the San Francisco Bay estuarine system. Limnology and Oceanography, 47(3), 713–729. https://doi.org/10.4319/lo.2002.47.3.0713
Connelly, T., McClelland, J., Crump, B., Kellogg, C., & Dunton, K. (2015). Seasonal changes in quantity and composition of suspended particulate organic matter in lagoons of the Alaskan Beaufort Sea. Marine Ecology Progress Series, 527, 31–45. https://doi.org/10.3354/meps11207
Connolly, C. T., Cardenas, M. B., Burkart, G. A., Spencer, R. G. M., & McClelland, J. W. (2020). Groundwater as a major source of dissolved organic matter to Arctic coastal waters. Nature Communications, 11(1), 1479. https://doi.org/10.1038/s41467-020-15250-8
Connolly, C. T., Crump, B. C., Dunton, K. H., & McClelland, J. W. (2021). Seasonality of dissolved organic matter in lagoon ecosystems along the Alaska Beaufort Sea coast. Limnology and Oceanography, 66(12), 4299–4313. https://doi.org/10.1002/lno.11962
Couture, N. J., Irrgang, A., Pollard, W., Lantuit, H., & Fritz, M. (2018). Coastal Erosion of Permafrost Soils Along the Yukon Coastal Plain and Fluxes of Organic Carbon to the Canadian Beaufort Sea. Journal of Geophysical Research: Biogeosciences, 123(2), 406–422. https://doi.org/10.1002/2017JG004166
Cuellar-Martinez, T., Ruiz-Fernández, A. C., Sanchez-Cabeza, J.-A., & Alonso-Rodríguez, R. (2017). Sedimentary record of recent climate impacts on an insular coastal lagoon in the Gulf of California. Quaternary Science Reviews, 160, 138–149. https://doi.org/10.1016/j.quascirev.2017.01.002
De Falco, G., Magni, P., Teräsvuori, L. M. H., & Matteucci, G. (2004). Sediment grain size and organic carbon distribution in the Cabras lagoon (Sardinia, Western

Mediterranean). Chemistry and Ecology, 20(sup1), 367–377. https://doi.org/10.1080/02757540310001629189
Dittmar, T., & Kattner, G. (2003). The biogeochemistry of the river and shelf ecosystem of the Arctic Ocean: A review. Marine Chemistry, 83(3–4), 103–120. https://doi.org/10.1016/S0304-4203(03)00105-1
Duarte, C. M. (2017). Reviews and syntheses: Hidden forests, the role of vegetated coastal habitats in the ocean carbon budget. Biogeosciences, 14(2), 301–310. https://doi.org/10.5194/bg-14-301-2017
Duarte, C. M., Middelburg, J. J., & Caraco, N. (2005). Major role of marine vegetation on the oceanic carbon cycle, Biogeosciences, 2, 1-8, https://doi.org/10.5194/bg-2-1-2005.
Dunton, K. H., Schonberg, S. V., & Cooper, L. W. (2012). Food Web Structure of the Alaskan Nearshore Shelf and Estuarine Lagoons of the Beaufort Sea. Estuaries and Coasts, 35(2), 416–435. https://doi.org/10.1007/s12237-012-9475-1
Dunton, K. H., Weingartner, T., & Carmack, E. C. (2006). The nearshore western Beaufort Sea ecosystem: Circulation and importance of terrestrial carbon in arctic coastal food webs. Progress in Oceanography, 71(2–4), 362–378. https://doi.org/10.1016/j.pocean.2006.09.011
Eicken, H., Gradinger, R., Gaylord, A., Mahoney, A., Rigor, I., & Melling, H. (2005). Sediment transport by sea ice in the Chukchi and Beaufort Seas: Increasing importance due to changing ice conditions? Deep Sea Research Part II: Topical Studies in Oceanography, 52(24–26), 3281–3302. https://doi.org/10.1016/j.dsr2.2005.10.006
Eidam, E. F., Thomson, J., Malito, J. G., & Hošeková, L. (2024). Morphology and Sediment Dynamics of Blossom Shoals at Icy Cape, Alaska. Journal of Geophysical Research: Earth Surface, 129(4), e2023JF007398. https://doi.org/10.1029/2023JF007398
Fraley, K. M., Robards, M. D., Rogers, M. C., Vollenweider, J., Smith, B., Whiting, A., & Jones, T. (2021). Freshwater input and ocean connectivity affect habitats and trophic ecology of fishes in Arctic coastal lagoons. Polar Biology, 44(7), 1401–1414. https://doi.org/10.1007/s00300-021-02895-4
Glud, R., Holby, O., Hoffmann, F., & Canfield, D. (1998). Benthic mineralization and exchange in Arctic sediments (Svalbard, Norway). Marine Ecology Progress Series, 173, 237–251. https://doi.org/10.3354/meps173237
Goñi, M. A., O'Connor, A. E., Kuzyk, Z. Z., Yunker, M. B., Gobeil, C., & Macdonald, R. W. (2013). Distribution and sources of organic matter in surface marine sediments across the North American Arctic margin. Journal of Geophysical Research: Oceans, 118(9), 4017–4035. https://doi.org/10.1002/jgrc.20286
Goñi, M. A., Yunker, M. B., Macdonald, R. W., & Eglinton, T. I. (2000). Distribution and sources of organic biomarkers in arctic sediments from the Mackenzie River and Beaufort Shelf. Marine Chemistry, 71(1–2), 23–51. https://doi.org/10.1016/S0304-4203(00)00037-2
Günther, F., Overduin, P. P., Baranskaya, A., Opel, T., & Grigoriev, M. N. (2013). Observing Muostakh Island disappear: Erosion of a ground-ice-rich coast in response to summer warming and sea ice reduction on the East Siberian shelf. https://doi.org/10.5194/tcd-7-4101-2013

Guo, L., Semiletov, I., Gustafsson, Ö., Ingri, J., Andersson, P., Dudarev, O., & White, D. (2004). Characterization of Siberian Arctic coastal sediments: Implications for terrestrial organic carbon export. Global Biogeochemical Cycles, 18(1), 2003GB002087. https://doi.org/10.1029/2003GB002087

Hanna, A. J., Shanahan, T. M., Allison, M. A., Bianchi, T. S., & Schreiner, K. M. (2018). A multi-proxy investigation of late-Holocene temperature change and climate-driven fluctuations in sediment sourcing: Simpson Lagoon, Alaska. The Holocene, 28(6), 984–997. https://doi.org/10.1177/0959683617752845

Harris, C. M., McClelland, J. W., Connelly, T. L., Crump, B. C., & Dunton, K. H. (2017). Salinity and Temperature Regimes in Eastern Alaskan Beaufort Sea Lagoons in Relation to Source Water Contributions. Estuaries and Coasts, 40(1), 50–62. https://doi.org/10.1007/s12237-016-0123-z

Hoffmann, R., Braeckman, U., Hasemann, C., & Wenzhöfer, F. (2018). Deep-sea benthic communities and oxygen fluxes in the Arctic Fram Strait controlled by sea-ice cover and water depth. Biogeosciences, 15(16), 4849–4869. https://doi.org/10.5194/bg-15-4849-2018

Ito, M., Ohshima, K. I., Fukamachi, Y., Hirano, D., Mahoney, A. R., Jones, J., Takatsuka, T., & Eicken, H. (2019). Favorable Conditions for Suspension Freezing in an Arctic Coastal Polynya. Journal of Geophysical Research: Oceans, 124(12), 8701–8719. https://doi.org/10.1029/2019JC015536

Jones, B. M., Arp, C. D., Jorgenson, M. T., Hinkel, K. M., Schmutz, J. A., & Flint, P. L. (2009). Increase in the rate and uniformity of coastline erosion in Arctic Alaska. Geophysical Research Letters, 36(3), 2008GL036205. https://doi.org/10.1029/2008GL036205

Jong, D., Bröder, L., Tesi, T., Tanski, G., Oudenhuijsen, M., Fritz, M., Lantuit, H., Haghipour, N., Eglinton, T., & Vonk, J. (2024). Selective Sorting and Degradation of Permafrost Organic Matter in the Nearshore Zone of Herschel Island (Yukon, Canada). Journal of Geophysical Research: Biogeosciences, 129(1), e2023JG007479. https://doi.org/10.1029/2023JG007479

Jørgensen, B. B., Wenzhöfer, F., Egger, M., & Glud, R. N. (2022). Sediment oxygen consumption: Role in the global marine carbon cycle. Earth-Science Reviews, 228, 103987. https://doi.org/10.1016/j.earscirev.2022.103987

Jorgenson, M. T., & Brown, J. (2005). Classification of the Alaskan Beaufort Sea Coast and estimation of carbon and sediment inputs from coastal erosion. Geo-Marine Letters, 25(2–3), 69–80. https://doi.org/10.1007/s00367-004-0188-8

Karlsson, E., Gelting, J., Tesi, T., Van Dongen, B., Andersson, A., Semiletov, I., Charkin, A., Dudarev, O., & Gustafsson, Ö. (2016). Different sources and degradation state of dissolved, particulate, and sedimentary organic matter along the Eurasian Arctic coastal margin. Global Biogeochemical Cycles, 30(6), 898–919. https://doi.org/10.1002/2015GB005307

Kiesel, J., Bienhold, C., Wenzhöfer, F., & Link, H. (2020). Variability in Benthic Ecosystem Functioning in Arctic Shelf and Deep-Sea Sediments: Assessments by Benthic Oxygen Uptake Rates and Environmental Drivers. Frontiers in Marine Science, 7, 426. https://doi.org/10.3389/fmars.2020.00426

Knoblauch, C., Jørgensen, B. B., & Harder, J. (1999). Community Size and Metabolic Rates of Psychrophilic Sulfate-Reducing Bacteria in Arctic Marine Sediments.

Applied and Environmental Microbiology, 65(9), 4230–4233. https://doi.org/10.1128/AEM.65.9.4230-4233.1999
Lantuit, H., Overduin, P. P., Couture, N., Wetterich, S., Aré, F., Atkinson, D., Brown, J., Cherkashov, G., Drozdov, D., Forbes, D. L., Graves-Gaylord, A., Grigoriev, M., Hubberten, H.-W., Jordan, J., Jorgenson, T., Ødegård, R. S., Ogorodov, S., Pollard, W. H., Rachold, V., … Vasiliev, A. (2012). The Arctic Coastal Dynamics Database: A New Classification Scheme and Statistics on Arctic Permafrost Coastlines. Estuaries and Coasts, 35(2), 383–400. https://doi.org/10.1007/s12237-010-9362-6
Lantuit, H., Overduin, P. P., & Wetterich, S. (2013). Recent Progress Regarding Permafrost Coasts. Permafrost and Periglacial Processes, 24(2), 120–130. https://doi.org/10.1002/ppp.1777
Lavoie, D., Macdonald, R. W., & Denman, K. L. (2009). Primary productivity and export fluxes on the Canadian shelf of the Beaufort Sea: A modelling study. Journal of Marine Systems, 75(1–2), 17–32. https://doi.org/10.1016/j.jmarsys.2008.07.007
Lawson, S. E., Wiberg, P. L., McGlathery, K. J., & Fugate, D. C. (2007). Wind-driven sediment suspension controls light availability in a shallow coastal lagoon. Estuaries and Coasts, 30(1), 102–112. https://doi.org/10.1007/BF02782971
Lehmann, M. F., Bernasconi, S. M., Barbieri, A., & McKenzie, J. A. (2002). Preservation of organic matter and alteration of its carbon and nitrogen isotope composition during simulated and in situ early sedimentary diagenesis. Geochimica et Cosmochimica Acta, 66(20), 3573–3584. https://doi.org/10.1016/S0016-7037(02)00968-7
Link, H., Archambault, P., Tamelander, T., Renaud, P. E., & Piepenburg, D. (2011). Spring-to-summer changes and regional variability of benthic processes in the western Canadian Arctic. Polar Biology, 34(12), 2025–2038. https://doi.org/10.1007/s00300-011-1046-6
Link, H., Chaillou, G., Forest, A., Piepenburg, D., & Archambault, P. (2013). Multivariate benthic ecosystem functioning in the Arctic – benthic fluxes explained by environmental parameters in the southeastern Beaufort Sea. Biogeosciences, 10(9), 5911–5929. https://doi.org/10.5194/bg-10-5911-2013
Lobbes, J. M., Fitznar, H. P., & Kattner, G. (2000). Biogeochemical characteristics of dissolved and particulate organic matter in Russian rivers entering the Arctic Ocean. Geochimica et Cosmochimica Acta, 64(17), 2973–2983. https://doi.org/10.1016/S0016-7037(00)00409-9
Macdonald, R. W., Kuzyk, Z. Z. A., & Johannessen, S. C. (2015). The vulnerability of Arctic shelf sediments to climate change. Environmental Reviews, 23(4), 461–479. https://doi.org/10.1139/er-2015-0040
Mahoney, A. R., Eicken, H., Gaylord, A. G., & Gens, R. (2014). Landfast sea ice extent in the Chukchi and Beaufort Seas: The annual cycle and decadal variability. Cold Regions Science and Technology, 103, 41–56. https://doi.org/10.1016/j.coldregions.2014.03.003
McArthur, J., Tyson, R., Thomson, J., & Mattey, D. (1991). Early diagenesis of marine organic matter: Alteration of the carbon isotopic composition. Marine Geology, 105, 51–61.

McClelland, J. W., Holmes, R. M., Dunton, K. H., & Macdonald, R. W. (2012). The Arctic Ocean Estuary. Estuaries and Coasts, 35(2), 353–368. https://doi.org/10.1007/s12237-010-9357-3

McClelland, J. W., Holmes, R. M., Peterson, B. J., Raymond, P. A., Striegl, R. G., Zhulidov, A. V., Zimov, S. A., Zimov, N., Tank, S. E., Spencer, R. G. M., Staples, R., Gurtovaya, T. Y., & Griffin, C. G. (2016). Particulate organic carbon and nitrogen export from major Arctic rivers. Global Biogeochemical Cycles, 30(5), 629–643. https://doi.org/10.1002/2015GB005351

McClelland, J. W., Townsend-Small, A., Holmes, R. M., Pan, F., Stieglitz, M., Khosh, M., & Peterson, B. J. (2014). River export of nutrients and organic matter from the North Slope of Alaska to the Beaufort Sea. Water Resources Research, 50(2), 1823–1839. https://doi.org/10.1002/2013WR014722

Mcleod, E., Chmura, G. L., Bouillon, S., Salm, R., Björk, M., Duarte, C. M., Lovelock, C. E., Schlesinger, W. H., & Silliman, B. R. (2011). A blueprint for blue carbon: Toward an improved understanding of the role of vegetated coastal habitats in sequestering CO 2. Frontiers in Ecology and the Environment, 9(10), 552–560. https://doi.org/10.1890/110004

Miller, A. (2020). leaps: Regression subset selection (3.1) [R]. https://CRAN.R-project.org/package=leaps

Miller, C. A., Bonsell, C., McTigue, N. D., & Kelley, A. L. (2021). The seasonal phases of an Arctic lagoon reveal the discontinuities of pH variability and CO₂ flux at the air–sea interface. Biogeosciences, 18(3), 1203–1221. https://doi.org/10.5194/bg-18-1203-2021

Morata, N., & Renaud, P. E. (2008). Sedimentary pigments in the western Barents Sea: A reflection of pelagic–benthic coupling? Deep Sea Research Part II: Topical Studies in Oceanography, 55(20–21), 2381–2389. https://doi.org/10.1016/j.dsr2.2008.05.004

Moriarty, J. M., Friedrichs, M. A. M., & Harris, C. K. (2021). Seabed Resuspension in the Chesapeake Bay: Implications for Biogeochemical Cycling and Hypoxia. Estuaries and Coasts, 44(1), 103–122. https://doi.org/10.1007/s12237-020-00763-8

Moriarty, J. M., Harris, C. K., Friedrichs, M. A. M., Fennel, K., & Xu, K. (2018). Impact of Seabed Resuspension on Oxygen and Nitrogen Dynamics in the Northern Gulf of Mexico: A Numerical Modeling Study. Journal of Geophysical Research: Oceans, 123(10), 7237–7263. https://doi.org/10.1029/2018JC013950

Morris, D. J., O'Connell, M. T., & Macko, S. A. (2015). Assessing the importance of terrestrial organic carbon in the CHUKCHI and Beaufort seas. Estuarine, Coastal and Shelf Science, 164, 28–38. https://doi.org/10.1016/j.ecss.2015.06.011

Muller-Karger, F., Varela, R., Thunell, R., Luerssen, R., Hu, C., & Walsh, J. (2005). The importance of continental margins in the global carbon cycle. Geophysical Research Letters, 32. https://doi.org/10.1029/2004GL021346

Naidu, A. S., Cooper, L. W., Finney, B. P., Macdonald, R. W., Alexander, C., & Semiletov, I. P. (2000). Organic carbon isotope ratios (δ13C) of Arctic Amerasian Continental shelf sediments. International Journal of Earth Sciences, 89(3), 522–532. https://doi.org/10.1007/s005310000121

Naidu, A. S., Kelley, J. J., Goering, J. J., & Venkatesan, M. I. (2003). Trace Metals and Hydrocarbons in Sediments of Elson Lagoon (Barrow, Northwest Arctic Alaska) as Related to the Prudhoe Bay Industrial Region.
Nichols, M. M. (1989). Sediment accumulation rates and relative sea-level rise in lagoons. Marine Geology, 88(3–4), 201–219. https://doi.org/10.1016/0025-3227(89)90098-4
Niemistö, J., & Lund-Hansen, L. C. (2019). Instantaneous Effects of Sediment Resuspension on Inorganic and Organic Benthic Nutrient Fluxes at a Shallow Water Coastal Site in the Gulf of Finland, Baltic Sea. Estuaries and Coasts, 42(8), 2054–2071. https://doi.org/10.1007/s12237-019-00648-5
Oksanen, J., Simpson, G., Blanchet, F., Kindt, R., Legendre, P., Minchin, P., O'Hara, R., Solymos, P., Szoecs, E., Wagner, H., Barbour, M., Bedward, M., Bolker, B., Borcard, D., Carvalho, G., Chirico, M., De Caceres, M., Durand, S., Evangelista, H., … Weedon, J. (2024). vegan: Community Ecology Package (2.6-7) [Computer software].
Overeem, I., Anderson, R. S., Wobus, C. W., Clow, G. D., Urban, F. E., & Matell, N. (2011). Sea ice loss enhances wave action at the Arctic coast: SEA ICE LOSS ENHANCES EROSION. Geophysical Research Letters, 38(17), https://doi.org/10.1029/2011GL048681
Pedrazas, M. N., Cardenas, M. B., Demir, C., Watson, J. A., Connolly, C. T., & McClelland, J. W. (2020). Absence of ice-bonded permafrost beneath an Arctic lagoon revealed by electrical geophysics. Science Advances, 6(43), eabb5083. https://doi.org/10.1126/sciadv.abb5083
Petti, M., Bosa, S., & Pascolo, S. (2018). Lagoon Sediment Dynamics: A Coupled Model to Study a Medium-Term Silting of Tidal Channels. Water, 10(5), 569. https://doi.org/10.3390/w10050569
Ping, C.-L., Michaelson, G. J., Guo, L., Jorgenson, M. T., Kanevskiy, M., Shur, Y., Dou, F., & Liang, J. (2011). Soil carbon and material fluxes across the eroding Alaska Beaufort Sea coastline. Journal of Geophysical Research, 116(G2), G02004. https://doi.org/10.1029/2010JG001588
Pusceddu, A., Grémare, A., Escoubeyrou, K., Amouroux, J. M., Fiordelmondo, C., & Danovaro, R. (2005). Impact of natural (storm) and anthropogenic (trawling) sediment resuspension on particulate organic matter in coastal environments. Continental Shelf Research, 25(19–20), 2506–2520. https://doi.org/10.1016/j.csr.2005.08.012
Rachold, V., Grigoriev, M. N., Are, F. E., Solomon, S., Reimnitz, E., Kassens, H., & Antonow, M. (2000). Coastal erosion vs riverine sediment discharge in the Arctic Shelf seas. International Journal of Earth Sciences, 89(3), 450–460. https://doi.org/10.1007/s005310000113
Radosavljevic, B., Lantuit, H., Knoblauch, C., Couture, N., Herzschuh, U., & Fritz, M. (2022). Arctic Nearshore Sediment Dynamics—An Example from Herschel Island—Qikiqtaruk, Canada. Journal of Marine Science and Engineering, 10(11), 1589. https://doi.org/10.3390/jmse10111589
Ramaswamy, V., Gaye, B., Shirodkar, P. V., Rao, P. S., Chivas, A. R., Wheeler, D., & Thwin, S. (2008). Distribution and sources of organic carbon, nitrogen and their isotopic signatures in sediments from the Ayeyarwady (Irrawaddy) continental

shelf, northern Andaman Sea. Marine Chemistry, 111(3–4), 137–150. https://doi.org/10.1016/j.marchem.2008.04.006
Rawlins, M. A. (2021). Increasing freshwater and dissolved organic carbon flows to Northwest Alaska's Elson lagoon. Environmental Research Letters, 16(10), 105014. https://doi.org/10.1088/1748-9326/ac2288
Reimnitz, E., Graves, S., & Barnes, P. (1988). Beaufort Sea coastal erosion, sediment flux, shoreline evolution, and the erosional shelf profile. USGS Report 1182G; IMAP, https://doi.org/10.3133/i1182G
Renaud, P. E., Morata, N., Carroll, M. L., Denisenko, S. G., & Reigstad, M. (2008). Pelagic–benthic coupling in the western Barents Sea: Processes and time scales. Deep Sea Research Part II: Topical Studies in Oceanography, 55(20–21), 2372–2380. https://doi.org/10.1016/j.dsr2.2008.05.017
Rowland, J. C., Jones, C. E., Altmann, G., Bryan, R., Crosby, B. T., Hinzman, L. D., Kane, D. L., Lawrence, D. M., Mancino, A., Marsh, P., McNamara, J. P., Romanvosky, V. E., Toniolo, H., Travis, B. J., Trochim, E., Wilson, C. J., & Geernaert, G. L. (2010). Arctic Landscapes in Transition: Responses to Thawing Permafrost. Eos, Transactions American Geophysical Union, 91(26), 229–230. https://doi.org/10.1029/2010EO260001
Rysgaard, S., Thamdrup, B., Risgaard-Petersen, N., Fossing, H., Berg, P., Christensen, P., & Dalsgaard, T. (1998). Seasonal carbon and nutrient mineralization in a high-Arctic coastal marine sediment, Young Sound, Northeast Greenland. Marine Ecology Progress Series, 175, 261–276. https://doi.org/10.3354/meps175261
Schreiner, K. M., Bianchi, T. S., Eglinton, T. I., Allison, M. A., & Hanna, A. J. M. (2013). Sources of terrigenous inputs to surface sediments of the Colville River Delta and Simpson's Lagoon, Beaufort Sea, Alaska. Journal of Geophysical Research: Biogeosciences, 118(2), 808–824. https://doi.org/10.1002/jgrg.20065
Snedden, G., Cable, J., & Kjerfve, B. (2023). Geomorphology, circulation, and mixing. In Estuarine Ecology.
Sørensen, H., Meire, L., Juul-Pedersen, T., De Stigter, H., Meysman, F., Rysgaard, S., Thamdrup, B., & Glud, R. (2015). Seasonal carbon cycling in a Greenlandic fjord: An integrated pelagic and benthic study. Marine Ecology Progress Series, 539, 1–17. https://doi.org/10.3354/meps11503
Tanski, G., Lantuit, H., Ruttor, S., Knoblauch, C., Radosavljevic, B., Strauss, J., Wolter, J., Irrgang, A. M., Ramage, J., & Fritz, M. (2017). Transformation of terrestrial organic matter along thermokarst-affected permafrost coasts in the Arctic. Science of The Total Environment, 581–582, 434–447. https://doi.org/10.1016/j.scitotenv.2016.12.152
Thamdrup, B., & Fleischer, S. (1998). Temperature dependence of oxygen respiration, nitrogen mineralization, and nitrification in Arctic sediments. Aquatic Microbial Ecology, 15, 191–199. https://doi.org/10.3354/ame015191
Thamdrup, B., Hansen, J. W., & JÃ¸rgensen, B. B. (1998). Temperature dependence of aerobic respiration in a coastal sediment. FEMS Microbiology Ecology, 25(2), 189–200. https://doi.org/10.1111/j.1574-6941.1998.tb00472.x
Trishchenko, A. P., Kostylev, V. E., Luo, Y., Ungureanu, C., Whalen, D., & Li, J. (2022). Landfast ice properties over the Beaufort Sea region in 2000–2019 from MODIS

and Canadian Ice Service data. Canadian Journal of Earth Sciences, 59(11), 847–865. https://doi.org/10.1139/cjes-2021-0011

Unisense. (2020). Unisense: Oxygen sensor manual. Unisense A/S.

Van Dongen, B. E., Semiletov, I., Weijers, J. W. H., & Gustafsson, Ö. (2008). Contrasting lipid biomarker composition of terrestrial organic matter exported from across the Eurasian Arctic by the five great Russian Arctic rivers. Global Biogeochemical Cycles, 22(1), 2007GB002974. https://doi.org/10.1029/2007GB002974

Wainright, S., & Hopkinson, C. (1997). Effects of sediment resuspension on organic matter processing in coastal environments: Simulation model. Journal of Marine Science, 11, 353–368.

Ward, N. D. (2017). Editorial: Integrative Research on Organic Matter Cycling across Aquatic Gradients. Frontiers in Marine Science, 4, 131. https://doi.org/10.3389/fmars.2017.00131

Wegner, C., Wittbrodt, K., Hölemann, J. A., Janout, M. A., Krumpen, T., Selyuzhenok, V., Novikhin, A., Polyakova, Ye., Krykova, I., Kassens, H., & Timokhov, L. (2017). Sediment entrainment into sea ice and transport in the Transpolar Drift: A case study from the Laptev Sea in winter 2011/2012. Continental Shelf Research, 141, 1–10. https://doi.org/10.1016/j.csr.2017.04.010

Weingartner, T. J., Danielson, S. L., Potter, R. A., Trefry, J. H., Mahoney, A., Savoie, M., Irvine, C., & Sousa, L. (2017). Circulation and water properties in the landfast ice zone of the Alaskan Beaufort Sea. Continental Shelf Research, 148, 185–198. https://doi.org/10.1016/j.csr.2017.09.001

Whalen, D., Forbes, D. L., Kostylev, V., Lim, M., Fraser, P., Nedimović, M. R., & Stuckey, S. (2022). Mechanisms, volumetric assessment, and prognosis for rapid coastal erosion of Tuktoyaktuk Island, an important natural barrier for the harbour and community. Canadian Journal of Earth Sciences, 59(11), 945–960. https://doi.org/10.1139/cjes-2021-0101

Yahel, G., Yahel, R., Katz, T., Lazar, B., Herut, B., & Tunnicliffe, V. (2008). Fish activity: A major mechanism for sediment resuspension and organic matter remineralization in coastal marine sediments. Marine Ecology Progress Series, 372, 195–209. https://doi.org/10.3354/meps07688

3.8 Tables

Table 3.1. Lagoon geomorphology (length (km), average depth (m), area (km^2), volume (km^3), % shallow, % deep), annual river discharge (km^3), and ocean connectivity at Elson Lagoon (EWL, EEL), Simpson Lagoon (SIL), Stefansson Sound (SSL), Kaktovik Lagoon (KAL), and Jago Lagoon (JAL). Freshwater sources sampled by the BLE-LTER program are grouped by lagoon. Lagoon geomorphology was measured using the base World Imagery map on ArcGIS.
(---) represents rivers with no published annual discharge rates.
*McClelland et al. 2014, Rawlins et al. 2019
**Stuefer et al. 2017
NA applies to lagoons with primarily diffusive inputs that cannot be or are difficult to quantify.

Lagoon	Length (km)	Average depth (m)	Area (km^2)	Volume (km^3)	% shallow | % deep (by area)	Freshwater sources sampled	Annual river discharge (km^3)*	Ocean connectivity
Elson Lagoon West (EWL) and Elson Lagoon East (EEL)	25	2.4	207	0.50	21% | 79%	Avak Creek No Name River Mayoeak River	--- --- ---	Several intermittent channels
Simpson Lagoon (SIL)	25	1.8	173	0.30	30% | 70 %	Kuparak River Colville River	1.3-1.4* 13.3-19.7*	Several intermittent channels
Stefansson Sound (SSL)	35	4.3	749	3.25	15% | 85%	Sagavanirktok River Putuligauyuk River Atigun River	1.6-3.0* 0.05** ---	Semi-enclosed
Kaktovik Lagoon (KAL)	7	2.8	20	0.05	14% | 86%	Streams, runoff	NA	1 channel to JAL
Jago Lagoon (JAL)	7	2.6	28	0.07	13% | 87%	Jago River	---	1 channel to Beaufort Sea

Table 3.2. Sediment organic carbon (SOC, %) and nitrogen (SON %) content, C:N ratio, and carbon ($\delta^{13}C$) and nitrogen ($\delta^{15}N$) stable isotope composition (‰) in Shallow and Deep stations or averaged across Shallow and Deep stations (All Depths), at each node (BRW, SCC, BTI) or averaged across nodes (All Nodes) across all three seasons (Ice Cover, Break Up Open Water) or averaged across Seasons (All Seasons). Values are average +/- standard error (n = number of samples). (---) represents samples not collected due to the presence of landfast ice.

		Shallow					Deep					All Depths				
	Node	**C %**	**N %**	**C:N**	**$\delta^{13}C$ ‰**	**$\delta^{15}N$ ‰**	**C %**	**N %**	**C:N**	**$\delta^{13}C$ ‰**	**$\delta^{15}N$ ‰**	**C %**	**N %**	**C:N**	**$\delta^{13}C$ ‰**	**$\delta^{15}N$ ‰**
Ice Cover	BRW	---	---	---	---	---	2.6 ± 0.1 (n=7)	0.19 ± 0.00 (n=7)	15.8 ± 0.6 (n=7)	-22.7 ± 0.1 (n=7)	3.1 ± 0.1 (n=7)	2.6 ± 0.1 (n=7)	0.19 ± 0.00 (n=7)	15.8 ± 0.6 (n=7)	-22.7 ± 0.1 (n=7)	3.1 ± 0.1 (n=7)
	SCC	---	---	---	---	---	0.9 ± 0.2 (n=7)	0.07 ± 0.02 (n=7)	13.0 ± 1.9 (n=7)	-26.3 ± 0.2 (n=7)	2.6 ± 0.1 (n=7)	0.9 ± 0.2 (n=7)	0.07 ± 0.02 (n=7)	13.0 ± 1.9 (n=7)	-26.3 ± 0.2 (n=7)	2.6 ± 0.1 (n=7)
	BTI	---	---	---	---	---	1.9 ± 0.1 (n=5)	0.17 ± 0.01 (n=5)	12.5 ± 0.7 (n=5)	-26.1 ± 1.2 (n=5)	3.6 ± 0.2 (n=5)	1.9 ± 0.1 (n=5)	0.17 ± 0.01 (n=5)	12.5 ± 0.7 (n=5)	-26.1 ± 1.2 (n=5)	3.6 ± 0.2 (n=5)
	All Nodes	**---**	**---**	**---**	**---**	**---**	**1.8 ± 0.2 (n=19)**	**0.14 ± 0.01 (n=19)**	**13.9 ± 0.5 (n=19)**	**-26.4 ± 0.1 (n=19)**	**3.1 ± 0.1 (n=19)**	**1.8 ± 0.2 (n=19)**	**0.14 ± 0.01 (n=19)**	**13.9 ± 0.5 (n=19)**	**-26.4 ± 0.1 (n=19)**	**3.1 ± 0.1 (n=19)**
Break Up	BRW	0.6 ± 0.2 (n=6)	0.05 ± 0.01 (n=6)	14.1 ± 2.2 (n=6)	-24.8 ± 0.4 (n=6)	4.0 ± 0.5 (n=6)	3.9 ± 1.6 (n=3)	0.35 ± 0.16 (n=3)	13.6 ± 1.0 (n=3)	-24.5 ± 0.7 (n=3)	2.7 ± 0.7 (n=3)	1.7 ± 0.7 (n=9)	0.15 ± 0.07 (n=9)	13.9 ± 1.4 (n=9)	-24.7 ± 0.3 (n=9)	3.6 ± 0.4 (n=9)
	SCC	1.8 ± 0.6 (n=8)	0.13 ± 0.04 (n=8)	15.8 ± 0.8 (n=8)	-26.7 ± 0.3 (n=8)	2.2 ± 0.2 (n=8)	1.0 ± 0.3 (n=4)	0.08 ± 0.01 (n=4)	13.8 ± 1.7 (n=4)	-26.4 ± 0.1 (n=4)	2.8 ± 0.1 (n=4)	1.5 ± 0.4 (n=12)	0.11 ± 0.03 (n=12)	15.1 ± 0.8 (n=12)	-26.6 ± 0.2 (n=12)	2.4 ± 0.1 (n=12)
	BTI	1.5 ± 1.3 (n=2)	0.12 ± 0.1 (n=2)	11.2 ± 3.6 (n=2)	-25.9 ± 1.2 (n=2)	2.3 ± 0.6 (n=2)	1.8 ± 0.3 (n=2)	0.16 ± 0.02 (n=2)	12.9 ± 0.4 (n=2)	-26.0 ± 0.1 (n=2)	3.3 ± 0.3 (n=2)	1.6 ± 0.6 (n=4)	0.14 ± 0.04 (n=4)	12.1 ± 1.6 (n=4)	-25.9 ± 0.5 (n=4)	2.8 ± 0.4 (n=4)
	All Nodes	**1.3 ± 0.3 (n=16)**	**0.10 ± 0.02 (n=16)**	**14.6 ± 1.0 (n=16)**	**-25.9 ± 0.3 (n=16)**	**2.9 ± 0.3 (n=16)**	**2.1 ± 0.7 (n=9)**	**0.19 ± 0.06 (n=9)**	**13.6 ± 0.8 (n=9)**	**-25.7 ± 0.4 (n=9)**	**2.9 ± 0.2 (n=9)**	**1.6 ± 0.3 (n=25)**	**0.13 ± 0.03 (n=25)**	**14.2 ± 0.7 (n=25)**	**-25.8 ± 0.2 (n=25)**	**2.9 ± 0.2 (n=25)**
Open Water	BRW	1.0 ± 0.4 (n=12)	0.07 ± 0.02 (n=12)	14.7 ± 1.2 (n=12)	-25.3 ± 0.3 (n=12)	3.5 ± 0.3 (n=12)	2.8 ± 0.3 (n=13)	0.19 ± 0.01 (n=13)	16.7 ± 0.9 (n=13)	-26.2 ± 0.3 (n=13)	3.1 ± 0.1 (n=13)	1.9 ± 0.3 (n=25)	0.14± 0.02 (n=25)	15.7± 0.7 (n=25)	-25.8 ± 0.2 (n=25)	3.3 ± 0.2 (n=25)
	SCC	0.7 ± 0.2 (n=12)	0.06 ± 0.02 (n=12)	12.0 ± 0.9 (n=12)	-25.9 ± 0.2 (n=12)	2.8 ± 0.3 (n=12)	1.0 ± 0.1 (n=11)	0.08 ± 0.01 (n=11)	14.1 ± 0.4 (n=11)	-26.4 ± 0.1 (n=11)	2.9 ± 0.1 (n=11)	0.8 ± 0.1 (n=23)	0.07 ± 0.01 (n=23)	13.0 ± 0.5 (n=23)	-26.1 ± 0.1 (n=23)	2.8 ± 0.2 (n=23)
	BTI	1.0 ± 0.3 (n=8)	0.09 ± 0.03 (n=8)	11.2 ± 1.2 (n=8)	-25.6 ± 0.4 (n=8)	2.7 ± 0.2 (n=8)	1.8 ± 0.1 (n=10)	0.16 ± 0.01 (n=10)	13.0 ± 0.3 (n=10)	-26.0 ± 0.2 (n=10)	3.6 ± 0.1 (n=10)	1.4 ± 0.2 (n=18)	0.13 ± 0.01 (n=18)	12.2 ± 0.6 (n=18)	-25.9 ± 0.2 (n=18)	3.2 ± 0.2 (n=18)
	All Nodes	**0.9 ± 0.2 (n=32)**	**0.07 ± 0.01 (n=32)**	**12.8 ± 0.7 (n=32)**	**-25.6 ± 0.2 (n=32)**	**3.1 ± 0.2 (n=32)**	**1.9 ± 0.2 (n=34)**	**0.15 ± 0.01 (n=34)**	**14.8 ± 0.5 (n=34)**	**-26.2 ± 0.1 (n=34)**	**3.2 ± 0.1 (n=34)**	**1.4 ± 0.1 (n=66)**	**0.11 ± 0.01 (n=66)**	**13.8 ± 0.4 (n=66)**	**-25.9 ± 0.1 (n=66)**	**3.1 ± 0.1 (n=66)**
All Seasons	BRW	0.9 ± 0.3 (n=18)	0.07 ± 0.01 (n=18)	14.5 ± 1.0 (n=18)	-25.1 ± 0.2 (n=18)	3.7 ± 0.3 (n=18)	2.9 ± 0.3 (n=23)	0.21 ± 0.02 (n=23)	16.0 ± 0.6 (n=23)	-26.1 ± 0.2 (n=23)	3.0 ± 0.1 (n=23)	2.0 ± 0.2 (n=41)	0.15 ± 0.02 (n=41)	15.3 ± 0.6 (n=41)	-25.7 ± 0.2 (n=41)	3.3 ± 0.1 (n=41)
	SCC	1.2 ± 0.3 (n=20)	0.09 ± 0.02 (n=20)	13.5 ± 0.7 (n=20)	-26.2 ± 0.2 (n=20)	2.6 ± 0.2 (n=20)	0.9 ± 0.1 (n=22)	0.08 ± 0.01 (n=22)	13.7 ± 0.4 (n=22)	-26.4 ± 0.1 (n=22)	2.8 ± 0.1 (n=22)	1.0 ± 0.1 (n=42)	0.08 ± 0.01 (n=42)	13.6 ± 0.4 (n=42)	-26.3 ± 0.1 (n=42)	2.7 ± 0.1 (n=42)
	BTI	1.1 ± 0.3 (n=10)	0.09 ± 0.03 (n=10)	11.2 ± 1.1 (n=10)	-25.7 ± 0.4 (n=10)	2.6 ± 0.2 (n=10)	1.8 ± 0.1 (n=17)	0.16 ± 0.00 (n=17)	12.8 ± 0.3 (n=17)	-26.0 ± 0.1 (n=17)	3.5 ± 0.1 (n=17)	1.5 ± 0.1 (n=27)	0.14 ± 0.01 (n=27)	12.2 ± 0.4 (n=27)	-25.9 ± 0.1 (n=27)	3.2 ± 0.1 (n=27)
	All Nodes	**1.0 ± 0.2 (n=48)**	**0.08 ± 0.01 (n=48)**	**13.4 ± 0.6 (n=48)**	**-25.7 ± 0.2 (n=48)**	**3.0 ± 0.2 (n=48)**	**1.9 ± 0.1 (n=62)**	**0.15 ± 0.01 (n=62)**	**14.3 ± 0.3 (n=62)**	**-26.2 ± 0.1 (n=62)**	**3.1 ± 0.1 (n=62)**	**1.5 ± 0.1 (n=110)**	**0.12 ± 0.01 (n=110)**	**13.9 ± 0.3 (n=110)**	**-26.0 ± 0.1 (n=110)**	**3.1± 0.1 (n=110)**

Table 3.3. Grain size average contribution (%) from sand (62.5 µm - 2000 µm), silt (4 µm - 62.5 µm), and clay (<4 µm) fractions (Wentworth, 1922) and median grain size values (µm) of BLE-LTER core program sediment samples (0 -10 cm) grouped by water depth (Shallow, Deep), and node (BRW, SCC, BTI). Values are average +/- standard error (n = number of samples).

Node	Shallow				Deep				All depths			
	Sand (%)	Silt (%)	Clay (%)	Median (µm)	Sand (%)	Silt (%)	Clay (%)	Median (µm)	Sand (%)	Silt (%)	Clay (%)	Median (µm)
BRW	61 ± 26 (n=3)	23 ± 14 (n=3)	17 ± 12 (n=3)	95 ± 45 (n=3)	28 ± 6 (n=7)	54 ± 3 (n=7)	19 ± 3 (n=7)	30 ± 8 (n=7)	37 ± 9 (n=10)	44 ± 6 (n=10)	18 ± 4 (n=10)	50 ± 16 (n=10)
SCC	58 ± 11 (n=6)	34 ± 9 (n=6)	8 ± 2 (n=6)	109 ± 36 (n=6)	32 ± 6 (n=7)	49 ± 5 (n=7)	19 ± 2 (n=7)	31 ± 2 (n=7)	44 ± 7 (n=13)	42 ± 5 (n=13)	14 ± 2 (n=13)	67 ± 20 (n=13)
BTI	---	---	---	---	6 ± 5 (n=2)	68 ± 2 (n=2)	26 ± 3 (n=2)	9 ± 1 (n=2)	6 ± 5 (n=2)	68 ± 2 (n=2)	26 ± 3 (n=2)	9 ± 1 (n=2)
All nodes	59 ± 10 (n=9)	30 ± 7 (n=9)	11 ± 4 (n=9)	105 ± 25 (n=9)	27 ± 4 (n=16)	53 ± 3 (n=16)	19 ± 2 (n=16)	28 ± 5 (n=16)	34.5 ± 5.4 (n=25	45 ± 4 (n=25	55 ± 12 (n=25)	56 ± 12 (n=25)

Table 3.4. Elson Lagoon Focused Study: Sediment grain size, porosity (%), organic carbon (SOC, %) organic nitrogen (SON, %), C:N ratio, bottom water temperature (°C), and DOU rate (mmol O_2 m^{-2} d^{-1}) from Elson Lagoon surface sediments (0-2 cm) at Shallow and Deep stations during Ice Cover and Open Water. Values are average ± standard error (n = number of samples). Shallow stations were not sampled during Ice Cover due to landfast ice. Asterisk (*) indicates p < 0.10 from t-tests comparing Water Depth (Shallow vs. Deep) during Open Water; # indicates p < 0.10 from t-tests comparing deep stations across Season (Ice Cover vs. Open Water).

Parameter	Ice Cover		Open Water	
	Shallow	Deep	Shallow	Deep
Sand (%)	---	22 ± 7 (n=4)	70 ± 9 (n=6)*	23 ± 4 (n=4)*
Silt (%)	---	57 ± 4 (n=4)	21 ± 7 (n=6)*	56 ± 2 (n=4)*
Clay (%)	---	21 ± 3 (n=4)	7 ± 3 (n=6)*	21 ± 2 (n=4)*
Grain Size Median (μm)	---	22 ± 7 (n=4)	119 ± 28 (n=6)*	19 ± 5 (n=4)*
Porosity (%)	---	52 ± 4 (n=4)	23 ± 2 (n=6)*	50 ± 3 (n=4)*
SOC (%)	---	2.5 ± 0.1 (n=4)	0.5 ± 0.2 (n=6)*	2.6 ± 0.1 (n=4)*
SON (%)	---	0.20 ± 0.01 (n=4)	0.05 ± 0.01 (n=6)*	0.20 ± 0.01 (n=4)*
C:N ratio	---	15.7 ± 0.6 (n=4)	15.0 ± 2.9 (n=6)	14.8 ± 0.8 (n=4)
Temperature (°C)	---	-2.0 ± 0.1 (n=4)#	7.1 ± 0.8 (n=6)*	4.3 ± 0.5 (n=4)*, #
DOU (mmol O_2 m^{-2} d^{-1})	---	0.75 ± 0.07 (n=4)#	0.48 ± 0.08 (n=6)*	1.42 ± 0.27 (n=4)*, #

Table 3.5. Multiple linear regression analysis results for select characteristics (bottom water temperature, SOC content (%), C:N ratio, porosity (%), median grain size (μm)) that may influence benthic diffusive oxygen uptake (DOU, mmol O_2 m^{-2} d^{-1}). For each parameter we calculated 1) slope: the estimated regression coefficient of the linear regression, 2) p-value: the statistical significance of the regression coefficient, 3) lmg: the relative importance of each parameter in explaining data variability, and 4) variance inflation factor (VIF): a measure of collinearity among independent variables, where values between 1 and 4 were considered an acceptable level of correlation between independent variables.

Multiple Regression	slope	p value	lmg	VIF
Intercept	-0.75	0.0646	NA	NA
Temperature (°C)	0.13	0.0055	0.28	2.36
SOC (%)	0.68	0.0009	0.72	2.36

Table 3.6. Benthic DOU was scaled up to the area of Elson Lagoon (207 km^2) over all three seasons (Ice Cover, Break Up, Open Water) between shallow and deep stations to calculate an annual sediment microbial respiration rate.

Depth	Annual DOU (megamoles O_2)			% Total
	Ice Cover (7.5 month)	Break Up (1 month)	Open Water (3.5 months)	
Shallow	NA	1.1	6.1	**5%**
Deep	67.9	11.4	51.1	**95%**
% Total	**49%**	**9%**	**42%**	

3.9 Figures

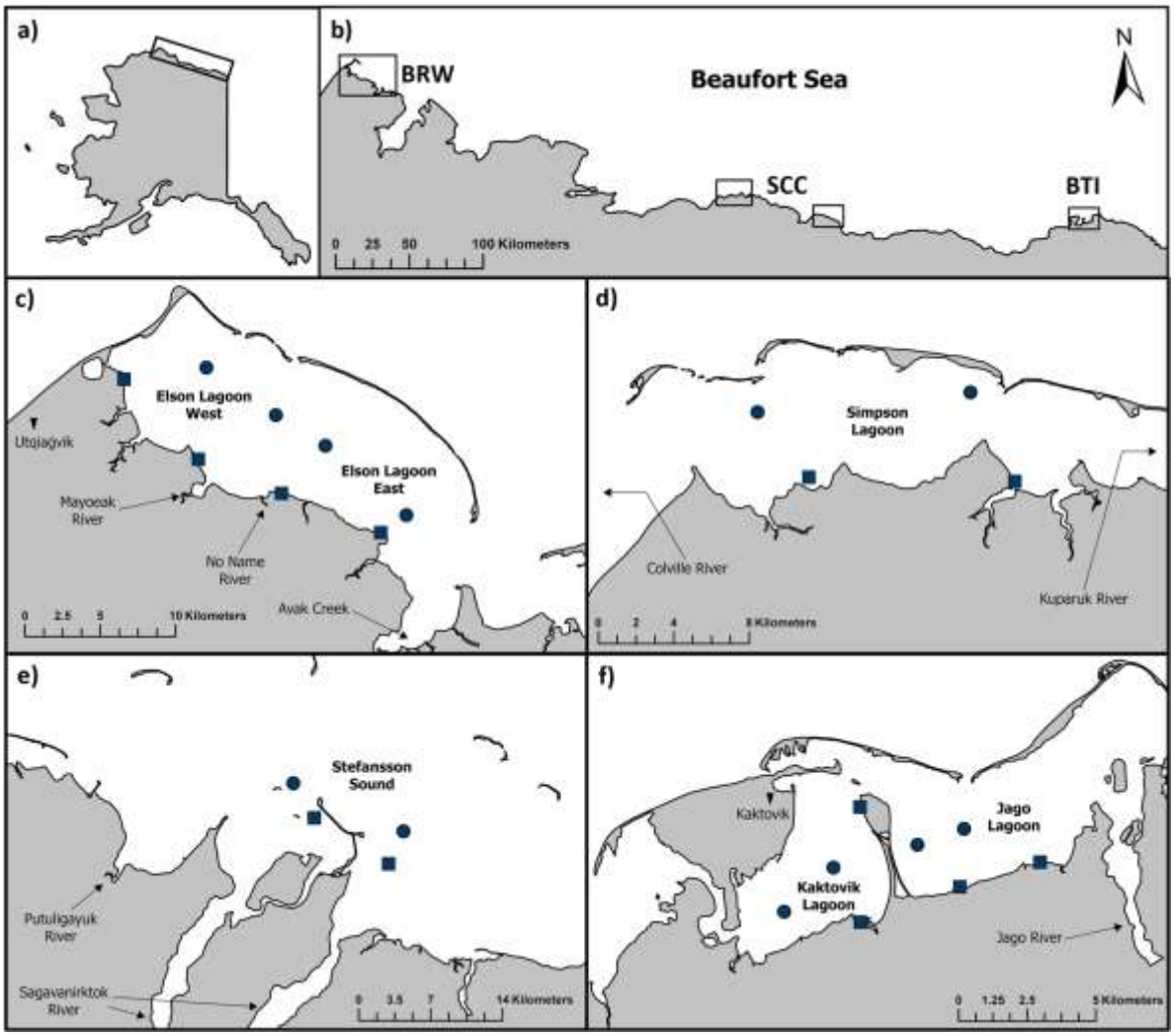

Figure 3.1 Location of the study sites at the Beaufort Lagoon Ecosystems Long-Term Ecological Research (BLE-LTER) program. a) Map of Alaska with Beaufort Sea Alaskan coast in box. b) Beaufort Sea Coast with BLE-LTER research nodes in boxes. c) The westernmost node (BRW) is based out of Utqiaġvik where Elson Lagoon is located. The central node (SCC) contains d) Simpson Lagoon and e) Stefansson Sound. The eastern node (BTI) is based out of Kaktovik and contains f) Kaktovik Lagoon and Jago Lagoon. Each sampled lagoon has two shallow (squares) and two deep (circles) stations.

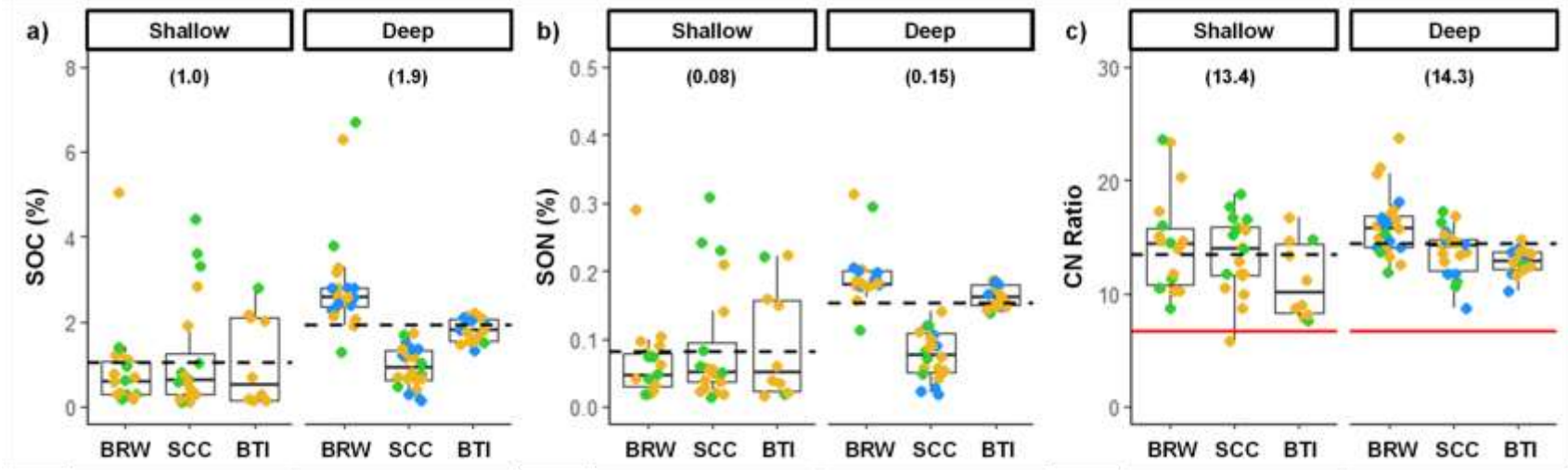

Figure 3.2. BLE-LTER Core Program dataset (2019-2021) of a) sediment organic carbon (SOC, %), b) sediment organic nitrogen (SON, %), and c) C:N ratio across nodes (BRW, SCC, BTI), separated by water depth (Shallow, Deep) and colored by season: Ice Cover (blue), Break Up (green), and Open Water (yellow). The lower and upper extent of the boxplot represent the 25th (Q1) and 75th (Q3) percentiles, while the lower and upper extent of the whiskers represent 1.5 times the interquartile range (Q3-Q1) below Q1 and above Q3. The solid black line within each box represents the median value and the dashed black line and parentheses at the top of each panel denote the mean across all nodes at each depth. The solid red line in c) represents the Redfield ratio of 106C:16N.

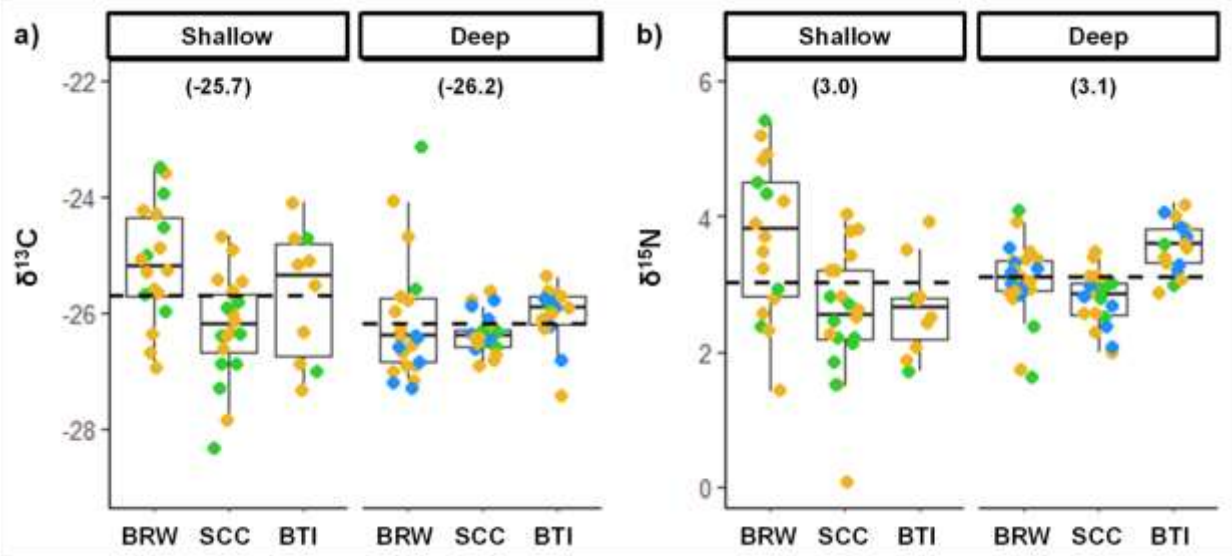

Figure 3.3. a) $\delta^{13}C$ and b) $\delta^{15}N$ values (‰) of lagoon sediments across nodes (BRW, SCC, BTI), separated by water depth (Shallow, Deep) and colored by season: Ice Cover (blue), Break Up (green), and Open Water (yellow). The lower and upper extent of the boxplot represent the 25th (Q1) and 75th (Q3) percentiles, while the lower and upper extent of the whiskers represent 1.5 times the interquartile range (Q3-Q1) below Q1 and above Q3. The mean across all nodes at each depth is denoted by the dashed black line and written in parentheses at the top of the panel.

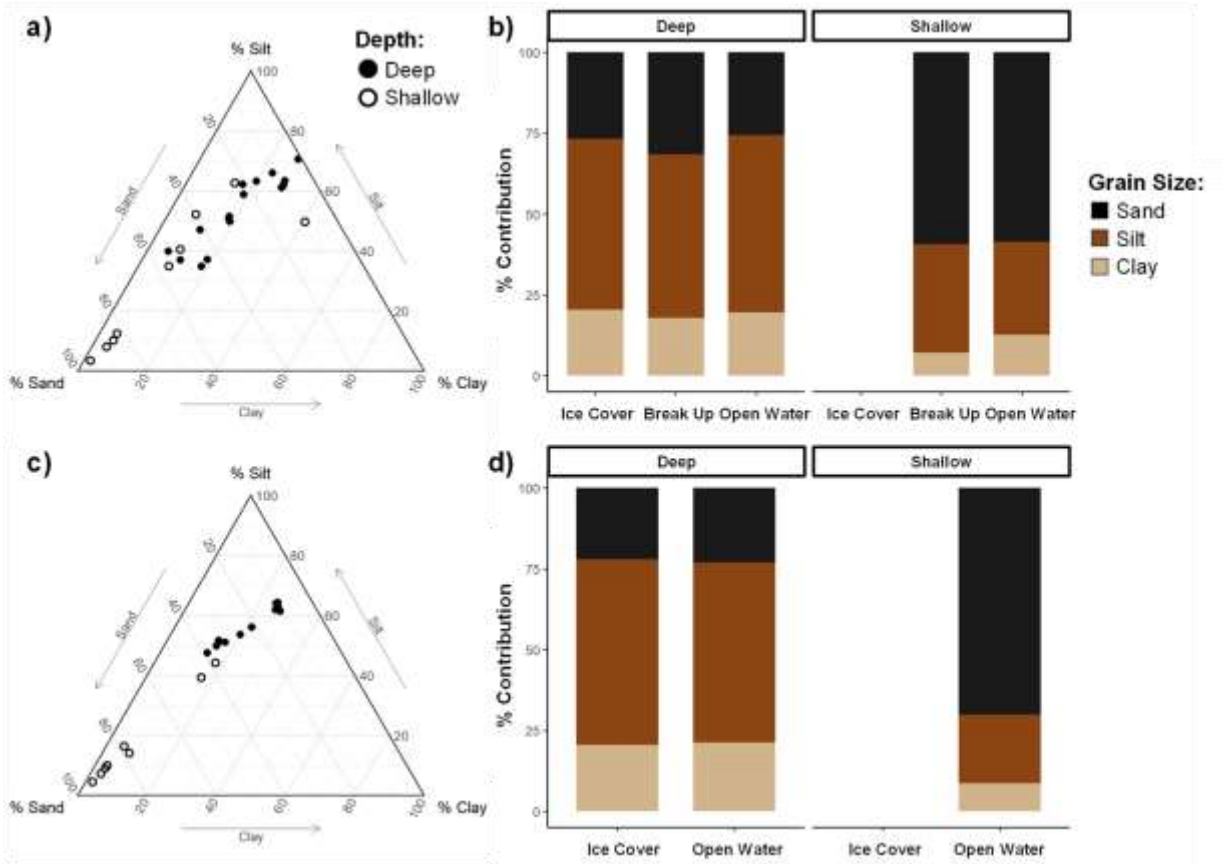

Figure 3.4. a) Ternary plot of grain size distribution showing % Sand (62.5 µm - 2000 µm), % Silt (4 µm - 62.5 µm), and % Clay (<4 µm) at Shallow (empty circle) and Deep stations (filled circle) for BLE-LTER sediments and c) Elson Lagoon case study sediments. b) The same grain size data grouped by season (Ice Cover, Break Up, Open Water) and water depth (Deep, Shallow) for BLE-LTER sediments and d) Elson Lagoon case study sediments. Shallow stations were not sampled during Ice Cover and Break Up was not sampled in the Elson Lagoon case study.

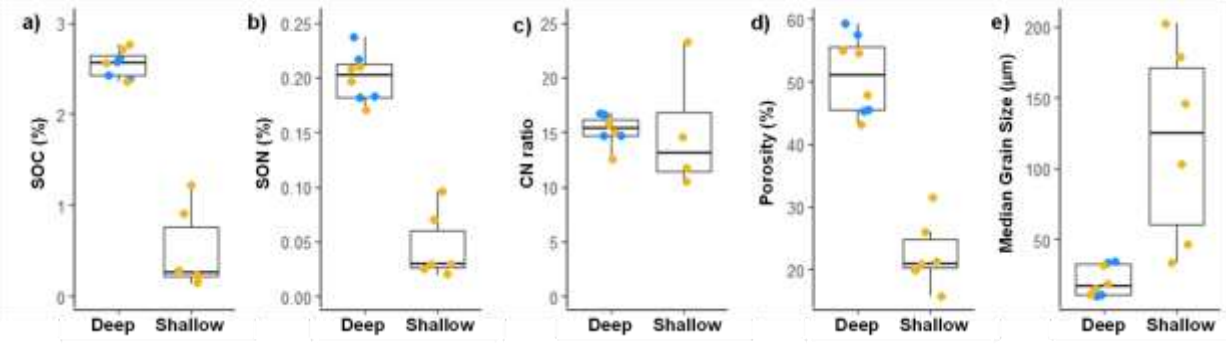

Figure 3.5. Elson Lagoon focused study: Surface sediment (0-2 cm depth) characteristics of a) SOC (%), b) SON (%), c) C:N ratio, d) porosity (%), and e) median grain size (µm) in Elson Lagoon separated by water depth (Deep, Shallow) and colored by season (blue=Ice Cover, yellow=Open Water). The lower and upper extent of the boxplot represent the 25th (Q1) and 75th (Q3) percentiles, while the lower and upper extent of the whiskers represent 1.5 times the interquartile range (Q3-Q1) below Q1 and above Q3. The solid black line within each box represents the median value. In the Elson Lagoon focused study, samples were not collected during Break Up or at shallow stations during Ice Cover.

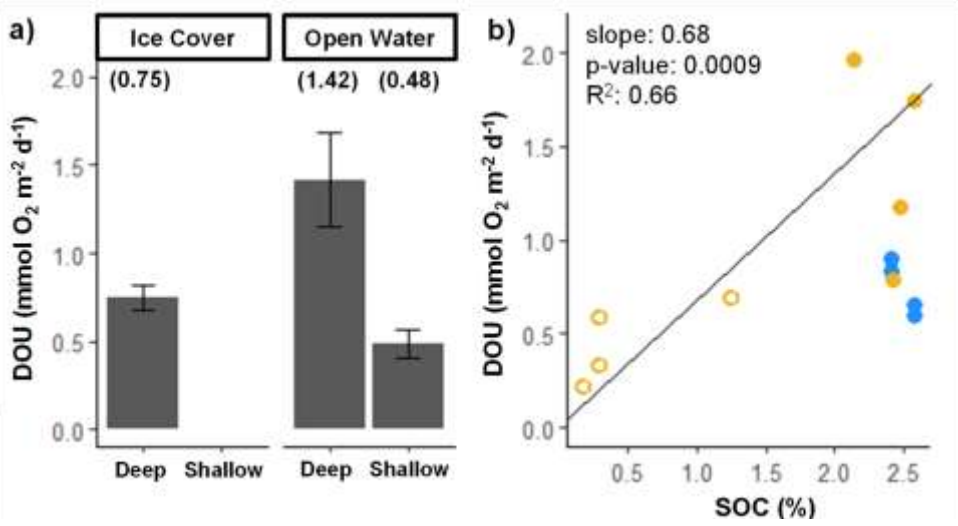

Figure 3.6. a) Diffusive oxygen uptake (DOU, mmol O_2 m^{-2} d^{-1}) for Elson Lagoon focused study (2022) grouped by season (Ice Cover, Open Water) and water depth (Deep, Shallow). The average DOU rate for each season and depth is denoted in parentheses at the top of the panel. b) Regression of sediment organic carbon content (SOC, %) and DOU (mmol O_2 m^{-2} d^{-1}) grouped by season (blue=Ice Cover, yellow=Open Water) and water depth (filled=Shallow, hollow=Deep), with associated slope, R^2, and p-value. DOU was not measured during the Break Up season.

3.10 Appendix B

Supplemental Table 3.1. List of historical (1945-53) smooth sheets created from National Ocean Service (NOS) hydrographic surveys. Soundings were collected by fathometers, and navigation was conducted by hydrographic sextant (visual triangulation) or Shoran (radio).

Site	Smooth Sheet ID	Scale	Correction
Elson Lagoon	H07071	1:20,000	digitized
Simpson Lagoon	H07917	1:20,000	digitized
	H07196	1:20,000	digitized
Stefansson Sound	H07760	1:20,000	digitized
	H07857	1:20,000	digitized
	H07757	1:20,000	digitized
	H07758	1:20,000	digitized
Kaktovik Lagoon	H07657	1:20,000	digitized
Jago Lagoon			

Supplemental Table 3.2. PERMANOVA results on the effect of node, season and water depth on sediment organic carbon (SOC, %), organic nitrogen (SON, %), and C:N ratio. When significant, post-hoc pairwise comparisons were performed on independent and interaction factors.

SOC	Df	Sum of Squares	R2	F	P
node	2	1.2957	0.08682	7.1093	0.0004
season	2	0.3803	0.02548	2.0866	0.0915
depth	1	2.4583	0.16472	26.9765	0.0001
node:season	4	0.7237	0.04849	1.9854	0.058
node:depth	2	1.2128	0.08127	6.6545	0.0004
season:depth	1	0.0739	0.00495	0.8107	0.4171
node:season:depth	2	0.1222	0.00819	0.6702	0.5929

ADONIS pairwise node	p adj
central - west	0.0036
east - west	1
east - central	0.0144

ADONIS pairwise depth	p adj	node:depth p_adj West	Central	East
shallow - deep	0.0001	0.0015	1	0.009

SON	Df	Sum of Squares	R2	F	P
node	2	1.3065	0.10554	9.3237	0.0001
season	2	0.3782	0.03055	2.6993	0.0463
depth	1	2.2386	0.18084	31.9521	0.0001
node:season	4	0.6606	0.05336	2.3572	0.0322
node:depth	2	0.9575	0.07734	6.8329	0.0006
season:depth	1	0.0386	0.00312	0.5514	0.5318
node:season:depth	2	0.1433	0.01158	1.0228	0.3743

ADONIS pairwise node	p adj
central - west	0.0036
east - west	1
east - central	0.0012

ADONIS pairwise season	p adj	node:season p_adj West	Central	East
break up - open water	1	1	1	1
break up - ice cover	0.2031	0.198	1	1
open water - ice cover	0.2115	1	1	1

ADONIS pairwise depth	p adj	node:depth p_adj West	Central	East
shallow - deep	0.0001	0.0015	1	0.0135

CN Ratio	Df	Sum of Squares	R2	F	P
node	2	0.18135	0.12463	8.2302	0.0003
season	2	0.00372	0.00256	0.169	0.9037
depth	1	0.07751	0.05327	7.0351	0.0063
node:season	4	0.0797	0.05477	1.8084	0.1196
node:depth	2	0.01117	0.00767	0.5067	0.6303
season:depth	1	0.03514	0.02415	3.1898	0.0715
node:season:depth	2	0.01985	0.01364	0.9008	0.402

ADONIS pairwise node	p adj	node:depth p_adj shallow	deep
central - west	0.072	1	0.0285
east - west	0.0015	0.6285	0.0015
east - central	0.1452	1	1

ADONIS pairwise depth	p adj
shallow - deep	0.0255

Supplemental Table 3.3. PERMANOVA results on the effect of node, season and water depth on sediment organic carbon and nitrogen stable isotopes ($\delta^{13}C$ and $\delta^{15}N$, ‰). When significant, post-hoc pairwise comparisons were performed on independent and interaction factors.

$\delta^{13}C$	Df	Sum of Squares	R2	F	P
node	2	0.003122	0.08729	6.5431	0.002
season	2	0.001883	0.05265	3.9462	0.0216
depth	1	0.0013	0.03636	5.45	0.0192
node:season	4	0.005421	0.15158	5.6807	0.0006
node:depth	2	0.000188	0.00525	0.3932	0.6747
season:depth	1	0.001025	0.02865	4.2955	0.0434
node:season:depth	2	0.000161	0.00451	0.3381	0.7096
ADONIS pairwise season	**p adj**				
break up - open water	1				
break up - ice cover	0.1302				
open water - ice cover	0.0792				
ADONIS pairwise node	**p adj**	**node:season p_adj**			
		West	**Central**	**East**	
central - west	0.0066	1	0.0036	1	
east - west	1	1	1	1	
east - central	0.0723	1	1	1	
ADONIS pairwise depth	**p adj**	**node:depth p_adj**			
		West	**Central**	**East**	
shallow - deep	0.008	---	1	0.053	

$\delta^{15}N$	Df	Sum of Squares	R2	F	P
node	2	0.19879	0.07593	4.7548	0.0018
season	2	0.04601	0.01757	1.1006	0.3538
depth	1	0.03231	0.01234	1.5458	0.1867
node:season	4	0.0899	0.03434	1.0751	0.3778
node:depth	2	0.19202	0.07334	4.5929	0.0024
season:depth	1	0.00476	0.00182	0.2277	0.8
node:season:depth	2	0.06849	0.02616	1.6381	0.1781
ADONIS node	**p adj**	**node:depth p_adj**			
		shallow	**deep**		
central - west	0.0036	0.0855	0.0036		
east - west	1	0.267	0.0495		
east - central	0.0219	1	0.0015		
ADONIS pairwise depth	**p adj**				
shallow - deep	0.0255				

Supplemental Table 3.4. PERMANOVA results on the effect of node, season and water depth on sediment grain size distribution (Sand %, Silt %, Clay %) for BLE-LTER core program sediment samples. When significant, post-hoc pairwise comparisons were performed on independent and interaction factors.

Sand (%)	Df	Sum of Squares	R2	F	P
node	2	0.68355	0.22743	3.0339	0.0385
season	2	0.09479	0.03154	0.4207	0.8181
depth	1	0.23764	0.07907	2.1095	0.1273
node:season	2	0.30841	0.10261	1.3689	0.2619
node:depth	1	0.03103	0.01032	0.2754	0.8229
season:depth	1	0.04483	0.01492	0.398	0.7097
node:season:depth	1	0.02819	0.00938	0.2503	0.8165

ADONIS node	p adj
central - west	0.8739
east - west	0.0555
east - central	0.2211

Silt (%)	Df	Sum of Squares	R2	F	P
node	2	0.10634	0.05281	0.7689	0.4974
season	2	0.08941	0.0444	0.6465	0.5964
depth	1	0.46657	0.2317	6.747	0.0102
node:season	2	0.21472	0.10663	1.5525	0.2235
node:depth	1	0.06405	0.03181	0.9262	0.3829
season:depth	1	0.00488	0.00242	0.0706	0.9478
node:season:depth	1	0.09959	0.04946	1.4402	0.2516

ADONIS depth	p adj
shallow - deep	0.002

node	2	0.18924	0.08711	1.517	0.2207
season	2	0.21508	0.099	1.7241	0.175
depth	1	0.46731	0.2151	7.4921	0.0076
node:season	2	0.29339	0.13505	2.3519	0.103
node:depth	1	0.07309	0.03364	1.1718	0.3005
season:depth	1	0.03378	0.01555	0.5415	0.558
node:season:depth	1	0.02735	0.01259	0.4385	0.6148

ADONIS depth	p adj
shallow - deep	0.0007

Grain Size Median (um)	Df	Sum of Squares	R2	F	P
node	2	0.18924	0.08711	1.517	0.2207
season	2	0.21508	0.099	1.7241	0.175
depth	1	0.46731	0.2151	7.4921	0.0076
node:season	2	0.29339	0.13505	2.3519	0.103
node:depth	1	0.07309	0.03364	1.1718	0.3005
season:depth	1	0.03378	0.01555	0.5415	0.558
node:season:depth	1	0.02735	0.01259	0.4385	0.6148

ADONIS depth	p adj
shallow - deep	0.0025

Supplemental Table 3.5. p values for T-tests comparing sediment characteristics (Sand %, Silt %, Clay %, median grain, porosity %) and organic matter content (SOC %, SON %, C:N ratio) between deep stations across Seasons (Ice Cover vs. Open Water) and Water Depth (Shallow vs. Deep) during the Open Water period.

Parameter	T-test p value	
	Season	Water Depth
Sand (%)	0.9069	0.0028
Silt (%)	0.6983	0.0027
Clay (%)	0.8496	0.0054
Median Grain Size (um)	0.7407	0.0166
Sort	0.7859	0.5490
Skew	0.7235	0.0554
Kurtosis	0.5716	0.1517
Porosity (%)	0.6966	0.0002
SOC (%)	0.4557	0.0025
SON (%)	0.478	0.0030
C:N	0.3981	0.9443
Temperature (C)	0.0012	0.0347
DOU (mmol O_2 m^{-2} d^{-1})	0.0844	0.0348

Supplemental Table 3.6. The stepwise selection regression model output for DOU rates displays the model with the lowest prediction error using a defined number of parameters (1-4). For each model, we calculated RMSE and MAE, which measure the prediction error of each model, with lower values indicating a better model. Adjusted R^2 values represent the correlation between values observed and predicted by the model, with higher values indicating a better model.

Model	Factor				
	Temp (C)	SOC (%)	C:N	Porosity (%)	Median grain size (um)
1				*	
2	*	*			
3	*	*	*		
4	*	*		*	*

Model	Nvmax	RMSE	MAE	Adj R2
1	1	17.97	17.88	0.38
2	2	12.13	11.96	0.63
3	3	19.40	17.42	0.62
4	4	18.23	16.46	0.75

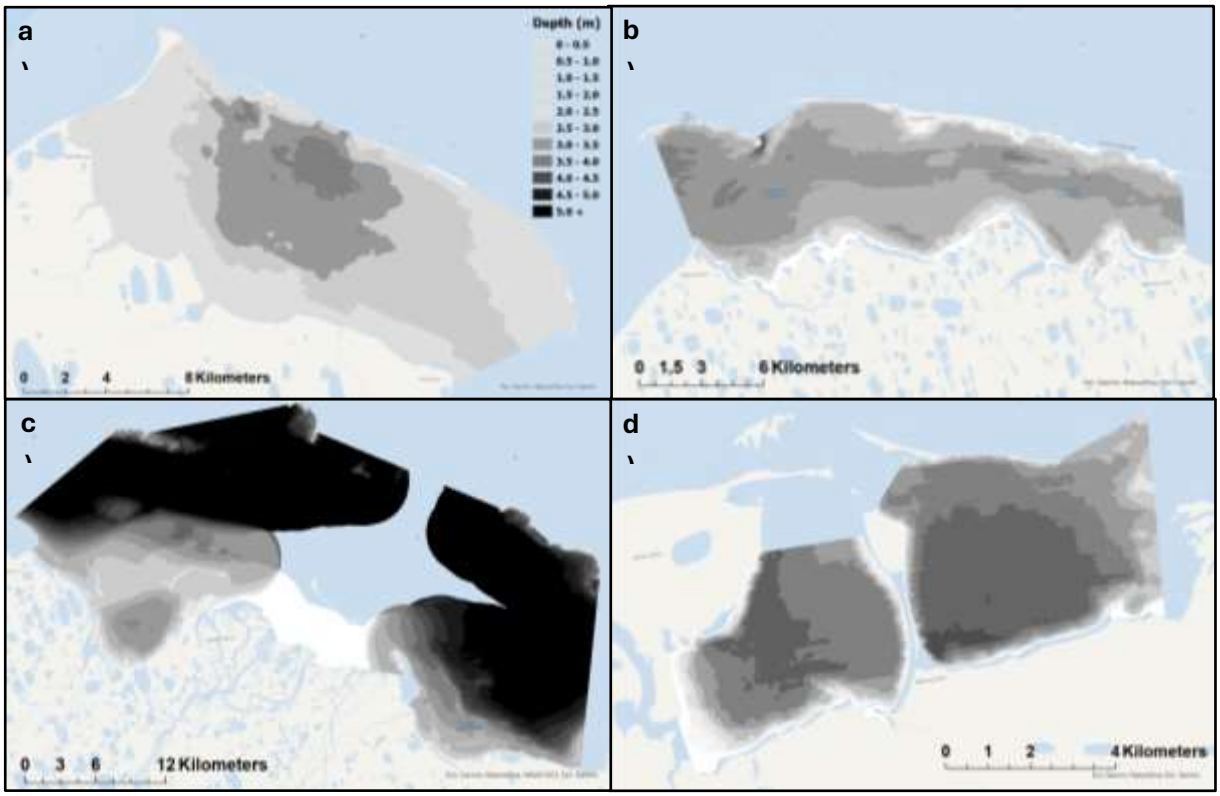

Supplemental Figure 3.1. Bathymetry of study sites derived from inverse distance weighted (IDW) interpolation of point depth soundings from National Ocean Services surveys from 1945 to 1953 for a) Elson Lagoon, b) Simpson Lagoon, c) Stefansson Sound, Kaktovik Lagoon (d, left) and Jago Lagoon (d, right). Lagoon depth is colored in 0.5 m increments with white denoting a depth of 0 and black representing a depth > 5.0 m.

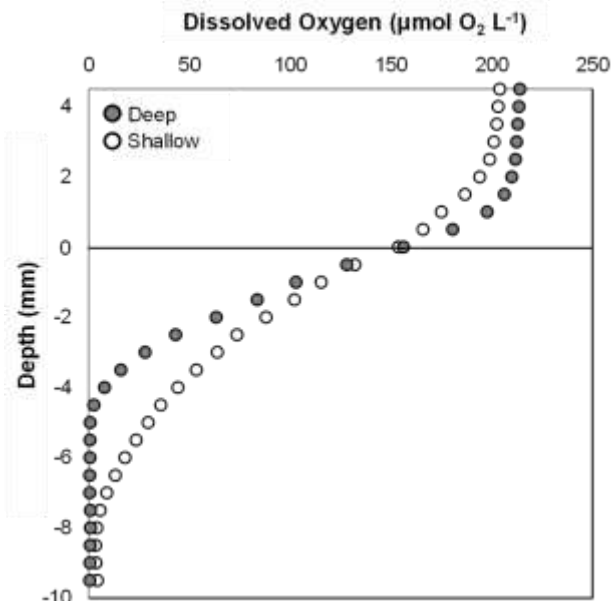

Supplemental Figure 3.2. Example sediment O_2 microprofiles from Unisense oxygen sensor. Two profiles during Open Water are shown to highlight the differences between Deep (EEL D1, filled circles) and Shallow (EWL S1, empty circles) stations.

Chapter 4: Seasonality of benthic metabolism and nutrient cycling in Beaufort Sea lagoons

4.1 Abstract

Alaska's Beaufort Sea coast is bordered by a discontinuous chain of barrier islands that enclose numerous shallow lagoons and sounds. Seasonally influenced by river discharge and coastal erosion, these lagoons receive and process ample terrestrial material and nutrients creating a "hotspot" of biogeochemical activity. Because of their shallow nature, sediments can exhibit high rates of primary production (PP) removing nutrients from the overlying water column. In contrast, organic matter remineralization can release nutrients from the sediments potentially fueling water column PP. While rising rates of PP in the Arctic Ocean appear to be driven by increasing terrestrial inputs, the seasonal trends and microbial processes driving nearshore coastal productivity remain underexplored. To that end, we quantified seasonal and spatial variations in sediment metabolism and nutrient fluxes in five Arctic lagoons. As part of the BLE-LTER program, we sampled the lagoons during Ice Cover, Break Up, and Open Water in alignment with the major hydrological phases. Sediment cores were incubated in the lab to measure net benthic fluxes of O_2, DIC, N_2, and dissolved inorganic nutrients (NH_4^+, NO_3^-, PO_4^{3-}, DSi). We calculated daily rates of benthic respiration (BR), gross benthic primary production (GBP), and net benthic metabolism (NBM). During Ice Cover, we observed net heterotrophy (3.3 ± 1.1 mmol C m^{-2} d^{-1}), inorganic nutrient release, and net nitrogen removal through denitrification (1.9 ± 0.6 mmol N m^{-2} d^{-1}). With melting sea ice and light availability during Break Up, benthic microalgae rapidly colonize the benthos, turning the sediments net autotrophic (Break Up: -20.8 ± 8.0 mmol C m^{-2} d^{-1}, Open Water: -8.9 ± 2.6 mmol C m^{-2} d^{-1}). This shift in productivity increased sediment nutrient demand which was shown through net nutrient

uptake and nitrogen fixation. As the coastal Arctic undergoes rapid changes in temperature, duration of sea ice, terrestrial nutrient export, and coastal erosion, our understanding of seasonal metabolism will help to better constrain future projections of coastal Arctic ecosystem productivity.

4.2 Introduction

Coastal lagoons are present on all continents making up ~12% of global (De Witt, 2011) and over half of the Alaskan Arctic coastline (Wiseman et al. 1973; Dunton et al., 2006). They are unique compared to deeper estuaries due to their shallow depth which allows for an extended photic zone, tight benthic-pelagic coupling, and high rates of productivity and nutrient cycling (Borges & Abril, 2011; McGlathery et al., 2001, 2007). Along the Alaskan Beaufort Sea coast, there are several irregular and discontinuous chains of barrier islands that enclose numerous shallow (<7 m) lagoons and sounds (Fig. 4.1). Beginning in late September, seasonal ice cover extends for nine months of the year, with shallow areas of the lagoons developing ice down to the sediment surface (Fig. 4.2). Annually, water column temperatures range from -2 to 14 ^{o}C, and salinities vary drastically, from fresh (0) to hypersaline (45+) (Harris et al., 2017). This large salinity range is a result of both the spring freshet introducing large volumes of freshwater into the lagoons during the break up period, and the hypersaline conditions under ice due to salt exclusion during ice formation (Harris et al., 2017; Macdonald & Yu, 2006; Yamamoto-Kawai et al., 2005). In addition to extreme fluctuations in temperature, salinity, and sea ice conditions, the lagoons are subject to polar light conditions, which include low overall sunlight intensities due to the low angle of incidence as well as months-long periods of continuous light (“midnight sun”) or dark (“polar night”; Fig. 4.2). Despite these extreme seasonal variations in environmental conditions, the biota in these shallow waters are abundant and diverse, including a variety of benthic infauna and epifauna that represent nearly every major invertebrate taxonomic group, along with several species of fish such as Arctic cod (*Boreogadus saida*) (Craig et al., 1984; Dunton et al., 2012).

During a short period from May to July, Arctic rivers discharge >90% of their annual nutrient and organic matter export and most of their water inputs (Dittmar & Kattner, 2003; Holmes et al., 2012; McClelland et al., 2014). Relative to lower latitudes, Arctic rivers have some of the highest concentrations of organic matter, with annual exports on par with the Amazon River, while inorganic nutrients in Arctic rivers are among the lowest worldwide (Dittmar & Kattner, 2003). This pattern of high organic matter and low inorganic nutrients is due to the Arctic watershed, which contains large areas of permafrost and wetlands that release high concentrations of dissolved organic carbon (DOC) (Bristol et al., 2021; Johnston et al., 2019; Connolly et al. 2020).

During the summer when the coast is free of sea ice cover for 3-4 months, the lagoons receive additional terrestrial inputs in the form of eroding tundra soils and underlying permafrost (Overduin et al., 2014). During this period, coastal bluffs are exposed to wind and wave activity that facilitate erosion. This is exacerbated by mechanical permafrost degradation (Barnhart et al., 2014b; Overeem et al., 2011). Average rates of coastal erosion for the Arctic (0.5 m $year^{-1}$) are among the highest in the world, due in part to the ice-bonded nature of the coast (Jones et al., 2009; Lantuit et al., 2011). The Beaufort Sea coastline is characterized by the strongest retreat, with coastal erosion rates exceeding 1.1 m $year^{-1}$ on average (Lantuit et al., 2011).

Due to climate change and changes in freshwater inflow, coastal erosion, ice cover, and exchange with the ocean, Alaska's northern Arctic coastal ecosystem is experiencing dramatic changes in the input and availability of organic matter and nutrients. For example, primary production in the Arctic Ocean has increased ~30% over the past several decades (Ardyna & Arrigo, 2020; Arrigo et al., 2008; Arrigo & Van Dijken,

2015; Lannuzel et al., 2020) with terrestrial nitrogen inputs playing a crucial role in supporting Arctic Ocean production (Terhaar et al., 2021; Thibodeau et al., 2017). Although thick sea ice and surface snow can diminish irradiance to <2% of surface PAR, Arctic marine productivity is supported by benthic microalgae (BMA) and macroalgae, pelagic phytoplankton, and sea ice algae (Attard et al., 2024; Glud et al., 2009; Lannuzel et al., 2020). In addition to sea ice algae and phytoplankton waters, the shallow nature of coastal lagoons allows for an extended photic zone to the sediments, supporting the prolific growth of benthic primary producers such as micro- and macroalgae (Hardison et al., 2013; Karsten et al., 2006, 2006, 2012). In fact, in a low-nutrient, oligotrophic environment like the coastal Arctic, benthic primary production tends to exceed pelagic primary production since BMA can gain nutrients from the sediments as well as the water column (R. N. Glud et al., 2009; Karsten et al., 2012).

While coastal lagoon sediments can be a source of nutrients (from remineralization of organic matter) released to the overlying waters, fueling benthic and pelagic primary production (Dalsgaard, 2003; Manini et al., 2003; McGlathery et al., 2007; Nowicki & Nixon, 1985), they can also function as sites of nutrient retention through biomass accumulation, removal through denitrification, and input through nitrogen fixation (Canion et al., 2014; Damashek & Francis, 2018; Fulweiler, 2023; Hardison et al., 2011; Newell et al., 2016). Within anoxic sediments, nitrogen (N) may be removed via denitrification or anaerobic ammonium oxidation (anammox) and released as dinitrogen gas (N_2). Denitrification is the stepwise reduction of nitrate (NO_3^-) to N_2 gas by denitrifying microbes. Recent work in the Chukchi Sea shelf shows sediments can be a source of ammonium (NH_4^+) release, but high rates of denitrification resulted in net N removal by the sediments

(Hardison et al., 2017; McTigue et al., 2016). However, recent studies have shown that benthic nitrogen fixation may also play an important role in marine systems with rates on par or even exceeding rates of denitrification (Newell et al., 2016).

Currently, the Arctic climate system is in a transitional state, marked by declining summer sea ice extent, altered ecosystem dynamics, shifts in circulation patterns, and potential tipping points. Arctic-wide average surface temperatures have increased at four times the rate of global mean temperatures (Rantanen et al., 2022) — a phenomenon known as Arctic amplification (Serreze & Barry, 2011). Arctic amplification is largely attributed to the loss of sea ice cover (Previdi et al., 2021; Serreze & Barry, 2011). In response to increasing atmospheric temperatures, more snow and ice on land is melting, driving increasing river discharge from major Arctic rivers, with a noticeable “freshening” of the coastal Arctic (Ahmed et al., 2020; Fichot et al., 2013; Peterson et al., 2002; Proshutinsky et al., 2015). Increasing atmospheric and water temperatures are expanding the open water period of the coastal Arctic by approximately 1-2 days per year (Markus et al., 2009; Stroeve et al., 2014), leading to increased thaw and more physical degradation of permafrost through winds, waves, and storms.

While recent studies have confirmed an increase in primary production in the Arctic in response to increasing terrestrial inputs alongside sea ice retreat (Arrigo and Dijken 2015; Lewis et al. 2020), the nearshore ecosystem processes that determine the magnitude and form of these nutrient exports are systematically understudied (Fritz et al. 2017). To that end, in this study, we conducted batch sediment incubations to measure benthic metabolism, N_2 fluxes, and nutrient fluxes during three distinct hydrological

seasons (Ice Cover, Break Up, Open Water) to quantify annual rates of nearshore benthic carbon and nitrogen cycling in coastal Arctic lagoons along the North coast of Alaska.

4.3 Methods

4.3.1 Study site

The study area is composed of several lagoons and sounds along the Alaskan coast of the Beaufort Sea in alignment with the Beaufort Lagoon Ecosystems Long-Term Ecological Research (BLE-LTER) program (ble.lternet.edu). The BLE-LTER program operates out of three nodes, spanning ~100 km of the Alaskan coastline: Utqiaġvik (formerly Barrow; BRW), Prudhoe Bay (SCC), and Barter Island (BTI) to represent the western, central, and eastern Beaufort Sea coast, respectively (Fig. 4.1). Each node has two lagoons. In the western node, the BLE-LTER samples Elson Lagoon, which divides into Elson Lagoon West and Elson Lagoon East for sampling purposes. The central node has Simpson Lagoon and Stefansson Sound, and the eastern node has Kaktovik Lagoon and Jago Lagoon. The western node is located near the village of Utqiaġvik at the boundary between the Chukchi Sea to the west and the Beaufort Sea to the north (Fig. 4.1). It is delineated by a 25 km chain of barrier islands and receives freshwater inputs from many streams (Lewellen, 1972). Exchange between Elson Lagoon and the Beaufort Sea occurs through three channels within the barrier island chain (Okkonen, 2008). In addition to these channels, the eastern side of the lagoon contains the mouth of Avak Creek as well as a wide passage to the Beaufort Sea. The central node, based in the Prudhoe Bay oil field region, contains Simpson Lagoon and Stefansson Sound. Simpson Lagoon receives the most of its freshwater inputs from the Kuparuk and Colville Rivers

(Craig et al., 1984). Stefansson Sound, which has the smallest barrier islands and is the least enclosed of the BLE-LTER lagoons, is located roughly 50 km east of Simpson Lagoon and receives inputs from the Sagavanirktok River. The two smallest sites, Kaktovik Lagoon and Jago Lagoon represent the eastern node and are located near the village of Kaktovik. With no tidal inlet or major river, Kaktovik Lagoon experiences the least marine exchange and freshwater through surface run off. In contrast, Jago Lagoon receives freshwater inputs from the Jago River and connects directly to the open ocean through a passage near its eastern end.

4.3.2 Sampling scheme

Samples were collected as part of the BLE-LTER program. To examine seasonal and interannual variations of benthic metabolism, N_2 fluxes, and inorganic nutrient fluxes, incubations were conducted three times during the year in conjunction with key phases of the hydrological cycle (i.e., Ice Cover, Break Up, and Open Water periods; Fig. 4.2) from 2019-2022. To determine spatial variation, six BLE-LTER lagoons were sampled, with each lagoon consisting of one shallow (<1 m water depth) and one deep (3-5 m water depth) station (Fig. 4.1). During the Ice Cover period, samples were not collected at shallow stations due to the presence of landfast ice. Sample timing was impacted by the COVID-19 pandemic. In 2019, samples were collected in all six lagoons. In 2020, no samples were collected due to travel restrictions. In 2021 and 2022 sampling resumed, but only for Elson Lagoon. At each station, undisturbed, intact sediment cores (inner diameter: 10 cm, core height 30 cm, sediment height ~10 cm) were collected in triplicate using a modified HYPOX corer (Gardner et al., 2009) along with 20 L of unfiltered bottom

water using a bilge pump. Once collected, sediment cores were transported to the field lab, aerated, and kept at in-situ temperatures in the dark to equilibrate overnight before incubations commenced.

4.3.3. Batch sediment incubations

After the equilibration period, two sediment cores from each station were set up for batch sediment incubations as described by Rysgaard and colleagues (2004). Two cores containing sediment with overlying water were sealed with a gas-tight lid containing a built-in stir bar. To isolate the influence of benthic activity, a third core was filled with site water only and sealed and incubated to quantify and subtract the influence of water column metabolism. The water blanks and water overlying sediment were stirred slowly with built-in stir bars throughout the incubations. Dark incubations were run first. The cores were wrapped in aluminum foil, incubated at in-situ temperatures in the dark, and sampled four times over 12 to 30 hours to determine dark fluxes. After the dark incubations, full spectrum (430 – 740 nm) 1000-watt grow lights were turned on and adjusted with shade sheets until in-situ light levels were achieved (range: 18.0 – 238 µmol s^{-1} m^{-2}). Sediment cores were exposed to the light for at least four hours to allow for acclimation to the lights. Then, cores were sampled four times over 12 hours to measure light fluxes. During the Ice Cover period, the dark incubations were longer than 12 hours in anticipation of slow rates due to low temperatures, and light incubations were not conducted due to the presence of thick (>1.5m) sea ice and snow and little to no light availability at the sediment surface (Bonsell and Dunton, 2018; Dunton, 1984).

For each sampling during the dark and light incubations, water from each core was collected using an outflow port connected to Tygon tubing to measure dissolved oxygen (DO), dissolved inorganic carbon (DIC, n=2), N_2 gas (n=2), and dissolved inorganic nutrients (n=1). To create flow during sampling and to offset the volume removed during each sampling (~15% core water volume), an elevated carboy containing site water was connected through a series of airtight valves and tubing to the inflow port at the top of each core. By opening and closing these valves, we were able to direct and control the gravity-fed flow of water through the air-tight incubation system (following Cornwell et al. 2014; Miller-Way et al. 1994; Margalhaes et al., 2002).

4.3.4 Dissolved oxygen (O_2)

Dissolved oxygen (mmol O_2 L^{-1}) was measured using an optical fiber flow-through cell oxygen sensor (PreSens FTC-PSt7) connected to the core outflow Tygon tubing. Outflow rates were approximately 1.0 mL s^{-1}, and DO measurements took ~90 seconds to stabilize before measurements were recorded in triplicate.

4.3.5 Dissolved inorganic carbon (DIC)

To collect DIC samples, the outflow tube was placed into the bottom of a 13mL Exetainer (Labco) before allowing the water to slowly fill and overflow for 3 volume equivalents before collecting the sample. Care was taken to avoid bubbles in the Exetainer. Once collected, the samples were preserved with 20 µL of a saturated mercuric chloride ($HgCl_2$) solution and refrigerated submerged in water until analysis. DIC samples were transported in a cooler to the Virginia Institute of Marine Science (VIMS), where DIC

concentration was determined with an infrared CO_2 detector-based DIC analyzer (Apollo SciTech-C3/LICOR-7000). Standards were made by dissolving known amounts of sodium carbonate in deionized water and purging it with helium before running dilution standards and checks. Occasionally, certified reference materials from A. G. Dickson of Scripps Institution of Oceanography were used as external reference checks.

4.3.6 N_2 gas

N_2 samples were collected in the same manner as for DIC but were preserved using 20 µL saturated zinc chloride ($ZnCl_2$). Samples were transported submerged in a cooler to VIMS, where they were analyzed for dissolved N_2 on a Bay Instruments membrane inlet mass spectrometer (MIMS) and quantified relative to ^{40}Ar using the N_2/Ar calculation (Kana et al. 1994). Samples were referenced against an air-equilibrated, deionized water standard at incubation temperature. This method provides net N_2 flux only and does not differentiate or quantify individual N cycling pathways (i.e., denitrification, nitrogen fixation). For this reason, positive N_2 fluxes indicate net denitrification, while negative fluxes indicate net nitrogen fixation.

4.3.7 Inorganic nutrients

For nutrients, water from the outflow tube was collected in a 30 mL acid-washed syringe, passed through a 0.45 µm polyethersulfone (PES) filter, and then frozen in a Whirl-Pak bag at -20℃ until analyses. Dissolved inorganic nutrient analyses included ammonium (NH_4^+), nitrite + nitrate (NO_2^- + NO_3^-), orthophosphate (PO_4^{3-}), and dissolved silica (DSi, only for 2021-2022). Nutrients were measured at the Core Facilities Laboratory at the University of Texas Marine Science Institute (UTMSI) on a continuous

flow-analyzer Lachat Quick Chem 8500 (2018-2020) and in the Hardison Lab at VIMS on a multi-channel FIAlyzer-1000 from Fluidic Intelligently Automated (FIA, 2021-2022). Duplicates were analyzed on both instruments to test precision and continuity during the transition from UTMSI to VIMS.

4.3.8 Benthic flux calculations

To calculate areal hourly benthic flux rates (mmol m^{-2} hr^{-1}) for dark and light incubations, a simple linear regression model was applied to each parameter using Equation 4.1 (Boynton et al. 2018):

Equation 4.1. Net benthic flux (mmol m^{-2} hr^{-1}) = $\left(\frac{dC_s}{dt} - \frac{dC_b}{dt}\right) x \left(\frac{V}{A}\right)$,

where dC_s/dt is the rate of change in concentration (mmol L^{-1} hr^{-1}) in the "sediment + water" core, dC_b/dt is the rate of change in concentration (mmol L^{-1} hr^{-1}) in the "water blank" core, V is the volume of water in the "sediment + water" core (L), and A is the surface area of the sediment core (m^2). Note that the estimated water activity from the "water blank" was subtracted from the "sediment + water" core to isolate "sediment only" flux. Positive fluxes indicate net benthic production of each parameter (DO, DIC, N_2, etc.) while negative fluxes indicate net benthic consumption of each parameter.

4.3.9. Benthic metabolism calculations

Rates of daily benthic respiration (BR), gross benthic production (GBP), and net benthic metabolism (NBM) were calculated using hourly light and dark benthic fluxes of O_2 using the following equations (Kemp & Testa, 2011):

Equation 4.2. BR (mmol O_2 m^{-2} d^{-1}) = F_D x 24 hrs

Equation 4.3. GBP (mmol O_2 m^{-2} d^{-1}) = (F_L – F_D) x h_L

Equation 4.4. NBM (mmol O_2 m^{-2} d^{-1}) = BR + GBP,

where F_D and F_L are fluxes of DO (mmol O_2 m^{-2} h^{-1}) during dark and light incubations respectively, and h_L represents the hours of daylight (www.timeanddate.com) during the season (Ice Cover = 17 hours; Break Up = 24 hours; Open Water = 19 hours). Based on the respiratory quotient (RQ) derived from the linear regression of DO and DIC fluxes of dark and light incubations for each season (this study), the units were then converted to units of carbon (mmol C m^{-2} d^{-1}).

Similarly, hourly rates of N_2 and inorganic nutrient (NH_4^+, NO_3^-, PO_4^{3-}, DSi) fluxes were also scaled up to daily net benthic flux rates (Eq. 4.5):

Equation 4.5. Net benthic flux (mmol [N_2, nutrients] m^{-2} d^{-1}) = (F_L x h_L) + (F_D x h_L).

4.3.10. Environmental data

At each sampling point, a suite of environmental parameters was measured in the field to identify potential physical and biological drivers of benthic fluxes. Handheld YSI ProDSS sonde meters were used to measure water column temperature, salinity, DO, pH, chlorophyll-a (chl-a), and phycoerythrin. Water column dissolved inorganic nutrients (NH_4^+, NO_3^-, PO_4^{3-}, DSi) were also analyzed. Surface sediment parameters were measured for sediment organic carbon (SOC), SOC-$\delta^{13}C$, C:N ratio, and porewater inorganic nutrients (NH_4^+, NO_3^-, PO_4^{3-}, DSi). All environmental data, except for photosynthetically active radiation (PAR), were sourced from the BLE-LTER core program, available at the Environmental Data Initiative (EDI) data catalog (Beaufort Lagoon Ecosystems LTER, Core Program, 2024). Light at the sediment surface (PAR) for this study was measured with a LICOR-193SA.

4.3.11. Statistical analyses

Given the unbalanced nature of the dataset due to COVID travel restrictions, lagoons were combined, and the data were analyzed to assess the impact of season and water depth (not node) on all benthic fluxes (DO, N_2, DIC, NH_4^+, NO_x^-, PO_4^{3-}, DSi). We used a two-way analysis of variance (ANOVA) to assess the impact of season (Ice Cover, Break Up, Open Water) and water depth (shallow <1.5 m, deep >1.5 m) on benthic fluxes. Because of the presence of landfast ice and frozen sediments at shallow stations during Ice Cover, for the ANOVAs, we assumed a benthic flux rate equal to 0 for the factorial combination of Ice Cover / shallow, with a sample size of 8 (n = 8, the average n of all other factorial treatments). When the ANOVA showed a significant effect (a = 0.05), a post-hoc Tukey multiple comparisons of means was used to determine how benthic fluxes varied across these season and water depth with 95% confidence intervals.

To identify potential environmental drivers of the benthic fluxes, a stepwise multivariate regression model was used to find relationships between flux rates and environmental parameters. A stepwise selection linear regression functions by iteratively adding and removing predictors in the model to find the subset of variables in the dataset resulting in the lowest prediction error (R package: leaps; Miller, 2020). With the addition and removal of each parameter, the significance of each regression term is tested. Parameter selection and elimination are repeated until the model cannot be significantly improved with new parameters. Three metrics were used to compare the accuracy of the models. Root mean square error (RMSE) and mean absolute error (MAE) measure the prediction error of each model, with lower values indicating a better model. R^2 indicates

the correlation between the predicted and observed values, with values closer to 1 indicating a better model. To narrow down the number of input parameters, the environmental variables were grouped into five categories (physical, water column nutrients, sediment organic matter, sediment nutrients, and sediment pigments). Within each category, a Pearson's correlation was performed to identify and remove highly correlated variables. Prior to the stepwise regression, the environmental data were tested for normality using a Shapiro-Wilk test, and any necessary transformations were applied.

4.4 Results

4.4.1 Benthic metabolism

For all seasons, sediment DO fluxes were negative for dark incubations and positive for light incubations (Fig. 4.3a; Table 4.1). Averaged across depths and seasons, dark O_2 fluxes were -0.38 ± 0.04 mmol O_2 m^{-2} h^{-1}, and light fluxes were 0.99 ± 0.19 mmol O_2 m^{-2} h^{-1} (Table 4.1). Sediment DIC fluxes exhibited a complementary pattern, with mostly DIC production during dark incubations and DIC consumption during light incubations (Fig. 4.3b, Supplementary Table 4.1). Averaged across depths and seasons, dark DIC fluxes were 0.06 ± 0.15 mmol C m^{-2} h^{-1} and light DIC fluxes were -0.96 ± 0.20 mmol C m^{-2} h^{-1}. Dark O_2 fluxes were more negative during Break Up (-0.37 ± 0.08 mmol O_2 m^{-2} h^{-1}) and Open Water (-0.48 ± 0.06 mmol O_2 m^{-2} h^{-1}) compared to Ice Cover (-0.19 ± 0.06 mmol O_2 m^{-2} h^{-1}) (Fig. 4.3a; Table 4.1; Supplementary Table 4.2). This was reflected in dark DIC fluxes which increased from consumption during Break Up (-0.38 ± 0.22 mmol C m^{-2} h^{-1}) to production during Open Water (0.42 ± 0.26 mmol C m^{-2} h^{-1}) (Fig. 4.3b; Supplementary Table 4.1). During light incubations, there was consistent production of O_2 during both Break Up (1.41 ± 0.38 mmol O_2 m^{-2} h^{-1}) and Open Water (0.79 ± 0.19 mmol

O_2 m^{-2} h^{-1}) (Fig. 4.3a; Table 4.1; Supplementary Table 4.2). In concert, we saw a significant negative flux of DIC during Break Up (-1.22 ± 0.34 mmol C m^{-2} h^{-1}) and Open Water (-0.83 ± 0.24 mmol C m^{-2} h^{-1}) (Fig. 4.3b; Supplementary Table 4.2).

Linear regressions of sediment DIC and DO fluxes across seasons and averaged annually displayed seasonally distinct respiratory quotients (RQ; i.e., DIC flux : DO flux, molar units), (Fig. 4.3c). The RQ value for Ice Cover was 0.53, though not statistically robust ($p = 0.66$). The RQ value for Break Up was 0.50 ($p < 0.001$), and the RQ value for Open Water was 0.89 ($p < 0.001$). The RQ values for Ice Cover and Break Up were lower than expected, while the value for Open Water fell within established literature values for marine sediments (0.69 - 1.31; Jorgensen et al. 2022 and citations therein). To best represent all of the DO and DIC fluxes, the overall RQ value (0.71, $p < 0.001$) using all data from all seasons was used to convert sediment flux units from O_2 to C (Supplemental Table 4.14).

Daily benthic metabolism rates revealed consistent seasonal patterns but no effect of water depth (Table 4.2, Supplemental Table 4.3, Fig. 4.4). The lowest BR rates were observed during Ice Cover (3.3 ± 1.1 mmol C m^{-2} d^{-1}), then rates doubled during Break Up (6.4 ± 1.3 mmol C m^{-2} d^{-1}), and then increased again during Open Water (8.2 ± 1.1 mmol C m^{-2} d^{-1}) (Fig. 4.4a). Averaged across depths, GBP was higher during Break Up (-29.7 ± 7.1 mmol C m^{-2} d^{-1}) compared to Open Water (-17.1 ± 2.9 mmol C m^{-2} d^{-1}) (Table 4.2, Fig. 4.4b). Due to the lack of light during Ice Cover, light incubations were not conducted, and thus GBP was set to 0 mmol C m^{-2} d^{-1}. Like BR and GBP, NBM varied seasonally, shifting from net heterotrophy during Ice Cover (3.3 ± 1.1 mmol C m^{-2} d^{-1}) to

net autotrophy during both the Break Up (-24.0 ± 6.5 mmol C m^{-2} d^{-1}) and Open Water (-8.9 ± 2.6 mmol C m^{-2} d^{-1}) (Table 4.2, Fig. 4.4c).

4.4.2 Sediment N_2 gas and nutrient (NH_4^+, NO_3^-, PO_4^{3-}, DSi) fluxes

Benthic nutrient fluxes did not exhibit as strong a seasonal pattern as benthic metabolism, but ANOVAs did reveal seasonal effects on benthic fluxes of N_2, NH_4^+ and potentially some effects of depth on DSi (Table 4.3, Supplemental Table 4.4, Fig. 4.5). Net N_2 fluxes varied significantly across seasons, with high rates of N_2 production (i.e., net denitrification) during Ice Cover (1903 ± 580 µmol N m^{-2} d^{-1}) compared to both the Break Up (-164 ± 382 µmol N m^{-2} d^{-1}) and Open Water (-352 ± 251 µmol N m^{-2} d^{-1}) periods, which not only showed smaller fluxes but also net N_2 uptake by the sediments (i.e., net N-fixation)(Fig. 4.5, Supplemental Fig. 4.1).

Net NH_4^+ fluxes varied seasonally, with average net NH_4^+ production during Ice Cover (38.5 ± 73.9 µmol N m^{-2} d^{-1}), which decreased closer to zero during Break Up (8.1 ± 26.4 µmol N m^{-2} d^{-1}), and then shifted to consistent net uptake during the Open Water period (-76.1± 22.1 µmol N m^{-2} d^{-1}) (Table 4.4, Supplemental Table 4.5, Fig. 4.6a). Benthic fluxes for NO_3^- and PO_4^{3-} did not vary significantly across seasons or depth (Table 4.4, Supplemental Table 4.5, Fig. 4.6b,c). Averaged across seasons and depth, NO_3^- fluxes were 22.3 ± 23.6 µmol N m^{-2} d^{-1}, and PO_4^{3-} fluxes were 5.2 ± 17.9 µmol P m^{-2} d^{-1}. When sediment fluxes of NH_4^+ and NO_3^- were combined to represent dissolved inorganic nitrogen flux (DIN = NH_4^+ + NO_3^-), DIN concentrations shifted from net production to net consumption from Ice Cover (103 ± 99 µmol N m^{-2} d^{-1}) to Open Water (-67 ± 36 µmol N m^{-2} d^{-1}) (Table 4.3, Supplemental Table 4.4, Fig. 4.5b). In contrast to all other parameters,

net DSi fluxes varied mostly by depth (p-value= 0.13) and not season, with annual net production at deep stations (69.5 ± 49.4 μmol SiO_2 m^{-2} d^{-1}) and annual net consumption at shallow stations (-61.9 ± 45.0 μmol SiO_2 m^{-2} d^{-1}, Table 4.4, Supplemental Table 4.5, Fig. 4.6d).

4.4.3 Environmental drivers

From a dataset of 23 measured environmental parameters, Pearson's Correlation was used to identify nine parameters to represent the environmental factors in the model. The correlation analysis identified parameters that displayed strong correlations so that they would not be added together in the model (i.e., avoiding collinearity in the model). The selected parameters fell broadly into categories representing physical variables (temperature, salinity, PAR), water column nutrients (DIN concentration), sediment porewater nutrients (NO_3^-, DSi concentrations), and sediment organic matter (SOC, δ^{13}C-SOC, chla) (Supplemental Table 4.6). Prior to analysis, the selected environmental data were normalized using log (water column DIN, sediment chla, porewater DSi), square root (PAR), or cube root (SOC, porewater NO_3^-) transformations, if required for normality. We then ran separate multiple linear regression models for metabolism parameters (BR, GBP, NBM), N_2 fluxes, and nutrient fluxes.

Based on accuracy metrics of the model (RMSE, MAE, Adj R^2), the stepwise multiple linear regression of BR identified the model with two parameters as the best fit (Table 4.6). Analysis of the model demonstrated that SOC and temperature were the dominant drivers of benthic respiration accounting for 47% and 53% of the variance, respectively. Based on the slope of the regressions, both SOC and temperature

correlated positively with BR (Table 4.6). For GBP the model of best fit indicated that two parameters (PAR and sediment chl-a) best explained the variance in rates (Supplemental Table 4.7). The model showed that GBP was primarily driven by PAR (75%), followed by sediment chlorophyll-a (25%). As expected, both PAR and sediment chlorophyll-a correlated negatively with GBP. Interestingly, when identifying the drivers of NBM, a metric that combines both BR and GBP, the stepwise regression identified a one parameter model with salinity having a positive relationship with NBM (Supplemental Table 4.8).

Variances in net N_2 flux were best explained by a one parameter model with a strong positive relationship with bottom water DIN concentrations (Supplemental Table 4.9). In contrast, net NH_4^+ and DSi fluxes were best explained by one parameter models with strong negative relationships to temperature (Supplemental Tables 4.10, 4.13). Environmental factors included in the model did not sufficiently explain net benthic fluxes of NO_3^- or PO_4^{3-}. Although not significant, net NO_3^- was best explained by a three parameter model (temperature, salinity, and δ^{13}C-SOC; Supplemental Table 4.11) while net PO_4^{3-} flux was best explained by a one parameter model (sediment chlorophyll-a; Supplemental Table 4.12).

4.5 Discussion

Studying seasonal variability in the Arctic is challenging due to logistical constraints posed by the darkness, extensive sea ice cover, and very low temperatures during the winter months. As a result, observations recorded during the winter are scarce (Bourgeois et al., 2017). Benthic metabolism (BR, GBP, NBM) in the Beaufort Sea coastal lagoons changed seasonally in response to physical factors such as temperature, light availability,

and salinity. However, BR, as well as net N_2 production (denitrification), were also influenced by biogeochemical factors like SOC and bottom water DIN, respectively. During Ice Cover, the sediments were net heterotrophic, facilitating sediment nutrient release from remineralization as well as anaerobic processes like denitrification. In contrast during Break Up and Open Water, high rates of benthic primary production resulted in significant carbon fixation as well as sediment nutrient demand and drawdown. On an annual scale, coastal sediments along the Beaufort Sea were a net sink of C and N from the environment. Here, we will discuss the seasonal dynamics and environmental constraints on nearshore benthic metabolism and nutrient cycling in coastal Arctic lagoons.

4.5.1 Seasonal patterns of benthic metabolism

Benthic respiration increased seasonally, more than doubling from Ice Cover to Break Up and increasing again to Open Water. The rates observed in this study (range: 3.3 – 8.5 mmol C m^{-2} d^{-1}) fell within the range previously observed in the Arctic Ocean basin (0 – 52.6 mmol C m^{-2} d^{-1}; Bourgeois et al., 2017) and were very similar to rates observed in the Beaufort Sea (1.3 – 8.0 mmol C m^{-2} d^{-1}, Renaud, Morata, et al., 2007; 1.26 – 14.36 mmol C m^{-2} d^{-1}, Renaud, Riedel, et al., 2007; 0.36 – 8.17 mmol C m^{-2} d^{-1} Link et al., 2013; 0.97 – 3.7 mmol C m^{-2} d^{-1}, Link et al., 2011). In general, studies of benthic respiration in Arctic sediments suggest that SOC remineralization is primarily influenced by organic matter supply in the form of fresh and labile particulate organic carbon (POC) deposition (Bourgeois et al., 2017; Hoffmann et al., 2018; Kiesel et al., 2020; Kotwicki et al., 2018) rather than temperature. However, the stepwise regression in this study

identified SOC (47%) as a secondary driver to temperature (53%) of BR in Beaufort Sea coastal lagoons.

Although multi-season studies in the Arctic are uncommon, especially those outside of the summer Open Water period, a synthesis by Bourgeois et al. (2017) reported that sediment DO demand in the Beaufort Sea exhibited the lowest values in winter and increased through the spring until peaking in summer. This trend is also confirmed by multi-season studies that reported an increase in sediment DO demand from winter to spring caused by increased macroinfaunal activity in response to temperature (Kotwicki et al., 2018; Renaud, Riedel, et al., 2007) and from spring to summer in response to increasing sediment chl-a concentrations (Link et al., 2011, 2013). Therefore, in these lagoons, while baseline sediment microbial respiration rates (DOU) may be driven by SOC (Chapter 3), temperature, and by proxy microbial as well as infaunal activity, played a crucial role in enhancing benthic community respiration during the Break Up and Open Water periods.

Seasonally, as light became available, the lagoons shifted from net heterotrophy during Ice Cover to net autotrophy during Break Up and Open Water. BMA can contribute significantly to benthic primary production under polar conditions, serving as a crucial food source for both heterotrophs and higher trophic consumers in high-latitude regions (Attard et al., 2024; Bridier et al., 2021; Woelfel et al., 2010). In shallow coastal areas where light reaches the sediment surface, benthic primary production from BMA can exceed that of the water column by up to a factor of 1.5 for water depths down to 30 meters (Glud et al., 2009). The GBP rates observed in this study (13.0 - 31.2 mmol C m^{-2} d^{-1}) were comparable to those found previously in coastal Arctic sediments (1.4 - 46.2

mmol C m^{-2} d^{-1}, Woelfel et al., 2010; 16.4 mmol C m^{-2} d^{-1}, Ask et al., 2016; 28.3 - 35 C m^{-2} d^{-1}, Glud et al., 2000).

The stepwise regression identified PAR (70%) and sediment chlorophyll-a (30%) as the primary drivers of GBP. The northern distribution limit of benthic algae in the Arctic is 80ºN, where the annual solar radiation is 30–50% lower than in temperate or tropical regions (Karsten et al., 2012). Although Arctic regions receive less light overall, the primary producers they host are remarkably adapted to low-light conditions (Glud et al., 2009; Karsten et al., 2006). The minimum light requirement for BMA is not well defined, but communities of benthic diatoms have been observed at depths down to 200 meters with maximum light availability < 0.2 µmol photons m^{-2} s^{-1} (McGee et al., 2008). In fact, polar BMA production has been recorded with light ranges down to 0.5 and 2.5 µmol photons m^{-2} s^{-1} (Glud et al., 2009; Karsten et al., 2006; Woelfel et al., 2014). However, it is important to note that the lagoons are also covered in sea ice for 8 months of the year, with ice onset occurring in late September and break up occurring in late May (Mahoney et al., 2014). Due to the presence of thick and sediment-laden sea ice, light levels at Simpson Lagoon are essentially undetectable from December to April, and increase to detectable levels (1.16 - 4.63 µmol photons m^{-2} s^{-1}) during the Break Up and Open Water periods (Bonsell & Dunton, 2018). Even then, during the Open Water period, light transmittance also decreases due to the formation of pelagic phytoplankton blooms, turbid river discharge, and wind-driven sediment resuspension (Aumack et al., 2007; Bonsell & Dunton, 2021; Hanelt et al., 2001) which was reflected in our study with higher rates of GBP during Break Up compared to Open Water.

Although benthic primary production clearly occurred during both the Break Up and Open Water periods, the higher BR and lower GBP during Open Water resulted in a lower NBM during Open Water compared to Break Up. The stepwise regression identified a one parameter model with salinity expressing a positive relationship to NBM. Salinity was likely a significant factor because it is very distinct during each season, going from hypersaline (37.6 ± 0.8) during Ice Cover to fresher (10.3 ± 3.7) during Break Up and estuarine (24.7 ± 0.8) during Open Water (Table 4.5). Previous studies in the coastal Arctic have observed this seasonal shift from net heterotrophy to net autotrophy from Ice Cover to the Open Water period. Ice Cover has been characterized by under-ice nutrient accumulation (Connolly et al., 2021; Cota et al., 1996; Macdonald & Yu, 2006), a decrease in POC and DOC quantity and quality (Connolly et al., 2021; Riedel et al., 2008), as well as decreased DO and pH (Miller et al., 2021), all reflecting a respiration-dominant system. In contrast, during the spring and summer, inorganic nutrients tend to be very low (Carey et al., 2020; Holmes et al., 2012; McClelland et al., 2012) and lagoon microbial communities shift toward primary producers in response to increasing availability of light for photosynthesis (Kellogg et al., 2019).

4.5.2 Seasonal net denitrification and nitrogen fixation

Arctic shelf sediments have been identified as substantial contributors to global N removal, with denitrification rates influenced by organic carbon burial rates (Canion et al., 2014; Chang & Devol, 2009; Christensen, 2008; Hardison et al., 2017). The high rates of denitrification in coastal marine sediments lead to the conversion of NO_3^- and NO_2^- to N_2 gas, resulting in the loss of fixed N from the system. This denitrification process is crucial

for maintaining N balance in coastal marine environments and has large implications for coastal nutrient export. In this study, sediment net N_2 flux varied seasonally, shifting from net denitrification (N_2 removal) during Ice Cover to net N fixation (N_2 production) during Break Up and Open Water, reflecting seasonal shifts in water column DIN availability and benthic DIN demand.

During Ice Cover, sediments exhibited extremely high rates of denitrification (mean: 1903 μmol N m^{-2} d^{-1}), far exceeding associated benthic fluxes of DIN (-106 – 397 μmol N m^{-2} d^{-1}). Previous studies in the coastal Arctic have observed the presence of net N_2 production, although with significant variability in magnitude. On the lower end, rates <500 μmol N m^{-2} d^{-1} were observed in the fjords and shelves of Greenland (34 – 344 μmol N m^{-2} d^{-1}, Rysgaard et al., 2004**;** 110 - 480 μmol N m^{-2} d^{-1}, Glud et al., 2000; 168 μmol N m^{-2} d^{-1}, Sørensen et al., 2015), Norway (160 – 630 μmol N m^{-2} d^{-1}, Glud et al., 1998**;** 11 - 35 μmol N m^{-2} d^{-1}, Gazeau et al., 2014**)**, and both the Beaufort (32 - 200 μmol N m^{-2} d^{-1}, Devol et al., 1997) and Chukchi Seas (-27 - 286 μmol N m^{-2} d^{-1}, Souza et al., 2014; 152-453 μmol N m^{-2} d^{-1}, Gihring et al., 2010; 108 - 490 μmol N m^{-2} d^{-1}, McTigue et al., 2016)**.** However, in these same regions, patches of sediments could also exhibit rates of net denitrification that are double or even an order of magnitude higher, exemplifying the heterogeneity of sediments and their metabolic processes. These hotspots of net denitrification have been observed across the Arctic including the Chukchi (576 - 1320 μmol N m^{-2} d^{-1}, Hardison et al., 2017; 1600 μmol N m^{-2} d^{-1}, Chang & Devol, 2009) and Beaufort Seas (293 - 2534 μmol N m^{-2} d^{-1}, Christensen, 2008)).

Arctic sediments have been identified as active sites of denitrification, with microbial communities playing a crucial role in mediating this process. Denitrifying

bacteria in permanently cold Arctic fjord sediments have been found to be psychrophilic, exemplifying microbial adaptations to the extreme Arctic conditions (Canion et al., 2014). As denitrification is an anaerobic process that requires the presence of NO_3^- as an electron acceptor, the availability of oxygen, SOC and NO_3^- concentrations in sediments are critical factors driving N_2 production (Damashek & Francis, 2018). In addition to SOC content and water column DIN, variability of denitrification rates in the Arctic suggests that the source of OC can be a critical factor (Payne & Arrigo, 2022), as well as interactions with other redox processes such as sulfate reduction and the subsequent inhibition of denitrification by sulfide accumulation (Damashek & Francis, 2018).

The results of the stepwise regression for net N_2 flux selected a one-parameter model driven solely by bottom water DIN concentration, which provides support for the importance of electron acceptors (NO_3^-) in Arctic sediments. In this study, rates of net denitrification may have been particularly high due to the ideal, conducive condition during Ice Cover. Due to the heterotrophic and enclosed nature (both to the atmosphere and the Beaufort Sea) of the lagoons during ice cover, water column oxygen can easily become suboxic, facilitating anaerobic respiration in the sediments (Miller et al., 2021; Spangenberg et al., 2021). Furthermore, with the presence of sea ice up to 1.5 m thick (Pedrazas et al., 2020) which significantly reduces light to the benthos (Bonsell & Dunton, 2018), there is a lack of competition for sediment porewater and accumulated water column DIN by photosynthetic primary producers (Risgaard-Petersen et al., 2004). A combination of high bottom water DIN, a cold-adapted microbial community, and a hypoxic sediment-water interface likely resulted in the high rates of N removal from the system.

As the lagoons shifted from Ice Cover to Break Up and eventually Open Water, we observed a significant decrease in net sediment N_2 flux, switching from net denitrification to net N fixation. This shift likely reflects the depletion of DIN in the water column by the spring diatom bloom fueling sediment N demand (Chapter 2). This is reflected in previous microbial work in the lagoons that observed a shift in the dominance of inorganic N-using chemoautotrophs (nitrifiers) during Ice Cover to organic N-consuming microbes with the depletion of DIN when light limitation was released (Baker et al., 2021). Several studies have confirmed an inverse relationship between DIN and N fixation rates due to the higher energetic cost of fixing N_2 than of assimilating NH_4^+ or NO_3^- (Damashek & Francis, 2018).

Nitrogen fixation has not been considered a prevalent process in Arctic sediments (Hardison et al., 2017; McTigue et al., 2016);, but it has been detected at low levels throughout the coast (0.96 – 7.92 $\mu mol\ N\ m^{-2}\ d^{-1}$, Haines et al., 1981), shelf (4.89 $\mu mol\ N\ m^{-2}\ d^{-1}$, Knowles & Wishart, 1977), and fjords (0 – 19.92 $\mu mol\ N\ m^{-2}\ d^{-1}$, Gihring et al., 2010). In comparison to N fixation found in these regions, our rates were high (184 – 478 $\mu mol\ N\ m^{-2}\ d^{-1}$). Once water column DIN is depleted, N fixation occurs to compensate for ecosystem N demand. In fact, although sediment N fixation is often disregarded in nutrient budgets, particularly in bare sediments, we now know that rates of sediment N fixation can exceed rates of denitrification (Fulweiler, 2023) by up to a factor of eight times (Newell et al., 2016) in response to N demand. Additionally, the high rates observed in this study may be due to the shallow nature (< 5 m) of these lagoons (Chapter 3), which likely amplifies benthic-pelagic interactions including nutrient use by both pelagic and benthic primary producers. Thus, the seasonal pattern observed in the sediments mirrors water column dynamics and

reinforces the concept of strong pelagic-benthic coupling in the Arctic (Bourgeois et al., 2017; Link et al., 2011, 2013).

4.5.3 Sediment inorganic nutrient supply and demand

In general, sediment fluxes of inorganic nutrients reflected the seasonal shift from net heterotrophy during Ice Cover to net autotrophy during Break Up and Open Water. Sediment fluxes of nutrients were variable during Ice Cover, but generally exhibited net nutrient release into the water column. During Break Up, the sediment fluxes were more balanced (~ net 0 flux) and showed less variability, and then fluxes became more negative during Open Water, particularly for NH_4^+ and DSi.

Net sediment fluxes of NH_4^+ and DSi were both best explained by a one-parameter model with a strong negative relationship to temperature. Temperature was likely the most significant factor due to its distinct values for each season, changing from sub-zero (-1.9 ^oC) during Ice Cover, to 2.8 ^oC by Break Up, and to 8 ^oC during Open Water (Table 4.5). Sediments exhibited mean net NH_4^+ and DSi production during Ice Cover and net consumption during Open Water. This seasonal shift in net NH_4^+ and DSi flux reflects the patterns of net benthic metabolism observed in this study, with net heterotrophy during Ice Cover transitioning to net autotrophy during Break Up and Open Water. During Ice Cover, the respiration-dominated system breaks down organic matter releasing inorganic nutrients into the overlying water column. The accumulation of inorganic nutrients during winter has been previously documented in these enclosed coastal Arctic systems (Cota et al., 1996; Macdonald & Yu, 2006). In fact, in Beaufort Sea lagoons, inorganic nutrients in the water column are highest during Ice Cover (NH_4^+: 2.1 µmol N L^{-1}, NO_3^-: 5.2 µmol N

L^{-1}, PO_4^{3-}: 2.2 µmol P L^{-1}, DSi: 18.8 µmol SiO_2 L^{-1}), and then decrease during Break Up and Open Water due to biological uptake and physical dilution from freshwater inputs (Chapter 2).

As BMA proliferated during Break Up and Open Water, the sediments shifted to net autotrophy, and high rates of benthic primary production quickly increased sediment N demand. BMA play a critical role in sediment nutrient uptake, influencing the movement of dissolved nutrients across the sediment-water interface by forming biofilms (Alsterberg et al., 2012; Tyler et al., 2003) that retain the nutrients within sediments as well as the ecosystem (Dalsgaard, 2003; Tyler et al., 2003). In fact, in shallow systems particularly, BMA can dominate sediment uptake of C and N, accounting for 100% of total nutrient uptake in certain environments (Hardison et al., 2011).

4.6 Conclusion

Arctic coastal environments are highly dynamic ecosystems at the intersection of cryospheric, terrestrial, and marine systems. Although covered in sea ice for most of the year, Arctic coastal lagoons experience intense productivity during ice-free summers. In response to these seasonal environmental changes, we observed seasonal shifts in benthic metabolism and sediment nutrient demand. We observed benthic net heterotrophy, inorganic nutrient production, and net denitrification during Ice Cover. During Break Up and Open Water, the sediments became net autotrophic, and sediment nutrient demand increased, supported by N fixation and sediment nutrient uptake. When scaled to annual rates by multiplying seasonal rates by season duration (Ice Cover: 7.5 months, Break Up: 1 month, Open Water: 3.5 months), the lagoon sediments were a net

sink of N mainly through denitrification and net autotrophic, acting as a carbon sink (Table 4.7).

BMA can make a substantial contribution to Arctic marine food webs, serving as a vital food source for both benthic and pelagic heterotrophs. These microalgae likely play a crucial role in supporting energy flow and trophic interactions in Arctic coastal ecosystems (Zacher et al., 2009). In fact, the Arctic ecosystem is particularly sensitive to changes in primary production due to its low number of trophic links (Arrigo et al., 2008). The loss of summer sea ice in the Arctic Ocean has been associated with an increase in annual primary production both in the water column as well as the sediments (Arrigo & Van Dijken, 2015; Attard et al., 2024). The lengthening growing season (Bonsell & Dunton, 2018) and enhanced nutrient fluxes from land (Ardyna & Arrigo, 2020; Le Fouest et al., 2013; Terhaar et al., 2021) play a crucial role in driving these changes in production.

Based on the current expansion rates of the Open Water period in the Beaufort Sea (~11 days per decade, Frey et al., 2015; Markus et al., 2009; Stroeve et al., 2014), in 20 years we can expect the Open Water period to increase by three weeks. This will result in a corresponding contraction of the Ice Covered period with no significant changes to the duration of Break Up (Bonsell & Dunton, 2021). As the Ice Cover period shrinks, winter nutrient accumulation, which fuels the spring bloom, will likely decrease. However, lower levels of DIN accumulation may decrease rates of winter denitrification resulting in more retention of N within the system. With the expansion of the Open Water period, annual BR will likely increase with rising water temperatures that begin earlier and persist later. In parallel, as benthic light exposure increases with decreasing sea ice duration, GBP is likely to increase as well. With regard to NBM, there are many complex

interactions to consider. A longer growth season may support more expansive microalgal mats decreasing sediment resuspension and potentially facilitating more benthic primary production. However, increasing terrestrial inputs and more frequent resuspension by wind and wave activity may reduce primary production and enhance respiration. As these lagoons are subject to drastic environmental fluctuations among seasons, it is critical to understand the drivers of primary production, nutrient cycling, and benthic-pelagic coupling between the sediment and water column during these distinct, sequential, seasonal periods.

4.7 References

Ahmed, R., Prowse, T., Dibike, Y., Bonsal, B., & O'Neil, H. (2020). Recent Trends in Freshwater Influx to the Arctic Ocean from Four Major Arctic-Draining Rivers. Water, 12(4), 1189. https://doi.org/10.3390/w12041189

Alsterberg, C., Sundbäck, K., & Hulth, S. (2012). Functioning of a Shallow-Water Sediment System during Experimental Warming and Nutrient Enrichment. PLoS ONE, 7(12), e51503. https://doi.org/10.1371/journal.pone.0051503

Ardyna, M., & Arrigo, K. R. (2020). Phytoplankton dynamics in a changing Arctic Ocean. Nature Climate Change, 10(10), 892–903. https://doi.org/10.1038/s41558-020-0905-y

Arrigo, K. R., & Van Dijken, G. L. (2015). Continued increases in Arctic Ocean primary production. Progress in Oceanography, 136, 60–70. https://doi.org/10.1016/j.pocean.2015.05.002

Arrigo, K. R., Van Dijken, G., & Pabi, S. (2008). Impact of a shrinking Arctic ice cover on marine primary production. Geophysical Research Letters, 35(19), 2008GL035028. https://doi.org/10.1029/2008GL035028

Ask, J., Rowe, O., Brugel, S., Strömgren, M., Byström, P., & Andersson, A. (2016). Importance of coastal primary production in the northern Baltic Sea. Ambio, 45(6), 635–648. https://doi.org/10.1007/s13280-016-0778-5

Attard, K., Singh, R. K., Gattuso, J.-P., Filbee-Dexter, K., Krause-Jensen, D., Kühl, M., Sejr, M. K., Archambault, P., Babin, M., Bélanger, S., Berg, P., Glud, R. N., Hancke, K., Jänicke, S., Qin, J., Rysgaard, S., Sørensen, E. B., Tachon, F., Wenzhöfer, F., & Ardyna, M. (2024). Seafloor primary production in a changing Arctic Ocean. Proceedings of the National Academy of Sciences, 121(11), e2303366121. https://doi.org/10.1073/pnas.2303366121

Aumack, C. F., Dunton, K. H., Burd, A. B., Funk, D. W., & Maffione, R. A. (2007). Linking light attenuation and suspended sediment loading to benthic productivity within an Arctic kelp-bed community 1. Journal of Phycology, 43(5), 853–863. https://doi.org/10.1111/j.1529-8817.2007.00383.x

Baker, K. D., Kellogg, C. T. E., McClelland, J. W., Dunton, K. H., & Crump, B. C. (2021). The Genomic Capabilities of Microbial Communities Track Seasonal Variation in Environmental Conditions of Arctic Lagoons. Frontiers in Microbiology, 12, 601901. https://doi.org/10.3389/fmicb.2021.601901

Barnhart, K. R., Overeem, I., & Anderson, R. S. (2014). The effect of changing sea ice on the physical vulnerability of Arctic coasts. The Cryosphere, 8(5), 1777–1799. https://doi.org/10.5194/tc-8-1777-2014

Beaufort Lagoon Ecosystems LTER, Core Program. (2024). Physiochemical water column parameters and hydrographic time series from river, lagoon, and open ocean sites along the Alaska Beaufort Sea coast, 2018-ongoing (Version 5) [dataset]. https://doi.org/10.6073/pasta/d459c2163f3d626635c9244cebe6b85a

Bonsell, C., & Dunton, K. H. (2018). Long-term patterns of benthic irradiance and kelp production in the central Beaufort sea reveal implications of warming for Arctic inner shelves. Progress in Oceanography, 162, 160–170. https://doi.org/10.1016/j.pocean.2018.02.016

Bonsell, C., & Dunton, K. H. (2021). Slow Community Development Enhances Abiotic Limitation of Benthic Community Structure in a High Arctic Kelp Bed. Frontiers in Marine Science, 8, 592295. https://doi.org/10.3389/fmars.2021.592295

Borges, A. V., & Abril, G. (2011). Carbon Dioxide and Methane Dynamics in Estuaries. In Treatise on Estuarine and Coastal Science (pp. 119–161). Elsevier. https://doi.org/10.1016/B978-0-12-374711-2.00504-0

Bourgeois, S., Archambault, P., & Witte, U. (2017). Organic matter remineralization in marine sediments: A Pan-Arctic synthesis. Global Biogeochemical Cycles, 31, 190–213. https://doi.org/10.1002/2016GB005378

Bridier, G., Olivier, F., Chauvaud, L., Sejr, M. K., & Grall, J. (2021). Food source diversity, trophic plasticity, and omnivory enhance the stability of a shallow benthic food web from a HIGH-ARCTIC fjord exposed to freshwater inputs. Limnology and Oceanography, 66(S1). https://doi.org/10.1002/lno.11688

Bristol, E. M., Connolly, C. T., Lorenson, T. D., Richmond, B. M., Ilgen, A. G., Choens, R. C., Bull, D. L., Kanevskiy, M., Iwahana, G., Jones, B. M., & McClelland, J. W. (2021). Geochemistry of Coastal Permafrost and Erosion-Driven Organic Matter Fluxes to the Beaufort Sea Near Drew Point, Alaska. Frontiers in Earth Science, 8, 598933. https://doi.org/10.3389/feart.2020.598933

Canion, A., Overholt, W. A., Kostka, J. E., Huettel, M., Lavik, G., & Kuypers, M. M. M. (2014). Temperature response of denitrification and anaerobic ammonium oxidation rates and microbial community structure in Arctic fjord sediments. Environmental Microbiology, 16(10), 3331–3344. https://doi.org/10.1111/1462-2920.12593

Carey, J. C., Gewirtzman, J., Johnston, S. E., Kurtz, A., Tang, J., Vieillard, A. M., & Spencer, R. G. M. (2020). Arctic River Dissolved and Biogenic Silicon Exports—Current Conditions and Future Changes With Warming. Global Biogeochemical Cycles, 34(3). https://doi.org/10.1029/2019GB006308

Chang, B. X., & Devol, A. H. (2009). Seasonal and spatial patterns of sedimentary denitrification rates in the Chukchi sea. Deep Sea Research Part II: Topical Studies in Oceanography, 56(17), 1339–1350. https://doi.org/10.1016/j.dsr2.2008.10.024

Christensen, J. P. (2008). Sedimentary Carbon Oxidation and Denitrification on the Shelf Break of the Alaskan Beaufort and Chukchi Seas. The Open Oceanography Journal, 2(1), 6–17. https://doi.org/10.2174/1874252100802010006

Connolly, C. T., Crump, B. C., Dunton, K. H., & McClelland, J. W. (2021). Seasonality of dissolved organic matter in lagoon ecosystems along the Alaska Beaufort Sea coast. Limnology and Oceanography, 66(12), 4299–4313. https://doi.org/10.1002/lno.11962

Cota, G., Pomeroy, L., Harrison, W., Jones, E., Peters, F., Sheldon, W., & Weingartner, T. (1996). Nutrients, primary production and microbial heterotrophy in the southeastern Chukchi Sea:Arctic summer nutrient depletion and heterotrophy. Marine Ecology Progress Series, 135, 247–258. https://doi.org/10.3354/meps135247

Craig, P. C., Griffiths, W. B., Johnson, S. R., & Schell, D. M. (1984). TROPHIC DYNAMICS IN AN ARCTIC LAGOON. In The Alaskan Beaufort Sea (pp. 347–380). Elsevier. https://doi.org/10.1016/B978-0-12-079030-2.50023-X
Dalsgaard, T. (2003). Benthic primary production and nutrient cycling in sediments with benthic microalgae and transient accumulation of macroalgae. Limnology and Oceanography, 48(6), 2138–2150. https://doi.org/10.4319/lo.2003.48.6.2138
Damashek, J., & Francis, C. A. (2018). Microbial Nitrogen Cycling in Estuaries: From Genes to Ecosystem Processes. Estuaries and Coasts, 41(3), 626–660. https://doi.org/10.1007/s12237-017-0306-2
De Witt, R. (2011). Biodiversity of Coastal Lagoon Ecosystems and Their Vulnerability to Global Change. In O. Grillo (Ed.), Ecosystems Biodiversity. InTech. https://doi.org/10.5772/24995
Devol, A. H., Codispoti, L. A., & Christensen, J. P. (1997). Summer and winter denitrification rates in western Arctic shelf sediments. Continental Shelf Research, 17(9), 1029–1050. https://doi.org/10.1016/S0278-4343(97)00003-4
Dittmar, T., & Kattner, G. (2003). The biogeochemistry of the river and shelf ecosystem of the Arctic Ocean: A review. Marine Chemistry, 83(3–4), 103–120. https://doi.org/10.1016/S0304-4203(03)00105-1
Dunton, K. H., Schonberg, S. V., & Cooper, L. W. (2012). Food Web Structure of the Alaskan Nearshore Shelf and Estuarine Lagoons of the Beaufort Sea. Estuaries and Coasts, 35(2), 416–435. https://doi.org/10.1007/s12237-012-9475-1
Dunton, K. H., Weingartner, T., & Carmack, E. C. (2006). The nearshore western Beaufort Sea ecosystem: Circulation and importance of terrestrial carbon in arctic coastal food webs. Progress in Oceanography, 71(2–4), 362–378. https://doi.org/10.1016/j.pocean.2006.09.011
Fichot, C. G., Kaiser, K., Hooker, S. B., Amon, R. M. W., Babin, M., Bélanger, S., Walker, S. A., & Benner, R. (2013). Pan-Arctic distributions of continental runoff in the Arctic Ocean. Scientific Reports, 3(1), 1053. https://doi.org/10.1038/srep01053
Frey, K. E., Moore, G. W. K., Cooper, L. W., & Grebmeier, J. M. (2015). Divergent patterns of recent sea ice cover across the Bering, Chukchi, and Beaufort seas of the Pacific Arctic Region. Progress in Oceanography, 136, 32–49. https://doi.org/10.1016/j.pocean.2015.05.009
Fulweiler, R. W. (2023). More Foxes than Hedgehogs: The Case for Nitrogen Fixation in Coastal Marine Sediments. Global Biogeochemical Cycles, 37(8), e2023GB007777. https://doi.org/10.1029/2023GB007777
Gazeau, F., Van Rijswijk, P., Pozzato, L., & Middelburg, J. J. (2014). Impacts of Ocean Acidification on Sediment Processes in Shallow Waters of the Arctic Ocean. PLoS ONE, 9(4), e94068. https://doi.org/10.1371/journal.pone.0094068
Gihring, T. M., Lavik, G., Kuypers, M. M. M., & Kostka, J. E. (2010). Direct determination of nitrogen cycling rates and pathways in Arctic fjord sediments (Svalbard, Norway). Limnology and Oceanography, 55(2), 740–752. https://doi.org/10.4319/lo.2010.55.2.0740
Glud, R., Holby, O., Hoffmann, F., & Canfield, D. (1998). Benthic mineralization and exchange in Arctic sediments (Svalbard, Norway). Marine Ecology Progress Series, 173, 237–251. https://doi.org/10.3354/meps173237

Glud, R. N., Woelfel, J., Karsten, U., Kühl, M., & Rysgaard, S. (2009). Benthic microalgal production in the Arctic: Applied methods and status of the current database. Botm, 52(6), 559–571. https://doi.org/10.1515/BOT.2009.074

Glud, R., Risgaard-Petersen, N., Thamdrup, B., Fossing, H., & Rysgaard, S. (2000). Benthic carbon mineralization in a high-Arctic sound (Young Sound, NE Greenland). Marine Ecology Progress Series, 206, 59–71. https://doi.org/10.3354/meps206059

Haines, J. R., Atlas, R. M., Griffiths, R. P., & Morita, R. Y. (1981). Denitrification and Nitrogen Fixation in Alaskan Continental Shelf Sediments. Applied and Environmental Microbiology, 41(2), 412–421. https://doi.org/10.1128/aem.41.2.412-421.1981

Hanelt, D., Tüg, H., Bischof, K., Groß, C., Lippert, H., Sawall, T., & Wiencke, C. (2001). Light regime in an Arctic fjord: A study related to stratospheric ozone depletion as a basis for determination of UV effects on algal growth. Marine Biology, 138(3), 649–658. https://doi.org/10.1007/s002270000481

Hardison, A. K., Anderson, I. C., Canuel, E. A., Tobias, C. R., & Veuger, B. (2011). Carbon and nitrogen dynamics in shallow photic systems: Interactions between macroalgae, microalgae, and bacteria. Limnology and Oceanography, 56(4), 1489–1503. https://doi.org/10.4319/lo.2011.56.4.1489

Hardison, A. K., Canuel, E. A., Anderson, I. C., Tobias, C. R., Veuger, B., & Waters, M. N. (2013). Microphytobenthos and benthic macroalgae determine sediment organic matter composition in shallow photic sediments. Biogeosciences, 10(8), 5571–5588. https://doi.org/10.5194/bg-10-5571-2013

Hardison, A. K., McTigue, N. D., Gardner, W. S., & Dunton, K. H. (2017). Arctic shelves as platforms for biogeochemical activity: Nitrogen and carbon transformations in the Chukchi Sea, Alaska. Deep Sea Research Part II: Topical Studies in Oceanography, 144, 78–91. https://doi.org/10.1016/j.dsr2.2017.08.004

Harris, C. M., McClelland, J. W., Connelly, T. L., Crump, B. C., & Dunton, K. H. (2017). Salinity and Temperature Regimes in Eastern Alaskan Beaufort Sea Lagoons in Relation to Source Water Contributions. Estuaries and Coasts, 40(1), 50–62. https://doi.org/10.1007/s12237-016-0123-z

Hoffmann, R., Braeckman, U., Hasemann, C., & Wenzhöfer, F. (2018). Deep-sea benthic communities and oxygen fluxes in the Arctic Fram Strait controlled by sea-ice cover and water depth. Biogeosciences, 15(16), 4849–4869. https://doi.org/10.5194/bg-15-4849-2018

Holmes, R. M., McClelland, J. W., Peterson, B. J., Tank, S. E., Bulygina, E., Eglinton, T. I., Gordeev, V. V., Gurtovaya, T. Y., Raymond, P. A., Repeta, D. J., Staples, R., Striegl, R. G., Zhulidov, A. V., & Zimov, S. A. (2012). Seasonal and Annual Fluxes of Nutrients and Organic Matter from Large Rivers to the Arctic Ocean and Surrounding Seas. Estuaries and Coasts, 35(2), 369–382. https://doi.org/10.1007/s12237-011-9386-6

Johnston, S. E., Carey, J. C., Kellerman, A., Podgorski, D., Jonathan, G., & Robert, S. (2019). Controls on Riverine Dissolved Organic Matter Composition Across an Arctic-Boreal Latitudinal Gradient. Geophysical Research Letters, 47. https://doi.org/10.1029/2019GL085897

Jones, B. M., Arp, C. D., Jorgenson, M. T., Hinkel, K. M., Schmutz, J. A., & Flint, P. L. (2009). Increase in the rate and uniformity of coastline erosion in Arctic Alaska. Geophysical Research Letters, 36(3), 2008GL036205. https://doi.org/10.1029/2008GL036205

Karsten, U., Schlie, C., Woelfel, J., & Becker, B. (2012). Benthic Diatoms in Arctic Seas – Ecological Functions and Adaptations. Polarforschung, 81(2), 77–84.

Karsten, U., Schumann, R., Rothe, S., Jung, I., & Medlin, L. (2006). Temperature and light requirements for growth of two diatom species (Bacillariophyceae) isolated from an Arctic macroalga. Polar Biology, 29(6), 476–486. https://doi.org/10.1007/s00300-005-0078-1

Kellogg, C. T. E., McClelland, J. W., Dunton, K. H., & Crump, B. C. (2019). Strong Seasonality in Arctic Estuarine Microbial Food Webs. Frontiers in Microbiology, 10, 2628. https://doi.org/10.3389/fmicb.2019.02628

Kemp, W., & Testa, J. (2011). Metabolic balance between ecosystem production and consumption. In Treatise on Estuarine and Coastal Science (pp. 83–118).

Kiesel, J., Bienhold, C., Wenzhöfer, F., & Link, H. (2020). Variability in Benthic Ecosystem Functioning in Arctic Shelf and Deep-Sea Sediments: Assessments by Benthic Oxygen Uptake Rates and Environmental Drivers. Frontiers in Marine Science, 7, 426. https://doi.org/10.3389/fmars.2020.00426

Knowles, R., & Wishart, C. (1977). Nitrogen fixation in arctic marine sediments: Effect of oil and hydrocarbon fractions. Environmental Pollution (1970), 13(2), 133–149. https://doi.org/10.1016/0013-9327(77)90098-2

Kotwicki, L., Grzelak, K., Opaliński, K., & Węsławski, J. M. (2018). Total benthic oxygen uptake in two Arctic fjords (Spitsbergen) with different hydrological regimes. Oceanologia, 60(2), 107–113. https://doi.org/10.1016/j.oceano.2017.11.005

Lannuzel, D., Tedesco, L., Van Leeuwe, M., Campbell, K., Flores, H., Delille, B., Miller, L., Stefels, J., Assmy, P., Bowman, J., Brown, K., Castellani, G., Chierici, M., Crabeck, O., Damm, E., Else, B., Fransson, A., Fripiat, F., Geilfus, N.-X., … Wongpan, P. (2020). The future of Arctic sea-ice biogeochemistry and ice-associated ecosystems. Nature Climate Change, 10(11), 983–992. https://doi.org/10.1038/s41558-020-00940-4

Lantuit, H., Atkinson, D., Paul Overduin, P., Grigoriev, M., Rachold, V., Grosse, G., & Hubberten, H.-W. (2011). Coastal erosion dynamics on the permafrost-dominated Bykovsky Peninsula, north Siberia, 1951–2006. Polar Research, 30(1), 7341. https://doi.org/10.3402/polar.v30i0.7341

Le Fouest, V., Babin, M., & Tremblay, J.-É. (2013). The fate of riverine nutrients on Arctic shelves. Biogeosciences, 10(6), 3661–3677. https://doi.org/10.5194/bg-10-3661-2013

Link, H., Archambault, P., Tamelander, T., Renaud, P. E., & Piepenburg, D. (2011). Spring-to-summer changes and regional variability of benthic processes in the western Canadian Arctic. Polar Biology, 34(12), 2025–2038. https://doi.org/10.1007/s00300-011-1046-6

Link, H., Chaillou, G., Forest, A., Piepenburg, D., & Archambault, P. (2013). Multivariate benthic ecosystem functioning in the Arctic – benthic fluxes explained by environmental parameters in the southeastern Beaufort Sea. Biogeosciences, 10(9), 5911–5929. https://doi.org/10.5194/bg-10-5911-2013

Macdonald, R. W., & Yu, Y. (2006). The Mackenzie Estuary of the Arctic Ocean. In P. J. Wangersky (Ed.), Estuaries (Vol. 5H, pp. 91–120). Springer-Verlag. https://doi.org/10.1007/698_5_027

Mahoney, A. R., Eicken, H., Gaylord, A. G., & Gens, R. (2014). Landfast sea ice extent in the Chukchi and Beaufort Seas: The annual cycle and decadal variability. Cold Regions Science and Technology, 103, 41–56. https://doi.org/10.1016/j.coldregions.2014.03.003

Manini, E., Fiordelmondo, C., Gambi, C., Pusceddu, A., & Danovaro, R. (2003). Benthic microbial loop functioning in coastal lagoons: A comparative approach. Oceanologica Acta, 26(1), 27–38. https://doi.org/10.1016/S0399-1784(02)01227-6

Markus, T., Stroeve, J. C., & Miller, J. (2009). Recent changes in Arctic sea ice melt onset, freezeup, and melt season length. Journal of Geophysical Research: Oceans, 114(C12), 2009JC005436. https://doi.org/10.1029/2009JC005436

McClelland, J. W., Holmes, R. M., Dunton, K. H., & Macdonald, R. W. (2012). The Arctic Ocean Estuary. Estuaries and Coasts, 35(2), 353–368. https://doi.org/10.1007/s12237-010-9357-3

McClelland, J. W., Townsend-Small, A., Holmes, R. M., Pan, F., Stieglitz, M., Khosh, M., & Peterson, B. J. (2014). River export of nutrients and organic matter from the North Slope of Alaska to the Beaufort Sea. Water Resources Research, 50(2), 1823–1839. https://doi.org/10.1002/2013WR014722

McGee, D., Laws, R., & Cahoon, L. (2008). Live benthic diatoms from the upper continental slope: Extending the limits of marine primary production. Marine Ecology Progress Series, 356, 103–112. https://doi.org/10.3354/meps07280

McGlathery, K., Anderson, I., & Tyler, A. (2001). Magnitude and variability of benthic and pelagic metabolism in a temperate coastal lagoon. Marine Ecology Progress Series, 216, 1–15. https://doi.org/10.3354/meps216001

McGlathery, K., Sundbäck, K., & Anderson, I. (2007). Eutrophication in shallow coastal bays and lagoons: The role of plants in the coastal filter. Marine Ecology Progress Series, 348, 1–18. https://doi.org/10.3354/meps07132

McTigue, N. D., Gardner, W. S., Dunton, K. H., & Hardison, A. K. (2016). Biotic and abiotic controls on co-occurring nitrogen cycling processes in shallow Arctic shelf sediments. Nature Communications, 7(1), 13145. https://doi.org/10.1038/ncomms13145

Miller, A. (2020). leaps: Regression subset selection (3.1) [R]. https://CRAN.R-project.org/package=leaps

Miller, C. A., Bonsell, C., McTigue, N. D., & Kelley, A. L. (2021). The seasonal phases of an Arctic lagoon reveal the discontinuities of pH variability and CO_2 flux at the air–sea interface. Biogeosciences, 18(3), 1203–1221. https://doi.org/10.5194/bg-18-1203-2021

Newell, S. E., McCarthy, M. J., Gardner, W. S., & Fulweiler, R. W. (2016). Sediment Nitrogen Fixation: A Call for Re-evaluating Coastal N Budgets. Estuaries and Coasts, 39(6), 1626–1638. https://doi.org/10.1007/s12237-016-0116-y

Nowicki, B. L., & Nixon, S. W. (1985). Benthic Nutrient Remineralization in a Coastal Lagoon Ecosystem. Estuaries, 8(2), 182. https://doi.org/10.2307/1352199

Overduin, P. P., Strzelecki, M. C., Grigoriev, M. N., Couture, N., Lantuit, H., St-Hilaire-Gravel, D., Günther, F., & Wetterich, S. (2014). Coastal changes in the Arctic. Geological Society, London, Special Publications, 388(1), 103–129. https://doi.org/10.1144/SP388.13

Overeem, I., Anderson, R. S., Wobus, C. W., Clow, G. D., Urban, F. E., & Matell, N. (2011). Sea ice loss enhances wave action at the Arctic coast: SEA ICE LOSS ENHANCES EROSION. Geophysical Research Letters, 38(17), https://doi.org/10.1029/2011GL048681

Payne, C. M., & Arrigo, K. R. (2022). Increases in Benthic Particulate Export and Sedimentary Denitrification in the Northern Chukchi Sea Tied to Under-Ice Primary Production. Journal of Geophysical Research: Oceans, 127(2), e2021JC018110. https://doi.org/10.1029/2021JC018110

Pedrazas, M. N., Cardenas, M. B., Demir, C., Watson, J. A., Connolly, C. T., & McClelland, J. W. (2020). Absence of ice-bonded permafrost beneath an Arctic lagoon revealed by electrical geophysics. Science Advances, 6(43), eabb5083. https://doi.org/10.1126/sciadv.abb5083

Peterson, B. J., Holmes, R. M., McClelland, J. W., Vörösmarty, C. J., Lammers, R. B., Shiklomanov, A. I., Shiklomanov, I. A., & Rahmstorf, S. (2002). Increasing River Discharge to the Arctic Ocean. Science, New Series, 298(5601), 2171–2173.

Previdi, M., Smith, K. L., & Polvani, L. M. (2021). Arctic amplification of climate change: A review of underlying mechanisms. Environmental Research Letters, 16(9), 093003. https://doi.org/10.1088/1748-9326/ac1c29

Proshutinsky, A., Dukhovskoy, D., Timmermans, M.-L., Krishfield, R., & Bamber, J. L. (2015). Arctic circulation regimes. Philosophical Transactions of the Royal Society A: Mathematical, Physical and Engineering Sciences, 373(2052), 20140160. https://doi.org/10.1098/rsta.2014.0160

Rantanen, M., Karpechko, A. Yu., Lipponen, A., Nordling, K., Hyvärinen, O., Ruosteenoja, K., Vihma, T., & Laaksonen, A. (2022). The Arctic has warmed nearly four times faster than the globe since 1979. Communications Earth & Environment, 3(1), 168. https://doi.org/10.1038/s43247-022-00498-3

Renaud, P. E., Morata, N., Ambrose, W. G., Bowie, J. J., & Chiuchiolo, A. (2007). Carbon cycling by seafloor communities on the eastern Beaufort Sea shelf. Journal of Experimental Marine Biology and Ecology, 349(2), 248–260. https://doi.org/10.1016/j.jembe.2007.05.021

Renaud, P. E., Riedel, A., Michel, C., Morata, N., Gosselin, M., Juul-Pedersen, T., & Chiuchiolo, A. (2007). Seasonal variation in benthic community oxygen demand: A response to an ice algal bloom in the Beaufort Sea, Canadian Arctic? Journal of Marine Systems, 67(1–2), 1–12. https://doi.org/10.1016/j.jmarsys.2006.07.006

Riedel, A., Michel, C., Gosselin, M., & LeBlanc, B. (2008). Winter–spring dynamics in sea-ice carbon cycling in the coastal Arctic Ocean. Journal of Marine Systems, 74(3–4), 918–932. https://doi.org/10.1016/j.jmarsys.2008.01.003

Risgaard-Petersen, N., Nicolaisen, M. H., Revsbech, N. P., & Lomstein, B. A. (2004). Competition between Ammonia-Oxidizing Bacteria and Benthic Microalgae. Applied and Environmental Microbiology, 70(9), 5528–5537. https://doi.org/10.1128/AEM.70.9.5528-5537.2004

Rysgaard, S., Glud, R. N., Risgaard-Petersen, N., & Dalsgaard, T. (2004). Denitrification and anammox activity in Arctic marine sediments. Limnology and Oceanography, 49(5), 1493–1502. https://doi.org/10.4319/lo.2004.49.5.1493

Serreze, M. C., & Barry, R. G. (2011). Processes and impacts of Arctic amplification: A research synthesis. Global and Planetary Change, 77(1–2), 85–96. https://doi.org/10.1016/j.gloplacha.2011.03.004

Sørensen, H., Meire, L., Juul-Pedersen, T., De Stigter, H., Meysman, F., Rysgaard, S., Thamdrup, B., & Glud, R. (2015). Seasonal carbon cycling in a Greenlandic fjord: An integrated pelagic and benthic study. Marine Ecology Progress Series, 539, 1–17. https://doi.org/10.3354/meps11503

Souza, A. C., Gardner, W. S., & Dunton, K. H. (2014). Rates of nitrification and ammonium dynamics in northeastern Chukchi Sea shelf waters. Deep Sea Research Part II: Topical Studies in Oceanography, 102, 68–76. https://doi.org/10.1016/j.dsr2.2013.12.017

Spangenberg, I., Overduin, P. P., Damm, E., Bussmann, I., Meyer, H., Liebner, S., Angelopoulos, M., Biskaborn, B. K., Grigoriev, M. N., & Grosse, G. (2021). Methane pathways in winter ice of a thermokarst lake–lagoon–coastal water transect in north Siberia. The Cryosphere, 15(3), 1607–1625. https://doi.org/10.5194/tc-15-1607-2021

Stroeve, J. C., Markus, T., Boisvert, L., Miller, J., & Barrett, A. (2014). Changes in Arctic melt season and implications for sea ice loss. Geophysical Research Letters, 41(4), 1216–1225. https://doi.org/10.1002/2013GL058951

Terhaar, J., Lauerwald, R., Regnier, P., Gruber, N., & Bopp, L. (2021). Around one third of current Arctic Ocean primary production sustained by rivers and coastal erosion. Nature Communications, 12(1), 169. https://doi.org/10.1038/s41467-020-20470-z

Thibodeau, B., Bauch, D., & Voss, M. (2017). Nitrogen dynamic in Eurasian coastal Arctic ecosystem: Insight from nitrogen isotope. Global Biogeochemical Cycles, 31(5), 836–849. https://doi.org/10.1002/2016GB005593

Tyler, A. C., McGlathery, K. J., & Anderson, I. C. (2003). Benthic algae control sediment—Water column fluxes of organic and inorganic nitrogen compounds in a temperate lagoon. Limnology and Oceanography, 48(6), 2125–2137. https://doi.org/10.4319/lo.2003.48.6.2125

Woelfel, J., Eggert, A., & Karsten, U. (2014). Marginal impacts of rising temperature on Arctic benthic microalgae production based on in situ measurements and modelled estimates. Marine Ecology Progress Series, 501, 25–40. https://doi.org/10.3354/meps10688

Woelfel, J., Schumann, R., Peine, F., Flohr, A., Kruss, A., Tegowski, J., Blondel, P., Wiencke, C., & Karsten, U. (2010). Microphytobenthos of Arctic Kongsfjorden (Svalbard, Norway): Biomass and potential primary production along the shore line. Polar Biology, 33(9), 1239–1253. https://doi.org/10.1007/s00300-010-0813-0

Yamamoto-Kawai, M., Tanaka, N., & Pivovarov, S. (2005). Freshwater and brine behaviors in the Arctic Ocean deduced from historical data of D18O and alkalinity (1929–2002 A.D.). Journal of Geophysical Research, 110. https://doi.org/doi:10.1029/2004JC002793

Zacher, K., Rautenberger, R., Hanelt, D., Wulff, A., & Wiencke, C. (2009). The abiotic environment of polar marine benthic algae. Botm, 52(6), 483–490. https://doi.org/10.1515/BOT.2009.082

4.8 Tables

Table 4.1. Average hourly sediment fluxes of O_2 (mmol O_2 m^{-2} h^{-1}) and DIC (mmol C m^{-2} h^{-1}) across seasons (Ice Cover, Break Up, Open Water, Annual) and water depth (Deep, Shallow, Combined). n = sample size. Superscript letters denote significant differences between seasons. Asterisks (*) denote values which were set to 0 due to the lack of light incubations during ice cover. (---) represents samples not collected due to the presence of landfast ice.

Season	Dark (mmol O_2 m^{-2} h^{-1})			Light (mmol O_2 m^{-2} h^{-1})		
	Deep	Shallow	Combined	Deep	Shallow	Combined
Ice Cover	-0.19 ± 0.06 (n=10)	---	-0.19 ± 0.06 (n=10)[a]	0* (n=10)	---	0* (n=10)[a]
Break Up	-0.46 ± 0.19 (n=4)	-0.33 ± 0.08 (n=8)	-0.37 ± 0.08 (n=12)[b]	0.66 (n=1)	1.50 ± 0.42 (n=8)	1.41 ± 0.38 (n=9)[b]
Open Water	-0.52 ± 0.07 (n=8)	-0.45 ± 0.10 (n=10)	-0.48 ± 0.06 (n=18)[b]	1.13 ± 0.36 (n=8)	0.51 ± 0.17 (n=10)	0.79 ± 0.19 (n=18)[a,b]
Annual	-0.36 ± 0.06 (n=22)	-0.39 ± 0.07 (n=18)	-0.38 ± 0.04 (n=40)	1.07 ± 0.32 (n=9)	0.95 ± 0.32 (n=18)	0.99 ± 0.19 (n=27)

Table 4.2. Average benthic respiration (BR; mmol C m^{-2} d^{-1}), gross benthic production (GBP; mmol C m^{-2} d^{-1}), and net benthic metabolism (NBM; mmol C m^{-2} d^{-1}) across seasons (Ice Cover, Break Up, Open Water, Annual) and water depth (Deep, Shallow, Combined). n = sample size. Superscript letters denote significant differences between seasons. Asterisks (*) denote values which were set to 0 due to the lack of light incubations during Ice Cover. (---) represents samples not collected due to the presence of landfast ice.

Season	BR (mmol C m^{-2} d^{-1})			GBP (mmol C m^{-2} d^{-1})			NBM (mmol C m^{-2} d^{-1})		
	Deep	Shallow	Combined	Deep	Shallow	Combined	Deep	Shallow	Combined
Ice Cover	3.3 ± 1.1 (n=10)	---	3.3 ± 1.1[a] (n=10)	0 ± 0* (n=10)	---	0 ± 0*[a] (n=10)	3.3 ± 1.1 (n=10)	---	3.3 ± 1.1[a] (n=10)
Break Up	7.9 ± 3.3 (n=4)	5.6 ± 1.3 (n=8)	6.4 ± 1.3[b] (n=12)	-17.9 (n=1)	-31.2 ± 7.8 (n=8)	-29.7 ± 7.1[b] (n=9)	-11.2 (n=1)	-25.5 ± 7.2 (n=8)	-24.0 ± 6.5[b] (n=9)
Open Water	8.5 ± 1.2 (n=8)	7.6 ± 1.7 (n=10)	8.2 ± 1.1[b] (n=18)	-22.3 ± 5.6 (n=8)	-13.0 ± 2.3 (n=10)	-17.1 ± 2.9[c] (n=18)	-13.4 ± 4.7 (n=8)	-5.4 ± 2.3 (n=10)	-8.9 ± 2.6[c] (n=18)
Annual	6.2 ± 1.0 (n=22)	6.7 ± 1.1 (n=18)	6.4 ± 0.7 (n=40)	-10.3 ± 3.4 (n=19)	-21.0 ± 1.2 (n=18)	-15.5 ± 2.8 (n=37)	-4.5 ± 2.8 (n=19)	-14.3 ± 4.1 (n=18)	-9.3 ± 2.6 (n=37)

Table 4.3. Net benthic N_2 fluxes (µmol N m^{-2} d^{-1}) and DIN fluxes (µmol N m^{-2} d^{-1}) across seasons (Ice Cover, Break Up, Open Water, Annual) and water depth (Deep, Shallow, Combined). n = sample size. Superscript letters denote significant differences between seasons. (---) represents samples not collected due to the presence of landfast ice.

Season	N_2 Flux (µmol N m^{-2} d^{-1})			DIN Flux (µmol N m^{-2} d^{-1})		
	Deep	Shallow	Combined	Deep	Shallow	Combined
Ice Cover	1903 ± 580 (n=10)	---	1903 ± 580[a] (n=10)	103 ± 99 (n=10)	---	103 ± 99 (n=10)
Break Up	-7 (n=1)	-184 ± 433 (n=8)	-164 ± 382[b] (n=9)	-6 (n=1)	12 ± 30 (n=8)	10 ± 27 (n=9)
Open Water	-195 ± 158 (n=8)	-478 ± 441 (n=10)	-352 ± 251[b] (n=18)	-67 ± 73 (n=8)	-67 ± 33 (n=10)	-67 ± 36 (n=18)
Annual	919 ± 390 (n=19)	-347 ± 304 (n=18)	301 ± 268 (n=37)	26 ± 62 (n=19)	-32 ± 24 (n=18)	-2 ± 34 (n=37)

Table 4.4. Net benthic fluxes of NH_4^+ (µmol N m^{-2} d^{-1}), NO_3^- (µmol N m^{-2} d^{-1}), PO_4^{3-} (µmol P m^{-2} d^{-1}) and DSi (µmol SiO_2 m^{-2} d^{-1}) across seasons (Ice Cover, Break Up, Open Water, Annual) and water depth (Deep, Shallow, Combined). n = sample size. Superscript letters denote significant differences between seasons. (---) represents samples not collected due to the presence of landfast ice.

Season	NH_4^+ flux (µmol N m^{-2} d^{-1})			NO_3^- flux (µmol N m^{-2} d^{-1})			PO_4^{3-} flux (µmol P m^{-2} d^{-1})			DSi flux (µmol SiO_2 m^{-2} d^{-1})		
	Deep	Shallow	Combined	Deep	Shallow	Combined	Deep	Shallow	Combined	Deep	Shallow	Combined
Ice Cover	38.5 ± 73.9 (n=10)	---	38.5 ± 73.9[a] (n=10)	64.5 ± 65.3 (n=10)	---	64.5 ± 65.3 (n=10)	13.0 ± 56.1 (n=10)	---	13.0 ± 56.1 (n=10)	143.0 ± 94.4 (n=4)	---	143.0 ± 94.4 (n=4)
Break Up	-2.7 (n=1)	9.5 ± 29.8 (n=8)	8.1 ± 26.4[ab] (n=9)	-2.5 (n=1)	2.4 ± 8.0 (n=8)	1.8 ± 7.1 (n=9)	-2.5 (n=1)	-6.9 ± 4.6 (n=8)	-6.4 ± 4.1 (n=9)	31.2 (n=1)	-16.8 ± 48.1 (n=3)	-4.8 ± 36.1 (n=4)
Open Water	-103.3 ± 38.4 (n=8)	-54.4 ± 25.2 (n=10)	-76.1 ± 22.1[b] (n=18)	36.0 ± 63.7 (n=8)	-12.5 ± 31.4 (n=10)	9.1 ± 32.7 (n=18)	-18.0 ± 42.6 (n=8)	26.4 ± 18.7 (n=10)	6.7 ± 21.5 (n=18)	5.9 ± 49.8 (n=4)	-95.7 ± 70.9 (n=4)	-44.9 ± 44.5 (n=8)
Annual	-23.4 ± 44.1 (n=19)	-26.0 ± 20.2 (n=18)	-24.7 ± 24.3 (n=37)	48.0 ± 42.5 (n=19)	-5.9 ± 17.5 (n=18)	22.3 ± 23.6 (n=37)	-0.9 ± 33.7 (n=19)	11.6 ± 11.1 (n=18)	5.2 ± 17.9 (n=37)	69.5 ± 49.4 (n=9)	-61.9 ± 45.0 (n=7)	12.0 ± 37.0 (n=16)

Table 4.5. Seasonal average ± standard error (n=sample number) of environmental parameters that were selected as input variables for the stepwise multiple linear regression model. n = sample size.

Parameter	Ice Cover	Break Up	Open Water
Temperature (°C)	-1.9 ± 0.1 (n=10)	2.8 ± 0.9 (n=12)	8.0 ± 0.3 (n=18)
Salinity	37.6 ± 0.8 (n=10)	10.3 ± 3.7 (n=12)	24.7 ± 0.8 (n=18)
PAR (µmol m^{-2} s^{-1})	---	93.1 ± 22.9 (n=12)	88.5 ± 15.0 (n=18)
DIN (µmol N L^{-1})	9.6 ± 1.7 (n=10)	1.6 ± 0.8 (n=12)	0.9 ± 0.2 (n=18)
Sed NOx (µmol N L^{-1})	2.4 ± 0.5 (n=7)	2.01 ± 1.2 (n=10)	1.5 ± 0.9 (n=10)
Sed DSi (µmol SiO2 L^{-1})	88.7 ± 8.0 (n=7)	64.2 ± 17.3 (n=10)	165.1 ± 42.4 (n=10)
SOC (%)	2.0 ± 0.3 (n=9)	2.0 ± 0.7 (n=11)	1.5 ± 0.2 (n=18)
Sediment $\delta^{13}C$ (‰)	-26.4 ± 0.2 (n=9)	-25.1 ± 0.3 (n=11)	-25.9 ± 0.2 (n=18)
Sediment chl-a (mg m^{-2})	28.7 ± 7.9 (n=10)	78.2 ± 28.5 (n=10)	47.2 ± 14.7 (n=17)

Table 4.6 The stepwise selection regression model output for Benthic Respiration (BR) displaying the model with the lowest prediction error with two parameters (temperature, SOC; Model 2). For each model, we calculated RMSE and MAE, which measure the prediction error of each model, with lower values indicating a better model. Adjusted R^2 values represent the correlation between values observed and predicted by the model, with higher values indicating a better model. Once selected, the final model was assessed for 1) slope: the estimated regression coefficient of the linear regression, 2) p-value: the statistical significance of the regression coefficient, 3) Img: the relative importance of each parameter in explaining data variability, and 4) variance inflation factor (VIF): a measure of collinearity among independent variables, where values between 1 and 4 were considered an acceptable level of correlation between independent variables.

BR	Factors in Model									Model Fit Metrics		
Model	Temp	Sal	$\delta^{13}C$	SOC	PW NO_3^-	PW DSi	Sed chl-a	DIN	PAR	RMSE	MAE	R^2
1	*									8.38	7.32	0.14
2	*			*						5.94	5.07	0.38
3	*	*	*							7.42	6.51	0.06
4	*	*		*				*		6.97	6.06	0.44
5	*	*		*			*	*		7.43	6.33	0.47

Multiple Regression	slope	p value	Img	VIF
Intercept	-2.77	0.287	NA	NA
SOC	6.40	0.003	0.53	1.076
Temperature	0.51	0.002	0.47	1.076

Table 4.7. Seasonal rates of benthic metabolism (BR, GBP, NBM) and net nitrogen fluxes (N_2, DIN) were scaled up to annual rates based on the duration of each season (Ice Cover, Break Up, and Open Water).

Season (duration in months)	BR	GBP	NBM	N_2	DIN	Net N flux
	(mmol C m^{-2} d^{-1})			(mmol N m^{-2} d^{-1})		
Ice Cover (7.5)	3.3	0	3.3	-1.90	0.10	-1.80
Break Up (1)	6.4	-29.7	-24.0	0.16	0.01	0.17
Open Water (3.5)	8.2	-17.1	-9.3	0.35	-0.07	0.29
Annual Flux (mmol C, N m^{-2} y^{-1})	**1.9**	**-2.8**	**-0.9**	**-0.39**	**0.02**	**-0.37**

4.9 Figures

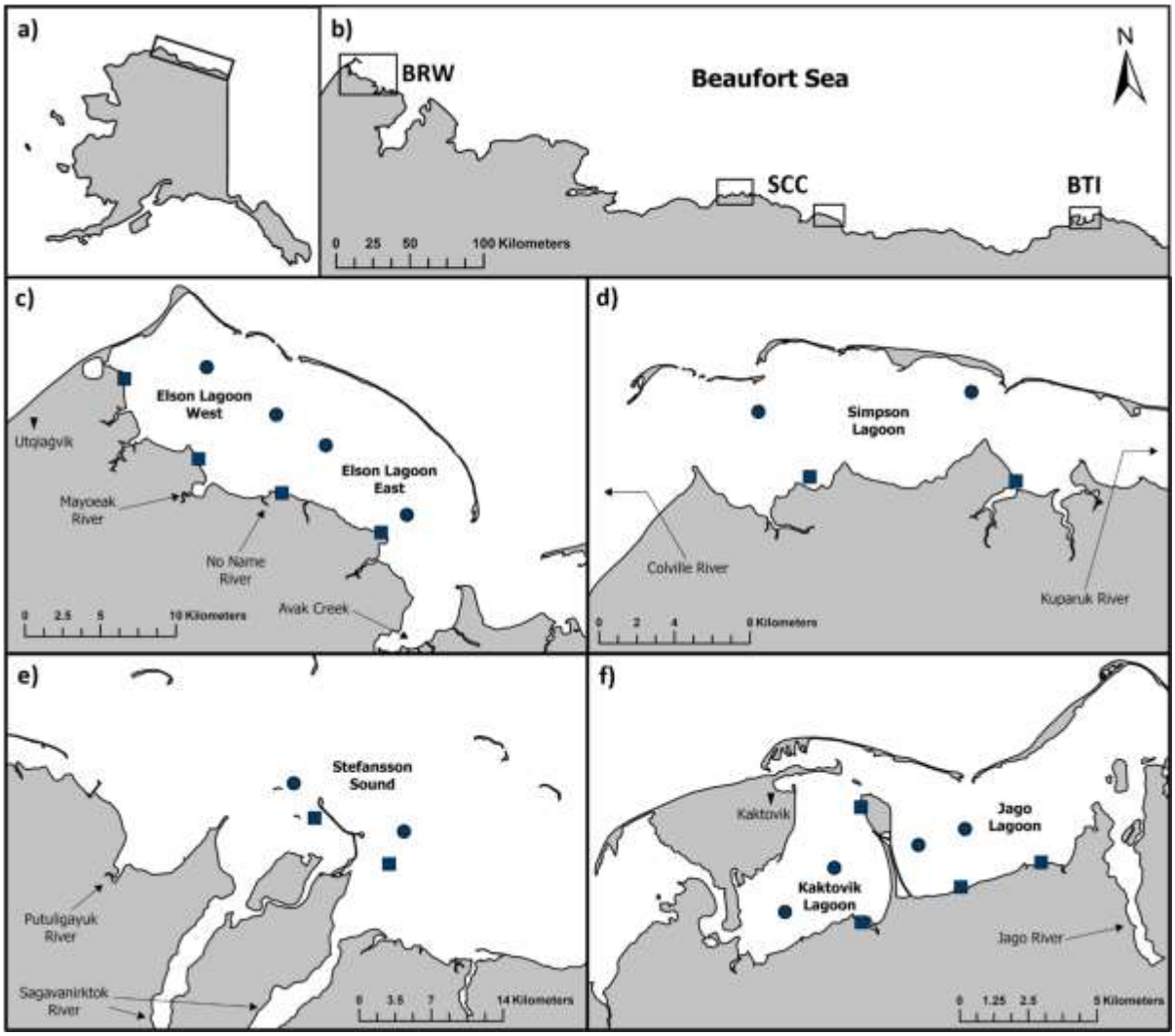

Figure 4.1. Location of the study sites at the Beaufort Lagoon Ecosystems Long-Term Ecological Research (BLE-LTER) program. a) Map of Alaska with Beaufort Sea Alaskan coast in box. b) Beaufort Sea Coast with BLE-LTER research nodes in boxes. c) The westernmost node (BRW) is based out of Utqiaġvik where Elson Lagoon is located. The central node (SCC) contains d) Simpson Lagoon and e) Stefansson Sound. The eastern node (BTI) is based out of Kaktovik and contains f) Kaktovik Lagoon and Jago Lagoon. Each sampled lagoon has two shallow (squares) and two deep (circles) stations.

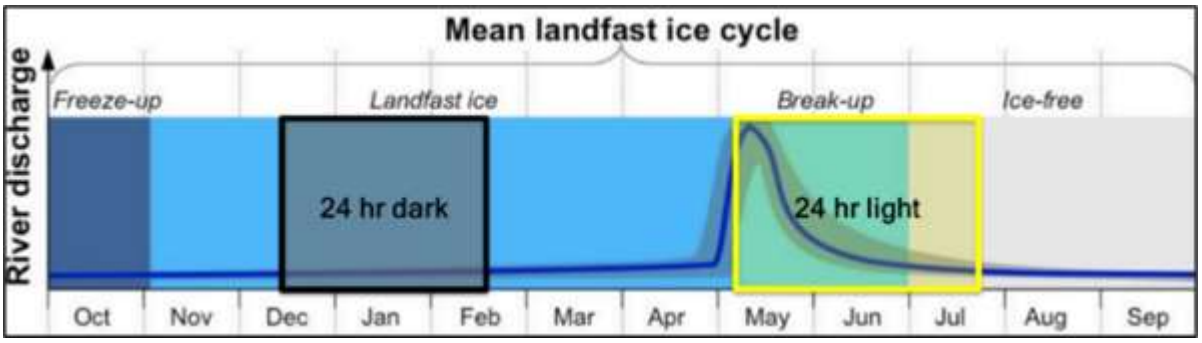

Figure 4.2. Conceptual diagram based on Mahoney et al. (2007) showing annual cycles of landfast sea ice (background color, freeze-up = dark blue, ice cover = light blue, break up = turquoise, open water = grey) and river discharge (solid blue line) along the Alaskan Beaufort Sea coast (Mahoney et al. 2007). Diagram has been modified to denote periods with 24 hours of light ("midnight sun") and 24 hours of darkness ("polar night").

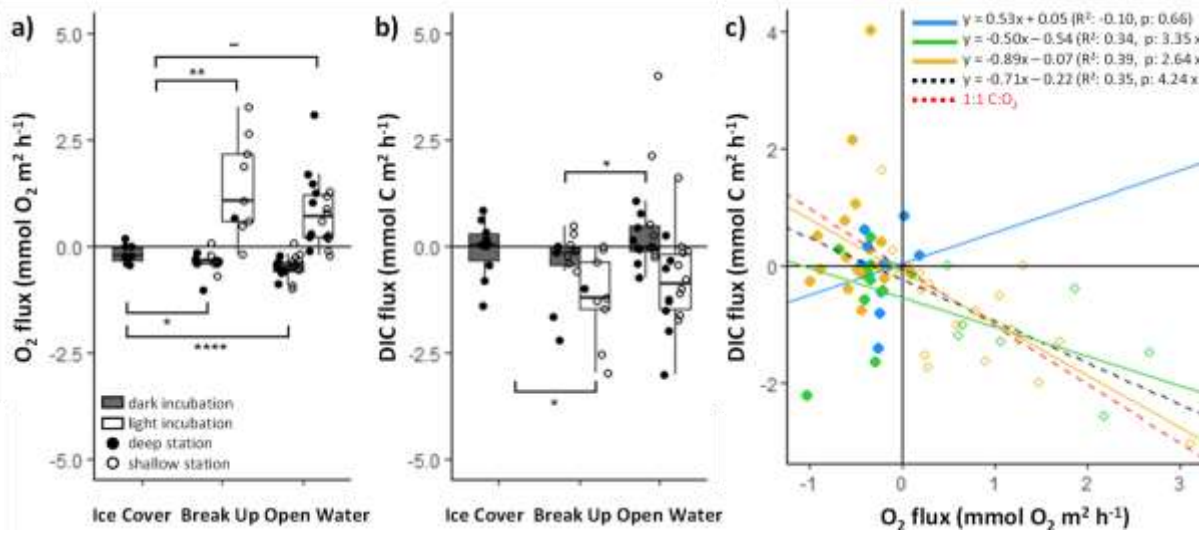

Figure 4.3. a) Hourly sediment O_2 flux (mmol O_2 m^{-2} h^{-1}) and b) hourly sediment DIC flux (mmol C m^{-2} h^{-1}) from dark (grey bars) and light (white bars) incubations across seasons (Ice Cover, Break Up, Open Water) and water depth (Deep = filled circles, Shallow = empty circles). The lower and upper extent of the boxplot represent the 25th (Q1) and 75th (Q3) percentiles while the lower and upper extent of the whiskers represent 1.5 times the interquartile range (Q3-Q1) below Q1 and above Q3. The solid black line within each box represents the median rate. Brackets represent significant seasonal differences (p-value: ~<0.10, *<0.05, **<0.01, ***<0.001, ****<0.0001). c) Scatterplot of sediment O_2 flux and DIC flux during light (open circles) and dark (filled circles) incubations across Ice Cover (blue), Break Up (green), and Open Water (yellow). The dashed red line through the scatterplot represents a 1:1, C:O_2 ratio (i.e., respiratory quotient, RQ), while the solid black line represents the linear regression between O_2 and DIC fluxes averaged across the entire year for this study (Annual RQ: 0.71). Season-specific linear regression lines are also shown for Ice Cover (blue), Break Up (green), and Open Water (yellow), with accompanying slopes, R^2, and p values.

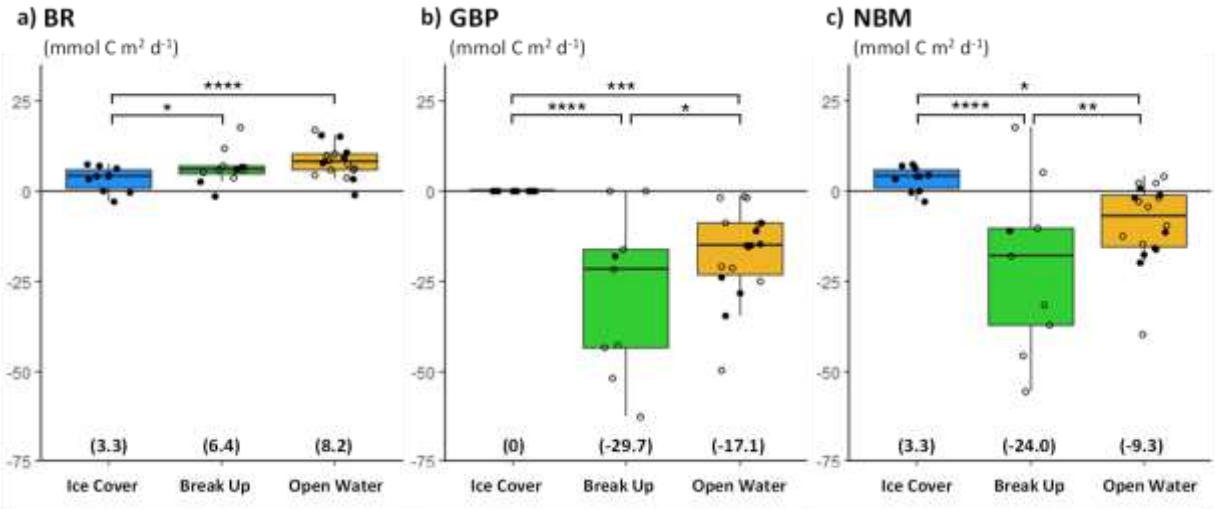

Figure 4.4. Daily rates of a) benthic respiration (BR, mmol C m^{-2} d^{-1}), b) gross benthic production (GBP, mmol C m^{-2} d^{-1}), and c) net benthic metabolism (NBM; mmol C m^{-2} d^{-1}) across seasons (Ice Cover [blue], Break Up [green], Open Water [yellow]) and water depth (Deep = filled circles, Shallow = empty circles). The lower and upper extent of the boxplot represent the 25th (Q1) and 75th (Q3) percentiles while the lower and upper extent of the whiskers represent 1.5 times the interquartile range (Q3-Q1) below Q1 and above Q3. The solid black line within each box represents the median rate. Brackets represent significant seasonal differences (p-value: ~<0.10, *<0.05, **<0.01, ***<0.001, ****<0.0001). Average rates of BR, GBP, and NBM (mmol C m^{-2} d^{-1}) by season are denoted in parentheses along the x-axis.

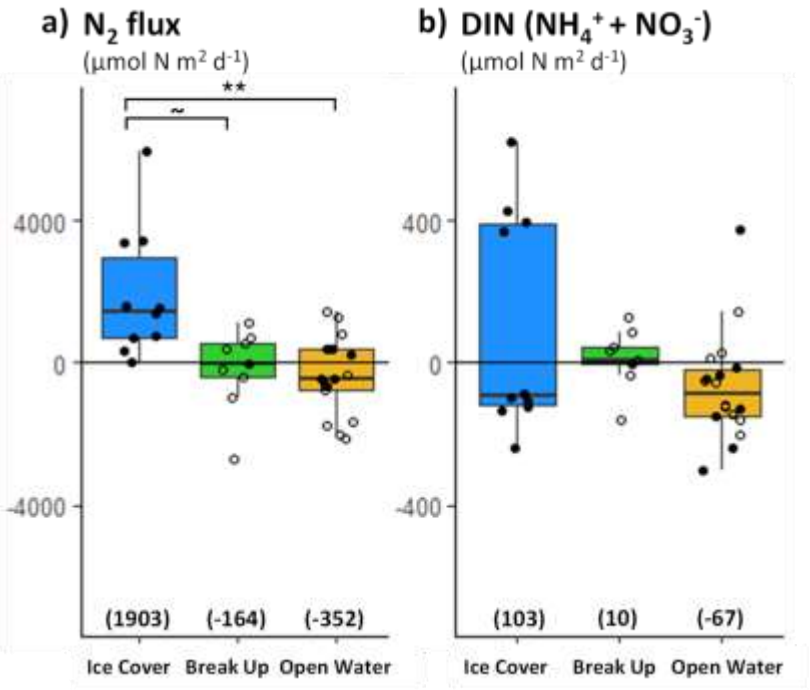

Figure 4.5. Daily net benthic a) N_2 flux (µmol N m^{-2} d^{-1}) and b) DIN flux (µmol N m^{-2} d^{-1}) across seasons (Ice Cover [blue], Break Up [green], Open Water [yellow]) and water depth (Deep = filled circles, Shallow = empty circles). The lower and upper extent of the boxplot represent the 25th (Q1) and 75th (Q3) percentiles while the lower and upper extent of the whiskers represent 1.5 times the interquartile range (Q3-Q1) below Q1 and above Q3. The solid black line within each box represents the median rate. Brackets represent significant seasonal differences (p-value: ~<0.10, *<0.05, **<0.01, ***<0.001, ****<0.0001). Average rates of sediment N_2 and DIN flux by season are denoted in parentheses along the x-axis. Note the difference in scale for y-axis in panels a and b.

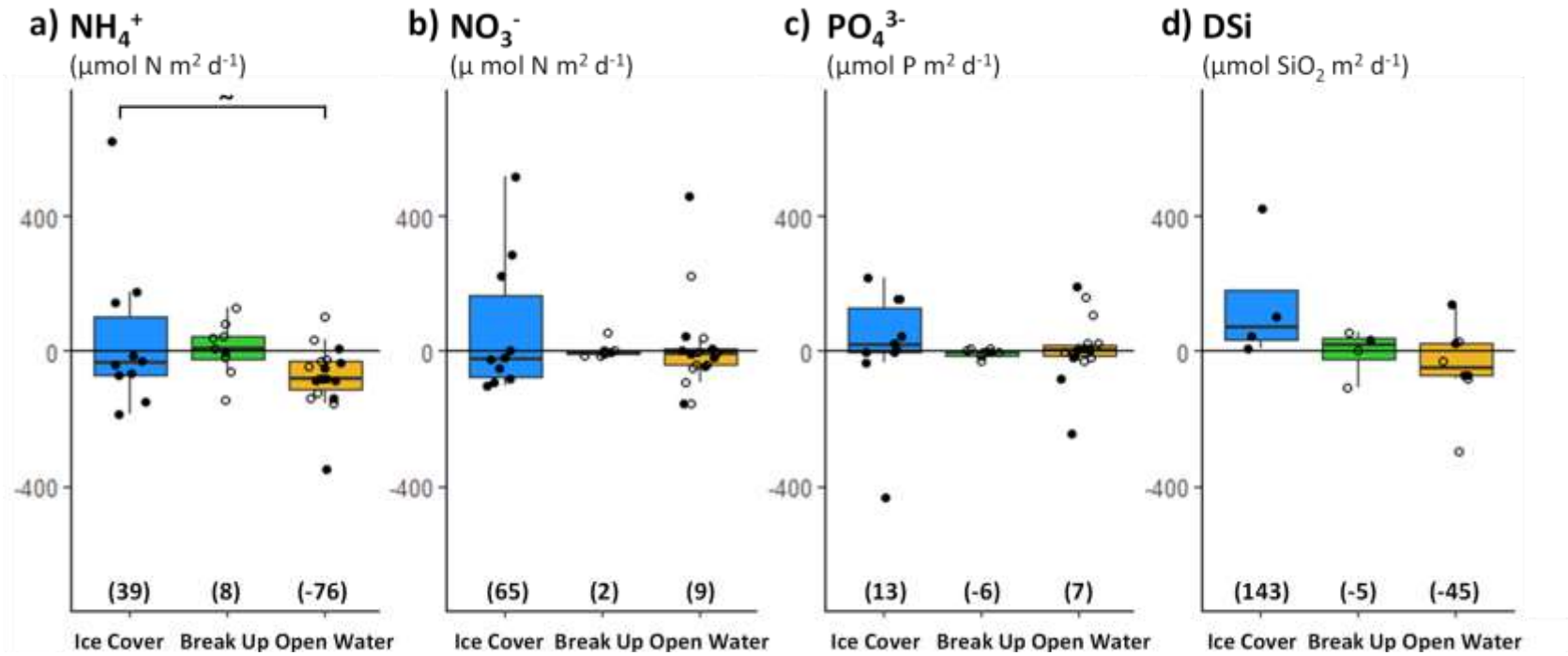

Figure 4.6. Daily benthic fluxes of a) NH_4^+ (µmol N m^{-2} d^{-1}), b) NO_3^- (µmol N m^{-2} d^{-1}), c) PO_4^{3-} (µmol P m^{-2} d^{-1}), and d) DSi (µmol SiO_2 m^{-2} d^{-1}) across seasons (Ice Cover [blue], Break Up [green], Open Water [yellow]) and water depth (Deep = filled circles, Shallow = empty circles). The lower and upper extent of the boxplot represent the 25th (Q1) and 75th (Q3) percentiles while the lower and upper extent of the whiskers represent 1.5 times the interquartile range (Q3-Q1) below Q1 and above Q3. The solid black line within each box represents the median rate. Brackets represent significant seasonal differences (p-value: ~<0.10, *<0.05, **<0.01, ***<0.001, ****<0.0001). Average rates of sediment nutrient flux by season are denoted in parentheses along the x-axis.

4.10 Appendix C

Supplementary Table 4.1. Average hourly sediment fluxes of DIC (mmol C m^{-2} h^{-1}) across seasons (Ice Cover, Break Up, Open Water, Annual) and water depth (Deep, Shallow, Combined). n = sample size. Superscript letters denote significant differences between seasons. Asterisks (*) denote values which were set to 0 due to the lack of light incubations during ice cover. (---) represents samples not collected due to the presence of landfast ice.

Season	Dark (mmol C m^{-2} h^{-1})			Light (mmol C m^{-2} h^{-1})		
	Deep	Shallow	Combined	Deep	Shallow	Combined
Ice Cover	-0.05 ± 0.21 (n=10)	---	-0.05 ± 0.21 (n=10)[a,b]	0* (n=10)	---	0* (n=10)[a]
Break Up	-0.99 ± 0.54 (n=4)	-0.07 ± 0.12 (n=8)	-0.38 ± 0.22 (n=12)[a]	-1.00 (n=1)	-1.24 ± 0.39 (n=8)	-1.22 ± 0.34 (n=9)[b]
Open Water	0.15 ± 0.21 (n=8)	0.63 ± 0.44 (n=10)	0.42 ± 0.26 (n=18)[b]	-1.21 ± 0.36 (n=8)	-0.52 ± 0.31 (n=10)	-0.83 ± 0.24 (n=18)[a,b]
Annual	-0.15 ± 0.17 (n=22)	0.32 ± 0.26 (n=18)	0.06 ± 0.15 (n=40)	-1.19 ± 0.32 (n=9)	-0.84± 0.25 1.0 (n=18)	-0.96 ± 0.20 (n=27)

Supplemental Table 4.2. Two-way ANOVA results on the effect of season (Ice Cover, Break Up, Open Water) and water depth (Shallow, Deep) on sediment fluxes of O_2 and DIC in dark and light incubations.

2-way ANOVA Dark DO	Sum of Squares	Df	Mean Square	F	P
season	1.3135	2	0.6568	11.385	0.000112
water depth	0.1261	1	0.1261	2.185	0.146817
season:water depth	0.0083	2	0.0042	0.072	0.930671
Tukey HSD Season	**p adj**				
ice cover-break up	0.01289				
open water-break up	0.46565				
open water-ice cover	0.00009				
2-way ANOVA Light DO	**Sum of Squares**	**Df**	**Mean Square**	**F**	**P**
season	8.384	2	4.192	6.170	0.00585
water depth	0.541	1	0.541	0.796	0.37950
season:water depth	1.771	2	0.885	1.303	0.28714
Tukey HSD Season	**p adj**				
ice cover-break up	0.00412				
open water-break up	0.17630				
open water-ice cover	0.07948				
2-way ANOVA Dark DIC	**Sum of Squares**	**Df**	**Mean Square**	**F**	**P**
season	4.726	2	2.3630	3.517	0.0387
water depth	2.185	1	2.1847	3.252	0.0785
season:water depth	1.122	2	0.5612	0.835	0.4408
Tukey HSD Season	**p adj**				
ice cover-break up	0.49765				
open water-break up	0.03367				
open water-ice cover	0.24217				
2-way ANOVA Light DIC	**Sum of Squares**	**Df**	**Mean Square**	**F**	**P**
season	6.570	2	3.285	3.880	0.0321
water depth	1.088	1	1.088	1.285	0.2663
season:water depth	1.055	2	0.527	0.623	0.5435
Tukey HSD Season	**p adj**				
ice cover-break up	0.02843				
open water-break up	0.56185				
open water-ice cover	0.10347				

Supplemental Table 4.3. Two-way ANOVA results on the effect of season (Ice Cover, Break Up, Open Water) and water depth (Shallow, Deep) on benthic respiration (BR), gross benthic production (GBP) and net benthic metabolism (NBM).

2-way ANOVA BR	Sum of Squares	Df	Mean Square	F	P
season	381.4	2	190.7	11.976	0.000112
water depth	36.6	1	36.6	2.185	0.146817
season:water depth	2.4	2	1.21	0.072	0.930674
Tukey HSD Season	**p adj**				
ice cover-break up	0.01289				
open water-break up	0.46565				
open water-ice cover	0.00009				
2-way ANOVA GBP	**Sum of Squares**	**Df**	**Mean Square**	**F**	**P**
season	5852	2	2926.1	20.240	9.35E-07
water depth	106	1	0.732	0732	0.397
season:water depth	439	2	1.520	1.520	0.231
Tukey HSD Season	**p adj**				
ice cover-break up	0.0000013				
open water-break up	0.0375421				
open water-ice cover	0.0003485				
2-way ANOVA NBM	**Sum of Squares**	**Df**	**Mean Square**	**F**	**P**
season	4038	2	2019.0	16.573	6.18E-06
water depth	29	1	29.1	0.239	0.628
season:water depth	456	2	228.2	1.873	0.167
Tukey HSD Season	**p adj**				
ice cover-break up	0.0000037				
open water-break up	0.0052331				
open water-ice cover	0.0155014				

Supplemental Table 4.4. Two-way ANOVA results on the effect of season (Ice Cover, Break Up, Open Water) and water depth (Shallow, Deep) on net benthic N_2 and DIN fluxes.

2-way ANOVA N2	Sum of Squares	Df	Mean Square	F	P
season	19.81	2	9.904	5.506	0.00783
water depth	3.78	1	3.778	2.1	0.15526
season:water depth	2.36	2	1.179	0.656	0.52478
Tukey HSD Season	**p adj**				
ice cover-break up	0.07845				
open water-break up	0.93702				
open water-ice cover	0.00852				
2-way ANOVA DIN	**Sum of Squares**	**Df**	**Mean Square**	**F**	**P**
season	140626	2	70313	2.029	0.145
water depth	5285	1	5285	0.152	0.698
season:water depth	11799	2	5900	0.170	0.844
Tukey HSD Season	**p adj**				
ice cover-break up	0.8093				
open water-break up	0.5727				
open water-ice cover	0.12498				

Supplemental Table 4.5. Two-way ANOVA results on the effect of season (Ice Cover, Break Up, Open Water) and water depth (Shallow, Deep) on net benthic inorganic nutrient fluxes (NH_4^+, NO_3^-, PO_4^{3-}, DSi).

2-way ANOVA NH_4^+	Sum of Squares	Df	Mean Square	F	P
season	94682	2	47341	2.693	0.0803
water depth	2418	1	2418	0.138	0.7128
season:water depth	10721	2	5361	0.305	0.7389
Tukey HSD Season	**p adj**				
ice cover-break up	0.96751				
open water-break up	0.27629				
open water-ice cover	0.08259				
2-way ANOVA NO_3^-	**Sum of Squares**	**Df**	**Mean Square**	**F**	**P**
season	9499	2	4749	0.259	0.773
water depth	14851	1	14851	0.81	0.374
season:water depth	2189	2	1094	0.06	0.942
2-way ANOVA PO_4^{3-}	**Sum of Squares**	**Df**	**Mean Square**	**F**	**P**
season	1280	2	640	0.06	0.942
water depth	3217	1	3217	0.3	0.587
season:water depth	5855	2	2927	0.273	0.762
2-way ANOVA DSi	**Sum of Squares**	**Df**	**Mean Square**	**F**	**P**
season	41831	2	20915	1.495	0.251
water depth	34069	1	34069	2.436	0.136
season:water depth	1908	2	954	0.068	0.934
Tukey HSD Depth	**p adj**				
shallow – deep	0.15403				

Supplemental Table 4.6. Matrix of p-values from Pearson's correlation of all environmental parameters. Colors denote level of significance (yellow <0.1, green <.05, red <0.01).

	wc_chla	btm_DO	WC_phy	pH	sal	temp_C	d13C	SOC	d15N	SON	CN	PW_NH4	PW_PO4	PW_Dsi	PW_Nox	PW_DIN	sed_chla	sed_pheo	wc_NH4	wc_PO4	wc_Dsi	wc_Nox	wc_DIN
wc_DIN	0.00	0.00	0.84	0.00	0.00	0.00	0.02	0.02	0.49	0.04	0.62	0.81	0.78	0.83	0.03	0.39	0.59	0.37	0.00	0.00	0.00	0.00	
wc_Nox	0.00	0.23	0.55	0.00	0.15	0.00	0.01	0.00	0.01	0.02	0.35	0.32	0.79	0.53	0.00	0.03	0.18	0.57	0.03	0.02	0.00		0.00
wc_Dsi	0.01	0.00	0.87	0.00	0.00	0.00	0.03	0.55	0.54	0.45	0.98	0.65	0.19	0.94	0.43	0.88	0.41	0.59	0.00	0.02		0.00	0.00
wc_PO4	0.02	0.59	0.39	0.01	0.06	0.00	0.84	0.39	0.24	0.42	0.30	0.42	0.60	0.59	0.11	0.44	0.85	0.40	0.00		0.02	0.02	0.00
wc_NH4	0.03	0.00	0.94	0.00	0.01	0.00	0.58	0.55	0.56	0.41	0.57	0.89	0.13	0.69	0.54	0.88	0.92	0.07		0.00	0.00	0.03	0.00
sed_pheo	0.77	0.98	0.19	0.94	0.12	0.06	0.80	0.00	0.90	0.00	0.54	0.90	1.00	0.20	0.13	0.92	0.00		0.07	0.40	0.59	0.57	0.37
sed_chla	0.88	0.36	0.82	0.07	0.49	0.84	0.30	0.84	0.00	0.48	0.18	0.90	0.30	1.00	0.15	0.92		0.00	0.92	0.85	0.41	0.18	0.59
PW_DIN	0.51	0.03	0.34	0.09	0.81	0.10	0.24	0.14	0.07	0.12	0.06	0.00	0.02	0.00	0.72		0.92	0.92	0.88	0.44	0.88	0.03	0.39
PW_Nox	0.37	0.48	0.45	0.67	0.18	0.19	0.02	0.30	0.10	0.65	0.01	0.42	0.44	0.07		0.72	0.15	0.13	0.54	0.11	0.43	0.00	0.03
PW_Dsi	0.42	0.02	0.32	0.86	0.13	0.01	0.16	0.38	0.05	0.50	0.42	0.00	0.03		0.07	0.00	1.00	0.20	0.69	0.59	0.94	0.53	0.83
PW_PO4	0.00	0.19	0.24	0.66	0.19	0.47	0.16	0.13	0.69	0.18	0.83	0.01		0.03	0.44	0.02	0.30	1.00	0.13	0.60	0.19	0.79	0.78
PW_NH4	0.44	0.08	0.57	0.14	0.71	0.15	0.08	0.43	0.21	0.31	0.03		0.01	0.00	0.42	0.00	0.90	0.90	0.89	0.42	0.65	0.32	0.81
CN	0.97	0.59	0.34	0.64	0.57	0.16	0.18	0.01	0.67	0.27		0.03	0.83	0.42	0.01	0.06	0.18	0.54	0.57	0.30	0.98	0.35	0.62
SON	0.33	0.63	0.42	0.94	0.36	0.01	0.27	0.00	0.00		0.27	0.31	0.18	0.50	0.65	0.12	0.48	0.00	0.41	0.42	0.45	0.02	0.04
d15N	0.36	0.27	0.02	0.26	0.53	0.24	0.11	0.00		0.00	0.67	0.21	0.69	0.05	0.10	0.07	0.00	0.90	0.56	0.24	0.54	0.01	0.49
SOC	0.30	0.51	0.80	0.86	0.39	0.04	0.19		0.00	0.00	0.01	0.43	0.13	0.38	0.30	0.14	0.84	0.00	0.55	0.39	0.55	0.00	0.02
d13C	0.27	0.00	0.90	0.07	0.00	0.48		0.19	0.11	0.27	0.18	0.08	0.16	0.16	0.02	0.24	0.30	0.80	0.58	0.84	0.03	0.01	0.02
temp_C	0.00	0.97	0.86	0.00	0.18		0.48	0.04	0.24	0.01	0.16	0.15	0.47	0.01	0.19	0.10	0.84	0.06	0.00	0.00	0.00	0.00	0.00
sal	0.92	0.00	0.86	0.00		0.18	0.00	0.39	0.53	0.36	0.57	0.71	0.19	0.13	0.18	0.81	0.49	0.12	0.01	0.06	0.00	0.15	0.00
pH	0.16	0.00	0.66		0.00	0.00	0.07	0.86	0.26	0.94	0.64	0.14	0.66	0.86	0.67	0.09	0.07	0.94	0.00	0.01	0.00	0.00	0.00
WC_phy	0.00	0.68		0.66	0.86	0.86	0.90	0.80	0.02	0.42	0.34	0.57	0.24	0.32	0.45	0.34	0.82	0.19	0.94	0.39	0.87	0.55	0.84
btm_DO	0.19		0.68	0.00	0.00	0.97	0.00	0.51	0.27	0.63	0.59	0.08	0.19	0.02	0.48	0.03	0.36	0.98	0.00	0.59	0.00	0.23	0.00
wc_chla		0.19	0.00	0.16	0.92	0.00	0.27	0.30	0.36	0.33	0.97	0.44	0.00	0.42	0.37	0.51	0.88	0.77	0.03	0.02	0.01	0.00	0.00

Supplemental Table 4.7. The stepwise selection regression model output for gross benthic production (GBP) displaying the model with the lowest prediction error with 2 parameters (Model 2; PAR, sediment chlorophyll-a). For each model, we calculated RMSE and MAE, which measure the prediction error of each model, with lower values indicating a better model. Adjusted R^2 values represent the correlation between values observed and predicted by the model, with higher values indicating a better model. Once selected, the final model was assessed for 1) slope: the estimated regression coefficient of the linear regression, 2) p-value: the statistical significance of the regression coefficient, 3) lmg: the relative importance of each parameter in explaining data variability, and 4) variance inflation factor (VIF): a measure of collinearity among independent variables, where values between 1 and 4 were considered an acceptable level of correlation between independent variables.

GBP	Factors in Model									Model Fit Metrics		
Model	Temp	Sal	$\delta^{13}C$	SOC	PW NO_3^-	PW DSi	Sed chl-a	DIN	PAR	RMSE	MAE	R^2
1									*	17.35	14.05	0.41
2							*		*	17.32	14.06	0.47
3		*					*		*	18.23	14.55	0.51
4		*					*	*	*	22.38	19.25	0.60
5		*				*	*	*	*	22.23	18.69	0.59

GBP - Multiple Regression	slope	p value	lmg	VIF
Intercept	15.62	0.039	NA	NA
Sed Chla	-4.95	0.025	0.25	1.078
PAR	-2.16	1.00e-05	0.75	1.078

Supplemental Table 4.8. The stepwise selection regression model output for net benthic metabolism (NBM) displaying the model with the lowest prediction error with one parameter (Model 1; salinity).

NBM	Factors in Model									Model Fit Metrics		
Model	Temp	Sal	$\delta^{13}C$	SOC	PW NO_3^-	PW DSi	Sed chl-a	DIN	PAR	RMSE	MAE	R^2
1		*								22.09	18.54	0.34
2		*							*	23.41	19.02	0.42
3		*					*		*	26.34	22.52	0.49
4		*					*	*	*	27.06	23.18	0.53
5		*				*	*	*	*	28.70	24.55	0.55

NBM - Multiple Regression	slope	p value	lmg	VIF
Intercept	-27.34	3.87e-07	NA	NA
Salinity	0.77	4.65e-05	NA	NA

Supplemental Table 4.9. The stepwise selection regression model output for net sediment N_2 flux displaying the model with the lowest prediction error with one parameter (Model 1; water column DIN concentration).

N_2 Model	Factors in Model									Model Fit Metrics		
	Temp	Sal	$\delta^{13}C$	SOC	PW NO_3^-	PW DSi	Sed chl-a	DIN	PAR	RMSE	MAE	R^2
1								*		1.22	1.05	0.31
2					*			*		1.60	1.36	0.32
3			*		*			*		1.64	1.37	0.35
4	*	*	*	*						1.58	1.38	0.24
5	*		*		*		*	*		1.90	1.63	0.38

N_2 - Linear Regression	slope	p value	Img	VIF
Intercept	0.23	0.28	NA	NA
DIN	0.63	1.49e-05	NA	NA

Supplemental Table 4.10. The stepwise selection regression model output for net sediment NH_4^+ flux displaying the model with the lowest prediction error with one parameter (Model 1; temperature).

NH_4^+ Model	Factors in Model									Model Fit Metrics		
	Temp	Sal	$\delta^{13}C$	SOC	PW NO_3^-	PW DSi	Sed chl-a	DIN	PAR	RMSE	MAE	R^2
1	*									147.28	129.47	0.16
2	*						*			169.51	147.50	0.17
3	*					*		*		173.00	155.49	0.16
4	*	*	*	*						168.62	148.11	0.04
5	*	*	*	*	*					190.92	163.67	0.00

NH_4^+ - Linear Regression	slope	p value	Img	VIF
Intercept	23.16	0.48	NA	NA
Temperature	-11.19	0.04	NA	NA

Supplemental Table 4.11. The stepwise selection regression model output for net sediment NO_3^- flux displaying the model with the lowest prediction error with three parameters (temperature, salinity, and $\delta^{13}C$-SOC). The parameters of the final model were not significant.

NO_3^- Model	Factors in Model									Model Fit Metrics		
	Temp	Sal	$\delta^{13}C$	SOC	PW NO_3^-	PW DSi	Sed chl-a	DIN	PAR	RMSE	MAE	R^2
1						*				182.56	156.78	0.03
2			*		*					179.20	154.50	0.05
3	*	*	*							154.36	135.69	-0.04
4	*		*	*	*					169.29	150.00	0.07
5	*		*	*	*					182.08	158.78	0.03

NO_3^- - Linear Regression	slope	p value	Img	VIF
Intercept	-254.06	0.71	NA	NA
Temperature	-4.16	0.50	0.44	1.16
Salinity	1.10	0.66	0.33	1.38
Sediment $\delta^{13}C$	-10.60	0.70	0.23	1.25

Supplemental Table 4.12. The stepwise selection regression model output for net sediment PO_4^{3-} flux displaying the model with the lowest prediction error with one parameter (sediment chlorophyll-a). The final model was not significant.

PO_4^{3-} Model	Factors in Model									Model Fit Metrics		
	Temp	Sal	$\delta^{13}C$	SOC	PW NO_3^-	PW DSi	Sed chl-a	DIN	PAR	RMSE	MAE	R^2
1							*			120.41	101.94	0.02
2				*			*			135.64	113.34	0.03
3				*	*		*			122.72	102.18	0.01
4	*			*	*		*			134.53	117.33	-0.01
5		*		*	*		*		*	163.34	144.84	-0.05

PO4 - Linear Regression	slope	p value	Img	VIF
Intercept	-96.91	0.16	NA	NA
Sediment chl-a	0.12	0.20	NA	NA

Supplemental Table 4.13. The stepwise selection regression model output for net sediment DSi flux displaying the model with the lowest prediction error with one parameter (temperature).

DSi Model	Factor in Model									Model Fit Metrics		
	Temp	Sal	$\delta^{13}C$	SOC	PW NO_3^-	PW DSi	Sed chl-a	DIN	PAR	RMSE	MAE	R^2
1	*									39.86	39.86	0.71
2	*					*				42.15	42.15	0.90
3	*			*	*					195.33	195.33	0.94
4	*			*	*	*				331.93	331.93	0.94
5	*	*			*	*	*			194.00	194.00	0.99

DSi - Linear Regression	slope	p value	Img	VIF
Intercept	91.43	0.52	NA	NA
Temperature	-21.14	0.02	NA	NA

Supplemental Table 4.14. Respiratory quotient (RQ, C:O_2) and photosynthetic quotient (PQ, O_2:C) calculated from linear regressions (R^2) of DO and DIC fluxes during dark and light incubations, respectively. Asterisks denote the levels of significance of the linear regression (p-value: ~<0.10, *<0.05, **<0.01, ***<0.001, ****<0.0001). RQ and PQ values were calculated for each season and annually. Due to the lack of significance of dark RQ values, RQ values were also calculated using both dark and light incubations.

Season	Dark (RQ - C:O_2)	Light (PQ - O_2:C)	Combined (RQ - C:O_2)
Ice Cover	0.53	NA	0.53
Break up	1.35	-1.43*	-0.5**
Open Water	0.22	-1.11***	-0.89***
Annual	0.23	-1.27***	-0.71***

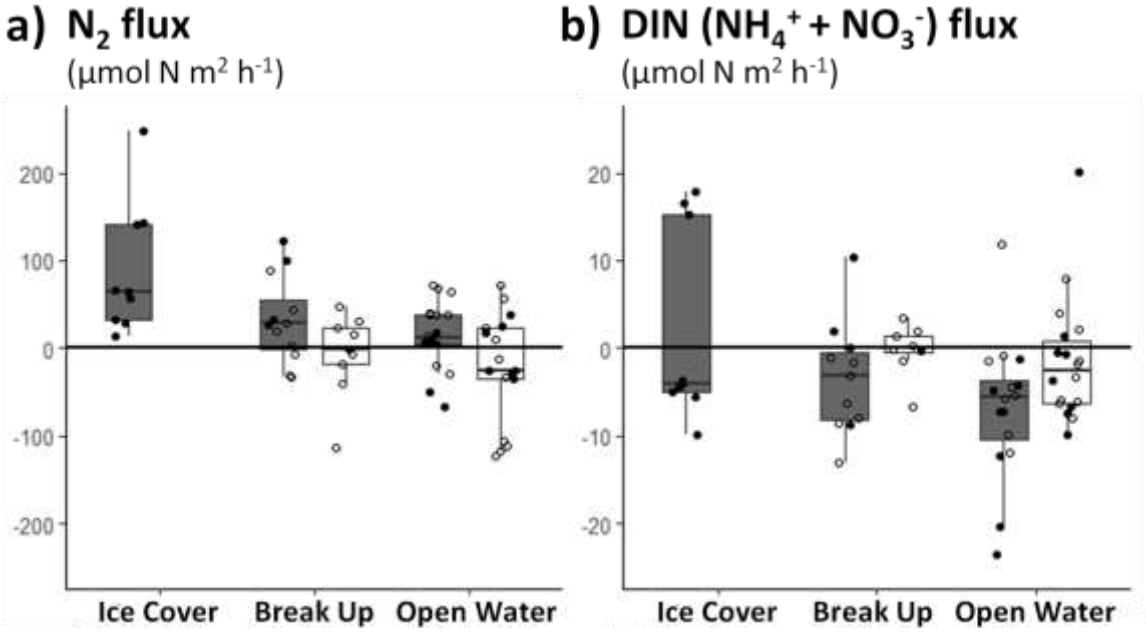

Supplementary Figure 4.1. Hourly net benthic a) N_2 flux (µmol N m^{-2} h^{-1}) and b) DIN flux (µmol N m^{-2} h^{-1}) across seasons. Fluxes are separated between dark (gray boxplot) and light (white boxplot) incubations with water depth denoted by filled circles (Deep) or empty circles (Shallow). The lower and upper extent of the boxplot represent the 25th (Q1) and 75th (Q3) percentiles while the lower and upper extent of the whiskers represent 1.5 times the interquartile range (Q3-Q1) below Q1 and above Q3. The solid black line within each box represents the median rate. Note the difference in scale for y-axis in panels a and b.

Chapter 5: Conclusion

5.1 Changing Arctic coastlines

Approximately half of Alaska's Beaufort Sea coast is fringed by barrier island chains that enclose shallow lagoons. These lagoons are subject to extreme seasonal variations in ice cover, temperature, and salinity, yet are home to a diverse and productive food web. Situated at the interface between the Arctic tundra and Beaufort Sea, these shallow systems receive and process resources from both land and sea as well as internal loading from the sediments. As the Arctic rapidly warms, these coastal lagoons will experience significant ecosystem state changes in the coming decades from both the land and sea. Warming is decreasing sea-ice extent during the summer across the Arctic, expanding the duration of the Open Water period. Changes in the timing and the magnitude of freshwater and marine inputs are likely to impact both hydrologic and biological processes in these lagoons. Studies across the Arctic have observed increases in nutrient delivery, temperature, and dissolved inorganic carbon, all linked to enhanced phytoplankton production. Specifically on the North coast of Alaska, studies indicate increasing inputs from land are providing more resources to support lagoon food webs and coastal primary productivity.

Although foundational knowledge of coastal Arctic systems has gradually developed over the past few decades, process studies that quantify nutrient transformations, ecosystem metabolism, and exchanges across the sediment-water interface in the shallow nearshore are sorely needed to develop a complete understanding of complex biogeochemical cycling within these lagoons. Understanding seasonal patterns and biological mechanisms driving coastal Arctic ecosystem

metabolism and nutrient cycling is urgently needed to form a baseline for predictions about the changing Arctic system.

5.2 Summary of Results

In Chapter 2, we observed that inorganic nutrient concentrations in coastal Arctic lagoons change seasonally in response to both biotic and abiotic influences. Nutrients accumulated during Ice Cover likely due to net heterotrophic conditions and potentially brine exclusion during sea ice formation. Notably, the concentrations of DIN were lower than expected compared to PO_4^{3-} and DSi, suggesting high rates of N cycling and removal. During Break Up, waters within the lagoons were quickly replaced by freshwater river discharge and sea ice melt with low inorganic nutrients. Regardless, uptake of inorganic nutrients was highest during Break Up signaling a transition into net ecosystem autotrophy. During the Open Water period, nutrients became depleted and nominal deviation from the conservative mixing line suggested high rates of turnover and microbial recycling.

In Chapter 3, we found that coastal sediment characteristics were likely associated with lagoon geomorphology, terrestrial organic matter source, and internal lagoon processing. SOC content was consistent with values observed along Arctic shelf sediments but exhibited spatial variability between nodes with lower values at SCC compared to BRW and BTI likely due to higher connectivity with the Beaufort Sea and larger riverine discharge. Within the lagoons, deeper regions were zones of deposition and reflected higher SOC content and finer grain sizes. Lagoon sediments had a clear, defined terrestrial signal with C:N ratios falling between coastal permafrost and riverine POC. The influence of riverine POC was reflected in SOC-$\delta^{13}C$ which was more depleted

at SCC which is characterized by higher riverine POC inputs. Notably, this spatial pattern was not reflected in C:N ratios which demonstrated decreasing values moving eastward. However, diagenetic signals of $\delta^{13}C$ and C:N ratios can decouple over shorter time scales, suggesting $\delta^{13}C$ may better reflect source while C:N ratio reflects coastal processing. Sediment microbial respiration (DOU) was primarily driven by SOC content, then temperature, with higher rates observed at deeper stations during the Open Water period. On an annual scale, Elson Lagoon sediments respired approximately 1.7 Gg C y^{-1} representing roughly one third of carbon inputs into the lagoon from coastal erosion.

In Chapter 4 environmental drivers of benthic metabolism gleaned from Chapters 2 and 3 were confirmed with batch sediment incubations. Benthic metabolism (BR, GBP, NBM) in the Beaufort Sea coastal lagoons changed seasonally in response to physical factors such as temperature, light availability, and salinity. During Ice Cover, the sediments were net heterotrophic and released nutrients into the overlying water column, but high DIN concentrations also facilitated denitrification resulting in net N loss. During Break Up and Open Water, high rates of benthic primary production by microalgae made sediments net autotrophic, and this increase in nutrient demand was reflected in increased benthic nutrient uptake and a switch to benthic N fixation. On an annual scale, the lagoon sediments functioned as a sink of both carbon (-1.9 mmol C m^{-2} y^{-1}) and nitrogen (-3.7 mmol C m^{-2} y^{-1}), highlighting their role in processing organic matter and nutrients along the land to sea continuum.

5.3 Future Implications

Based on the current expansion rates of the Open Water period in the Beaufort Sea (~11 days per decade), in 20 years we can expect the Open Water period to increase

by almost three weeks. This will result in a corresponding contraction of the Ice Cover period with no significant changes to the duration of Break Up. Decreasing ice cover duration will likely diminish the amount of inorganic nutrient accumulation in the water column during the winter. In turn, it is possible that reduced accumulation of inorganic nutrients will result in decreased pelagic primary production during Break Up. However, a shorter Ice Cover period could also result in less benthic denitrification and more accumulation of nutrients in the water column. With the expansion of the Open Water period, primary production is likely to increase with the reduction of light limitation. However, lagoon sediments may not persist as coastal carbon sinks into the future due to increasing organic matter loading and enhanced respiration. With benthic respiration limited by SOC, increasing rates of permafrost erosion and riverine POC exports will likely increase carbon release from lagoon sediments. In addition, increasing storm frequency and duration during the Open Water period will promote more sediment resuspension, amplifying organic matter remineralization. However, it is also possible that as the growing season expands, BMA may be able to develop extensive algal mats, suppressing sediment resuspension and enhancing ecosystem primary productivity. As long-term changes accelerate, it is critical to understand these biogeochemical processes and the linkages between these distinct, sequential, seasonal periods to provide a more accurate and wholistic representation of annual coastal Arctic ecosystem dynamics.